BEILSTEIN JOURNAL OF ORGANIC CHEMISTRY

Photoredox catalysis for novel organic reactions

Edited by Markus Antonietti and Peter H. Seeberger

Imprint

Beilstein Journal of Organic Chemistry
www.bjoc.org
ISSN 1860-5397
Email: journals-support@beilstein-institut.de

The *Beilstein Journal of Organic Chemistry* is published by the Beilstein-Institut zur Förderung der Chemischen Wissenschaften.

Beilstein-Institut zur Förderung der Chemischen Wissenschaften
Trakehner Straße 7–9
60487 Frankfurt am Main
Germany
www.beilstein-institut.de

BEILSTEIN JOURNAL OF ORGANIC CHEMISTRY

Graphitic carbon nitride prepared from urea as a photocatalyst for visible-light carbon dioxide reduction with the aid of a mononuclear ruthenium(II) complex

Kazuhiko Maeda[*1], Daehyeon An[1], Ryo Kuriki[1,2], Daling Lu[3] and Osamu Ishitani[1]

Full Research Paper

Open Access

Address:
[1]Department of Chemistry, School of Science, Tokyo Institute of Technology, 2-12-1-NE-2 Ookayama, Meguro-ku, Tokyo 152-8550, Japan, [2]Japan Society for the Promotion of Science, Kojimachi Business Center Building, 5-3-1, Kojimachi, Chiyoda-ku, Tokyo 102-0083, Japan and [3]Suzukakedai Materials Analysis Division, Technical Department, Tokyo Institute of Technology, 4259 Nagatsuta-cho, Midori-ku, Yokohama 226-8503, Japan

Email:
Kazuhiko Maeda[*] - maedak@chem.titech.ac.jp

* Corresponding author

Keywords:
artificial photosynthesis; heterogeneous photocatalysis; hybrid material; metal complexes; solar fuels

Beilstein J. Org. Chem. **2018,** *14,* 1806–1812.
doi:10.3762/bjoc.14.153

Received: 21 April 2018
Accepted: 26 June 2018
Published: 17 July 2018

This article is part of the thematic issue "Photoredox catalysis for novel organic reactions".

Guest Editor: M. Antonietti

Abstract

Graphitic carbon nitride (g-C_3N_4) was synthesized by heating urea at different temperatures (773–923 K) in air, and was examined as a photocatalyst for CO_2 reduction. With increasing synthesis temperature, the conversion of urea into g-C_3N_4 was facilitated, as confirmed by X-ray diffraction, FTIR spectroscopy and elemental analysis. The as-synthesized g-C_3N_4 samples, further modified with Ag nanoparticles, were capable of reducing CO_2 into formate under visible light ($\lambda > 400$ nm) in the presence of triethanolamine as an electron donor, with the aid of a molecular Ru(II) cocatalyst (RuP). The CO_2 reduction activity was improved by increasing the synthesis temperature of g-C_3N_4, with the maximum activity obtained at 873–923 K. This trend was also consistent with that observed in photocatalytic H_2 evolution using Pt-loaded g-C_3N_4. The photocatalytic activities of RuP/g-C_3N_4 for CO_2 reduction and H_2 evolution were thus shown to be strongly associated with the generation of the crystallized g-C_3N_4 phase.

Introduction

Carbon nitride is one of the oldest synthetic polymers [1], and has several allotropes. Among them, graphitic carbon nitride (g-C_3N_4) is the most stable form and is an emerging material as an organic semiconductor photocatalyst active for various kinds of reactions such as water splitting, CO_2 reduction, and degradation of harmful organic compounds, because of its non-toxic, stable, and earth-abundant nature [2-7].

Our group has developed photocatalytic CO_2 reduction systems using g-C_3N_4-based materials, in combination with functional

metal complexes [8-16]. For example, mesoporous g-C_3N_4 (mpg-C_3N_4) modified with a mononuclear Ru(II) complex, such as *trans*-(Cl)-Ru{$(PO_3H_2)_2$bpy$(CO)_2Cl_2$} (bpy: 2,2'-bipyridine), abbreviated as RuP, is capable of photocatalyzing CO_2 reduction into formate with high selectivity under visible light irradiation, as confirmed by isotope tracer experiments with $^{13}CO_2$ [8-12]. After the first report of a metal complex/C_3N_4 hybrid for CO_2 reduction, several groups have presented similar reports using cobalt-based metal complexes as reduction cocatalysts [17-20].

In these systems, structural properties of g-C_3N_4 such as specific surface area and porosity have a strong impact on activity, because they strongly affect the efficiency of electron/hole utilization to the surface chemical reactions [21,22]. Apart from mpg-C_3N_4 that is usually prepared by a hard-template method with multistep procedures [9,23], g-C_3N_4 having a relatively higher surface area can be readily prepared by heating urea, which is an inexpensive and readily available precursor, in air [14,24]. In fact, the urea-derived g-C_3N_4 exhibited an enhanced activity for CO_2 reduction compared to mpg-C_3N_4, when modified with Ag nanoparticles and a binuclear Ru(II) complex [14].

Thermal heating of urea results in decomposition and formation of g-C_3N_4, whose physicochemical properties should be dependent on the heating temperature. In this work, we investigated photocatalytic activities of g-C_3N_4, which was synthesized by heating urea at different temperatures, for visible-light CO_2 reduction with the aid of a mononuclear Ru(II) complex, RuP (see Scheme 1). As mentioned earlier, g-C_3N_4 has been studied as a visible-light-responsive photocatalyst mostly for H_2 evolution from aqueous triethanolamine (TEOA) solution [2,3,5]. The present work also compares the activities for CO_2 reduction with those for H_2 evolution in order to obtain a better understanding on photocatalytic activities of g-C_3N_4 for different kinds of reactions.

Results and Discussion

Synthesis of g-C_3N_4 by thermal heating of urea at different temperatures

Figure 1 shows XRD patterns of g-C_3N_4 samples synthesized at different temperatures. Two peaks are observed at 2theta = 13 and 27.4°, which are assigned to an in-planar repeating motif and the stacking of the conjugated aromatic system, respectively [25]. This result confirms the successful synthesis of g-C_3N_4

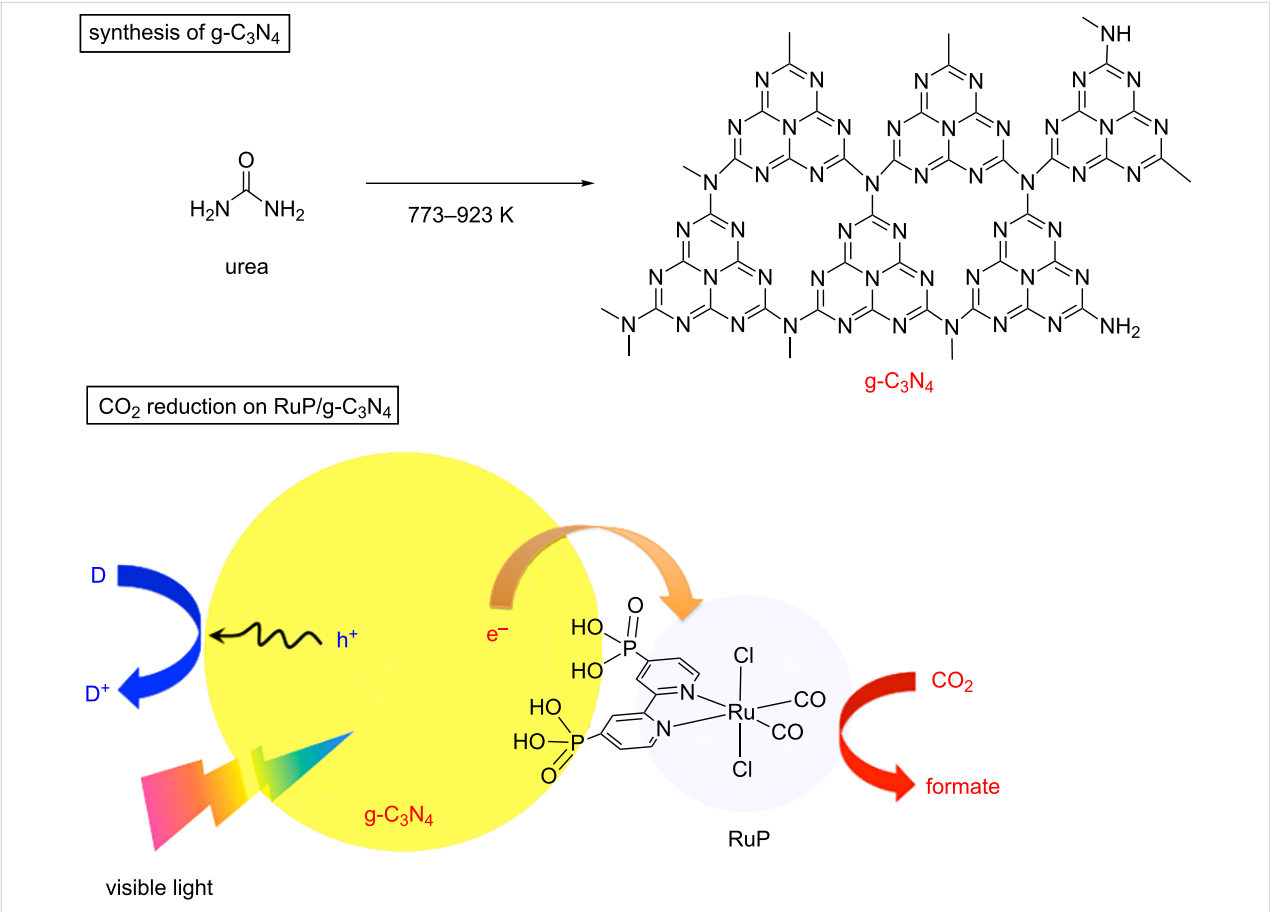

Scheme 1: Synthesis of g-C_3N_4 by thermal heating of urea and application to photocatalytic CO_2 reduction with a mononuclear Ru(II) complex (RuP).

at the present temperature range examined. With increasing temperature, the intensity of these peaks became stronger, indicating that the formation of g-C_3N_4 was facilitated at higher temperatures. It is, however, noted that the high-temperature heating also caused the loss of the product mass due to the decomposition of g-C_3N_4 itself [25].

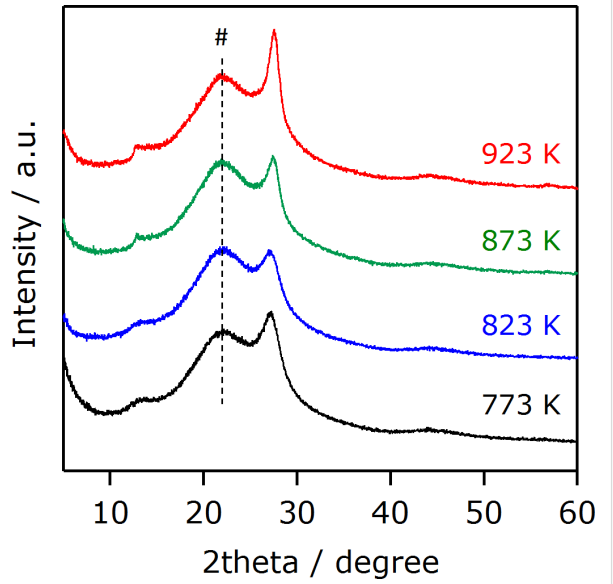

Figure 1: XRD patterns of g-C_3N_4 synthesized at different temperatures. A broad peak at around 22 degree, indicated by #, in XRD patterns originated from a glass folder for the measurement.

FTIR spectra for the same set of the samples are shown in Figure 2. Characteristic peaks can be seen in the 1650–1200 cm^{-1} region. The peaks at 1322 and 1243 cm^{-1} are assigned to the stretching vibration of connected units of C–N(–C)–C (full condensation) or C–NH–C (partial condensation) [26,27]. The leftovers of 1641, 1569, 1462 and 1412 cm^{-1} are assigned to stretching vibration modes of heptazine-derived repeating units, and are sharper with increasing temperature. This further indicates the production of g-C_3N_4 at elevated temperatures, consistent with the XRD analysis (Figure 1). The 812 cm^{-1} peak is attributed to the out-of-plane bending vibration characteristic of heptazine rings.

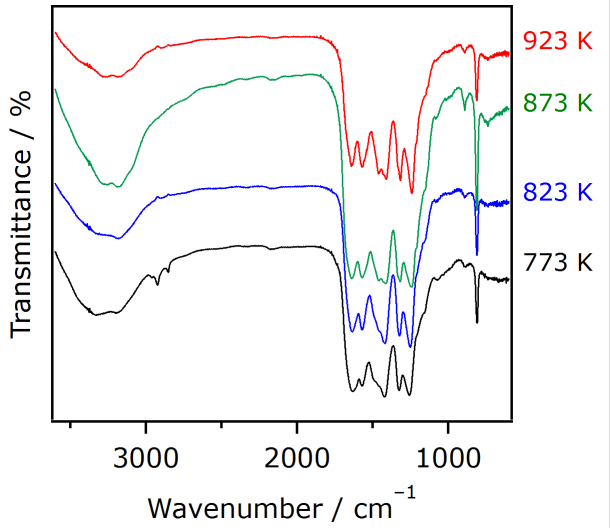

Figure 2: FTIR spectra of g-C_3N_4 synthesized at different temperatures. Each spectrum was acquired by a KBr method in N_2 atmosphere.

The results of elemental analyses for the as-prepared g-C_3N_4 samples were listed in Table 1. In all cases, not only carbon and nitrogen, which are the main constituent elements of g-C_3N_4, but also hydrogen and oxygen were detected. As the synthesis temperature increased, the compositions of carbon and nitrogen became closer to the ideal values, although the carbon content was obviously lower. The hydrogen and oxygen impurities were also reduced with an increase in the synthesis temperature. These results indicate that rising temperature is important to obtain purer g-C_3N_4 in terms of the chemical composition.

TEM images of the same samples are shown in Figure 3. The sample synthesized at 773 K had a lot of circular voids having 50–100 nm in size. At 823 K, this void structure was less prominent, and sheet-like morphology started to appear. With a further increase in the synthesis temperature, the synthesized samples consisted of disordered nanosheets. This change in par-

Table 1: Results of elemental analysis and specific surface area measurements.

synthesis temperature [K]	composition [wt %]				specific surface area [m^2 g^{-1}]
	C	N	H	O	
773	32.68	59.60	1.78	4.98	38
823	33.29	59.97	1.53	4.58	36
873	33.64	60.38	1.26	4.15	56
923	34.29	61.14	1.09	2.90	54
ideal C_3N_4	39.13	60.87	0	0	–

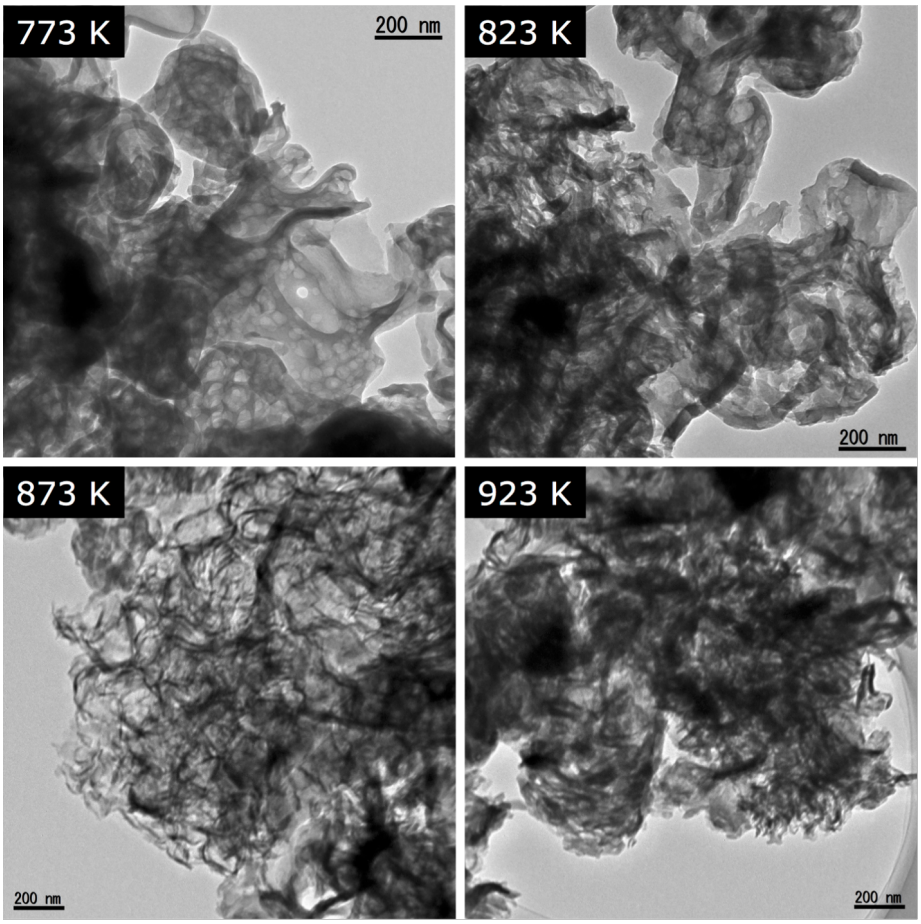

Figure 3: TEM images of g-C_3N_4 synthesized at different temperatures.

ticle morphology is in qualitative agreement with that in the specific surface area (see Table 1).

Figure 4 shows the UV–visible diffuse reflectance spectra of g-C_3N_4 synthesized at different temperatures. All of the samples exhibited an absorption edge at 420–450 nm, attributed to electron transitions from the valence band formed by nitrogen 2p orbitals to the conduction band formed by carbon 2p orbitals [25]. The band gaps of the synthesized g-C_3N_4 were estimated to be ca. 2.8–3.0 eV, from the onset wavelength of the diffuse reflectance spectra. This value is consistent with that reported previously [24]. As the synthesis temperature increases, the onset wavelength is shifted to longer wavelengths (i.e., band gap is decreased), with more pronounced tailing absorption extending to 550 nm that is assigned to n–π* transitions involving lone pairs on the edge nitrogen atoms of the heptazine rings [28,29]. While the n–π* transitions are forbidden for perfectly symmetric and planar heptazine units, they become partially allowed with increasing the condensation of layers in g-C_3N_4, which results from an increase in the synthesis temperature.

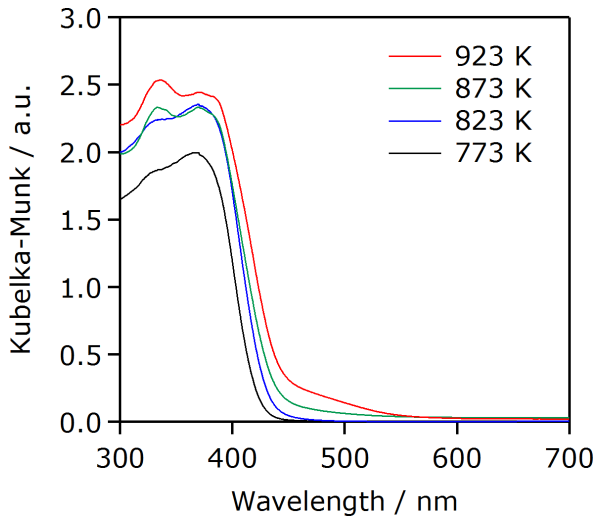

Figure 4: UV–visible diffuse reflectance spectra of g-C_3N_4 synthesized at different temperatures.

Photocatalytic activities for CO_2 reduction and H_2 evolution

Using the as-prepared g-C_3N_4, CO_2 reduction was conducted with the aid of RuP cocatalyst and Ag promoter in a *N,N*-dimethylacetamide (DMA)/TEOA mixed solution under visible light (λ > 400 nm). Here TEOA works as an effective electron donor that scavenges holes generated in the valence band of g-C_3N_4 [25]. The use of DMA as the solvent for CO_2 reduction using RuP/mpg-C_3N_4 has previously been shown to be the best choice of solvents to maximize the photocatalytic activity [10]. Because RuP does not absorb visible light efficiently, the g-C_3N_4 component can be activated selectively by visible light [10]. Our previous study also indicated that the amount of a molecular cocatalyst is very important in this kind of mononuclear-complex/C_3N_4 hybrid photocatalyst for visible-light CO_2 reduction [8]. To eliminate any other effects other than heating temperature of urea, we fixed the amount of RuP in this study. Ag nanoparticles loaded on mpg-C_3N_4 serves as a promoter of electron transfer from mpg-C_3N_4 to RuP, as discussed in our previous work [13]. TEM observation indicated that the loaded Ag is in the form of nanoparticles of 5–10 nm in size (Figure 5). Without Ag (i.e., RuP/g-C_3N_4), formate production was clearly observable, but the activity was typically 20% that of RuP/Ag/g-C_3N_4. Hence we employed Ag as an additional promoter in all cases. It should be also noted that no reaction took place using only g-C_3N_4.

As listed in Table 2, the main product during the reaction was formate with 90–95% selectivity. Minor products were CO and H_2. With increasing the synthesis temperature, the formate generation activity was improved to reach a maximum at 873–923 K, while almost unchanging the CO and H_2 evolution. The catalytic turnover number of formate generation calculated based on the mole amount of RuP at the optimal conditions reached 650, which confirms the catalytic cycle of the reaction.

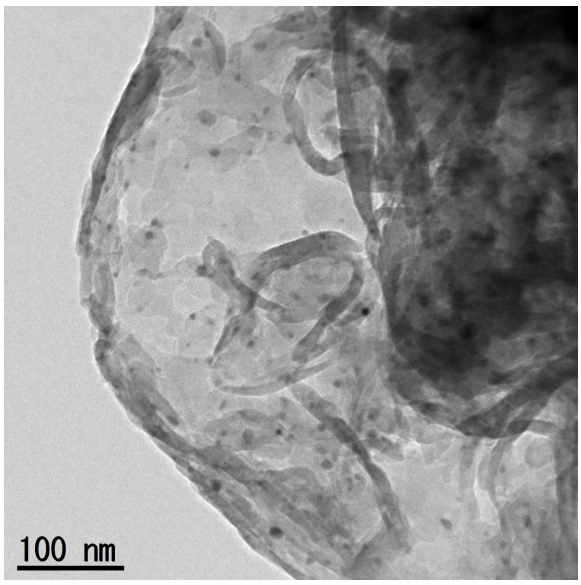

Figure 5: A typical TEM image of Ag-loaded g-C_3N_4. The synthesis temperature of g-C_3N_4 was 873 K in this case.

H_2 evolution was also conducted in a mixed solution of water and TEOA. It is also noted that Pt was in situ loaded on g-C_3N_4 as a cocatalyst to facilitate H_2 evolution. As listed in Table 2, all of the synthesized samples produced H_2. Similar to the trend in CO_2 reduction, the H_2 evolution activity was enhanced as the synthesis temperature was increased.

The results of the photocatalytic reactions thus indicated that photocatalytic activities of g-C_3N_4 derived from urea were dependent on the heating temperature of urea. The trend of activity observed in both CO_2 reduction and H_2 evolution could be explained in terms of the formation of the g-C_3N_4 structure. Physicochemical analyses indicated that increasing the synthesis temperature of g-C_3N_4 promotes conversion of urea into g-C_3N_4 (Figure 1 and Figure 2), which has even better visible-

Table 2: Photocatalytic activities of g-C_3N_4 synthesized at different temperatures for CO_2 reduction and H_2 evolution under visible light (λ > 400 nm)[a].

synthesis temperature [K]	CO_2 reduction[b] [μmol]			H_2 evolution[c] [μmol]
	formate	CO	H_2	
773	2.8	0.2	0.1	7.0
823	3.0	0.2	0.1	9.7
873	5.2	0.1	0.1	17.9
923	5.1	0.1	0.1	18.6

[a]Reaction conditions: photocatalyst (4.0 mg); reactant solution (4.0 mL); light source, 400 W high-pressure Hg lamp with a $NaNO_2$ aqueous solution filter. Reaction time: 5 h. [b]With 2.0 μmol g^{-1} RuP and 5.0 wt % Ag. Performed in a DMA/TEOA mixed solution (4:1 v/v). [c]With 3.0 wt % Pt. Performed in a water/TEOA mixed solution (9:1 v/v).

light absorption (Figure 4). The better light absorption profile as well as higher specific surface area of the g-C_3N_4 samples synthesized at elevated temperatures would have a positive impact on the activity to a certain extent. It is also noted that the photocatalytic activity for CO_2 reduction was much lower than that for H_2 evolution, even though the same electron donor, TEOA, was employed. This in turn implies that there still remains much room for the improvement of CO_2 reduction activity, for example, if a proper modification method, which allows for more efficient electron transfer, is developed. This is now under investigation in our laboratory.

Conclusion

Heating urea in air at 773–923 K resulted in the formation of g-C_3N_4, which exhibited photocatalytic activity for CO_2 reduction into formate under visible light with the aid of a molecular Ru(II) cocatalyst. Experimental results highlighted that higher heating temperature for the synthesis led to the production of more crystallized g-C_3N_4 with higher specific surface area and more pronounced visible-light absorption, which was preferable for photocatalytic reactions of both CO_2 reduction and H_2 evolution. However, too high synthesis temperature causes a mass loss of g-C_3N_4 due to thermal decomposition, which is not practically desirable.

Experimental

Materials and reagents

g-C_3N_4 samples were synthesized by heating 10 g of urea (99^+%, Wako Chemicals Co.) in air at a ramp rate of 2.3 K min^{-1} to a given temperature (773–923 K), keeping that temperature for 4 h, then cooling without temperature control.

Ag (5.0 wt %) was loaded as a promoter onto the surface of g-C_3N_4 by an impregnation method using $AgNO_3$ (>99.8%, Wako Pure Chemicals Co.) as the precursor according to the previous method [13]. g-C_3N_4 (50 mg) was dispersed in an aqueous $AgNO_3$ solution (10 mL). The water content was subsequently removed under reduced pressure at 317 K. The resulting solid sample was heated under a H_2 stream (20 mL min^{-1}) at 473 K for 1 h.

RuP was synthesized according to methods reported in our previous paper [10]. Adsorption of RuP onto Ag/g-C_3N_4 was conducted by dispersing 40 mg of Ag/g-C_3N_4 in an acetonitrile (MeCN) solution (20 mL) of RuP. The suspension was stirred overnight at room temperature in the dark to allow for the adsorption/desorption equilibrium, followed by filtration and washing with acetonitrile. The filtrates were collected and concentrated to a volume of 30 mL. The amount of the ruthenium complex absorbed was calculated based on the UV–vis spectrum of the filtrate, using Equation 1:

$$\text{adsorbed amount}\left(\text{mol g}^{-1}\right) = \frac{A_{\text{before}} - A_{\text{after}}}{A_{\text{before}}} \cdot \frac{C\left(\text{mol L}^{-1}\right) \times 20 \times 10^{-3}\left(\text{L}\right)}{40 \times 10^{-3}\left(\text{g}\right)}, \quad (1)$$

where A_{before} and A_{after} are the absorbance of the solution before and after the adsorption procedure, respectively, and C is the initial concentration of RuP.

Organic solvents used in this work were subject to purification prior to use. DMA was dried over molecular sieves 4 Å (which was heated at 373 K under reduced pressure (<1 Torr) overnight for several days), and distilled under reduced pressure (10–20 Torr). MeCN was distilled over P_2O_5 twice, and then distilled over CaH_2 prior to use. TEOA was distilled under reduced pressure (<1 Torr). The distilled DMA and TEOA were kept under Ar prior to use.

Characterization

The prepared materials were characterized by X-ray diffraction (XRD) (MiniFlex600, Rigaku; Cu Kα radiation), Fourier-transform infrared (FTIR) spectroscopy (FTIR-610, Jasco), transmission electron microscopy (TEM) (JEM-2010F, JEOL), and UV–visible diffuse reflectance spectroscopy (DRS) (V-565, Jasco). The Brunauer–Emmett–Teller (BET) surface area of each specimen was determined using a BELSOEP-mini instrument (BEL Japan) at liquid nitrogen temperature. The amount of carbon, nitrogen, hydrogen and oxygen were determined by elemental analysis (MICRO CORDER JM10, J-SCIENCE) by Suzukakedai Materials Analysis Division, Technical Department, Tokyo Institute of Technology.

Photocatalytic reactions

Reactions were performed at room temperature (298 K) using an 8 mL test tube containing 4 mL of solution by dispersing 4 mg of photocatalyst powder. For H_2 evolution, a mixed solution of water and TEOA (9:1 v/v) was used as the reactant solution, which was in prior purged with Ar for 20–30 min to remove residual air. Pt (3.0 wt %) was loaded in situ using H_2PtCl_6 (>98.5%, Wako Pure Chemicals Co.) as the precursor. For CO_2 reduction, a mixed solution of DMA and TEOA (4:1 v/v) was used. Prior to irradiation, the suspension was purged with CO_2 (Taiyo Nippon Sanso Co., >99.995%) for 20–30 min. A 400 W high-pressure Hg lamp (SEN) was used as a light source, in combination with a $NaNO_2$ solution as a filter to provide visible light irradiation ($\lambda > 400$ nm). The gaseous reaction products were analyzed using a gas chromatograph with a thermal conductivity detector (GL Science, Model GC323). The formate generated in the liquid phase was

analyzed via a capillary electrophoresis system (Otsuka Electronics Co., Model CAPI-3300).

Acknowledgements

This work was supported by a Grant-in-Aid for Young Scientists (A) (Project JP16H06130) from JSPS. It was also partially supported by a Grant-in-Aid for Scientific Research on Innovative Area "Mixed Anion (Project JP16H06441)" and a CREST program (Project JPMJCR13L1) (JST). K.M. acknowledges The Noguchi Institute and Murata Research Foundation financial support. R.K. wishes to acknowledge support by a JSPS Fellowship for Young Scientists (Project JP17J03705).

ORCID® iDs

Kazuhiko Maeda - https://orcid.org/0000-0001-7245-8318
Ryo Kuriki - https://orcid.org/0000-0002-3843-2867
Daling Lu - https://orcid.org/0000-0002-9084-480X
Osamu Ishitani - https://orcid.org/0000-0001-9557-7854

References

1. Liebig, J. *Ann. Pharm. (Lemgo, Ger.)* **1834,** *10,* 1–47. doi:10.1002/jlac.18340100102
2. Wang, Y.; Wang, X.; Antonietti, M. *Angew. Chem., Int. Ed.* **2012,** *51,* 68–89. doi:10.1002/anie.201101182
3. Zheng, Y.; Lin, L.; Wang, B.; Wang, X. *Angew. Chem., Int. Ed.* **2015,** *54,* 12868–12884. doi:10.1002/anie.201501788
4. Zhang, J.; Chen, Y.; Wang, X. *Energy Environ. Sci.* **2015,** *8,* 3092–3108. doi:10.1039/C5EE01895A
5. Kuriki, R.; Maeda, K. *Phys. Chem. Chem. Phys.* **2017,** *19,* 4938–4950. doi:10.1039/C6CP07973C
6. Yin, S.; Han, J.; Zhou, T.; Xu, R. *Catal. Sci. Technol.* **2015,** *5,* 5048–5061. doi:10.1039/C5CY00938C
7. Fang, Y.; Wang, X. *Chem. Commun.* **2018,** *54,* 5674–5687. doi:10.1039/C8CC02046A
8. Maeda, K.; Sekizawa, K.; Ishitani, O. *Chem. Commun.* **2013,** *49,* 10127–10129. doi:10.1039/c3cc45532g
9. Maeda, K.; Kuriki, R.; Zhang, X.; Wang, X.; Ishitani, O. *J. Mater. Chem. A* **2014,** *2,* 15146–15151. doi:10.1039/C4TA03128H
10. Kuriki, R.; Sekizawa, K.; Ishitani, O.; Maeda, K. *Angew. Chem., Int. Ed.* **2015,** *54,* 2406–2409. doi:10.1002/anie.201411170
11. Kuriki, R.; Ishitani, O.; Maeda, K. *ACS Appl. Mater. Interfaces* **2016,** *8,* 6011–6018. doi:10.1021/acsami.5b11836
12. Maeda, K.; Kuriki, R.; Ishitani, O. *Chem. Lett.* **2016,** *45,* 182–184. doi:10.1246/cl.151061
13. Kuriki, R.; Matsunaga, H.; Nakashima, T.; Wada, K.; Yamakata, A.; Ishitani, O.; Maeda, K. *J. Am. Chem. Soc.* **2016,** *138,* 5159–5170. doi:10.1021/jacs.6b01997
14. Kuriki, R.; Yamamoto, M.; Higuchi, K.; Yamamoto, Y.; Akatsuka, M.; Lu, D.; Yagi, S.; Yoshida, T.; Ishitani, O.; Maeda, K. *Angew. Chem., Int. Ed.* **2017,** *56,* 4867–4871. doi:10.1002/anie.201701627
15. Wada, K.; Eguchi, M.; Ishitani, O.; Maeda, K. *ChemSusChem* **2017,** *10,* 287–295. doi:10.1002/cssc.201600661
16. Wada, K.; Ranasinghe, C. S. K.; Kuriki, R.; Yamakata, A.; Ishitani, O.; Maeda, K. *ACS Appl. Mater. Interfaces* **2017,** *9,* 23869–23877. doi:10.1021/acsami.7b07484
17. Lin, J.; Pan, Z.; Wang, X. *ACS Sustainable Chem. Eng.* **2014,** *2,* 353–358. doi:10.1021/sc4004295
18. Wang, S.; Lin, J.; Wang, X. *Phys. Chem. Chem. Phys.* **2014,** *16,* 14656–14660. doi:10.1039/c4cp02173h
19. Walsh, J. J.; Jiang, C.; Tang, J.; Cowan, A. J. *Phys. Chem. Chem. Phys.* **2016,** *18,* 24825–24829. doi:10.1039/C6CP04525A
20. Zhao, G.; Pang, H.; Liu, G.; Li, P.; Liu, H.; Zhang, H.; Shi, L.; Ye, J. *Appl. Catal., B: Environ.* **2017,** *200,* 141–149. doi:10.1016/j.apcatb.2016.06.074
21. Maeda, K. *J. Photochem. Photobiol., C* **2011,** *12,* 237–268. doi:10.1016/j.jphotochemrev.2011.07.001
22. Maeda, K.; Domen, K. *Bull. Chem. Soc. Jpn.* **2016,** *89,* 627–648. doi:10.1246/bcsj.20150441
23. Goettmann, F.; Fischer, A.; Antonietti, M.; Thomas, A. *Angew. Chem., Int. Ed.* **2006,** *45,* 4467–4471. doi:10.1002/anie.200600412
24. Liu, J.; Zhang, T.; Wang, Z.; Dawson, G.; Chen, W. *J. Mater. Chem.* **2011,** *21,* 14398–14401. doi:10.1039/c1jm12620b
25. Wang, X.; Maeda, K.; Thomas, A.; Takanabe, K.; Xin, G.; Carlsson, J. M.; Domen, K.; Antonietti, M. *Nat. Mater.* **2009,** *8,* 76–80. doi:10.1038/nmat2317
26. Lotsch, B. V.; Döblinger, M.; Sehnert, J.; Seyfarth, L.; Senker, J.; Oeckler, O.; Schnick, W. *Chem. – Eur. J.* **2007,** *13,* 4969–4980. doi:10.1002/chem.200601759
27. Bojdys, M. J.; Müller, J.-O.; Antonietti, M.; Thomas, A. *Chem. – Eur. J.* **2008,** *14,* 8177–8182. doi:10.1002/chem.200800190
28. Jorge, A. B.; Martin, D. J.; Dhanoa, M. T. S.; Rahman, A. S.; Makwana, N.; Tang, J.; Sella, A.; Corà, F.; Firth, S.; Darr, J. A.; McMillan, P. F. *J. Phys. Chem. C* **2013,** *117,* 7178–7185. doi:10.1021/jp4009338
29. Zhang, H.; Yu, A. *J. Phys. Chem. C* **2014,** *118,* 11628–11635. doi:10.1021/jp503477x

License and Terms

BEILSTEIN JOURNAL OF ORGANIC CHEMISTRY

Applications of organocatalysed visible-light photoredox reactions for medicinal chemistry

Michael K. Bogdos*[1], Emmanuel Pinard[2] and John A. Murphy[1]

Review

Open Access

Address:
[1]Department of Pure and Applied Chemistry, University of Strathclyde, 295 Cathedral Street, Glasgow G1 1 XL, United Kingdom and [2]F. Hoffman-La Roche Ltd., pRED, Pharma Research & Early Development, Roche Innovation Center Basel, Grenzacherstrasse 124, 4070 Basel, Switzerland

Email:
Michael K. Bogdos* - michael.bogdos.2014@uni.strath.ac.uk

* Corresponding author

Keywords:
C–H functionalisation; heterocycles; late-stage functionalisation; medicinal chemistry; organic dyes; organic photocatalysts; peptide chemistry; photoredox catalysis

Beilstein J. Org. Chem. **2018,** *14,* 2035–2064.
doi:10.3762/bjoc.14.179

Received: 05 May 2018
Accepted: 13 July 2018
Published: 03 August 2018

This article is part of the thematic issue "Photoredox catalysis for novel organic reactions".

Associate Editor: C. Stephenson

Abstract

The focus of this review is to provide an overview of the field of organocatalysed photoredox chemistry relevant to synthetic medicinal chemistry. Photoredox transformations have been shown to enable key transformations that are important to the pharmaceutical industry. This type of chemistry has also demonstrated a high degree of sustainability, especially when organic dyes can be employed in place of often toxic and environmentally damaging transition metals. The sections are arranged according to the general class of the presented reactions and the value of these methods to medicinal chemistry is considered. An overview of the general characteristics of the photocatalysts as well as some electrochemical data is presented. In addition, the general reaction mechanisms for organocatalysed photoredox transformations are discussed and some individual mechanistic considerations are highlighted in the text when appropriate.

Review

1 Introduction

1.1 Main advantages of organocatalysed photoredox chemistry

Photoredox catalysis is an emerging field in organic synthesis and has been the subject of many reviews in recent years [1-9]. Some cover the manipulation or installation of various functional groups [10-17], the synthesis of particular bonds (C–C or C–N etc.) [18-21] or the synthesis of natural products or heterocycles [22-27]. Others provide an overview of catalysts and the

transformations they enable [28-33]. The most relevant review that links photoredox synthesis and medicinal chemistry is that of Stephenson [34].

Organocatalysis in general offers several advantages over transition metal-mediated catalysis. For example, removal of the catalyst during purification is much more straightforward. Furthermore, the organic molecules employed are typically much less environmentally damaging and toxic to various life forms.

Photochemistry also offers benefits compared to conventional thermally driven processes. Several transformation processes that utilise sunlight as the energy source to drive a particular reaction have been reported and some reactions presented in this review achieve this as well. This is the most energetically sustainable way possible to carry out a chemical transformation. A result of this use of the energy of photons is that photochemical transformations often require fewer and/or less reactive (which correlates to toxicity and environmental impact) components than traditional reactions.

Organocatalysed photoredox catalysis combines the advantages of both these fields. Thus, it is not only a new field filled with exciting discoveries, but also is sustainable and beneficial in the long term.

1.2 General characteristics of photocatalysts

1.2.1 Brief photophysical overview. There are several factors that affect the ability of an organic molecule to act as a photocatalyst. In a typical organocatalysed photoredox reaction, the photocatalyst transitions from a singlet ground state (S_0) to a long-lived and relatively stable excited state, either a singlet excited state (S_1) or a triplet excited state (T_1), by absorption of a photon with energy *hν*, which then undergoes photoinduced electron transfer (PET). Following this, the photocatalyst is reduced or oxidised accordingly, such that it returns to its ground state and native oxidation state (Figure 1 and Figure 2).

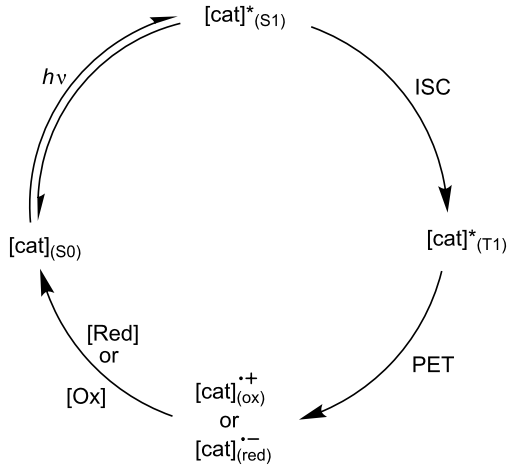

Figure 2: General catalytic cycle of a photocatalyst in a photoredox organocatalysed reaction. [cat] – photocatalyst, [cat]*x – photocatalyst in x (x = S_0, S_1, T_1) state, ox – oxidised, red – reduced. ISC does not always occur.

It is ideal if a photocatalyst has a local absorbance maximum (λ_{max}) at a relatively long wavelength. Lower energy photons avoid exciting other reactants and prevent competing photochemistry from occurring, cf. ultraviolet light. However, the energy of the absorbed photon also determines the energy of the excited state of the catalyst. Catalysts with a λ_{max} at a longer wavelength have excited states at relatively low energy and therefore do not have very strong oxidising or reducing capabilities. A good balance is achieved by molecules which have λ_{max} in the visible region. Many organic molecules have some UV absorbance, but little or no absorbance in the visible part of the spectrum, hence excitation of other reactants is unlikely. Visible light photons are high enough in energy to produce excited states of sufficient reactivity to undergo PET.

Once a molecule is electronically excited, there are multiple pathways through which it can decay back to S_0. The excited

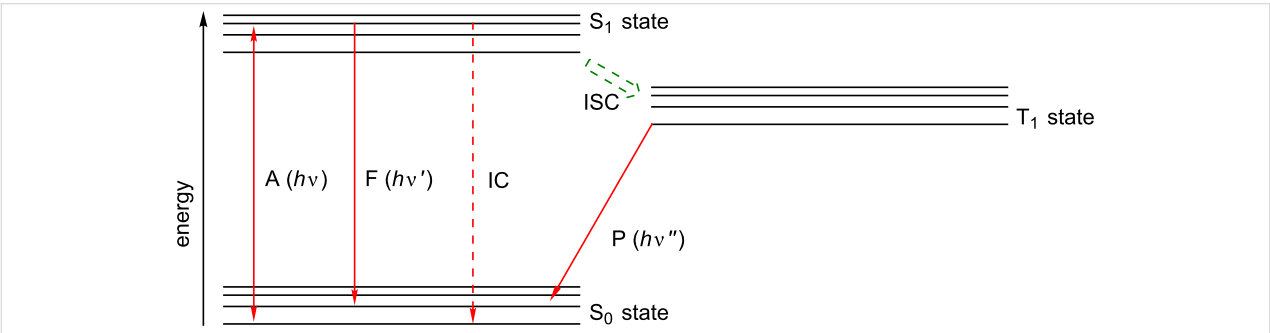

Figure 1: Depiction of the energy levels of a typical organic molecule and the photophysical processes it can undergo. A – absorption and emission, F – fluorescence, IC – internal conversion (non-radiative), ISC – intersystem crossing, P – phosphorescence.

state can decay via non-radiative processes, such as vibrational relaxation. It can also return to S_0 via fluorescence or non-radiative emission. While in S_1 (or T_1) Förster resonance electron transfer (FRET) can occur, a process through which energy is transferred between chromophores via non-radiative dipole–dipole coupling.

It is generally assumed that the non-radiative processes occur at a much slower rate than radiative processes. As such, the lifetime of S_1 (τ_{s1}) is roughly equal to the lifetime of fluorescence (τ_f). In general, if a molecule is to participate in a reaction in the S_1 state, its τ_f must be greater than 1 ns; N.B. the diffusion rate constant (k_{diff}) is ≈1–2 × 10^{10} s^{-1}.

The fluorescence quantum yield (Φ_f) is another key parameter to consider when determining whether the S_1 state of a molecule is likely to be involved in PET. A molecule with a low Φ_f will be unlikely to be found in the S_1 state, as this state will be highly susceptible to other decay pathways in the timescale of PET.

For a molecule to undergo PET when in the T_1 state, the intersystem crossing quantum yield (Φ_{ISC}) must be comparable to or larger than the Φ_f and, more importantly, the rate constant for ISC (k_{ISC}) must be similar to the rate constant for fluorescence (k_f). The lifetime of the T_1 state (τ_{T1}) is generally orders of magnitude longer than the timescale of electron transfer (ET), meaning that τ_{T1} does not alter the efficiency of the PET process.

The decay of T_1 is negligible as the processes which bring this about (phosphorescence mainly) are symmetry forbidden and hence very slow. Therefore, if a molecule can reach the T_1 state through excitation with visible light then it is one which can be considered as a photoredox catalyst, as it will likely be able to participate in ET.

1.2.2 Brief electrochemical overview. In this review, the notation proposed by Nicewicz in his comprehensive review is adopted [35]. Therefore, all reduction potentials will be referred to using notation of the form E_x (Ox/Red) where x = "red" or "ox" and the species in the brackets refer to the reactant and product of the half reaction (Equation 1).

$$\mathrm{Ox} + e^- \longrightarrow \mathrm{Red} \qquad (1)$$

where Ox = oxidised form and Red = reduced form of the species in question.

The half reaction is always assumed to be written in the direction where reduction occurs.

$$\text{Eosin Y} + e^- \longrightarrow \text{Eosin Y}^{\bullet -} \qquad (2)$$

So, for example in half reaction (2) the redox potential is referred to by the notation E_{red} (Eosin Y/Eosin $Y^{\bullet -}$). The symbol "*" serves to denote when a species is in an excited electronic state, which then leads the general format adopted in this review to describe redox potentials of photocatalysts to become E^*_x (Ox/Red).

The electrochemical data of a photocatalyst and a substrate which is to undergo PET allow for the estimation of the feasibility of the PET.

The following equations can be used to estimate whether PET from a substrate to an excited state photocatalyst is possible:

$$\Delta G_{PET} = -F(E^*_{red}(\mathrm{cat}^*/\mathrm{cat}^{\bullet -}) - E_{ox}(\mathrm{sub}^{\bullet +}/\mathrm{sub}))$$
$$\text{and } E^*_{red}(\mathrm{cat}^*/\mathrm{cat}^{\bullet -}) = E_{red}(\mathrm{cat}^*/\mathrm{cat}^{\bullet -}) + E_{0,0}$$

Conversely, the following equations can be used for predicting whether PET from an excited state photocatalyst to a substrate is spontaneous:

$$\Delta G_{PET} = -F(E_{red}(\mathrm{sub}^*/\mathrm{sub}^{\bullet -}) - E^*_{ox}(\mathrm{cat}^{\bullet +}/\mathrm{cat}^*))$$
$$\text{and } E^*_{ox}(\mathrm{cat}^{\bullet +}/\mathrm{cat}^*) = E_{red}(\mathrm{cat}^{\bullet +}/\mathrm{cat}^*) + E_{0,0}$$

In both cases ΔG_{PET} is the free energy change during PET, F is the Faraday constant and $E_{0,0}$ is the energy of the excited state.

From these equations one can conclude that for PET to take place such that the excited catalyst is reduced, E^*_{red} ($\mathrm{cat}^*/\mathrm{cat}^{\bullet -}$) must be greater (more positive) than E_{ox} ($\mathrm{sub}^{\bullet +}$/sub). Conversely, for PET to occur from the excited photocatalyst (oxidation) to the substrate, E^*_{ox} ($\mathrm{cat}^{\bullet +}/\mathrm{cat}^*$) must be more negative than E_{red} (sub/$\mathrm{sub}^{\bullet -}$).

Where comments or suggestions are made about the reducing or oxidising power of a photocatalyst, comparisons of relevant data and these electrochemical considerations have been undertaken.

1.3 Most common catalysts employed

The following photocatalysts are frequently encountered in the literature presented in this review. Here some basic data of these photocatalysts are presented, to serve as an easy reference to the reader, with respect to their structure, electrochemical and photophysical properties.

Figure 3 shows the structures of the various compounds that are used on multiple occasions as photocatalysts in the reactions presented in this review. In cases where photocatalysts other

than these are used, their structure will be given in the reaction scheme.

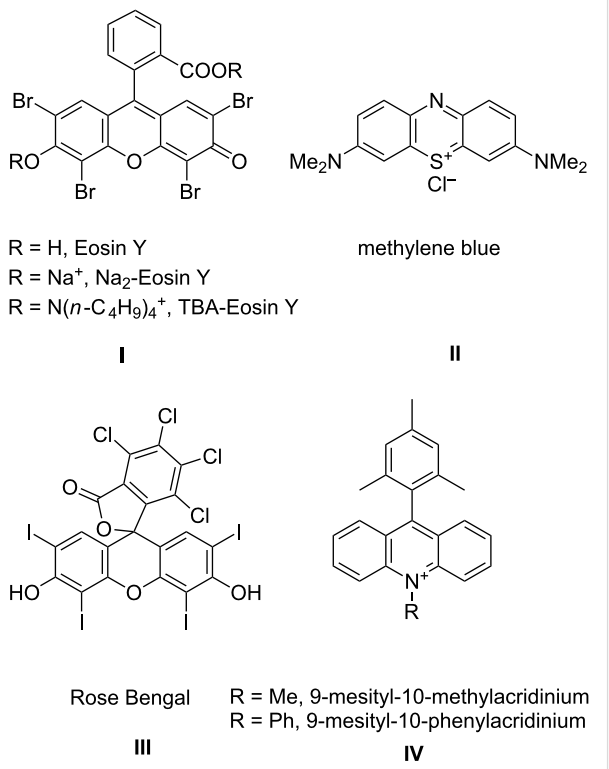

Figure 3: Structures and names of the most common photocatalysts encountered in the reviewed literature.

In Table 1 the redox potentials for the ground and excited states of these catalysts are shown.

Examination of these data reveals how excitation of these compounds changes their properties and makes them capable of redox chemistry. In some cases, e.g., MesAcr, the produced excited state is only strongly oxidising, in others the excited state is a molecule which can both reduce and oxidise different species, depending on their relative redox potentials.

1.4 General mechanism for organophotoredox-catalysed reactions

The general catalytic cycle of a photocatalyst in any given organocatalysed photoredox reaction (Figure 2) can be categorised based on the direction of ET involving the excited catalyst. If ET occurs such that the catalyst is reduced, the cycle is classed as a reductive quenching cycle (Figure 4). In a reductive quenching catalytic cycle, a species must act as an oxidant to return the photocatalyst to its native oxidation state.

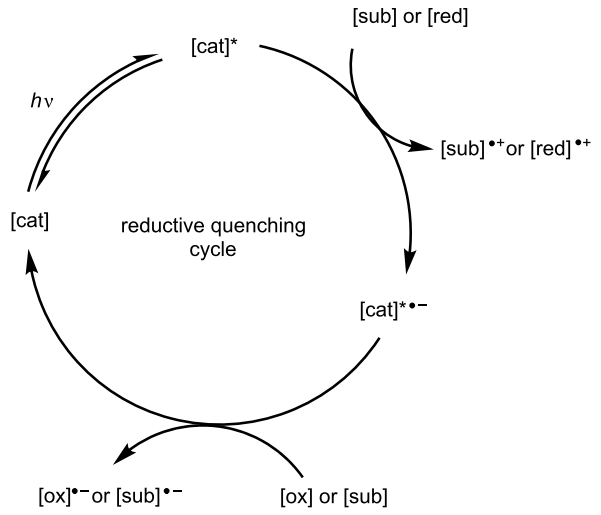

Figure 4: General example of a reductive quenching catalytic cycle. [cat] – photocatalyst, [cat]* – photocatalyst in excited state, [sub] – substrate, [red] – reductant, [ox] – oxidant.

If ET occurs such that the catalyst is oxidised, the cycle is classed as an oxidative quenching cycle (Figure 5). In an oxidative quenching catalytic cycle, a species must act as a reductant to return the photocatalyst to its native oxidation state.

Table 1: Electrochemical data for the four catalysts (**I** to **IV**) most commonly encountered in the reaction reported herein [33,35-37]. All values are with respect to the saturated calomel electrode (SCE).

catalyst	ground state redox potential		excited state redox potential		excited state	absorbance maximum (λ_{max})
	E_{red} (cat/cat$^{\bullet-}$)	E_{ox} (cat$^{\bullet+}$/cat)	E^*_{red} (cat*/cat$^{\bullet-}$)	E^*_{ox} (cat$^{\bullet+}$/cat*)		
Eosin Y (**I**)	−1.08 V	+0.76 V	+0.83 V	−1.15 V	triplet	520 nm
methylene blue (**II**)	−0.30 V	+1.13 V	+1.14 V	−0.33 V	triplet	650 nm
Rose Bengal (**III**)	−0.99 V	+.84 V	+0.81 V	−0.96 V	triplet	549 nm
MesAcr (**IV**)	−0.46 V to −0.79 V	–	+2.32 V	–	singlet	425 nm

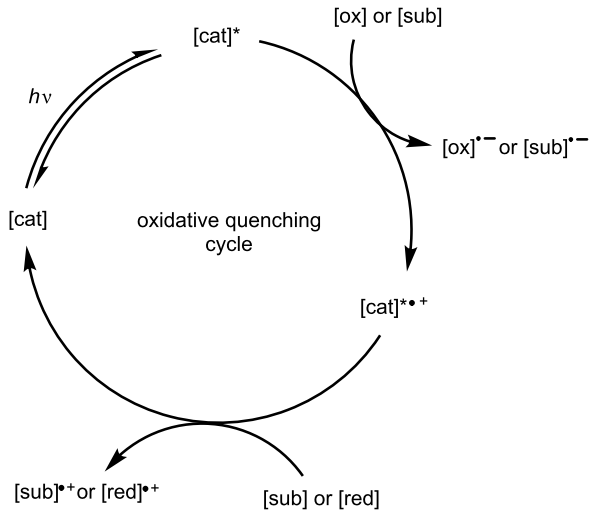

Figure 5: General example of an oxidative quenching catalytic cycle. [cat] – photocatalyst, [cat]* – photocatalyst in excited state, [sub] – substrate, [red] – reductant, [ox] – oxidant.

The reducing and oxidising species can be the substrate or an additive, since the classification of a catalytic cycle as either reductive or oxidative quenching considers only the ET with respect to the excited photocatalyst.

Photoredox reactions can also be classified with respect to the substrate. Depending on the change in oxidation state of the substrate, a photoredox reaction can be classified as either net oxidative, net reductive or redox neutral. The net result of the reaction is not dependent on the catalytic cycle characterisation – either reductive or oxidative quenching.

Net oxidative reactions require the presence of an oxidising agent. The advantage of photoredox net oxidative reactions, compared to conventional oxidation reactions, is that much milder oxidants are employed. For example, the oxidation of alcohols to carbonyls traditionally requires strong oxidants (Cr(VI) species, IBX, DMP), whereas similar reactions using photochemical methods can utilise oxygen (O_2) as the oxidising agent. The oxidising agent can accept electrons either from the excited photocatalyst or the radical anion catalyst in the catalyst turnover step. Irrespective of its role, the reaction is still classed as net oxidative.

Similarly, net reductive transformations require a reducing agent as an additive. As with net oxidative reactions, the reductant can act at any point in the catalytic cycle, which itself can be classed either as reductively or oxidatively quenched.

Net redox neutral processes see the substrate remain at the same oxidation state overall. These transformations are generally more complex, and the additives required as well as their mode of action vary in each case.

1.5 Scope, aim and selection criteria for presented publications

Unless otherwise stated, control experiments were completed to prove the necessity of the light source, photocatalyst and all additives in the reported reactions. In addition, unless otherwise stated, optimisation of the reaction conditions was carried out for all components of the reactions presented.

Only selected mechanisms are reported, as the focus is on the applications of the presented reactions in the synthesis of molecules for the purposes of medicinal chemistry. For the sake of brevity, most mechanisms are omitted completely, as they can be correctly inferred by the reagents, conditions and general mechanisms described previously (section 1.4). If the mechanism contains information vital to the understanding of various results, the key steps which contain this information will be presented and discussed.

This review aims to function as a kind of synthetic medicinal chemists' guide to organocatalysed visible light photoredox chemistry. For this reason, the review is structured such that reactions that fall under a broad category are grouped together. The main text is separated into three sections, which correspond to reactions frequently used in medicinal chemistry.

The existing literature on the topic is extensive. The papers reviewed were selected on the following criteria:

- The reactions described must not be extremely common, easy to undertake using more traditional methods or overly simplistic, e.g., simple functional group transformations.
- The publication presents a new idea or breakthrough that can potentially significantly impact the field of medicinal chemistry or synthetic organophotoredox catalysis.
- The conditions reported offer a distinct, unique or significant advantage over non-photocatalytic or transition metal photocatalysed processes.
- The reported chemistry has no precedent in the literature and is only possible using organophotoredox chemistry.
- The products presented must always be somehow important in medicinal chemistry.
- A combination of some of the above conditions.

As such, the number of research papers reviewed and presented is by no means exhaustive but is an attempt to present the content which is most relevant.

2 Coupling reactions

In this section, the bonds formed during the reactions are highlighted in red, as they are not always immediately and easily identifiable.

2.1 Peptide-type linkages

Medicinal chemists often draw inspiration from nature for the design of their molecules. With the exception of certain natural products, most naturally occurring biologically active molecules contain amides. The formation of the amide functional group is the most utilised reaction in medicinal chemistry. This is a reflection of the tendency of synthetic bioactive molecules to exhibit peptidomimetic properties. Though there is a vast number of procedures that generate amide bonds, an interesting approach is taken by Leow, who has demonstrated the synthesis of amides through the oxidative coupling of aromatic aldehydes and a wide range of secondary amines, using mesitylacridinium salts as the photocatalysts (Scheme 1) [38].

The main advantage is the use of air as the oxidant, which converts the formed α-hydroxy amine into the desired amide. This makes for a much more atom economical and environmentally benign process, when compared to traditionally used amide coupling methods where acid activating agents are needed, e.g., HATU or DCC, as the only byproduct is water.

Only arylaldehydes can be converted into amides and all but one of the examples of the amines used are secondary cyclic amines. Aliphatic aldehydes gave poor yields, with sterically hindered examples not reacting at all. The author attributed this to the formation of enamines. Under the reported reaction conditions primary aliphatic and aromatic amines all produced imines.

The benzamide moiety is somewhat common in biologically active molecules. Leow recognised this and provided some examples which are currently on the market or under investigation (Figure 6) [39]. An example of the formation of these bonds using his protocol would serve as a demonstration of utility of the reaction to complex, biologically relevant systems.

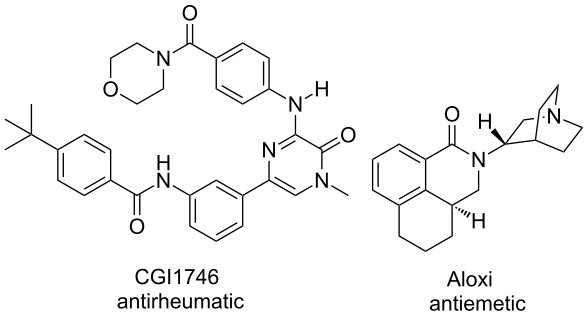

Figure 6: Biologically active molecules containing a benzamide linkage.

Naturally occurring amino acids, e.g., glycine, are often used in medicinal chemistry as linkers, structural components of scaffolds or even as precursors to useful building blocks.

Wallentin and co-workers have described a method for the reductive decarboxylation of amino acids, using bis(4-chlorophenyl)disulfide (empirical name – dichlorodiphenyl disulfide, abbreviated as DDDS), 2,6-lutidine and acridinium salts under blue LED irradiation, providing access to precious, non-commercially available and multifunctional amine building blocks in one step (Scheme 2) [40].

The group demonstrated the synthesis of protected naturally occurring amines such as GABA and phenylethylamine as well as diamines with orthogonal protecting groups, cf. product **2c**.

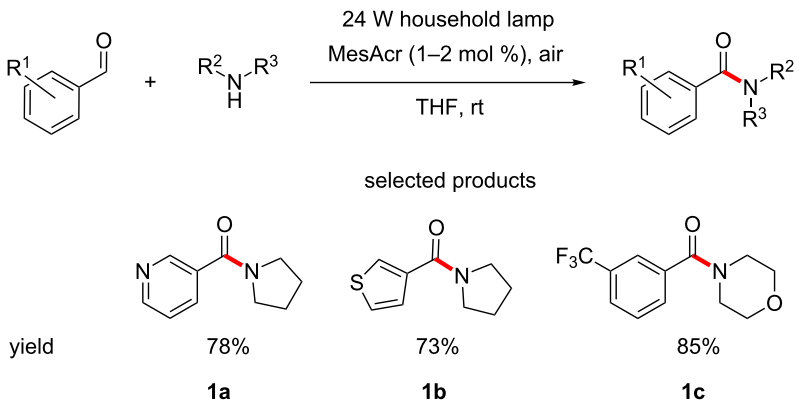

Scheme 1: Oxidative coupling of aldehydes and amines to amides using acridinium salt photocatalysis.

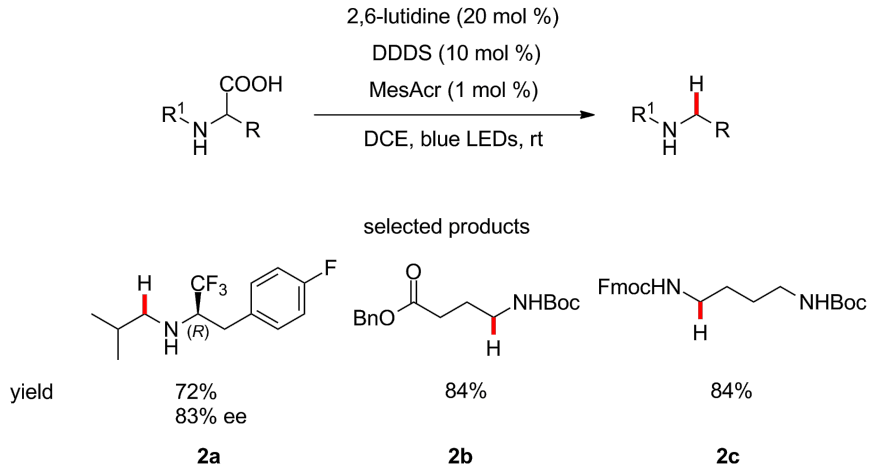

Scheme 2: The photocatalytic reduction of amino acids to produce the corresponding free or protected amines.

The combination of this protocol with the diastereoselective reductive amination reported by Hughes and Devine [41], provides access to very high value chiral α-trifluoromethylamines, which are attractive due to their low basicity, ability to act as amide bioisosteres [42] and higher metabolic stability.

The number of medicinal chemists who specialise in peptides has been increasing in recent years. This is largely due to the increasing interest in macrocyclic peptides. A key structural characteristic of peptides is the disulfide bridge formed by cysteines. This functional group is much more prevalent in peptide medicinal chemistry.

Noël et al. have published a protocol for the aerobic oxidation of thiols to disulfides, using Eosin Y photocatalysis and TMEDA (Scheme 3) [43].

The reaction specifically investigated the dimerization of thiols. Some of the experiments carried out by the group were in a flow chemistry set up, exemplifying the scalability of the proce-

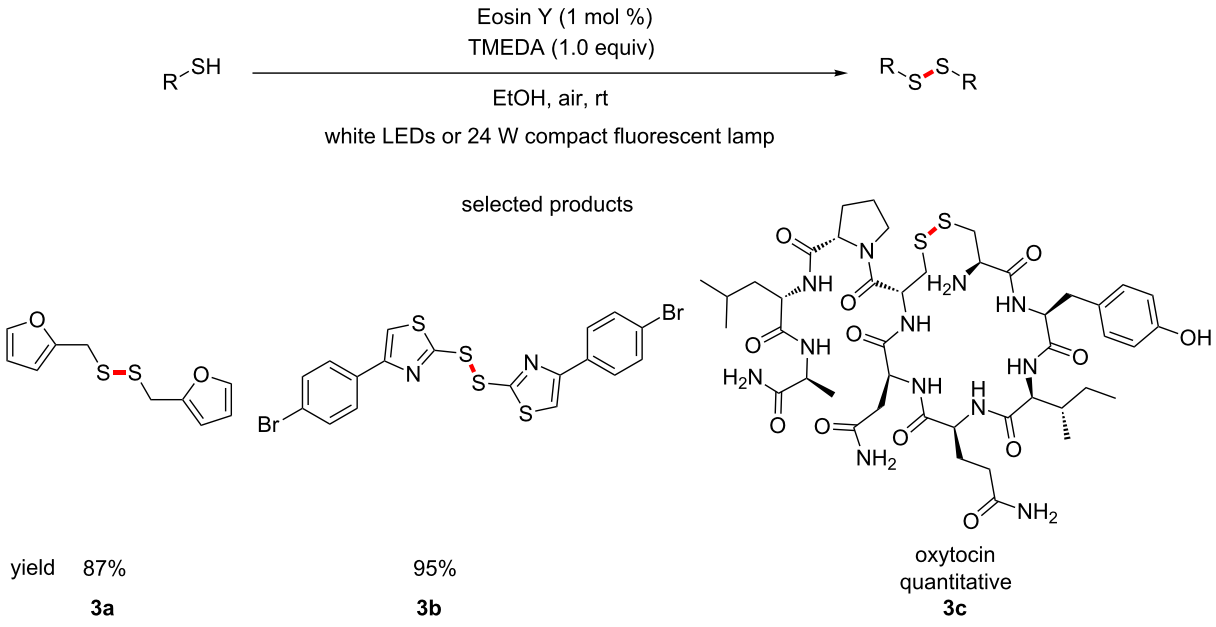

Scheme 3: The organocatalysed photoredox base-mediated oxidation of thiols to disulfides.

dure. In addition, the oxidant that achieves the transformation is molecular oxygen, making this a very sustainable route, in a similar manner to the amide coupling by Leow.

The demonstrated oxidation of the free thiols to a disulfide to afford oxytocin (**3c**) as the product in quantitative yield shows the value of this procedure. Medicinal chemists who specialise in creating artificial peptides could find much use for such a mild and selective oxidation.

MacMillan and co-workers have recently developed a method for the bioconjugation of peptides by radical decarboxylation of the C-terminus of peptides and subsequent Giese-type addition to Michael acceptors. This is performed under blue light irradiation, using lumiflavin (^{3}Lum E_{red}*(cat/cat$^{\bullet-}$) ≈ +1.5 V vs SCE) as the photocatalyst in aqueous buffer (Scheme 4) [44].

This work highlights the great biocompatibility of organophotoredox methodology and also is an excellent demonstration of the type of chemoselectivity achievable using these methods.

Apart from the immediately obvious application of this bioconjugation to biochemistry and molecular biology as a tool for protein labelling, it could also be used as a convenient tool for peptide chemists in medicinal chemistry programs for modification of peptides.

2.2 C(sp^2)–C(sp^2) bond formation

Suzuki–Miyaura and related transition metal-catalysed C–C bond forming reactions are in the top 5 most used reactions in medicinal chemistry [45]. Therefore, the development of metal-free variants of these types of reactions is a very attractive goal.

An interesting approach was taken by König et al., who report the reduction of aryl halides to the corresponding non-halogenated aromatics. This was extended to the coupling of aryl halides to a variety of substituted pyrroles, using *N,N*-bis(2,6-diisopropylphenyl)perylene-3,4,9,10-bis(dicarboximide) (PDI) as the photocatalyst, under blue LED irradiation, in DMSO and in the presence of triethylamine (Scheme 5) [46].

The biggest breakthrough in this case is the excitation of PDI by two photons, creating a radical anion in an excited state, giving the catalyst a much higher reducing power, allowing the reduction of aryl chlorides (see product **5b**). This is the first report of the reduction of aryl chlorides without the use of a strong base, UV radiation or highly reactive neutral organic reducing agents.

The PDI catalytic cycle is different to the general catalytic cycle presented in the introduction and is presented in Figure 7.

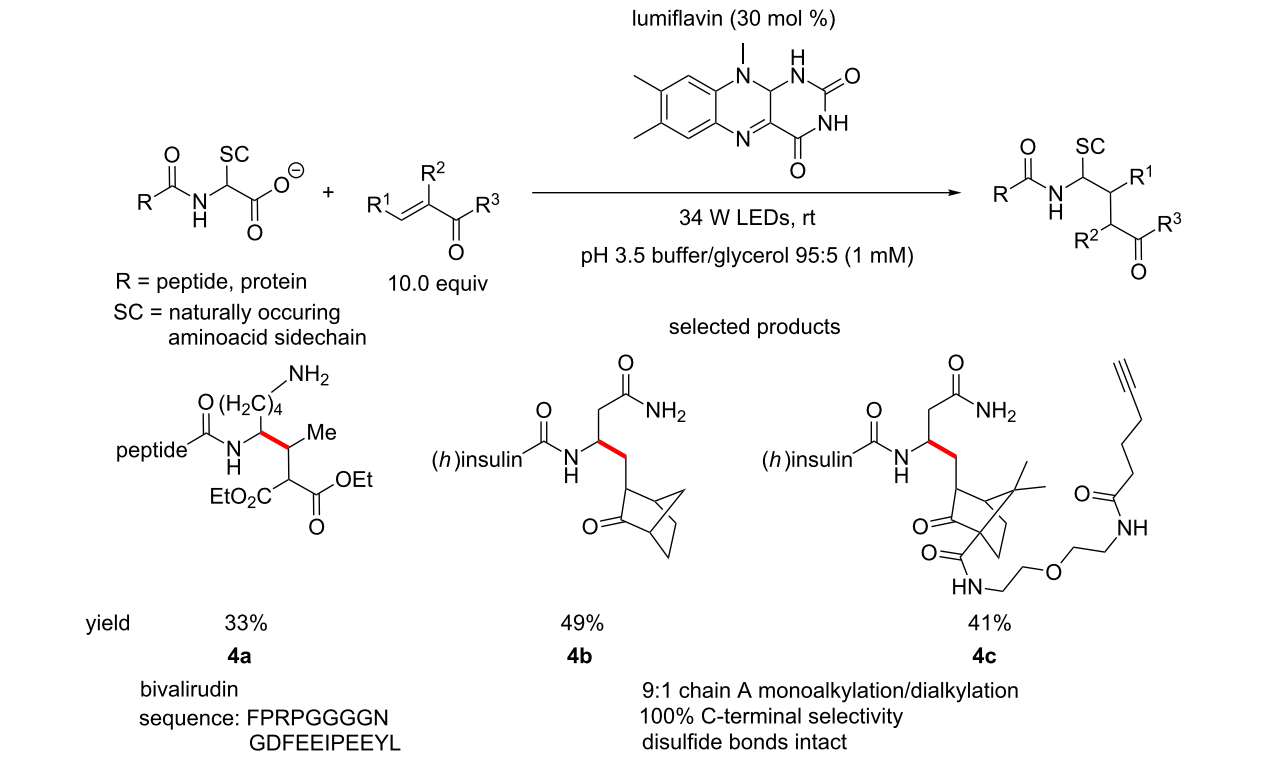

Scheme 4: C-Terminal modification of peptides and proteins using organophotoredox catalysis.

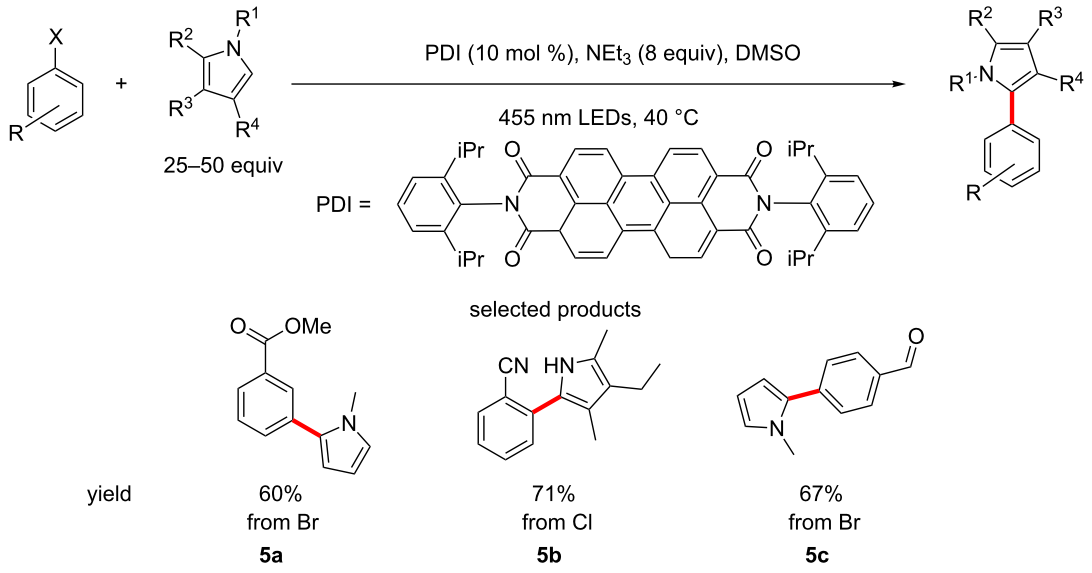

Scheme 5: The reduction and aryl coupling of aryl halides using a doubly excited photocatalyst (PDI).

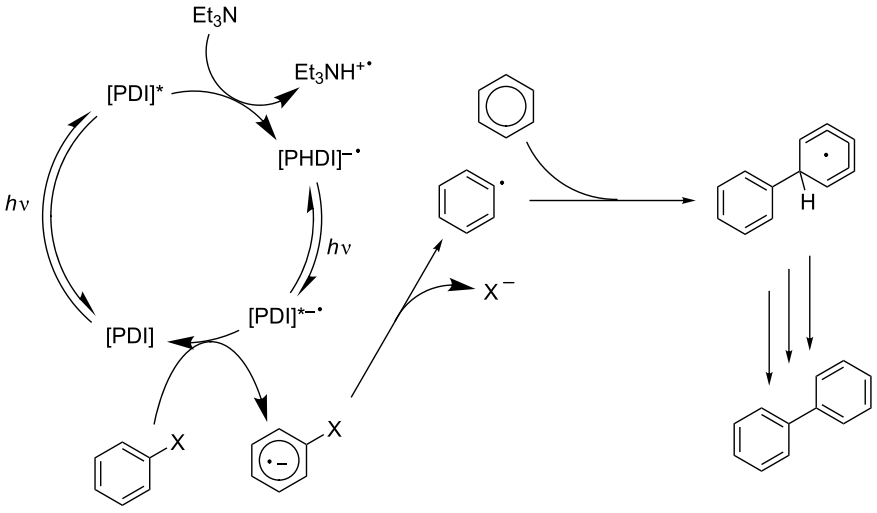

Figure 7: Mechanism for the coupling of aryl halides using PDI, which is excited sequentially by two photons.

The group also showed that it is possible to carry out these reactions using sunlight as the source of photons, leading them to term their newly discovered photocatalyst a "minimalistic chemical model of the Z-scheme in biological photosynthesis".

The König group has contributed a more traditional methodology as well, publishing a protocol for coupling simple five-membered heterocycles to substituted benzenes, using Eosin Y as the photocatalyst, starting from arenediazonium salts (Scheme 6) [47].

The scope of the reaction is limited to *N*-Boc-pyrroles, furans and a couple of simple substituted thiophenes with respect to the heterocycle, and the benzene moiety can tolerate all manner of substituents in all positions, however, only mono-substituted systems are explored. This is a powerful procedure, which allows for the circumvention of traditional Pd or Cu catalysed couplings of heteroarenes, which are notoriously difficult.

A publication by Kundu and Ranu provides a way of arylating the C2 position of electron-rich five-membered heterocycles, using anilines as the coupling partner. *tert*-Butyl nitrite (*t*-BuONO) is used as a diazotizing agent to generate diazonium salts transiently in situ. The reaction is catalysed by Eosin Y under irradiation with blue LEDs at room temperature (Scheme 7) [48].

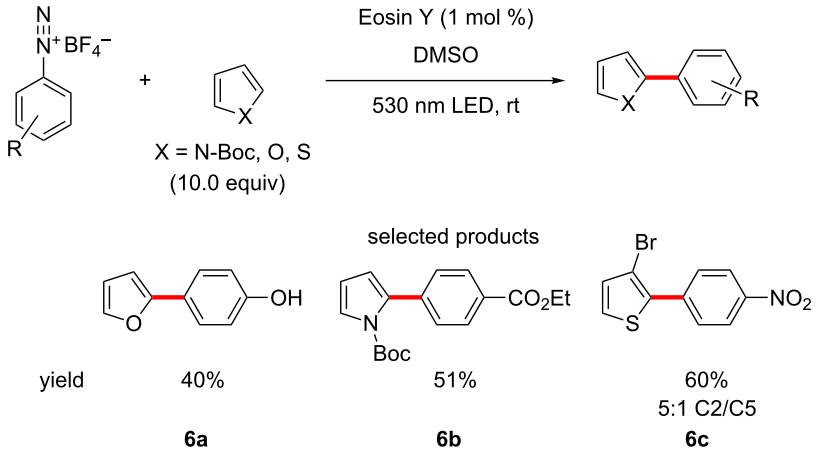

Scheme 6: The arylation of five-membered heteroarenes using arenediazonium salts under organophotoredox conditions.

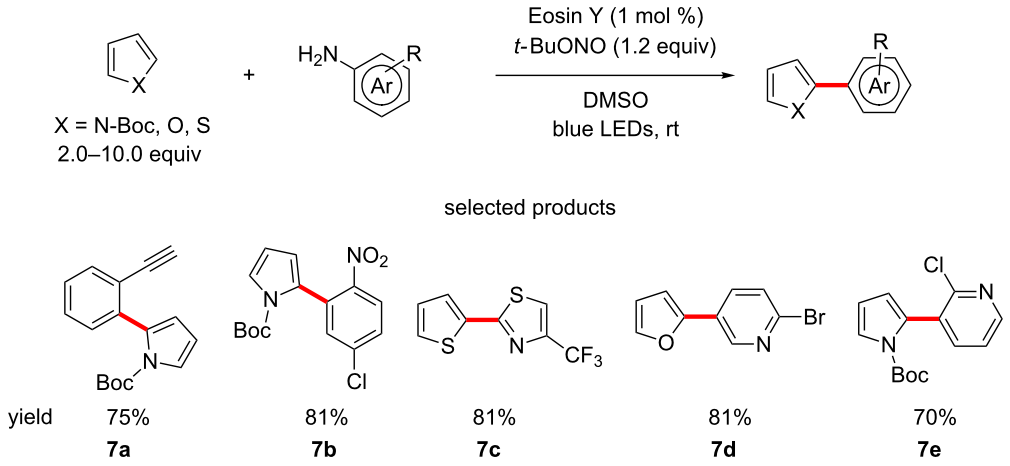

Scheme 7: The C–H (hetero)arylation of five-membered heterocycles under Eosin Y photocatalysis.

The authors report that in general their procedure allowed for better transformation of electron-poor anilines compared to their electron-rich counterparts. Unfortunately, it is also reported that the scope of the reaction cannot be extended to electron-poor heterocycles under the current conditions. However, the aniline coupling partner opens up a huge variety of opportunities, as arylamines and heteroarylamines are widely available.

Scaffolds such as **7b** have lots of potential for further elaboration. In addition, the presence of electron-poor pyridines, cf. **7e**, is also very encouraging, as these find widespread use in pharmaceuticals as benzene isosteres, which are more polar and metabolically stable, but lack the – often problematic – basicity of regular pyridines. Compounds such as **7c** are not commonly encountered, but definitely have the potential to be of interest if explored further. The good physical chemical properties of thiazoles, as well as their ability to act as isosteres to thiophenes, carbonyls and pyrazoles [49,50] make this scaffold an intriguing novel motif.

2.3 C(sp^2)–X bond formation

The obvious extension after considering C–C coupling reactions, is to consider the ability of organocatalysed photoredox reactions to perform reactions which create C–X (X = N, O, S) bonds, in reactions analogous to Buchwald or Chan–Lam couplings.

An example of the creation of C–S bonds is given by Wang and co-workers, who have reported the formation of aromatic thioethers by functionalising C–H bonds of imidazo[1,2-*a*]pyridines and benzo[*d*]imidazo[1,2-*b*]thiophenes using Eosin B and sulfinic acids (Scheme 8) [51].

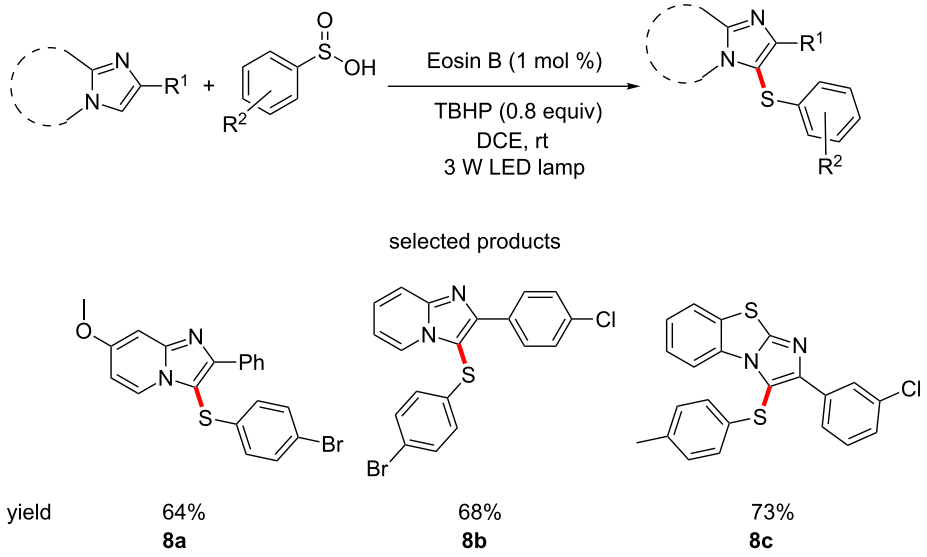

Scheme 8: The C–H sulfurisation of imidazoheterocycles using Eosin B-catalyzed photochemical methods.

The manipulated heterocycles, particularly the imidazopyridines, are motifs which are commonly encountered in medicinal chemistry. The formation of the thioether is also quite interesting, due to the possibility of accessing sulfones, which are abundant in drugs and drug-like molecules.

The scope of the reaction covers the basics in terms of substituents on both reactants and investigates various substitution patterns. Most of the reactions proceed in good yields. The use of *tert*-butyl hydroperoxide as the oxidant likely prohibits the use of oxidation-sensitive functional groups, such as alkenes or aldehydes. Use of a milder oxidant, e.g., oxygen – seen many times in this review, could help broaden the functional group compatibility.

Hajra et al. have reported the direct C–H thiocyanation of substituted imidazo[1,2-*a*]pyridines, using ammonium thiocyanate, in combination with Eosin Y under irradiation by blue LEDs (Scheme 9) [52]. This is another photoredox example of C–S bond formation, in this case to a highly versatile thiocyanate functional group, which is a precursor group to many sulfur-containing functional groups, as well as heterocycles such as thiazoles and isothiazoles.

The imidazo[1,2-*a*]pyridine core is a particularly interesting drug-like structure, e.g., electron poor, polar, of low basicity, etc. The scope of the modified substituted imidazo[1,2-*a*]pyridines contains scaffolds commonly found in pharmaceuticals, such as sulfones **9a** and trifluoromethyl groups **9b**.

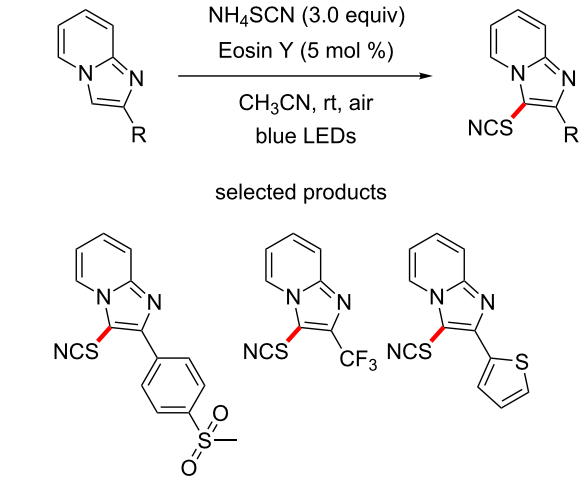

Scheme 9: The introduction of the thiocyanate group using Eosin Y photocatalysis.

Hence, this publication provides an easy route to access scaffolds with diverse aromatic systems, allowing for the construction of interesting molecules.

An interesting report of C–N bond formation is seen in König and co-workers' method for the formation of sulfonamidated pyrroles, using acridinium salts as photocatalysts, in the presence of oxygen and sodium hydroxide (Scheme 10) [53].

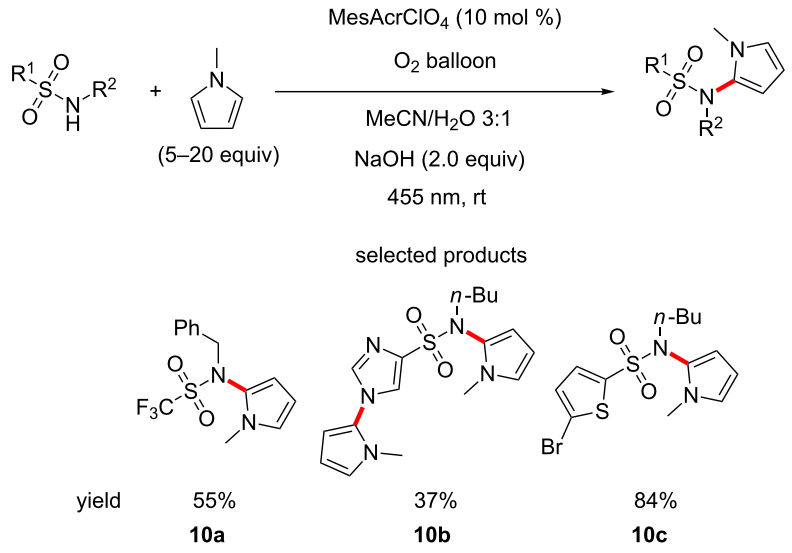

Scheme 10: Sulfonamidation of pyrroles using oxygen as the terminal oxidant.

Unfortunately, this protocol was investigated for its use in the sulfonamidation of other heterocycles and was not successful. The authors attribute this lack of reactivity to the limited oxidising power of the excited acridinium salts and to the relative instability of the heterocyclic radical cation, which is a key intermediate in the proposed mechanism. Considering that E_{red}*(cat/cat$^{\bullet-}$) is greater than +2 V (vs SCE) for acridinium salts, the limited oxidising power is not the most probable explanation. Instability of the heteroaromatic radical cation seems more plausible. The authors explore both aromatic and heteroaromatic pendant groups on the sulfonamide, as well as aliphatic chains. Unsurprisingly, esters and other base labile groups are not encountered.

A recent publication by König and his group shows the DDQ catalysed (^{3}DDQ E_{red}*(cat/cat$^{\bullet-}$) ≈ +3.18 V vs SCE) C–H amination of arenes and heteroarenes using weakly nucleophilic species such as carbamates, urea and non-basic heterocycles (Scheme 11) [54].

The scope covers a multitude of electron-poor and electron-rich arenes which can be reacted with carbamates, urea, pyrazole and triazole derivatives to furnish aminated products. The authors address the various reactivities observed with respect to both the electronics of the arene and the nucleophilicity of the amine. Particularly electron-rich arenes such as *N*-methylindole are not tolerated, as is the case for relatively nucleophilic amines such as imidazoles, anilines or alkylamines.

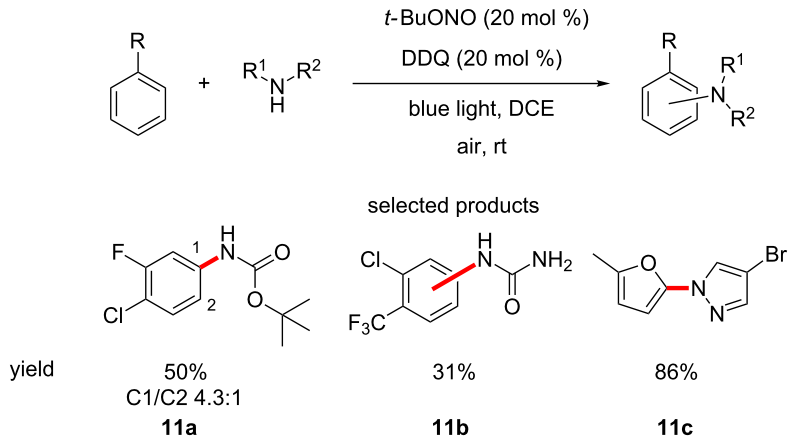

Scheme 11: DDQ-catalysed C–H amination of arenes and heteroarenes.

The reported substrates are particularly valuable to medicinal chemistry, since electron-deficient systems, as well as polar but weakly basic nitrogen atoms possess molecular properties desired in biologically active molecules.

More C(sp^2)–N bond forming reactions are reported in the literature; however, they are encountered further in this review, as they are better suited to be included in the late stage functionalisation (LSF) section.

2.4 Reactions manipulating hydrocarbon backbones

The reactions of hydrocarbons are central to building the scaffolds of molecules. This is also true in medicinal chemistry. There are countless C–C bond-forming reactions using traditional chemistry and organophotoredox synthesis can offer some interesting options as well.

Wu et al. reported the alkylation of unfunctionalised allylic and benzylic sp^3 C–H bonds by reaction with Michael acceptors, using blue LEDs and acridinium salts (Scheme 12) [55]. The main advantage is the absence of strong bases like *tert*-butyllithium (*t*-BuLi).

A very broad scope of Michael acceptors, allylic and benzylic substrates is reported, with an equally broad range of yields achieved (10–99%). Some selectivity is observed when asymmetric alkenes are used. The key to this selectivity is likely the proposed intermediate **Int 8**, which is formed selectively by SET from the alkene to the excited photocatalyst, in a reductive quenching of the catalytic cycle (Figure 8).

The more stable intermediate **Int 8** is formed selectively by the SET and the allylic radical species that is formed from the less hindered and more reactive, less substituted position of its two canonical forms.

In a similar manner, Rueping et al. demonstrated the functionalisation of C–H bonds α to tertiary amines with various nucleophiles. They also reported the formation of C–C bonds from α-amino C–H bonds using an organophotocatalytic version of the Ugi reaction. These procedures were undertaken in a flow chemistry set-up, using irradiation by green LEDs and Rose Bengal as the photocatalyst (Scheme 13) [56].

The scope of the reaction is fairly broad, especially considering the method was developed in a flow chemistry set-up, which requires a large amount of optimisation itself. A range of nucleophiles including nitroalkanes, cyanides, malonates and phosphonates are used to modify different *N*-aryltetrahydroisoquinolines. These products have the potential for quite a range of subsequent reactions for elaboration and their core structural characteristics are quite drug like.

The products of the Ugi-type reaction the group report are also interesting. The functional group (FG) compatibility of the reaction is very good, as many of the FGs tolerated can be further

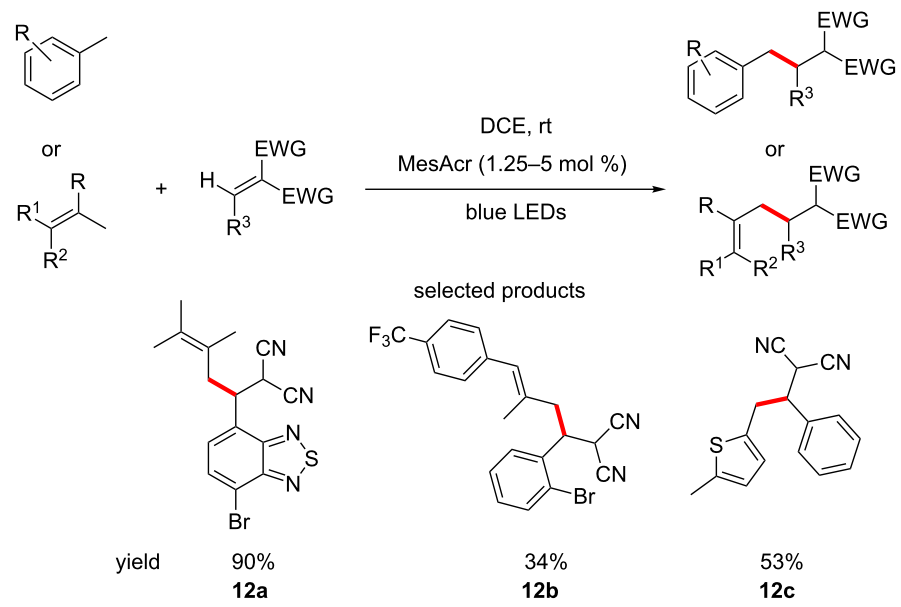

Scheme 12: Photoredox-promoted radical Michael addition reactions of allylic or benzylic carbons.

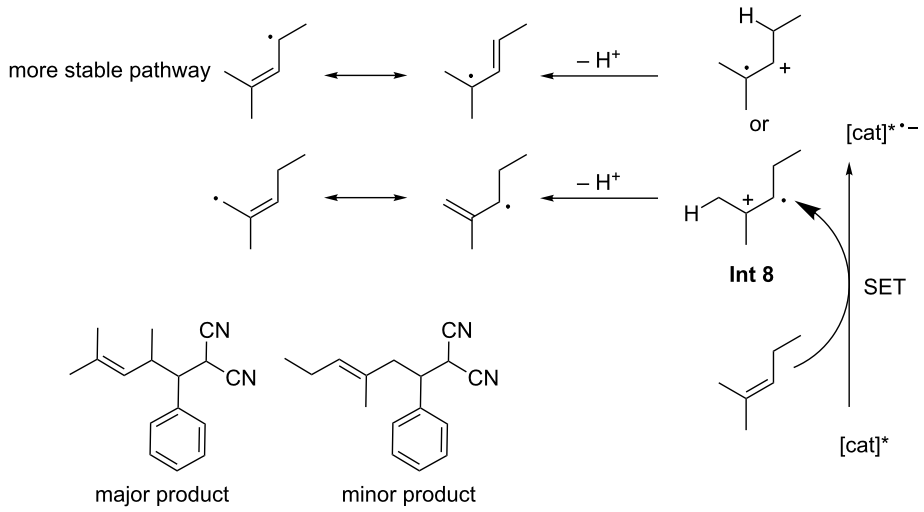

Figure 8: Proposed mechanistic rationale for the observed chemoselectivities.

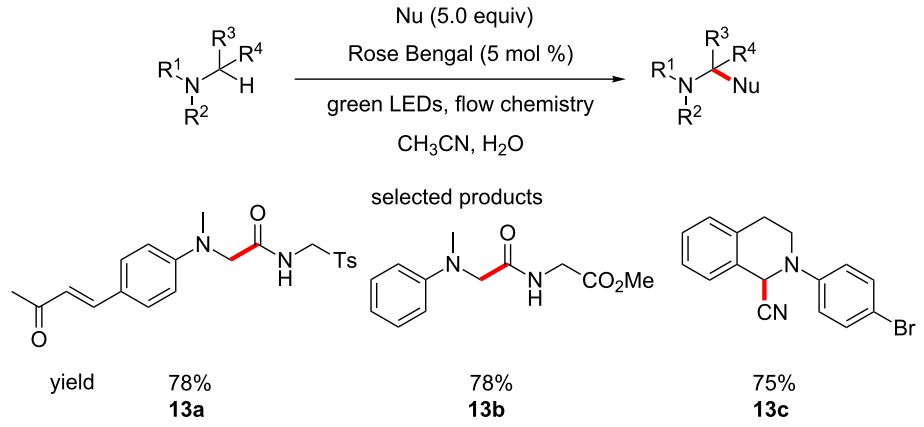

Scheme 13: The photocatalytic manipulation of C–H bonds adjacent to amine groups.

functionalised in a plethora of different ways. Examples of heterocyclic (e.g., pyridinyl) anilines would be more relevant to the pharmaceutical industry.

Medicinal chemistry often requires particularly furnished hydrocarbon backbones as bioisosteric replacements. One such interesting group is the difluoromethyl group. Akita et al. have described a novel difluoromethylating agent which was used to simultaneously install a difluoromethyl and an acetamide group on various styrene-type derivatives, under perylene-catalysed (E_{ox}* ($cat^{+\bullet}$/cat) = −2.23 V vs ferrocene in acetonitrile) photoredox conditions (Scheme 14) [57].

For the most part, the scope of the reaction is limited to relatively simple styrenes, however, some rather interesting substrates are reported, as shown in Scheme 12, in addition to some others, e.g., *meta*-aldehyde or *para*-bromo substituents. These types of motifs have the potential to be elaborated into very drug-like molecules.

Overall, this presents a decent method for the introduction of the typically difficult to introduce CF_2H group. However, this method is applied to quite simple substrates and so use of this protocol is limited to the early steps in the synthesis of compounds. The ability to extend this procedure to encompass

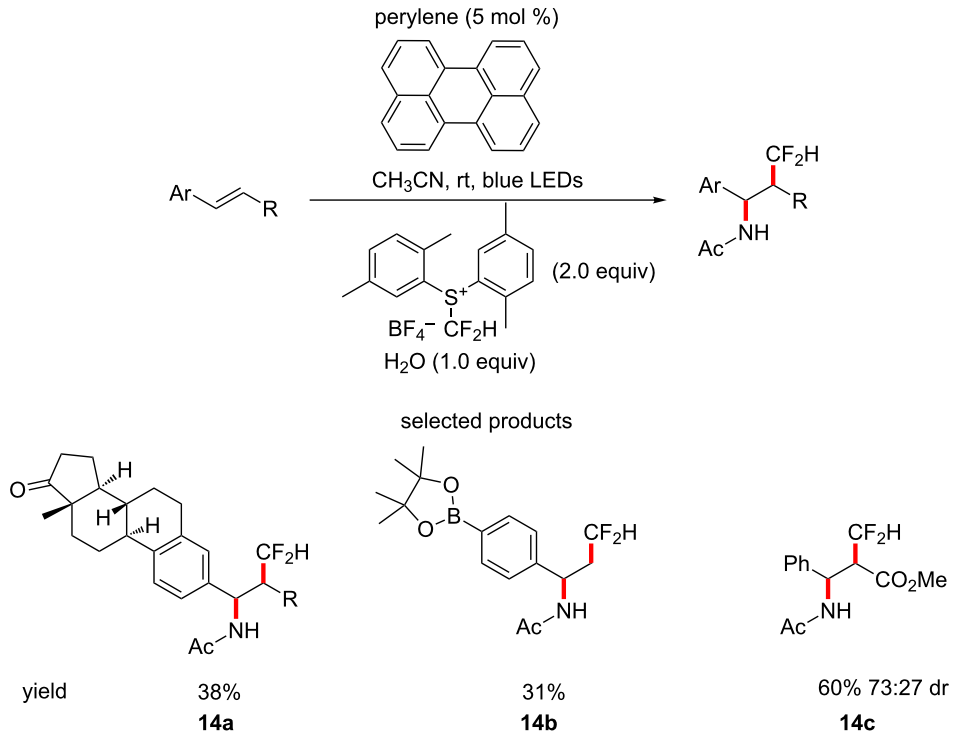

Scheme 14: The perylene-catalysed organophotoredox tandem difluoromethylation–acetamidation of styrene-type alkenes.

structurally diverse and relatively delicate scaffolds, making it suitable for LSF, would make this an incredibly valuable tool to the medicinal chemist.

3 Heterocycle formation

The importance and prevalence of heterocyclic systems in medicinal chemistry cannot be overstated. Although reactions for the formation of heterocycles are decreasing in frequency [45], the presence of heterocycles in drugs on the market is still extremely high. The former is more a reflection of the fact that heterocyclic building blocks are now more readily available as starting materials, so chemists opt to construct them less frequently.

Many biologically active synthetic compounds contain highly substituted five-membered heterocycles. In particular, pyrroles and oxazoles are quite commonly encountered (Figure 9) [58,59].

Xiao and co-workers have shown that highly substituted pyrroles can be synthesised by the [3 + 2]-cycloaddition of electron-poor alkynes and 2*H*-azirines [60]. The reaction is per-

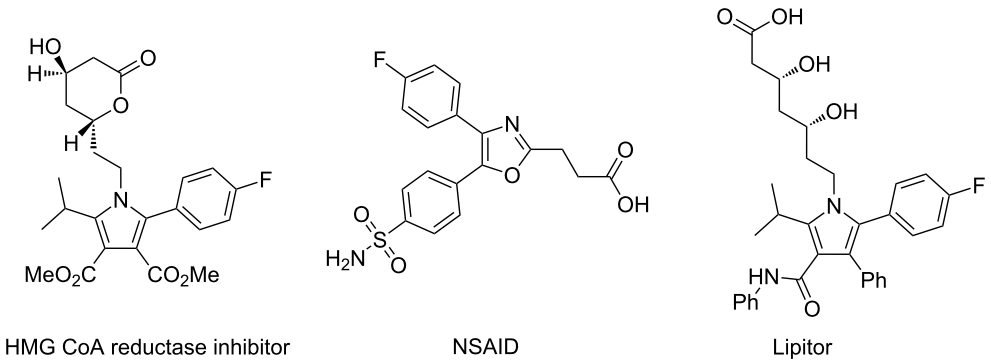

Figure 9: Examples of biologically active molecules containing highly functionalised five membered heterocycles.

formed under blue LED irradiation and using acridinium salts as a photocatalyst (Scheme 15).

With respect to 2*H*-azirine the scope of the reaction is demonstrated to be relatively broad, with aromatics, heteroaromatics and aliphatics all seen. However, the variation in the alkyne partner is limited, with only examples of esters and nitriles shown. The yields are variable (15–98%), with no general explanation being offered to rationalise this by the authors. An example of the reaction of two asymmetric substrates is provided and the reaction demonstrates reasonable regioselectivity (6.5:1). The synthesis of **15c**, a precursor to an active pharmaceutical ingredient (API), by the authors demonstrates how this method is immediately useful in the synthesis of biologically active molecules. Although the authors offer no direct explanation for the observed regioselectivity, the mechanism of the reaction could provide some insight. The key step of the reaction, which sets the regiochemistry of the product is seen in Figure 10.

The intermediate cation radical **Int 10** and the stability of the positive charge in the iminium radical cation are the keys in the mechanism and to understanding the selectivity of the reaction.

In an unsymmetrical reactant, the iminium carries most of the partial positive charge on the benzylic carbon (Figure 11). The radical is not stabilised by being borne on the benzylic carbon, as the aromatic ring must lie in conjugation with the iminium double bond, making the orbitals of the ring orthogonal to the orbital in which the unpaired electron resides.

The Xiao group have also published a method for making oxazoles using conditions that are very similar to those de-

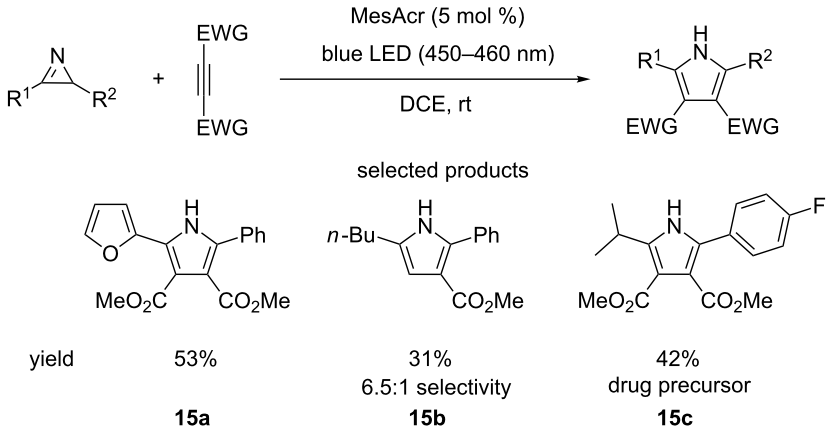

Scheme 15: The [3 + 2]-cycloaddition leading to the formation of pyrroles, through the reaction of 2*H*-azirines and alkynes via organophotoredox catalysis.

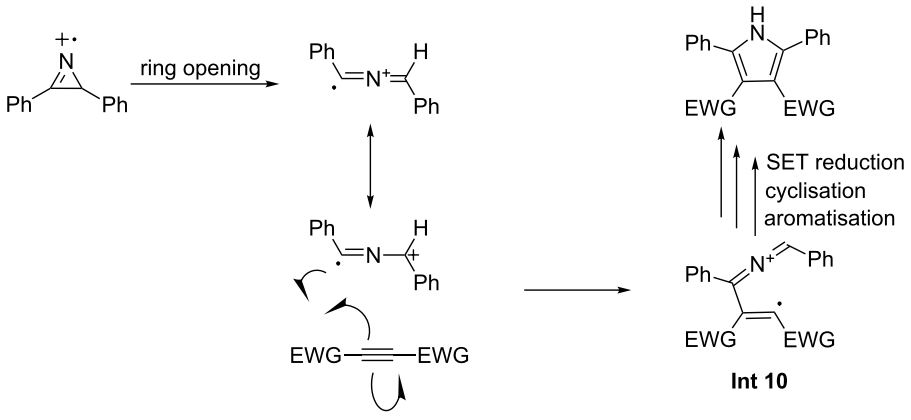

Figure 10: Proposed intermediate that determines the regioselectivity of the reaction.

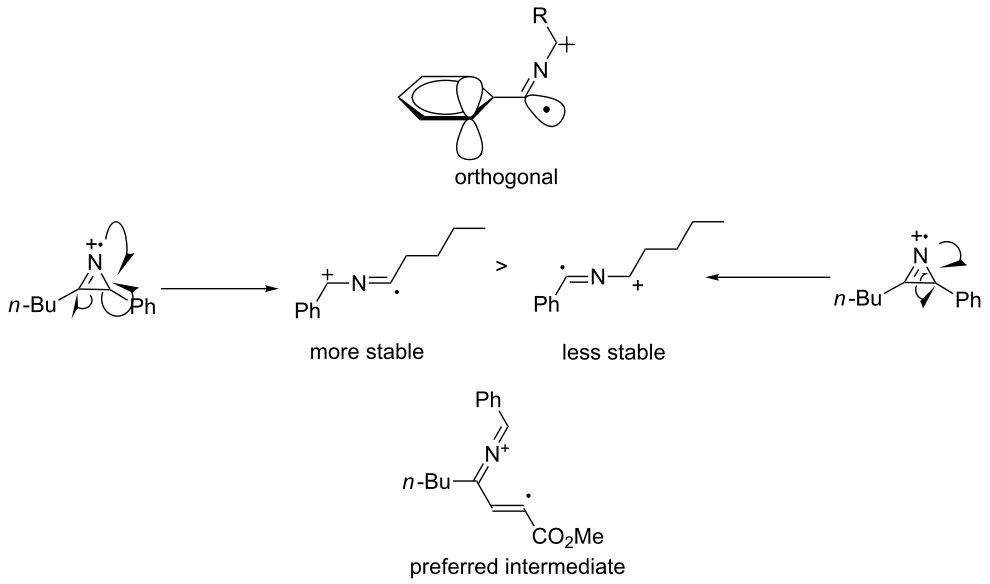

Figure 11: Comparison of possible pathways of reaction and various intermediates involved.

scribed above (Scheme 16). The reaction uses 2*H*-azirines and aldehydes to access the functionalised heterocycles [61].

Unlike the pyrrole-forming reaction, this protocol requires an oxidising agent, DDQ, for the desired oxazole to be obtained. This means that access to the corresponding 2,5-oxazolines is also possible. Aliphatic and heteroaromatic substituents on the 2*H*-azirine were not tolerated. The aldehyde substituents are much more diverse, with a variety of substituted benzenes, heteroaromatics, carbonyls and aliphatic side chains undergoing the cycloaddition.

Overall, these two methods provide much more mild, scalable and environmentally friendly reaction conditions than the traditional methods employed for making these highly substituted heteroaromatics.

Access to the saturated oxazolines and thaziolines from amides and thioamides, respectively, has been described by Nicewicz who used acridinium salt photocatalysts in cooperation with a disulfide cocatalyst, which is converted to the corresponding thiol and serves as a source of hydrogen atoms for the reduction of the double bond (Scheme 17) [62].

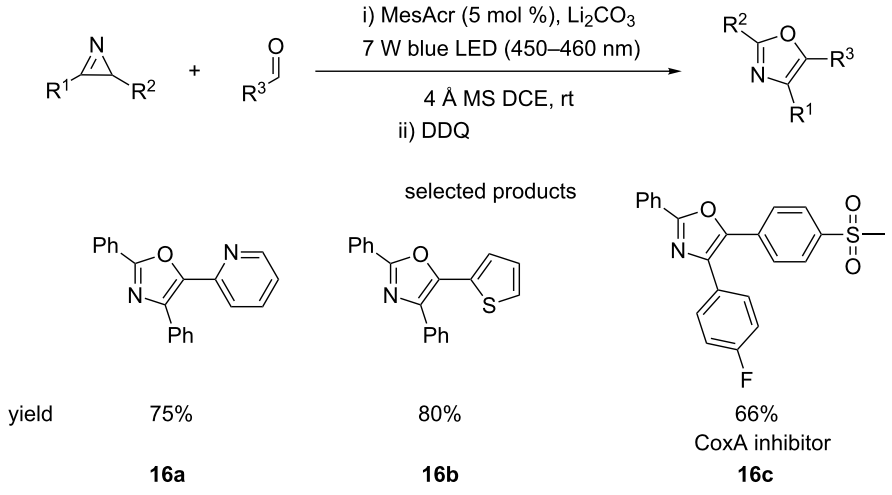

Scheme 16: The acridinium salt-catalysed formation of oxazoles from aldehydes and 2*H*-azirines.

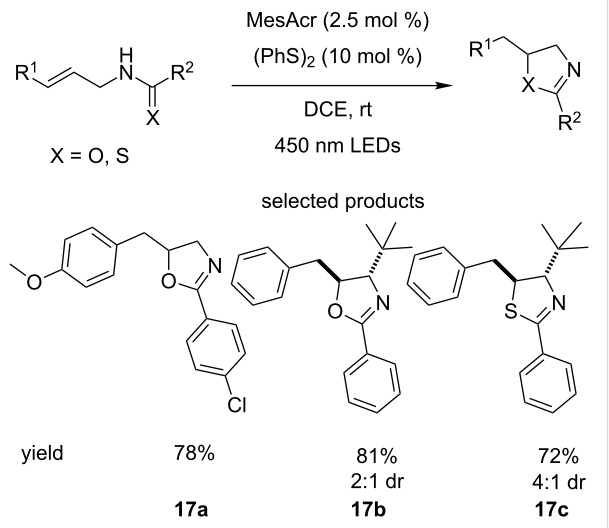

Scheme 17: The synthesis of oxazolines and thiazolines from amides and thioamides using organocatalysed photoredox chemistry.

The scope of the reaction is not particularly broad; electron-withdrawing groups such as pyridyl or trifluoromethyl are not tolerated. No functional group tolerance towards other carbonyls such as esters or aldehydes is demonstrated. The use of terminal or trisubstituted alkenes is limited and the reaction times are long.

However, the authors do report that the reaction is somewhat diastereoselective, favouring the *anti*-configuration in all cases. In addition, the option for oxidation to the oxazole or thiazole is always enticing as a way of easily accessing a diverse set of molecules.

Immediately akin to the oxazole moiety is the oxadiazole heterocycle, which exhibits similar properties. There are several examples of drugs on the market containing such heteroaromatics (Figure 12).

Yadav et al. reported the synthesis of 1,3,4-oxadiazoles from aldehyde semicarbazones, using CBr_4, green LEDs and Eosin Y as the photocatalyst, at room temperature, in the presence of air (Scheme 18) [63].

This procedure offers a much milder route to these heterocycles than traditional synthetic methodologies, which typically use harsh conditions. Semicarbazones are readily synthesised from the corresponding aldehydes, so these starting materials are easily accessible. The yields are very good to excellent (86–96%), while the variation on the ligands of the aromatic ring covers a sensible range. The 4-pyridyl **18a** example is particularly interesting, as is the hindered 2,6-disubstituted ring system **18b**. Only the synthesis of 2-amino-1,3,4-oxadiazoles is

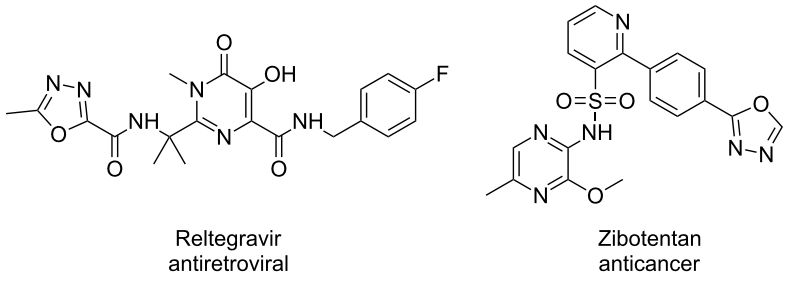

Figure 12: Biologically active molecules on the market containing 1,3,4-oxadiazole moieties.

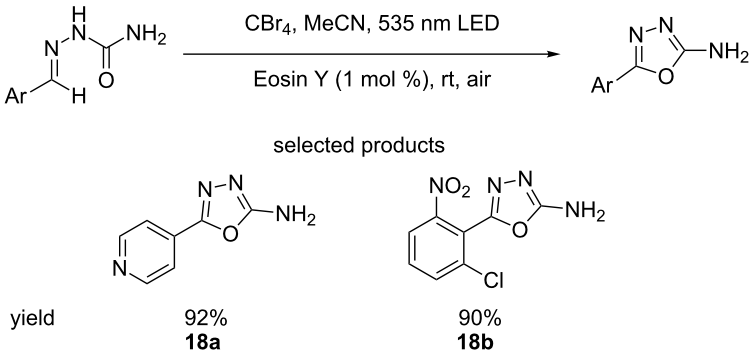

Scheme 18: The synthesis of 1,3,4-oxadiazoles from aldehyde semicarbazones using Eosin Y organophotocatalysis.

reported, which although useful building blocks, are not extremely common in drugs.

The Yadav research group have also published the homocoupling of primary thioamides for the formation of symmetrical 1,2,4-thiadiazoles, using visible light and Eosin Y as the photocatalyst, in air at room temperature (Scheme 19) [64].

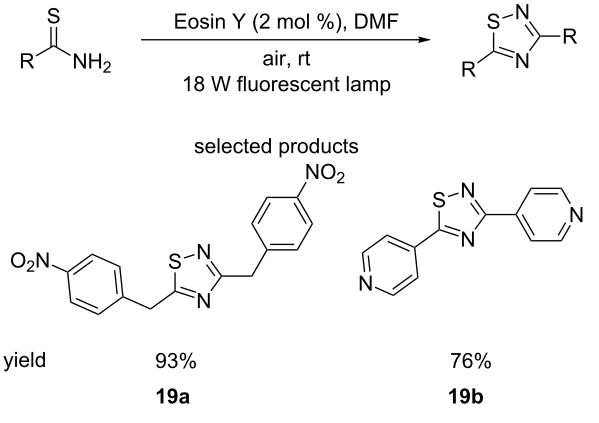

Scheme 19: The dimerization of primary thioamides to 1,2,4-thiadiazoles catalysed by the presence of Eosin Y and visible light irradiation.

The immediately obvious limitation of this reaction is the identical nature of the substituents on the product. This severely limits its potential applications, and the usefulness of this protocol is likely limited to the creation of linkers or pendant groups.

Benzo-fused five-membered heterocycles also find widespread use in medicinal chemistry, with indoles, benzothiophenes and benzimidazoles seen in many drugs. In another demonstration of the value of diazonium salts, the König group have published a protocol for the synthesis of substituted benzothiophenes using Eosin Y photocatalysis, starting from *o*-methylthioarenediazonium salts and substituted alkynes (Scheme 20) [65].

The scope of the substrates demonstrated is quite broad, with substituted aromatic and aliphatic alkynes being used and a variety of substituents tolerated on the diazonium salt starting material. Terminal alkynes selectively formed 2-substituted benzothiophenes, whereas the regioselectivity of unsymmetrical disubstituted alkynes was not explored. It is important to note the role of DMSO, which acts as a demethylating agent as well as solvent. Even so, the benzothiophene cores constructed by the authors are still valuable, as molecules such as **20b** can be further elaborated in many ways and **20c** is a precursor to an API.

Another method for benzothiopene construction is seen in Kumar and co-workers' report describing a dehydrogenative oxytrifluoromethylation cascade reaction of 1,6-enynes, catalysed by phenanthrene-9,10-dione (PQ) (E_{red}*(cat/cat$^{\bullet-}$) +1.6 V vs SCE) using visible light (Scheme 21) [66]. However, benzofurans and, most importantly, indoles are also accessible through this cascade.

The authors demonstrated the synthesis of an array of different, potentially drug-like compounds. The authors also showed the accessibility of their starting materials by synthesising the 1,6-enynes from the corresponding 2-halogenated phenols, benzenethiols or anilines, via a simple substitution–elimination–Sonogashira synthetic sequence. In addition, the group has synthesised trifluoromethylated modified versions of certain drugs (Figure 13).

Variations on the classical benzofused heterocycles (indole etc.) – such as benzimidazoles or tetrazolopyridines are often seen in

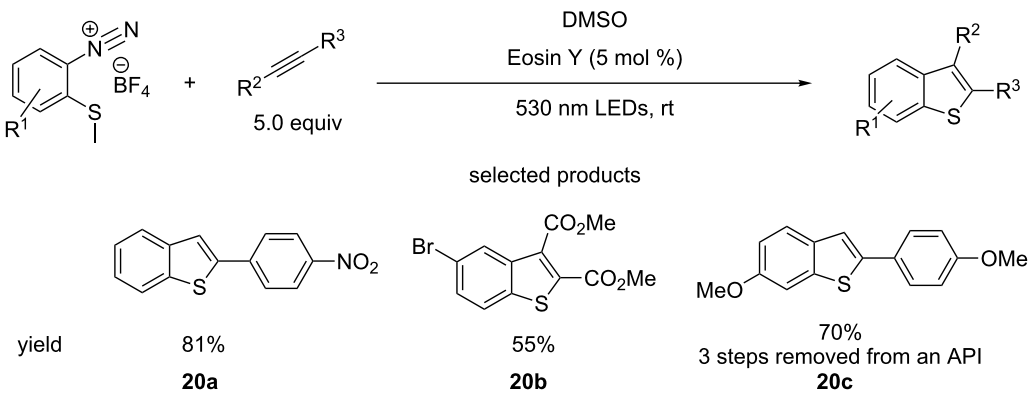

Scheme 20: The radical cycloaddition of *o*-methylthioarenediazonium salts and substituted alkynes towards the formation of benzothiophenes.

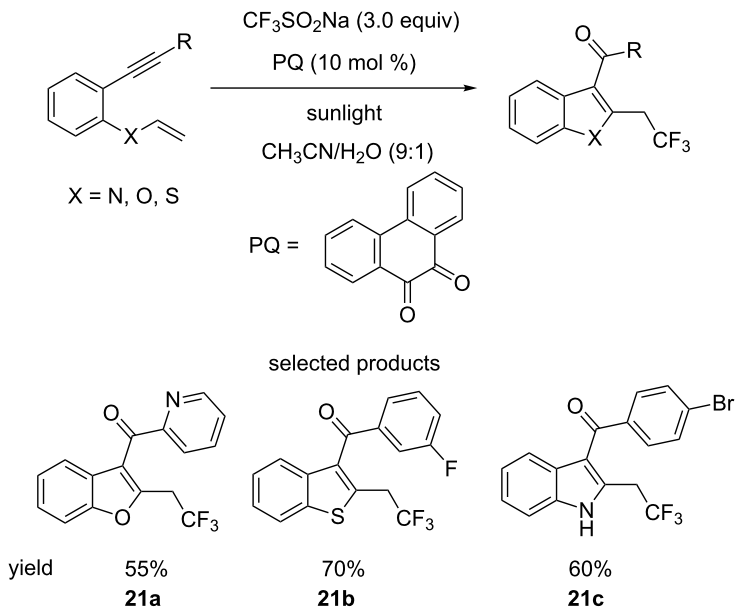

Scheme 21: The dehydrogenative cascade reaction for the synthesis of 5,6-benzofused heterocyclic systems.

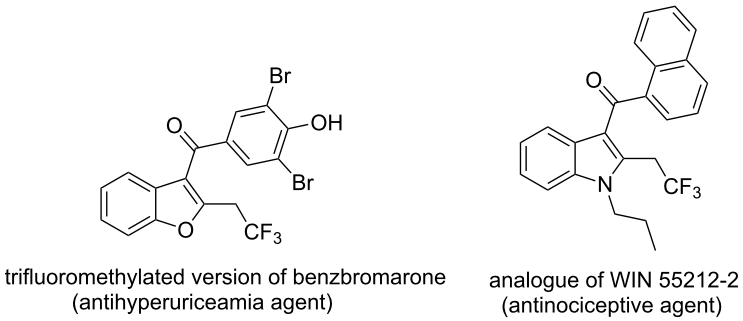

Figure 13: Trifluoromethylated version of compounds which have known biological activities.

medicinal chemistry. Singh et al. reported a method for preparing 3-arylnitrobenzimidazoles from 2-aminopyridines and nitroalkanes, using green LED Eosin Y photocatalysis, with molecular oxygen as the oxidant (Scheme 22) [67].

Heterocycles in drugs are not only restricted to five-membered rings. Pyridines, pyrazines, pyrimidines, pyridazines are all common functional groups in biologically active compounds.

Liu et al. have published the visible light-catalysed oxidation of dihydropyrimidines (DHPMs) using atmospheric oxygen as the stoichiometric oxidant, TBA-Eosin Y photocatalysis and carbonate as the base at room temperature (Scheme 23) [68].

The group also reported that this transformation is possible using sunlight as the source of photons, with a yield comparable to that obtained when blue LEDs were employed. Though the scope of the reaction is quite broad, variation is only investigated in the C4 and C5 positions of the DHPMs. Variability at C1 and C6 are not investigated. The variation of the ester and the C4 ligands, however, is good, with some interesting products being presented.

The authors do not justify the selection of the particular substitution pattern with the C6 methyl and the C2 heteroatom methyl, e.g., ease of access to this type of DHPM core. Therefore, it would be interesting to see whether this method is compatible with other DHPM systems.

In the same publication, the group described the use of similar – also mild – reaction conditions to synthesise benzoxazoles from 2-substituted phenolic imines (Scheme 24). This implies that the DHPM manipulation was perhaps a preliminary study that served to optimise mild oxidation conditions.

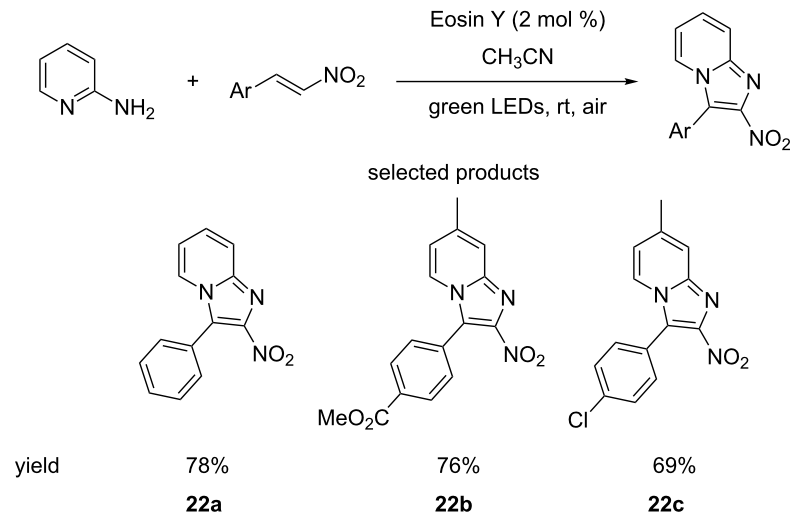

Scheme 22: Eosin Y-catalysed photoredox formation of 3-substituted benzimidazoles.

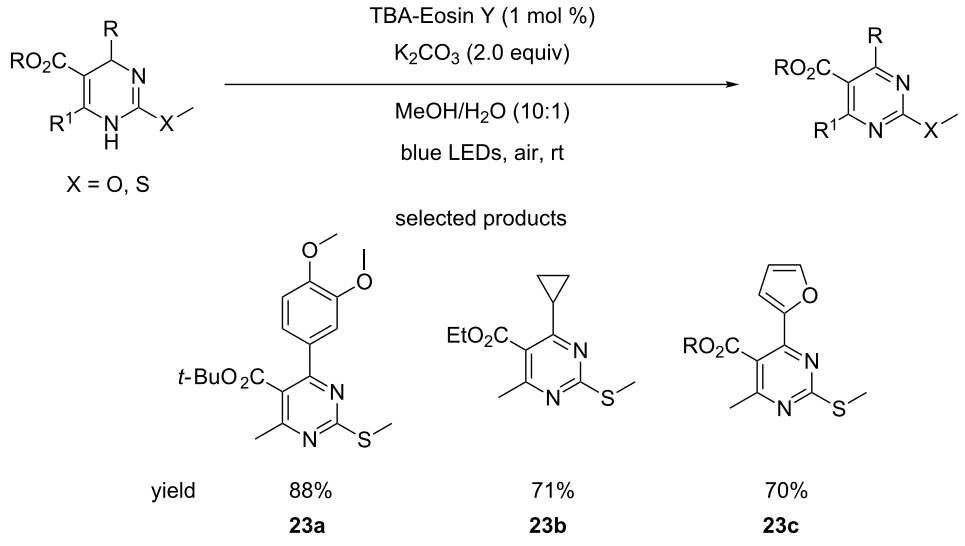

Scheme 23: Oxidation of dihydropyrimidines by atmospheric oxygen using photoredox catalysis.

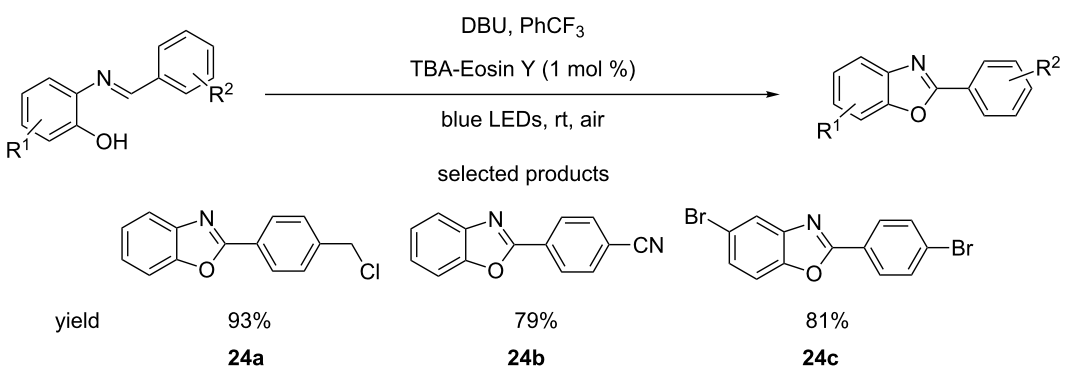

Scheme 24: Photoredox-organocatalysed transformation of 2-substituted phenolic imines to benzoxazoles.

Tang et al. reported a procedure for performing a visible light-driven oxidative cyclisation of arylamidines using Rose Bengal as the photocatalyst, in the presence of base and CBr_4 as the oxidant (Scheme 25) [69].

The scope of the reaction is restricted to mono-substituted benzenes and lacks any carbonyl derivatives as ligands. The reaction conditions are relatively harsh (high temperature) compared to the typical conditions encountered so far.

Overall, the synthesis of many of the most common heterocyclic systems has been reported using organophotocatalytic conditions, which offer several advantages over their traditional counterparts. Mainly, milder conditions are employed and easily elaborated structures are accessed in one step.

4 Late stage functionalisation

In this section, the bonds formed during the reactions are highlighted in red, as they are not always immediately and easily identifiable.

Late stage functionalisation (LSF) is a relatively new concept. It is the name given to the synthetic strategy in medicinal chemistry where lead structures are diversified by transformation of unactivated C–H bonds. In LSF C–H bonds are treated as distinct functional groups. This approach allows for diversification of lead structures without having to devise alternative syntheses [70].

There are numerous examples of novel methodologies for LSF published in recent years. The general theme is that these protocols employ mild conditions that are widely functional group-tolerant, as they usually operate on highly elaborate structures.

LSF can either be guided, e.g., selective fluorination of a molecule or can also follow an unselective approach, e.g., fluorination in various positions, but in either case the goal is exploration of SAR directly on a lead structure and easy diversification. In addition, LSF can explore the addition of small groups, e.g., methyl, fluoro, chloro, trifluoromethyl etc., or can be aimed at installing larger functional groups, e.g., heterocycles, amides or long alkyl chains.

The previous two sections outlined how mild the reaction conditions employed in visible light organophotoredox catalysis usually are, making it a uniquely suited method for LSF. For example, Scaiano et al. have demonstrated the direct C–H trifluoromethylation of heterocycles using TMEDA, visible light from white LEDs, Methylene Blue as the photocatalyst and Togni's reagent as the trifluoromethyl source (Scheme 26) [71].

The reaction is regioselective and follows the same substitution pattern as the electrophilic substitution of electron-rich heterocycles. Although highly elaborated structures are not presented, the mild reaction conditions and general functional group compatibility that the reaction exhibits make it well suited for LSF purposes. In the same study, the hydrotrifluoromethylation of terminal alkenes and alkynes is also reported and in this case the amine base acts as the hydrogen atom source to complete the reduction of the π-bond (Scheme 27).

The more electron-rich double bond is more reactive towards the electrophilic trifluoromethyl radical, providing some selectivity to the process, which indicates that it could be applied to a guided LSF strategy.

Itoh and co-workers have described a procedure for the direct C–H perfluoroalkylation of substrates, which can act as fluo-

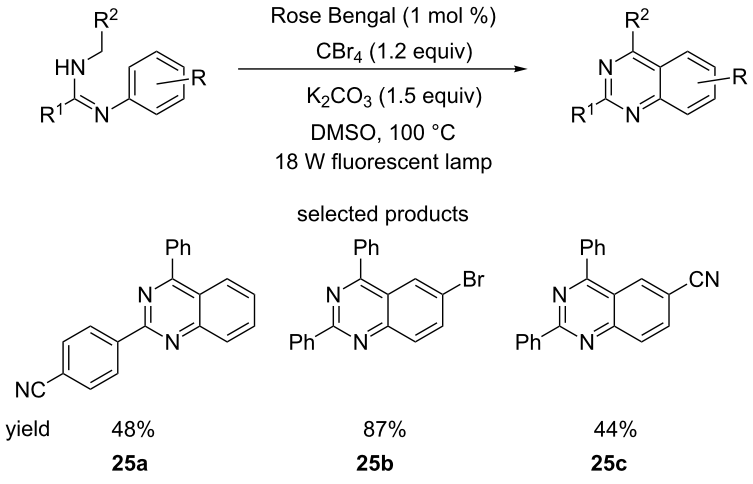

Scheme 25: Visible light-driven oxidative annulation of arylamidines.

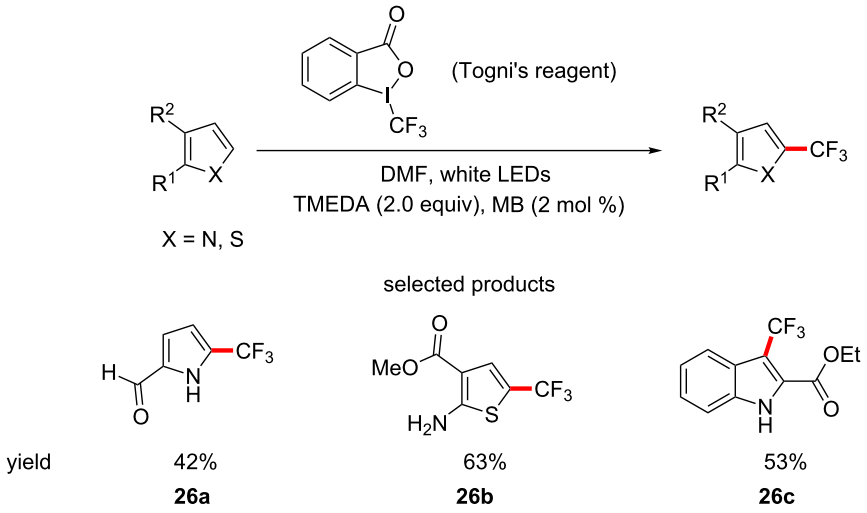

Scheme 26: Methylene blue-photocatalysed direct C–H trifluoromethylation of heterocycles.

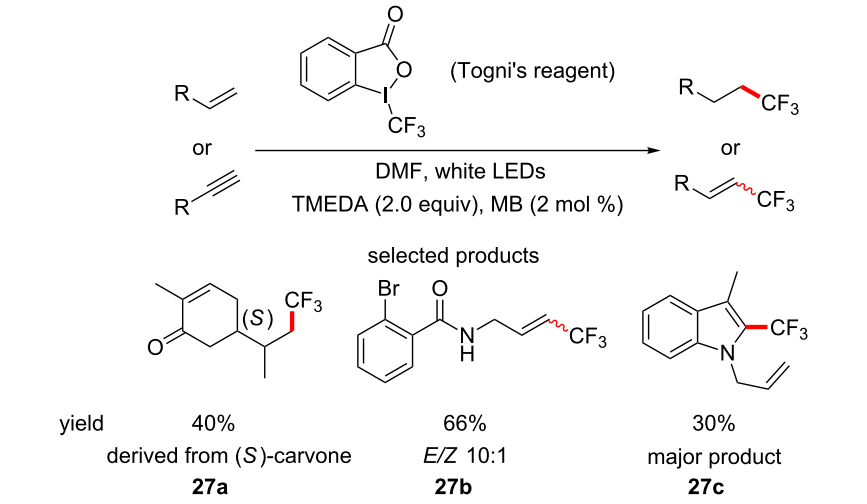

Scheme 27: Photoredox hydrotrifluoromethylation of terminal alkenes and alkynes.

rous tags. The group utilised the corresponding fluoroalkyl sulfinate salt as the fluoroalkyl source, in combination with TFA and Acid Red 94 as the photocatalyst, under 22 W fluorescent lamp irradiation to perform the transformation (Scheme 28) [72].

The substrate scope is limited to rather simple compounds, the most structurally complex of which is caffeine. The yields are good (44–92%), with regioselectivity being observed in a few cases. As with the trifluoromethylation by Pitre et al., this procedure does fit all the criteria for LSF, as it is very mild and simple, even though no complex structures are exemplified.

Although it does not fit the exact definition of a reaction employed in LSF, Jiang and co-workers have described a procedure that allows the enantioselective aerobic olefination of α-amino sp^3 C–H bonds, using cooperative asymmetric and organocatalysed photoredox catalysis (Scheme 29) [73].

This may not allow for direct diversification of leads, however, the products shown can, in one or two steps, be converted into functionalised versions of a lead compound (vide infra). The study revolves around two types of substrates, tetrahydroisoquinolines (THIQs) and tetrahydro-β-carbolines (THCs), both of which are scaffolds encountered in biologically active molecules.

This reaction was included due to the ability to introduce chirality into lead structures, something that is valuable in medicinal chemistry. The straightforward synthesis of isoxazoline

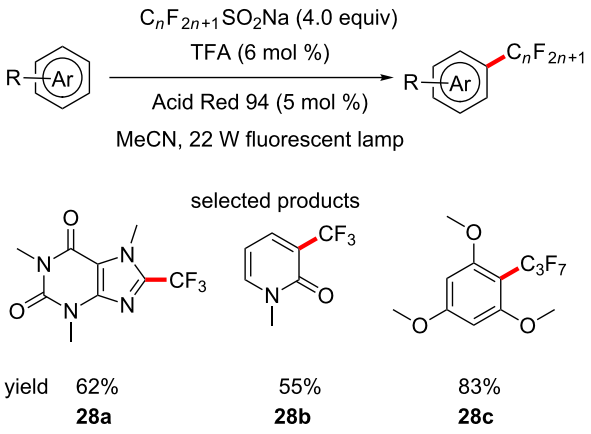

Scheme 28: Trifluoromethylation and perfluoroalkylation of aromatics and heteroaromatics.

29a from the corresponding vinyl aldehyde is a perfect example of the potential for application to LSF.

Leonori et al. have demonstrated the coupling of amide derivatives to aromatics using aryloxy amides, under Eosin Y photocatalysis with green LEDs and potassium carbonate (Scheme 30) [74].

The reaction is well suited for LSF, as is demonstrated by the authors in the diversification of derivatives of lysergic acid such as **30c**. The overall scope of the reaction is quite diverse with respect to both the amide and aromatic coupling partner. The authors also address the issue of availability of the starting aryloxy amides by accessing their starting materials in two simple steps.

Molander and his group report the selective, direct C–H alkylation of various heterocycles, using their staple BF_3K salts, visible light, persulfate and acridinium salts as the photocatalyst (Scheme 31) [75].

The scope of the reaction is truly exceptional, with a wide variety of heterocycles, ranging from nicotinamides to highly functionalised quinolines, such as the antimalarial drug quinine. The ability of this protocol to tolerate such highly functionalised molecules, with such a variety of functional groups present, really justifies the claims of the authors that this protocol is ideal for LSF in drug discovery programs.

The scope of the alkyl chains is also tremendous, with primary, secondary and tertiary alkyl trifluoroborates being used. The team also addresses the availability of these substrates, showing

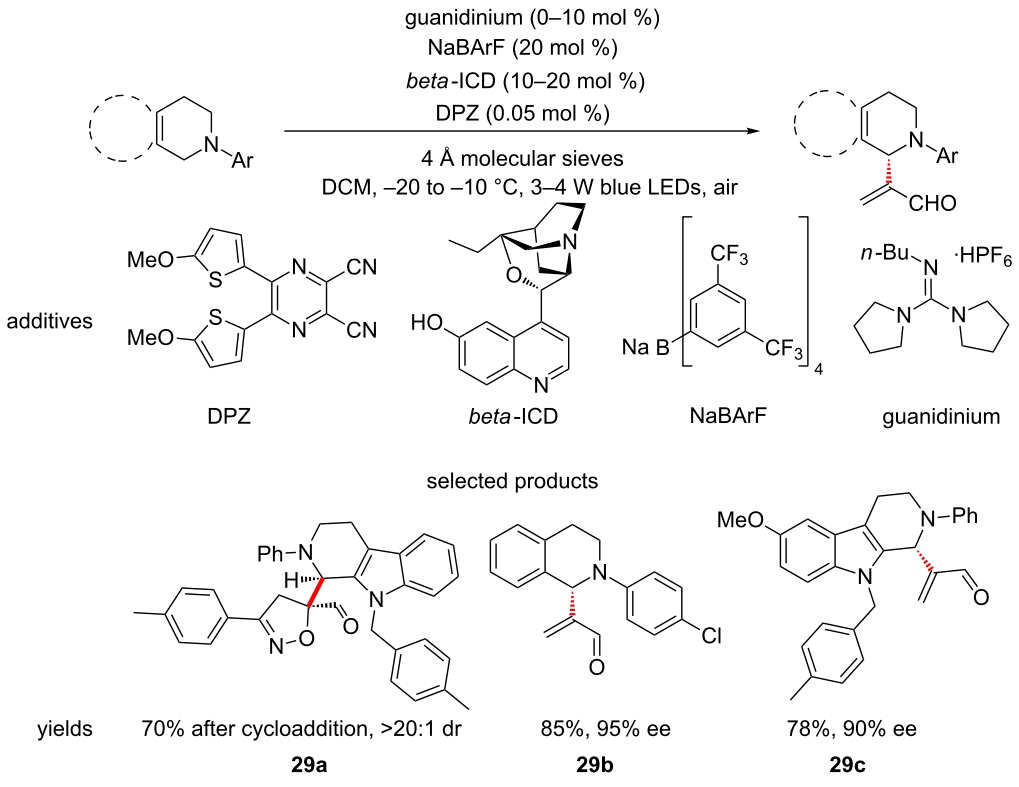

Scheme 29: The cooperative asymmetric and photoredox catalysis towards the functionalisation of α-amino sp^3 C–H bonds with electron-deficient olefins.

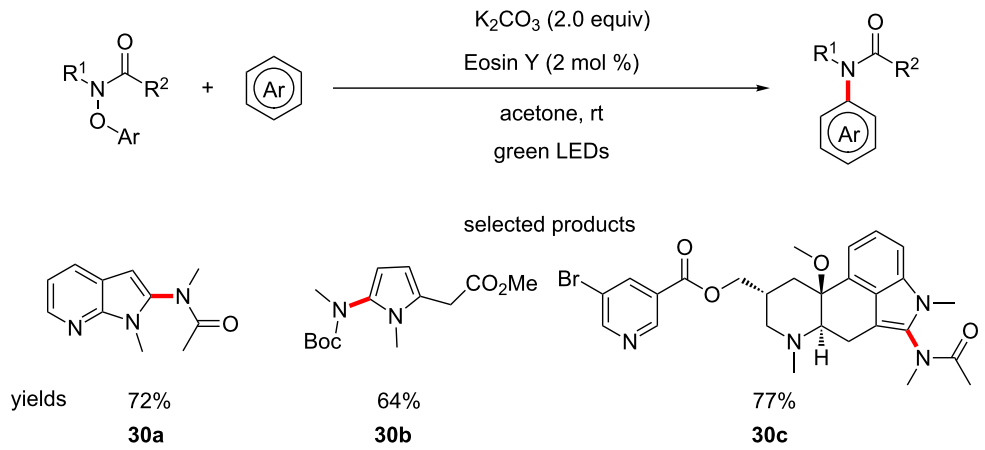

Scheme 30: Organophotoredox-catalysed direct C–H amidation of aromatics.

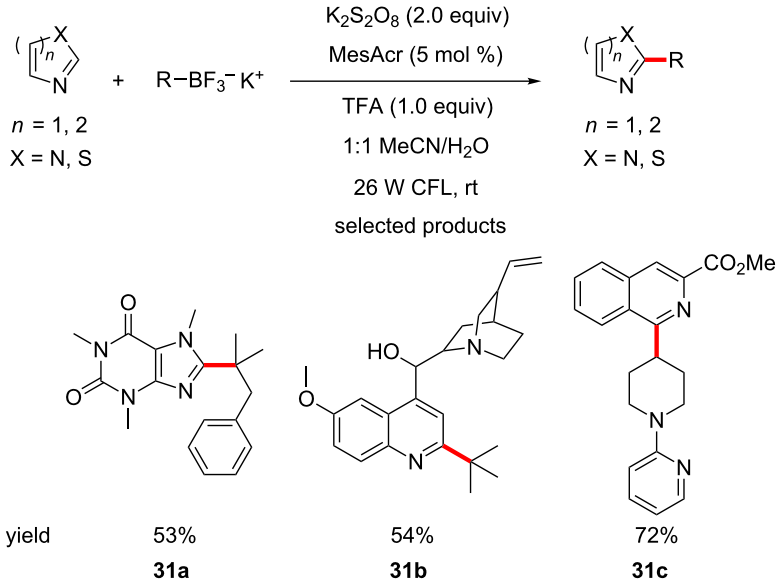

Scheme 31: Direct C–H alkylation of heterocycles using BF_3K salts. CFL – compact fluorescent lamp.

how these can be easily made in one step from the corresponding alkyl bromides, using a method published by Cook [76].

The authors also further establish the immediate value of the procedure to LSF by exploring SAR of camptothecin, a molecule identified as an anticancer drug candidate. The authors selectively manipulated the C-7 position, which has been shown to improve efficacy when alkylated (Figure 14) [77].

Nicewicz and co-workers have published a procedure for the aerobic C–H amination of aromatics, using acridinium salts as the photocatalyst under blue LED irradiation (Scheme 32) [78].

The authors have demonstrated a truly extensive scope for their protocol, subjecting a range of aromatics, heteroaromatics and fused aromatic and heteroaromatic systems with a variety of substituents to C–H amination using a wide range of heterocyclic amines. The functionalisation of molecules that are natural product-like such as **32c** is demonstrated by the authors, which is an excellent example of how this protocol translates seamlessly to drug discovery in the LSF strategy.

In a method that is complementary to their C–H amination strategy, Nicewicz et al. have reported the S_NAr-type addition of nucleophiles to methoxybenzene derivatives at the *ipso* position, as opposed to the C–H amination that operates on the

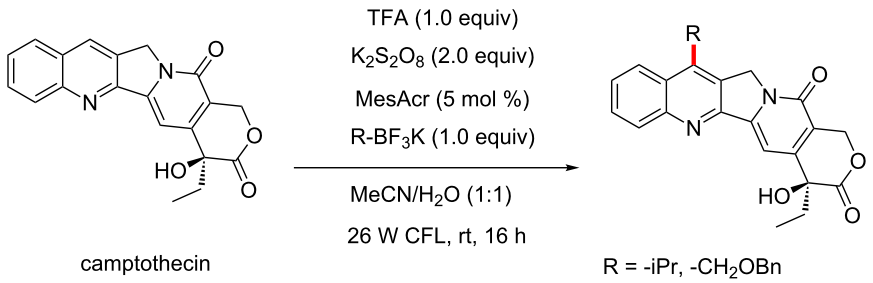

Figure 14: The modification of camptothecin, demonstrating the use of the Molander protocol in LSF.

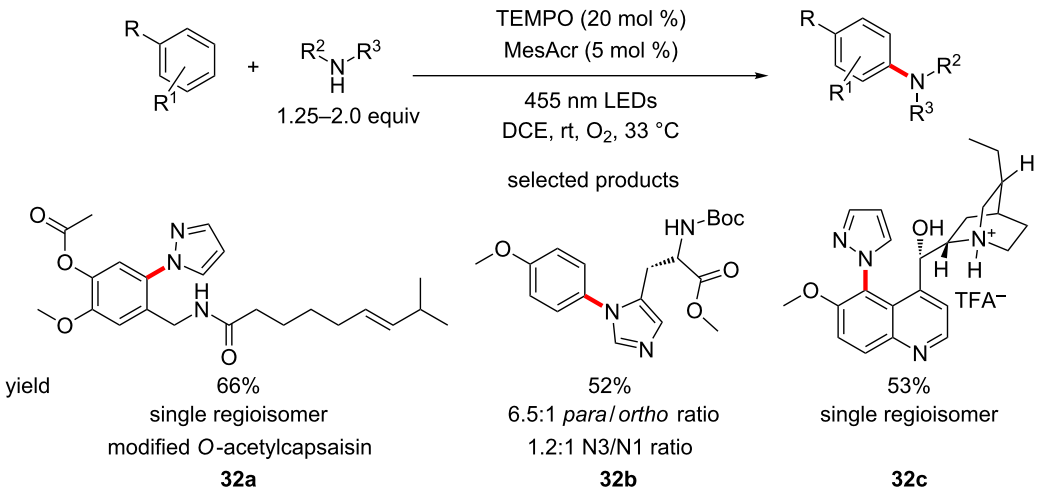

Scheme 32: Direct C–H amination of aromatics using acridinium salts.

ortho- and *para*-position of such EDGs. The reaction is catalysed by acridinium salts under anaerobic conditions and irradiation by blue LEDs (Scheme 33) [79].

The scope of substrates able to undergo the transformation is quite broad and many, if not all the substrates that the group report are scaffolds and moieties seen in typical medicinal chemistry syntheses. There are numerous examples of amino acid-derived substrates, either as the methoxybenzene electrophile (tyrosine type derivatives) or as the nucleophile (histidine and related structures such as the depicted triazole **33c**).

Examples such as the synthesis of a modified structure of naproxen, starting from the methyl ester of the well-known NSAID, demonstrate the full power of the protocol for its use as a LSF tool. The mild conditions, selectivity on certain substrates and the great opportunity for diversification of substrates make this an ideal method for introducing nucleophilic ligands onto aromatic rings.

Another publication from the Nicewicz group demonstrates the C–H direct cyanation of a variety of aromatic and heteroaromatic substrates. TMSCN is employed as the cyanide source, acridinium salts as the photocatalyst, under irradiation from blue LEDs and aerobic conditions (Scheme 34) [80]. The authors show a set of diverse molecules that underwent the transformation cleanly. The group again demonstrated the LSF applications by cyanating the methyl ester naproxen derivative **34a**.

In summary, organophotoredox chemistry has been developed to be applied to medicinal chemistry in the context of LSF and appears to be very broadly applicable and robust. As LSF becomes more popular in the ensuing decades, procedures such as the ones outlined above will become both more numerous and powerful.

Conclusion

Overall, the presented literature demonstrates that the recent developments in organophotoredox catalysis are increasingly in

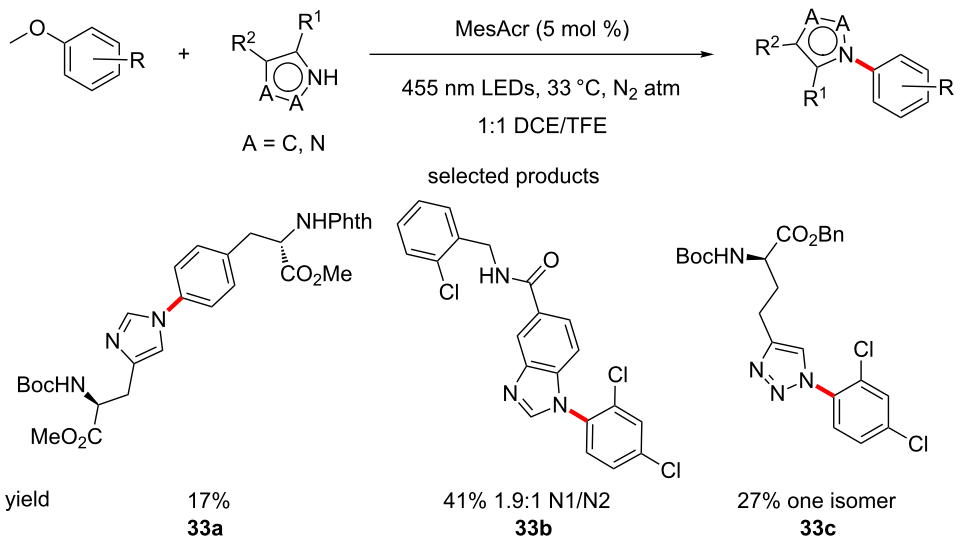

Scheme 33: Photoredox-catalysed nucleophilic aromatic substitution of nucleophiles onto methoxybenzene derivatives.

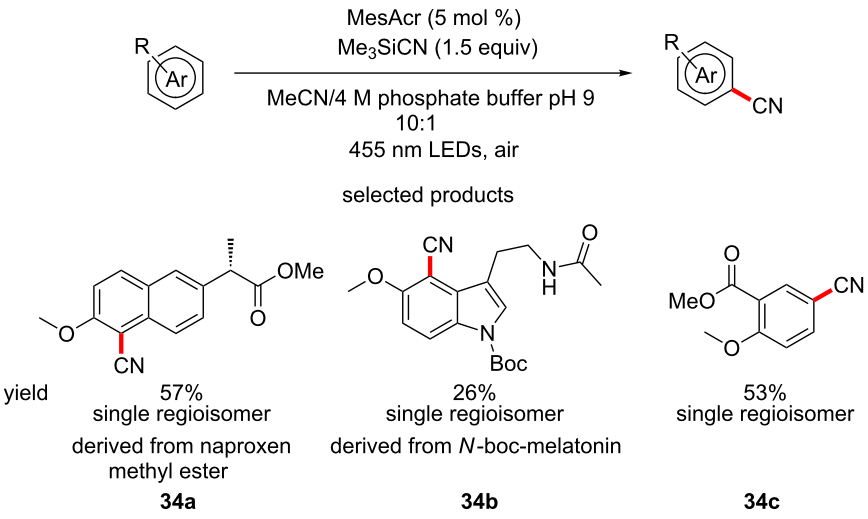

Scheme 34: The direct C–H cyanation of aromatics with a focus on its use for LSF.

line with the demands of medicinal chemistry. Not only has it been shown to be highly sustainable, versatile and mild, but in some cases, it enables transformations that are notoriously challenging, cf. heteroaryl–heteroaryl coupling (vide supra).

Possibly the most attractive application of these methods is LSF. Medicinal chemists are constantly exploring SAR and LSF is the concept that will expedite this process. Protocols that can be used as tools for LSF are being rapidly developed and organophotoredox catalysis is at an advantage when compared to other approaches, due to its mild nature, as has been highlighted repeatedly.

Great advances are constantly being made in this emerging field and even so, there are still numerous possibilities to be explored. For example, stereoselective photoredox chemistry is still quite sparse in the literature. Late-stage fluorination protocols are also rare and would be exhaustively used by the pharmaceutical industry. In addition, as has been pointed out in this review, mostly electron-rich heterocycles are manipulated, which are less valuable to the drug discovery process than their electron-poor counterparts. The growing number of academic and pharma laboratories entering organophotoredox catalysis and the development of even stronger photocatalysts ensures that the field will produce impactful research for years to come.

Abbreviations

Table 2: Abbreviations.

abbreviation	explanation
API	active pharmaceutical ingredient
BOC	*tert*-butyloxycarbonyl
DCC	dicyclohexyl carbodiimide
DDQ	2,3-dichloro-5,6-dicyano-1,4-benzoquinone
DMP	Dess–Martin periodinane
DMSO	dimethyl sulfoxide
EDG	electron-donating group
ET	electron transfer
EWG	electron-withdrawing group
GABA	γ-aminobutyric acid
HATU	1-[bis(dimethylamino)methylene]-1*H*-1,2,3-triazolo[4,5-b]pyridinium 3-oxide hexafluorophosphate
IBX	2-iodoxybenzoic acid
LED	light-emitting diode
LSF	late stage functionalisation
MB	methylene blue
MesAcr	mesityl acridinium salt
NSAID	non-steroidal anti-inflammatory drug
PET	photoinduced electron transfer
SAR	structure–activity relationship
SCE	saturated calomel electrode
SET	single electron transfer
TFA	trifluoroacetic acid
TMEDA	*N,N,N′,N′*-tetramethylethane-1,2-diamine
TMSCN	trimethylsilyl cyanide
UV	ultraviolet
X	heteroatom

Acknowledgements

M.K.B. would like to acknowledge his friends and former colleagues Gerhard Hofer and Nikos Kalivas, who invested time and effort proofreading this document in its earlier stages and for providing a valuable perspective on the content.

ORCID® iDs

John A. Murphy - https://orcid.org/0000-0003-3136-0845

References

1. Reckenthäler, M.; Griesbeck, A. G. *Adv. Synth. Catal.* **2013,** *355,* 2727–2744. doi:10.1002/adsc.201300751
2. Matsui, J. K.; Lang, S. B.; Heitz, D. R.; Molander, G. A. *ACS Catal.* **2017,** *7,* 2563–2575. doi:10.1021/acscatal.7b00094
3. Tucker, J. W.; Stephenson, C. R. J. *J. Org. Chem.* **2012,** *77,* 1617–1622. doi:10.1021/jo202538x
4. Narayanam, J. M. R.; Stephenson, C. R. J. *Chem. Soc. Rev.* **2011,** *40,* 102–113. doi:10.1039/B913880N
5. Zeitler, K. *Angew. Chem., Int. Ed.* **2009,** *48,* 9785–9789. doi:10.1002/anie.200904056
6. Staveness, D.; Bosque, I.; Stephenson, C. R. J. *Acc. Chem. Res.* **2016,** *49,* 2295–2306. doi:10.1021/acs.accounts.6b00270
7. Shaw, M. H.; Twilton, J.; MacMillan, D. W. C. *J. Org. Chem.* **2016,** *81,* 6898–6926. doi:10.1021/acs.joc.6b01449
8. Lefebvre, Q. *Synlett* **2017,** *28,* 19–23. doi:10.1055/s-0036-1588643
9. Akita, M.; Koike, T. *C. R. Chim.* **2015,** *18,* 742–751. doi:10.1016/j.crci.2015.01.013
10. Margrey, K. A.; Nicewicz, D. A. *Acc. Chem. Res.* **2016,** *49,* 1997–2006. doi:10.1021/acs.accounts.6b00304
11. Liu, Y.; Dong, W. *Chin. J. Chem.* **2017,** *35,* 1491–1500. doi:10.1002/cjoc.201700146
12. Yerien, D. E.; Barata-Vallejo, S.; Postigo, A. *Chem. – Eur. J.* **2017,** *23,* 14676–14701. doi:10.1002/chem.201702311
13. Koike, T.; Akita, M. *Org. Chem. Front.* **2016,** *3,* 1345–1349. doi:10.1039/C6QO00139D
14. Beatty, J. W.; Stephenson, C. R. J. *Acc. Chem. Res.* **2015,** *48,* 1474–1484. doi:10.1021/acs.accounts.5b00068
15. Nakajima, K.; Miyake, Y.; Nishibayashi, Y. *Acc. Chem. Res.* **2016,** *49,* 1946–1956. doi:10.1021/acs.accounts.6b00251
16. Lee, K. N.; Ngai, M.-Y. *Chem. Commun.* **2017,** *53,* 13093–13112. doi:10.1039/C7CC06287G
17. Sun, X.; Yu, S. *Synlett* **2016,** *27,* 2659–2675. doi:10.1055/s-0036-1588631
18. Shaaban, S.; Maulide, N. *Synlett* **2017,** *28,* 2707–2713. doi:10.1055/s-0036-1588776
19. Luo, K.; Yang, W.-C.; Wu, L. *Asian J. Org. Chem.* **2017,** *6,* 350–367. doi:10.1002/ajoc.201600512
20. Xie, J.; Jin, H.; Xu, P.; Zhu, C. *Tetrahedron Lett.* **2014,** *55,* 36–48. doi:10.1016/j.tetlet.2013.10.090
21. Xie, J.; Jin, H.; Hashmi, A. S. K. *Chem. Soc. Rev.* **2017,** *46,* 5193–5203. doi:10.1039/C7CS00339K
22. Morris, S. A.; Wang, J.; Zheng, N. *Acc. Chem. Res.* **2016,** *49,* 1957–1968. doi:10.1021/acs.accounts.6b00263
23. Chatterjee, T.; Iqbal, N.; You, Y.; Cho, E. J. *Acc. Chem. Res.* **2016,** *49,* 2284–2294. doi:10.1021/acs.accounts.6b00248
24. Chen, J.-R.; Hu, X.-Q.; Lu, L.-Q.; Xiao, W.-J. *Acc. Chem. Res.* **2016,** *49,* 1911–1923. doi:10.1021/acs.accounts.6b00254
25. Boubertakh, O.; Goddard, J.-P. *Eur. J. Org. Chem.* **2017,** *2017,* 2072–2084. doi:10.1002/ejoc.201601653
26. Kärkäs, M. D.; Porco, J. A., Jr.; Stephenson, C. R. J. *Chem. Rev.* **2016,** *116,* 9683–9747. doi:10.1021/acs.chemrev.5b00760
27. Nicholls, T. P.; Leonori, D.; Bissember, A. C. *Nat. Prod. Rep.* **2016,** *33,* 1248–1254. doi:10.1039/C6NP00070C
28. Cavalcanti, L. N.; Molander, G. A. *Top. Curr. Chem.* **2016,** *374,* 39. doi:10.1007/s41061-016-0037-z
29. Nicewicz, D. A.; Nguyen, T. M. *ACS Catal.* **2014,** *4,* 355–360. doi:10.1021/cs400956a
30. Larsen, C. B.; Wenger, O. S. *Chem. – Eur. J.* **2018,** *24,* 2039–2058. doi:10.1002/chem.201703602
31. Fukuzumi, S.; Ohkubo, K. *Org. Biomol. Chem.* **2014,** *12,* 6059–6071. doi:10.1039/C4OB00843J
32. Prier, C. K.; Rankic, D. A.; Macmillan, D. W. C. *Chem. Rev.* **2013,** *113,* 5322–5363. doi:10.1021/cr300503r
33. Hari, D. P.; König, B. *Chem. Commun.* **2014,** *50,* 6688–6699. doi:10.1039/C4CC00751D
34. Douglas, J. J.; Sevrin, M. J.; Stephenson, C. R. J. *Org. Process Res. Dev.* **2016,** *20,* 1134–1147. doi:10.1021/acs.oprd.6b00125

35. Romero, N. A.; Nicewicz, D. A. *Chem. Rev.* **2016,** *116,* 10075–10166. doi:10.1021/acs.chemrev.6b00057
36. Lambert, C. R.; Kochevar, I. E. *Photochem. Photobiol.* **1997,** *66,* 15–25. doi:10.1111/j.1751-1097.1997.tb03133.x
37. Joshi-Pangu, A.; Lévesque, F.; Roth, H. G.; Oliver, S. F.; Campeau, L.-C.; Nicewicz, D.; DiRocco, D. A. *J. Org. Chem.* **2016,** *81,* 7244–7249. doi:10.1021/acs.joc.6b01240
38. Leow, D. *Org. Lett.* **2014,** *16,* 5812–5815. doi:10.1021/ol5029354
39. Di Paolo, J. A.; Huang, T.; Balazs, M.; Barbosa, J.; Barck, K. H.; Bravo, B. J.; Carano, R. A. D.; Darrow, J.; Davies, D. R.; Deforge, L. E.; Diehl, L.; Ferrando, R.; Gallion, S. L.; Giannetti, A. M.; Gribling, P.; Hurez, V.; Hymowitz, S. G.; Jones, R.; Kropf, J. E.; Lee, W. P.; Maciejewski, P. M.; Mitchell, S. A.; Rong, H.; Staker, B. L.; Whitney, J. A.; Yeh, S.; Young, W. B.; Yu, C.; Zhang, J.; Reif, K.; Currie, K. S. *Nat. Chem. Biol.* **2011,** *7,* 41–50. doi:10.1038/nchembio.481
40. Cassani, C.; Bergonzini, G.; Wallentin, C.-J. *Org. Lett.* **2014,** *16,* 4228–4231. doi:10.1021/ol5019294
41. Hughes, G.; Devine, P. N.; Naber, J. R.; O'Shea, P. D.; Foster, B. S.; McKay, D. J.; Volante, R. P. *Angew. Chem., Int. Ed.* **2007,** *46,* 1839–1842. doi:10.1002/anie.200603745
42. Black, W. C.; Bayly, C. I.; Davis, D. E.; Desmarais, S.; Falgueyret, J.-P.; Léger, S.; Li, C. S.; Massé, F.; McKay, D. J.; Palmer, J. T.; Percival, M. D.; Robichaud, J.; Tsou, N.; Zamboni, R. *Bioorg. Med. Chem. Lett.* **2005,** *15,* 4741–4744. doi:10.1016/j.bmcl.2005.07.071
43. Talla, A.; Driessen, B.; Straathof, N. J. W.; Milroy, L.-G.; Brunsveld, L.; Hessel, V.; Noël, T. *Adv. Synth. Catal.* **2015,** *357,* 2180–2186. doi:10.1002/adsc.201401010
44. Bloom, S.; Liu, C.; Kölmel, D. K.; Qiao, J. X.; Zhang, Y.; Poss, M. A.; Ewing, W. R.; Macmillan, D. W. C. *Nat. Chem.* **2018,** *10,* 205–211. doi:10.1038/nchem.2888
45. Brown, D. G.; Boström, J. *J. Med. Chem.* **2016,** *59,* 4443–4458. doi:10.1021/acs.jmedchem.5b01409
46. Ghosh, I.; Ghosh, T.; Bardagi, J. I.; König, B. *Science* **2014,** *346,* 725–728. doi:10.1126/science.1258232
47. Hari, D. P.; Schroll, P.; König, B. *J. Am. Chem. Soc.* **2012,** *134,* 2958–2961. doi:10.1021/ja212099r
48. Maity, P.; Kundu, D.; Ranu, B. C. *Eur. J. Org. Chem.* **2015,** 1727–1734. doi:10.1002/ejoc.201500006
49. Rosen, T.; Nagel, A. A.; Rizzi, J. P.; Ives, J. L.; Daffeh, J. B.; Ganong, A. H.; Guarino, K.; Heym, J.; McLean, S.; Nowakowski, J. T.; Schmidt, A. W.; Seeger, T. F.; Siok, C. J.; Vincent, L. A. *J. Med. Chem.* **1990,** *33,* 2715–2720. doi:10.1021/jm00172a006
50. Lange, J. H. M.; Van Stuivenberg, H. H.; Coolen, H. K. A. C.; Adolfs, T. J. P.; McCreary, A. C.; Keizer, H. G.; Wals, H. C.; Veerman, W.; Borst, A. J. M.; De Looff, W.; Verveer, P. C.; Kruse, C. G. *J. Med. Chem.* **2005,** *48,* 1823–1838. doi:10.1021/jm040843r
51. Sun, P.; Yang, D.; Wei, W.; Jiang, M.; Wang, Z.; Zhang, L.; Zhang, H.; Zhang, Z.; Wang, Y.; Wang, H. *Green Chem.* **2017,** *19,* 4785–4791. doi:10.1039/C7GC01891F
52. Mitra, S.; Ghosh, M.; Mishra, S.; Hajra, A. *J. Org. Chem.* **2015,** *80,* 8275–8281. doi:10.1021/acs.joc.5b01369
53. Meyer, A. U.; Berger, A. L.; König, B. *Chem. Commun.* **2016,** *52,* 10918–10921. doi:10.1039/C6CC06111G
54. Das, S.; Natarajan, P.; König, B. *Chem. – Eur. J.* **2017,** *23,* 18161–18165. doi:10.1002/chem.201705442
55. Zhou, R.; Liu, H.; Tao, H.; Yu, X.; Wu, J. *Chem. Sci.* **2017,** *8,* 4654–4659. doi:10.1039/c7sc00953d
56. Rueping, M.; Vila, C.; Bootwicha, T. *ACS Catal.* **2013,** *3,* 1676–1680. doi:10.1021/cs400350j
57. Noto, N.; Koike, T.; Akita, M. *Chem. Sci.* **2017,** *8,* 6375–6379. doi:10.1039/C7SC01703K
58. Zhou, X.-p.; Zhang, M.-x.; Sun, W.; Yang, X.-h.; Wang, G.-s.; Sui, D.-y.; Yu, X.-f.; Qu, S.-c. *Biol. Pharm. Bull.* **2009,** *32,* 1986–1990. doi:10.1248/bpb.32.1986
59. Roth, B. D.; Blankley, C. J.; Chucholowski, A. W.; Ferguson, E.; Hoefle, M. L.; Ortwine, D. F.; Newton, R. S.; Sekerke, C. S.; Sliskovic, D. R.; Stratton, C. D.; Wilson, M. W. *J. Med. Chem.* **1991,** *34,* 357–366. doi:10.1021/jm00105a056
60. Xuan, J.; Xia, X.-D.; Zeng, T.-T.; Feng, Z.-J.; Chen, J.-R.; Lu, L.-Q.; Xiao, W.-J. *Angew. Chem.* **2014,** *126,* 5759–5762. doi:10.1002/ange.201400602
61. Zeng, T.-T.; Xuan, J.; Ding, W.; Wang, K.; Lu, L.-Q.; Xiao, W.-J. *Org. Lett.* **2015,** *17,* 4070–4073. doi:10.1021/acs.orglett.5b01994
62. Morse, P. D.; Nicewicz, D. A. *Chem. Sci.* **2015,** *6,* 270–274. doi:10.1039/C4SC02331E
63. Kapoorr, R.; Singh, S. N.; Tripathi, S.; Yadav, L. D. S. *Synlett* **2015,** *26,* 1201–1206. doi:10.1055/s-0034-1380493
64. Srivastava, V. P.; Yadav, A. K.; Yadav, L. D. S. *Synlett* **2013,** *24,* 465–470. doi:10.1055/s-0032-1318158
65. Hari, D. P.; Hering, T.; König, B. *Org. Lett.* **2012,** *14,* 5334–5337. doi:10.1021/ol302517n
66. Jana, S.; Verma, A.; Kadu, R.; Kumar, S. *Chem. Sci.* **2017,** *8,* 6633–6644. doi:10.1039/C7SC02556D
67. Yadav, S.; Srivastava, M.; Rai, P.; Tripathi, B. P.; Mishra, A.; Singh, J.; Singh, J. *New J. Chem.* **2016,** *40,* 9694–9701. doi:10.1039/C6NJ02365G
68. Wang, L.; Ma, Z.-G.; Wei, X.-J.; Meng, Q.-Y.; Yang, D.-T.; Du, S.-F.; Chen, Z.-F.; Wu, L.-Z.; Liu, Q. *Green Chem.* **2014,** *16,* 3752–3757. doi:10.1039/C4GC00337C
69. Shen, Z.-c.; Yang, P.; Tang, Y. *J. Org. Chem.* **2016,** *81,* 309–317. doi:10.1021/acs.joc.5b02366
70. Cernak, T.; Dykstra, K. D.; Tyagarajan, S.; Vachal, P.; Krska, S. W. *Chem. Soc. Rev.* **2016,** *45,* 546–576. doi:10.1039/C5CS00628G
71. Pitre, S. P.; McTiernan, C. D.; Ismaili, H.; Scaiano, J. C. *ACS Catal.* **2014,** *4,* 2530–2535. doi:10.1021/cs5005823
72. Cui, L.; Matusaki, Y.; Tada, N.; Miura, T.; Uno, B.; Itoh, A. *Adv. Synth. Catal.* **2013,** *355,* 2203–2207. doi:10.1002/adsc.201300199
73. Wei, G.; Zhang, C.; Bureš, F.; Ye, X.; Tan, C.-H.; Jiang, Z. *ACS Catal.* **2016,** *6,* 3708–3712. doi:10.1021/acscatal.6b00846
74. Davies, J.; Svejstrup, T. D.; Fernandez Reina, D.; Sheikh, N. S.; Leonori, D. *J. Am. Chem. Soc.* **2016,** *138,* 8092–8095. doi:10.1021/jacs.6b04920
75. Matsui, J. K.; Primer, D. N.; Molander, G. A. *Chem. Sci.* **2017,** *8,* 3512–3522. doi:10.1039/C7SC00283A
76. Atack, T. C.; Cook, S. P. *J. Am. Chem. Soc.* **2016,** *138,* 6139–6142. doi:10.1021/jacs.6b03157
77. Venditto, V. J.; Simanek, E. E. *Mol. Pharmaceutics* **2010,** *7,* 307–349. doi:10.1021/mp900243b
78. Romero, N. A.; Margrey, K. A.; Tay, N. E.; Nicewicz, D. A. *Science* **2015,** *349,* 1326–1330. doi:10.1126/science.aac9895
79. Tay, N. E. S.; Nicewicz, D. A. *J. Am. Chem. Soc.* **2017,** *139,* 16100–16104. doi:10.1021/jacs.7b10076
80. McManus, J. B.; Nicewicz, D. A. *J. Am. Chem. Soc.* **2017,** *139,* 2880–2883. doi:10.1021/jacs.6b12708

BEILSTEIN JOURNAL OF ORGANIC CHEMISTRY

Bioinspired cobalt cubanes with tunable redox potentials for photocatalytic water oxidation and CO_2 reduction

Zhishan Luo, Yidong Hou, Jinshui Zhang, Sibo Wang and Xinchen Wang*

Full Research Paper

Open Access

Address:
State Key Laboratory of Photocatalysis on Energy and Environment, College of Chemistry, Fuzhou University, Fuzhou 350002, China

Email:
Xinchen Wang* - xcwang@fzu.edu.cn

* Corresponding author

Keywords:
CO_2 reduction; cobalt cubane; photocatalysis; water oxidation; water splitting

Beilstein J. Org. Chem. **2018,** *14,* 2331–2339.
doi:10.3762/bjoc.14.208

Received: 14 May 2018
Accepted: 17 August 2018
Published: 05 September 2018

This article is part of the thematic issue "Photoredox catalysis for novel organic reactions".

Guest Editor: P. H. Seeberger

Abstract

The development of efficient, robust and earth-abundant catalysts for photocatalytic conversions has been the Achilles' heel of solar energy utilization. Here, we report on a chemical approach based on ligand designed architectures to fabricate unique structural molecular catalysts coupled with appropriate light harvesters (e.g., carbon nitride and $Ru(bpy)_3^{2+}$) for photoredox reactions. The "Co_4O_4" cubane complex $Co_4O_4(CO_2Me)_4(RNC_5H_4)_4$ (R = CN, Br, H, Me, OMe), serves as a molecular catalyst for the efficient and stable photocatalytic water oxidation and CO_2 reduction. A comprehensive structure–function analysis emerged herein, highlights the regulation of electronic characteristics for a molecular catalyst by selective ligand modification. This work demonstrates a modulation method for fabricating effective, stable and earth-abundant molecular catalysts, which might facilitate further innovation in the function-led design and synthesis of cubane clusters for photoredox reactions.

Introduction

The direct conversion of solar energy into chemical fuels (e.g., H_2, CO and hydrocarbons) through water splitting and carbon fixation reactions is a sustainable solution to environmental concerns and long-term access to adequate energy supplies [1-7]. To realize these reactions, extensive studies have focused on the design and synthesis of chemically stable light-harvesting antenna materials and efficient cocatalysts, and their assembly in integrated artificial photosynthetic systems [8-13]. However, such target reactions are typical thermodynamically uphill reactions with large overpotentials, leading to low conversion efficiency. Therefore, the search for suitable cocatalysts to reduce the multielectron involved kinetic barriers for water oxidation and CO_2 reduction is regarded as a critical step toward artificial photosynthesis, which can boost the photoconversion efficiency (PCE) significantly [14-19].

Molecular catalysts with complex and varied structural motifs are a class of promising catalysts for solar energy conversion, because of their well-controlled functions and tunable nature [20,21]. Their topologies and electron structures can be precisely engineered by ligand design, using the full arsenal of organic chemistry [22,23]. These unique structures benefit not only tailoring their redox and kinetic properties for catalysis, but also providing valuable structural information to understand the mechanistic insights of catalytic behavior [24-27]. In addition, the molecular catalysts can either be dissolved in liquids affording a homogeneous catalytic system [28,29], or immobilized on solid surfaces for application in heterogeneous catalysis [30-33], owing to their molecular nature with flexible ligand architectures [34,35]. In this regard, extensive attention has been contributed to the design and synthesis of molecular catalysts [36]. Unfortunately, most of the high-activity molecular catalysts are typically based on noble metals (e.g., Ru, Ir) [37-40], which seriously restricts their practical applications. Therefore, the development of effective, stable and sustainable molecular catalysts based on earth-abundant elements is highly desirable [41-43].

Inspired by the molecular Mn_4CaO_5 cubane of oxygen-evolving complex in photosystem II, there is an emerging number of molecular cubanes with metallic and heterobimetallic cores that are designed and synthesized for photosynthesis and electrochemistry. Cobalt-based molecular catalysts [44], in particular the ones containing a cubical Co_4O_4 core were studied extensively as energy conversion catalysts, because of their cubical topology that is structurally analogous to the biological Mn_4CaO_5 cubane [45,46]. Driess et al. have reported the smallest possible molecular building block "Co_4O_4" cluster with a singly deprotonated dipyridyldiol (LH) as a chelating ligand [47]. Generally, Co_4O_4-based molecular catalysts can be easily tuned by ligand design, owing to their molecular nature [48,49]. For example, Hill et al. demonstrated that using polytungstate ligands to stabilize "Co_4O_4" cubane units can produce a robust homogeneous catalyst for solar water oxidation [50]. After that, Berlinguette et al. reported that replacing the inorganic ligand with an organic ligand, such as the pentadentate Py5 ligand can also well stabilize the "Co_4O_4" unit to catalyze water oxidation [51]. This finding is very important, which means there is ample choice of organic ligand architectures to tailor the electronic properties of the "Co_4O_4" unit for catalysis. In this regard, Nocera et al. selected an organic ligand bearing an electron-withdrawing group (fluorine) to optimize the "Co_4O_4" cubane unit for electrocatalytic water oxidation [52]. As expected, the resultant catalyst exhibited a larger catalytic current and an earlier onset potential with respect to its analogs without a fluorine functional group. Thus, the control of catalytic properties via molecular design by tunable ligand substitution is essential in the development of Co_4O_4-based cubane catalysts. However, most of the researches focused on the oxidative properties of the Co_4O_4 core [53], and its use for reduction reactions is rarely covered. Theoretically, the redox potential of Co_4O_4 cubane clusters should be tuned by virtue of different ligand substitutions, thus it is highly possible to develop a Co_4O_4-based catalyst for reduction applications, such as H_2 evolution and CO_2 fixation.

Herein, we demonstrate that molecular Co_4O_4 cubanes (Figure 1) are readily and precisely manipulated to tune their redox functions through regulating their electronic structures by ligand engineering. The use of electron-withdrawing or donating ligands can easily adjust their catalytic properties for water oxidation and CO_2 reduction, respectively. For example, organic ligands with strong electron-withdrawing groups (R = CN, Br) enhance their oxidation capability for water oxi-

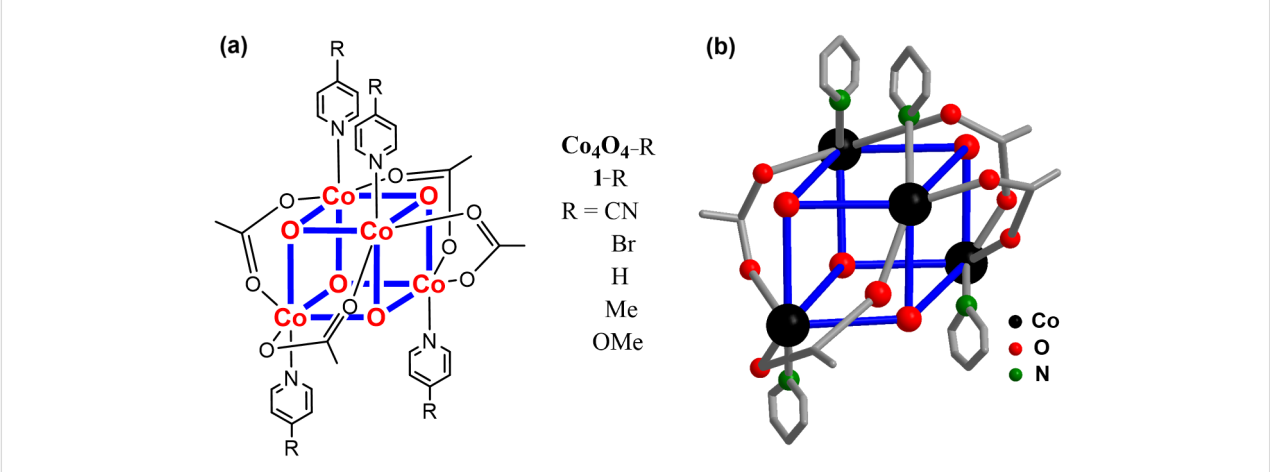

Figure 1: (a) Molecular structures of the Co_4O_4 cubane catalysts. (b) Ball-and-stick representation of complex **1**-H; H atoms are omitted for clarity.

dation by reducing the overpotential of O–O bond formation. In contrast, the incorporation of electron-donating groups (R = Me, OMe) significantly increases the electronic density at the metal centers, thus affording a Co_4O_4 core able to catalyze CO_2 reduction. This indicates that the change of substituents in the pyridine ligand provides further insight into the factors that affect the redox potential and tailor the catalytic performance. Furthermore, by exploring the structure–function relationship at the molecular level offers a useful guidance for the design and construction of high-performance earth-abundant molecular catalysts.

Results and Discussion

The molecular Co_4O_4 cubanes (**1**-R) were fabricated according to the literature [54], and their identities were confirmed by ^{1}H NMR and FTIR spectroscopy (see Supporting Information File 1 for details). Taking catalyst **1**-H as an example, it's ^{1}H NMR spectrum exhibits three sets of peaks at 8.20 (d, 8H), 7.71 (t, 4H) and 7.20 (t, 8H) ppm for the *o*-, *p*-, and *m*-ring protons, respectively, of the equivalent pyridines and the methyl protons of the acetate ligands appear as a sharp singlet at 2.06 (s, 12 H) ppm (see Supporting Information File 1, Figure S1). In the FTIR spectrum, the bands in the region 1530–1538 cm^{-1} are assigned to the ν_{asym}(COO) vibration and the stretching vibration of the pyridine ring [54], whereas the band at 1410 cm^{-1} designates to the $\delta_{asym}(CH_3)$. The most characteristic feature of the IR data is the appearance of a four-band pattern observed at ≈759, ≈692, ≈634 and ≈574 cm^{-1}, corresponding to the "Co_4O_4" cubane-like core present in the complex [54]. The XRD patterns for **1**-R cubanes are shown in Supporting Information File 1, Figure S8. Moreover, as shown in Scheme S1 (Supporting Information File 1), all aqueous solutions of **1**-R are transparent, homogeneous and clear, indicative of their similarities in structure. Based on the above analyses and comparison with the data in literatures [54,55], it is concluded that the **1**-R cubanes have been successfully fabricated.

Next, to investigate the effect of different ligands on the optical properties of the **1**-R complexes, UV–vis absorption measurements were conducted. As shown in Figure 2, three absorption bands are observed in the UV–vis spectra. The lowest energy absorption appearing as a shoulder at 645 to 660 nm, is associated with the d–d transitions involving $^1A_1 \rightarrow {}^1T_1$ and $^1A_1 \rightarrow {}^1T_2$ for the approximately octahedral Co complex [53-55]. As judged by the observed intensities, the other two bands are attributable to absorptions rather than d–d transitions. The bands in the range of 340 to 365 nm are likely due to a charge-transfer transition involving the μ-O–Co moiety present in these complexes [54,55]. The observed wavelength shift is dependent on the nature of the substituent present in the *p*-position of the pyridine-based ligand. As expected, the incorporation of the electron-withdrawing moiety R = CN reduces the

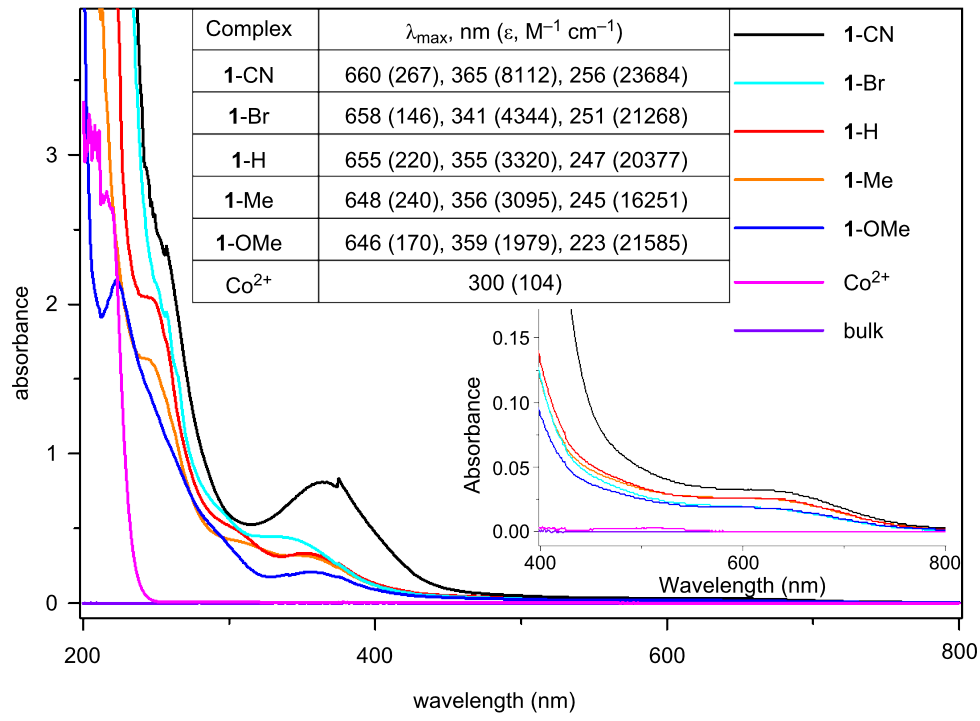

Figure 2: UV–vis absorption spectra of **1**-R in H_2O based on measurements in 10^{-4} M solution. Inset: scale from 400 nm to 800 nm and the λ_{max} for **1**-R.

electron densities of the Co centers and thus facilitates the charge-transfer transitions from μ-O atoms to the Co centers, which leads to a modest bathochromic shift from 355 (R = H) to 365 nm, however, with a remarkably enhanced intensity. In addition, the highest energy band between 220–260 nm is believed to be of ligand origin, most probably originating from the π → π* absorption of pyridine [54]. Similarly, a red shift in the order of **1**-CN (256 nm) > **1**-Br (251 nm) > **1**-H (247 nm) > **1**-Me (245 nm) > **1**-OMe (223 nm) is observed based on the increasing electron-withdrawing property of the ligands in these complexes (Figure 2 inset) [55]. This indicates that the different electronic properties have a significant influence on the optical performances, thus underlining the tuning effect of suitably substituted pyridine-based ligands for controlling the catalysts functions.

The subsequent cyclic voltammetry (CV) experiments supported the above results, i.e., that the variation of the ligands has a profound effect on the observed redox potentials. Figure 3 displays the plots of the Hammett σ_p parameters for the ligands versus the half-wave potentials ($E_{1/2}$) for **1**-R complexes, and the potentials increase linearly as a function of σ_p, giving an indicator of the electronic influence of the substituents on $E_{1/2}$. The $E_{1/2}$ values for the complexes increase in the following order: **1**-R, R = OMe < Me < H < Br < CN. The Hammett analysis provides a positive slope value, indicating that the $E_{1/2}$ value is favored by electron-withdrawing ligands [48,55]. As the ligand becomes more electron withdrawing, the reduced electron density at the metal center makes the Co center in the complex easier to reduce and more difficult to oxidize [55]. Most surprisingly, the potentials could be predicted simply by considering the Hammett σ_p values. Therefore, the observed redox potentials reflect a dependence on the electronic properties of the ligand. This again underlines, that the ligands are playing a significant role in the regulation of the redox properties of the **1**-R complexes.

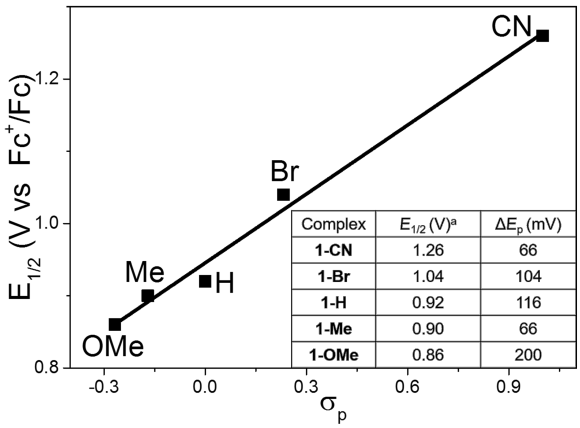

Complex	$E_{1/2}$ (V)[a]	ΔE_p (mV)
1-CN	1.26	66
1-Br	1.04	104
1-H	0.92	116
1-Me	0.90	66
1-OMe	0.86	200

Figure 3: Correlation of Hammett constants σ_p for the different ligands with midpoint potentials ($E_{1/2}$) in complexes **1**-R. [a]CV data for **1**-R in MeCN/0.1 M TBAP vs Fc^+/Fc under saturated Ar atmosphere.

To further estimate the impact of ligand substitution, the complexes were analyzed by linear sweep voltammetry (LSV). For this, we chose complexes **1**-CN, **1**-H and **1**-OMe to include ligand substitutions with electron-withdrawing and electron-donating properties (Figure 4). In Figure 4a, an abrupt onset of the catalytic anode current at 0.7 V, 1.0 V and 1.3 V for **1**-CN, **1**-H and **1**-OMe is observed, respectively, which is ascribed to an O_2 evolution reaction. The ligand substituted with the electron-withdrawing cyano (**CN**) group shows the lowest overpotential

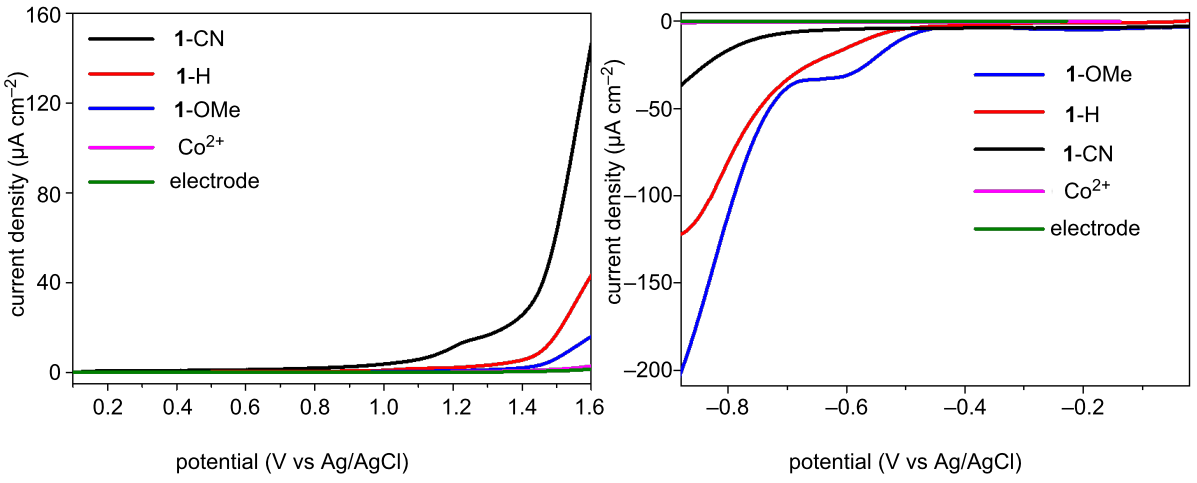

Figure 4: Linear sweep voltammetry of **1**-R (0.3 mM) or $Co(NO_3)_2{\cdot}6H_2O$ (1.2 mM); (a) at a 100 mV/s scan rate in 0.2 M Na_2SO_4, (b) at a 50 mV/s scan rate in MeCN (0.1 M $TBAPF_6$) under CO_2-saturated conditions. The working electrode used was 3 mm diameter glassy carbon electrode, the counter electrode was a platinum foil and the reference electrode was a Ag/AgCl.

for water oxidation activities, exhibiting a much higher current density compared to other cubane complexes and Co^{2+}. Meanwhile, we also studied the electrochemical reduction in a CO_2-saturated system (Figure 4b). It displays that **1**-OMe affords a current density of 200 μA·cm^{-2} at −0.88 V, a 5.5-fold enhancement over **1**-CN (36 μA·cm^{-2}). This suggests that the substituted ligand with the electron-donating group is suitable for the electrochemical reduction. It is important to note that ligands with different electronic structures exhibited starkly different activities for redox reaction. The ligand with an electron-withdrawing property favors water oxidation, and the one with electron-donating property is conducive to CO_2 reduction. Such a favorable electrochemical potential for **1**-R with tunable ligand substitutions suggests their great potential as redox catalysts for water oxidation and CO_2 reduction reactions.

Next, we studied the photocatalytic activity of a series of the **1**-R molecular complexes in the water oxidation reaction to release O_2 gas and CO_2-to-CO conversion (Figure 5). For the water oxidation, we have chosen carbon nitride [56-60] coupled with the **1**-R molecular complexes to evaluate the oxygen evolution performance. In Figure 5a, without the **1**-R molecular complexes, the O_2 production rate is rather low (1.2 μmol·h^{-1}). However, after introducing the molecular complexes, the oxygen evolution reaction is accelerated, and the reactivity of the reaction is expected to be tuned by the ligand modification, within the order of **1**-CN (10.2 μmol·h^{-1}) > **1**-Br (5.9 μmol·h^{-1}) > **1**-H (4.9 μmol·h^{-1}) > **1**-Me (4.5 μmol·h^{-1}) > **1**-OMe (3.3 μmol·h^{-1}), which is consistent with the effect of the substituent groups on the pyridine ligand of **1**-R on the electrochemical oxygen evolution. These results indicated that water oxidation is favored by the presence of electron-withdrawing ligands. Additionally, the activity of water oxidation over **1**-R is much higher than that over Co^{2+} ions, which may be due to the effect of the ligand for enhancing the stability of the entire cobalt metal center [48,49]. Furthermore, a long time course of water oxidation for **1**-CN and Co^{2+} are also compared in Figure 6. It is obvious that the overall amount of the produced O_2 gas for **1**-R is higher than that for Co^{2+}. As the reaction time increases,

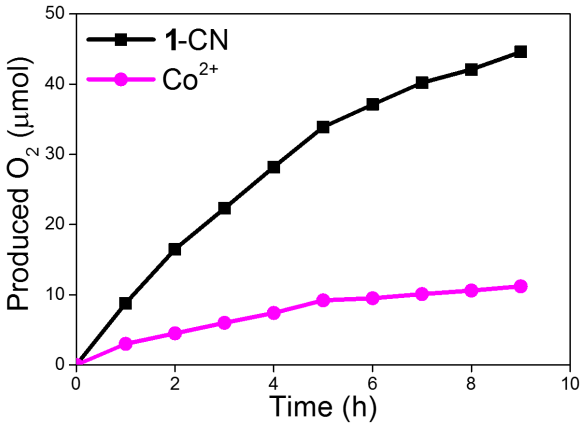

Figure 6: Long-time course of water oxidation for **1**-CN and Co^{2+} under UV–vis light irradiation (λ >300 nm).

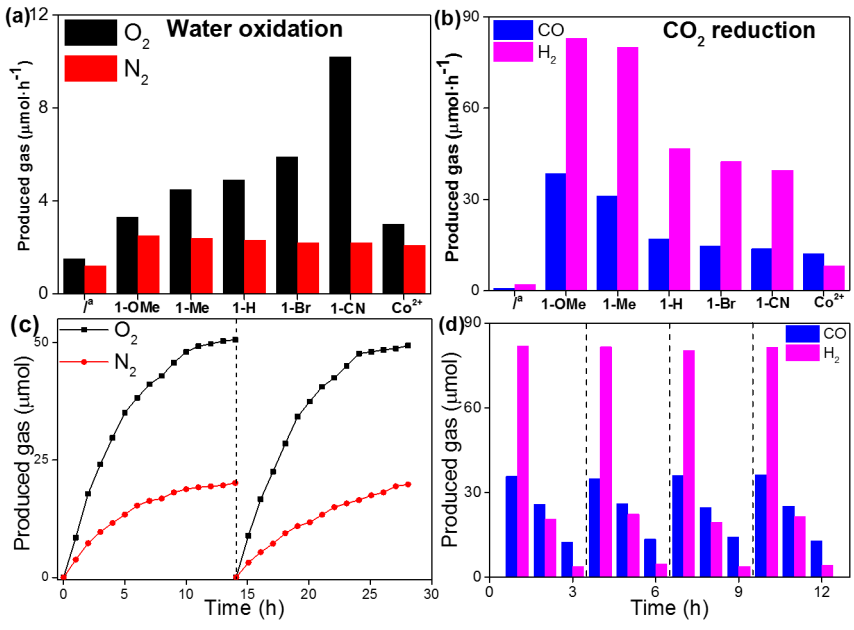

Figure 5: The activity of **1**-R for (a) water oxidation and (b) CO_2 reduction. (c) Long-time course of water oxidation for **1**-CN under UV–vis light irradiation (λ > 300 nm) in two recycling tests. (d) CO_2 reduction for **1**-OMe under visible light irradiation (λ > 420 nm) in four recycling tests. [a]Without **1**-R.

the decreasing trend of O_2 evolution rate for Co^{2+} is more pronounced than in case of **1**-CN. This can be ascribed to the instability of Co^{2+} and the tendency of this metal to be oxidized to form CoO_x nanoparticles in the reaction mixture (Supporting Information File 1, Figure S7). These results also support the above discussion. The presence of **1**-R with an enhanced electron-withdrawing ability can significantly reduce the overpotential for the O–O bond formation, and thus facilitates water oxidation.

Besides the CO_2 reduction performance of the molecular complexes was evaluated by cooperation with a ruthenium photosensitizer $Ru(bpy)_3^{2+}$ (bpy = 2',2-bipyridine) with visible light irradiation [61-67]. As shown in Figure 5b, the activity of the CO_2 reaction is reduced with the increase of electron-withdrawing ability of the ligand. In this case, **1**-OMe exhibits the highest CO_2 photoreduction activity with a CO evolution rate of 38.5 μmol·h^{-1}, together with a H_2 generation rate of 83 μmol·h^{-1}. The CO_2-to-CO conversion rate of **1**-OMe is 2.5-fold enhanced than that of **1**-CN (13.8 μmol·h^{-1}). It is found that the introduction of a simple substituent greatly influenced the activity of CO_2 reduction, that is, the ligand substitution with an electron-donating property is more beneficial for the CO_2 reduction reaction. The above results demonstrate that the **1**-R molecular complexes are highly active for both water oxidation and CO_2 reduction reactions, which is in good agreement with the results of the optical, CV and LSV measurements. Importantly, the photoredox functions of the molecular complexes can be modulated deliberately by ligand substitutions with different electronic properties.

The stabilities of the molecular catalysts for photoredox reactions were also examined. Firstly, in 14 h long term water oxidation tests for 2 cycles, the total O_2 evolution in each run was almost the same (Figure 5c). The gradually reduced reaction rate after about 5 h is ascribed to the deposition of Ag particles on the surface of polymeric carbon nitride (p-C_3N_4, PCN), which leads to a light shading effect hindering optical absorption. In the stability test for CO_2 reduction reactions, no noticeable losses in the yields of CO and H_2 were observed in 4 cycles (Figure 5d). The deactivation after 3 h reaction in each case is due to photobleaching of the used dye photosensitizer. Moreover, after water oxidation and CO_2 reduction reactions, the structures of **1**-CN and **1**-OMe were studied by ^{1}H NMR spectroscopy, and no obvious changes were observed compared with the fresh samples (Supporting Information File 1, Figure S6).

Conclusion

In summary, we have developed molecular cubane catalysts with tunable redox potentials through the ligand architectures, which are coupled with the light harvesters (e.g., carbon nitride and $Ru(bpy)_3^{2+}$) for photocatalytic water oxidation and CO_2 reduction. The electronic properties of the ligands have a significant effect on the catalysts photoredox reaction. The ligands with electron-withdrawing substituents are beneficial for the water oxidation and the CO_2 reduction is favored by the presence of electron-donating ligands. The comparative study reported here allows us to scrutinize the interplay between electronic effects and redox potential caused by ligand modifications within the series of Co_4O_4 cubane clusters. The ligand modification strategy developed here provides a rational, precise and cost-effective way for the chemical design and synthesis of biomimetic cubane clusters with metal cores (i.e., Co, Mn, and Ni) or even heterobimetallic cores for a wide range of redox applications in catalysis and photosynthesis.

Experimental

Materials: All chemicals are commercially available and were used without further purification. All solutions were prepared with Milli-Q ultrapure water (>18 MΩ) unless otherwise stated.

Synthesis of p-C_3N_4: p-C_3N_4 was synthesized by annealing urea (10 g) at 550 °C for 2 h under the muffle furnace with the ramping rate at 5 °C/min, and the resulted buff powder was collected and denoted as PCN.

Synthesis of ATCN/p-C_3N_4: The ATCN/p-C_3N_4 sample was synthesized according to the literature procedures [68]. 2-Aminothiophene-3-carbonitrile (ATCN, 10 mg) and 10 g urea were mixed with 10 mL pure water, and stirring at room temperature for 12 h and then stirring at 80 °C to remove water. The mixtures were ground into powder and calcined at 550 °C for 2 h under the muffle furnace with the ramping rate at 5 °C/min. The samples thus obtained were denoted as ATCN/PCN.

Synthesis of $Co_4O_4(O_2CMe)_4(NC_5H_5)_4$, 1-H: Complex **1**-H was synthesized according to the literature procedures [30,48,54]. Typically, to a mixture of $Co(NO_3)_2{\cdot}6H_2O$ (2.9 g, 10 mmol) and $CH_3CO_2Na{\cdot}3H_2O$ (2.7 g, 20 mmol) in methanol (30 mL) heated to refluxing temperature, is added pyridine (0.8 mL, 10 mmol) while stirring. Then a portion of 30% hydrogen peroxide (v/v, 5 mL, 50 mmol) is slowly added to the reaction mixture, and stirring under refluxing conditions is continued for 4 h. After cooling to room temperature and reducing the volume, the latter is placed in a separating funnel and CH_2Cl_2 added. The pink aqueous phase was discarded, while the dark green organic phase dried over anhydrous Na_2SO_4 and filtered. After removal of the solvent, the residue was purified by column chromatography on silica gel with

CH_2Cl_2/CH_3OH 15:1 (v/v) as the eluent to afford 1.50 g (70%) of the pure complex as a dark green solid.

Synthesis of $Co_4O_4(O_2CMe)_4(NC_5H_4$-OMe$)_4$, 1-OMe: The same procedure as described above was adopted except replacing pyridine with 4-methoxypyridine (1.02 mL, 10 mmol), to afford 2.07 g (85%) of the dark green product.

Synthesis of $Co_4O_4(O_2CMe)_4(NC_5H_4$-Me$)_4$, 1-Me: A similar procedure as described above was adopted using 4-methylpyridine (0.98 mL, 10 mmol) to afford 1.82 g (80%) of the dark green product.

Synthesis of $Co_4O_4(O_2CMe)_4(NC_5H_4$-Br$)_4$, 1-Br: The same procedure as described above was adopted except replacing pyridine with 4-bromopyridine hydrochloride (1.94 g, 10 mmol) to afford 0.9 g (31%) of the dark green product.

Synthesis of $Co_4O_4(O_2CMe)_4(NC_5H_4$-CN$)_4$, 1-CN: The same procedure as described above was adopted except replacing pyridine with 4-cyanopyridine (1.04 mL, 10 mmol) to afford 2.01 g (84%) of the product as dark brown solid.

Characterization: The UV–vis absorption spectra were measured on a SHIMADZU UV-1780 spectrometer (Kyoto, Japan). Fourier transform infrared (FTIR) spectra were taken on a thermo Nicolet Nexus 670 FTIR spectrometer with KBr as the diluents. Electrochemical measurements were conducted with a Biologic VSP-300 Electrochemical System in a conventional three electrode cell. The ^{1}H NMR experiments were performed on Bruker AVANCE 400M spectrometers. Transmission electron microscopy (TEM) was obtained using a FEI TECNAIG2F20 instrument. Powder X-ray diffraction (XRD) patterns were collected on Bruker D8 Advance diffractometer with Cu K1 radiation (λ = 1.5406 Å).

Photocatalytic test for water oxidation system [69]**:** Photocatalytic O_2 production was carried out in a Pyrex top-irradiation reaction vessel connected to a glass closed gas circulation system. For each reaction, PCN powder (50 mg) was well dispersed in an aqueous solution (100 mL) containing $AgNO_3$ (0.17 g) as an electron acceptor, La_2O_3 (0.2 g) as a pH buffer agent and **1**-R (0.25 μmol) or $Co(NO_3)_2{\cdot}6H_2O$ (1.0 μmol). The reaction solution was evacuated several times to remove air completely prior to irradiation with a 300 W xenon lamp with a working current of 15 A (Shenzhen ShengKang Technology Co., Ltd, China, LX300F). The wavelength of the incident light was controlled by applying some appropriate long-pass cut-off filters (λ > 300 nm). The temperature of the reaction solution was maintained at room temperature by a flow of cooling water during the reaction. The evolved gases were analyzed in-situ by gas chromatography equipped with a thermal conductive detector (TCD) and a 5 Å molecular sieves column, using Argon as the carrier gas.

Photocatalytic test for CO_2 reduction system [70]**:** The photocatalytic test was performed in a Schlenk flask (80 mL) under an atmospheric pressure of CO_2. In the Schlenk flask, the photocatalytic CO_2 reduction reaction was carried out by dispersing $Ru(bpy)_3^{2+}$ (7.8 mg) in MeCN (4 mL) containing triethanolamine (TEOA, 1 mL) and **1**-R (0.25 μmol) or $Co(NO_3)_2{\cdot}6H_2O$ (1.0 μmol). This mixture was subjected to vacuum degassing and then back filling with pure CO_2 gas. This process was repeated three times, and after the last cycle, the flask was back filled with CO_2 (1 bar). The temperature of the reaction solution was maintained at 30 °C controlled by a flow of warm water during the reaction. Then, the system was irradiated with a 300 W Xenon lamp with a 420 nm cut-off filter under vigorous stirring. The produced gases (CO and H_2) were detected using a gas chromatograph equipped with a packed molecular sieves column (TDX-1 mesh 42/10); Argon was used as the carrier gas.

Supporting Information

Supporting Information File 1

Additional data.
[https://www.beilstein-journals.org/bjoc/content/supplementary/1860-5397-14-208-S1.pdf]

Acknowledgements

This work was financially supported by the National Key Technologies R & D Program of China (2018YFA0209301), the National Natural Science Foundation of China (21425309, 21761132002, and 21861130353), and the 111 Project.

ORCID® iDs

Jinshui Zhang - https://orcid.org/0000-0003-4649-6526
Sibo Wang - https://orcid.org/0000-0003-2656-9169

References

1. Garrido-Barros, P.; Gimbert-Suriñach, C.; Matheu, R.; Sala, X.; Llobet, A. *Chem. Soc. Rev.* **2017,** *46,* 6088–6098. doi:10.1039/C7CS00248C
2. Chu, S.; Majumdar, A. *Nature* **2012,** *488,* 294–303. doi:10.1038/nature11475
3. Wang, S.; Guan, B. Y.; Lu, Y.; Lou, X. W. D. *J. Am. Chem. Soc.* **2017,** *139,* 17305–17308. doi:10.1021/jacs.7b10733
4. Wang, S.; Wang, X. *Angew. Chem., Int. Ed.* **2016,** *55,* 2308–2320. doi:10.1002/anie.201507145
5. Wang, S.; Guan, B. Y.; Lou, X. W. D. *Energy Environ. Sci.* **2018,** *11,* 306–310. doi:10.1039/C7EE02934A

6. Wang, S.; Guan, B. Y.; Lou, X. W. D. *J. Am. Chem. Soc.* **2018,** *140,* 5037–5040. doi:10.1021/jacs.8b02200
7. Liu, Y.; Huang, B.; Xie, Z. *Appl. Surf. Sci.* **2018,** *427,* 693–701. doi:10.1016/j.apsusc.2017.08.098
8. Zhang, M.; Luo, Z.; Zhou, M.; Zhang, G.; Alamry, K. A.; Taib, L. A.; Asiri, A. M.; Wang, X. *Appl. Catal., B: Environ.* **2017,** *210,* 454–461. doi:10.1016/j.apcatb.2017.03.080
9. Kärkäs, M. D.; Verho, O.; Johnston, E. V.; Åkermark, B. *Chem. Rev.* **2014,** *114,* 11863–12001. doi:10.1021/cr400572f
10. Guo, F.; Hou, Y.; Asiri, A. M.; Wang, X. *Chem. Commun.* **2017,** *53,* 13221–13224. doi:10.1039/C7CC07805F
11. Zhang, G.; Lan, Z.-A.; Wang, X. *Chem. Sci.* **2017,** *8,* 5261–5274. doi:10.1039/C7SC01747B
12. Chen, L.; Gu, Q.; Hou, L.; Zhang, C.; Lu, Y.; Wang, X.; Long, J. *Catal. Sci. Technol.* **2017,** *7,* 2039–2049. doi:10.1039/C7CY00495H
13. Pang, A.; Sun, X.; Ruan, H.; Li, Y.; Dai, S.; Wei, M. *Nano Energy* **2014,** *5,* 82–90. doi:10.1016/j.nanoen.2014.02.007
14. Ran, J.; Zhang, J.; Yu, J.; Jaroniec, M.; Qiao, S. Z. *Chem. Soc. Rev.* **2014,** *43,* 7787–7812. doi:10.1039/C3CS60425J
15. Yang, J.; Wang, D.; Han, H.; Li, C. *Acc. Chem. Res.* **2013,** *46,* 1900–1909. doi:10.1021/ar300227e
16. Tachibana, Y.; Vayssieres, L.; Durrant, J. R. *Nat. Photonics* **2012,** *6,* 511–518. doi:10.1038/nphoton.2012.175
17. Sun, J.; Zhang, J.; Zhang, M.; Antonietti, M.; Fu, X.; Wang, X. *Nat. Commun.* **2012,** *3,* No. 1139. doi:10.1038/ncomms2152
18. Yang, P.; Wang, R.; Zhou, M.; Wang, X. *Angew. Chem., Int. Ed.* **2018,** *57,* 8674–8677. doi:10.1002/anie.201804996
19. Yang, P.; Ou, H.; Fang, Y.; Wang, X. *Angew. Chem., Int. Ed.* **2017,** *56,* 3992–3996. doi:10.1002/anie.201700286
20. Bonin, J.; Maurin, A.; Robert, M. *Coord. Chem. Rev.* **2017,** *334,* 184–198. doi:10.1016/j.ccr.2016.09.005
21. Wu, X.; Li, F.; Zhang, B.; Sun, L. *J. Photochem. Photobiol., C* **2015,** *25,* 71–89. doi:10.1016/j.jphotochemrev.2015.07.002
22. Nguyen, A. I.; Wang, J.; Levine, D. S.; Ziegler, M. S.; Tilley, T. D. *Chem. Sci.* **2017,** *8,* 4274–4284. doi:10.1039/C7SC00627F
23. Das, B.; Ezzedinloo, L.; Bhadbhade, M.; Bucknall, M. P.; Colbran, S. B. *Chem. Commun.* **2017,** *53,* 10006–10009. doi:10.1039/C7CC06294J
24. McAlpin, J. G.; Stich, T. A.; Ohlin, C. A.; Surendranath, Y.; Nocera, D. G.; Casey, W. H.; Britt, R. D. *J. Am. Chem. Soc.* **2011,** *133,* 15444–15452. doi:10.1021/ja202320q
25. Hodel, F. H.; Luber, S. *ACS Catal.* **2016,** *6,* 1505–1517. doi:10.1021/acscatal.5b02507
26. Nguyen, A. I.; Ziegler, M. S.; Oña-Burgos, P.; Sturzbecher-Hohne, M.; Kim, W.; Bellone, D. E.; Tilley, T. D. *J. Am. Chem. Soc.* **2015,** *137,* 12865–12872. doi:10.1021/jacs.5b08396
27. Li, X.; Siegbahn, P. E. M. *J. Am. Chem. Soc.* **2013,** *135,* 13804–13813. doi:10.1021/ja4053448
28. Song, F.; Moré, R.; Schilling, M.; Smolentsev, G.; Azzaroli, N.; Fox, T.; Luber, S.; Patzke, G. R. *J. Am. Chem. Soc.* **2017,** *139,* 14198–14208. doi:10.1021/jacs.7b07361
29. Bi, W.; Li, X.; Zhang, L.; Jin, T.; Zhang, L.; Zhang, Q.; Luo, Y.; Wu, C.; Xie, Y. *Nat. Commun.* **2015,** *6,* No. 8647. doi:10.1038/ncomms9647
30. Wang, Y.; Li, F.; Zhou, X.; Yu, F.; Du, J.; Bai, L.; Sun, L. *Angew. Chem., Int. Ed.* **2017,** *56,* 6911–6915. doi:10.1002/anie.201703039
31. Wang, Y.; Li, F.; Li, H.; Bai, L.; Sun, L. *Chem. Commun.* **2016,** *52,* 3050–3053. doi:10.1039/C5CC09588C
32. Schreier, M.; Luo, J.; Gao, P.; Moehl, T.; Mayer, M. T.; Grätzel, M. *J. Am. Chem. Soc.* **2016,** *138,* 1938–1946. doi:10.1021/jacs.5b12157
33. Zhang, B.; Li, F.; Yu, F.; Wang, X.; Zhou, X.; Li, H.; Jiang, Y.; Sun, L. *ACS Catal.* **2014,** *4,* 804–809. doi:10.1021/cs401109u
34. Azcarate, I.; Costentin, C.; Robert, M.; Savéant, J.-M. *J. Am. Chem. Soc.* **2016,** *138,* 16639–16644. doi:10.1021/jacs.6b07014
35. Smith, P. F.; Kaplan, C.; Sheats, J. E.; Robinson, D. M.; McCool, N. S.; Mezle, N.; Dismukes, G. C. *Inorg. Chem.* **2014,** *53,* 2113–2121. doi:10.1021/ic402720p
36. Blakemore, J. D.; Crabtree, R. H.; Brudvig, G. W. *Chem. Rev.* **2015,** *115,* 12974–13005. doi:10.1021/acs.chemrev.5b00122
37. Kang, P.; Chen, Z.; Nayak, A.; Zhang, S.; Meyer, T. J. *Energy Environ. Sci.* **2014,** *7,* 4007–4012. doi:10.1039/C4EE01904K
38. Duan, L.; Bozoglian, F.; Mandal, S.; Stewart, B.; Privalov, T.; Llobet, A.; Sun, L. *Nat. Chem.* **2012,** *4,* 418–423. doi:10.1038/nchem.1301
39. Chen, Z.; Concepcion, J. J.; Brennaman, M. K.; Kang, P.; Norris, M. R.; Hoertz, P. G.; Meyer, T. J. *Proc. Natl. Acad. Sci. U. S. A.* **2012,** *109,* 15606–15611. doi:10.1073/pnas.1203122109
40. Huang, H.; Lin, J.; Zhu, G.; Weng, Y.; Wang, X.; Fu, X.; Long, J. *Angew. Chem., Int. Ed.* **2016,** *55,* 8314–8318. doi:10.1002/anie.201602796
41. Han, X.-B.; Zhang, Z.-M.; Zhang, T.; Li, Y.-G.; Lin, W.; You, W.; Su, Z.-M.; Wang, E.-B. *J. Am. Chem. Soc.* **2014,** *136,* 5359–5366. doi:10.1021/ja412886e
42. Zhang, G.; Zhang, M.; Ye, X.; Qiu, X.; Lin, S.; Wang, X. *Adv. Mater.* **2014,** *26,* 805–809. doi:10.1002/adma.201303611
43. Zhang, J.; Zhang, G.; Chen, X.; Lin, S.; Möhlmann, L.; Dołęga, G.; Lipner, G.; Antonietti, M.; Blechert, S.; Wang, X. *Angew. Chem., Int. Ed.* **2012,** *51,* 3183–3187. doi:10.1002/anie.201106656
44. Artero, V.; Chavarot-Kerlidou, M.; Fontecave, M. *Angew. Chem., Int. Ed.* **2011,** *50,* 7238–7266. doi:10.1002/anie.201007987
45. Sartorel, A.; Bonchio, M.; Campagna, S.; Scandola, F. *Chem. Soc. Rev.* **2013,** *42,* 2262–2280. doi:10.1039/C2CS35287G
46. La Ganga, G.; Puntoriero, F.; Campagna, S.; Bazzan, I.; Berardi, S.; Bonchio, M.; Sartorel, A.; Natali, M.; Scandola, F. *Faraday Discuss.* **2012,** *155,* 177–190. doi:10.1039/C1FD00093D
47. Polarz, S.; Orlov, A. V.; van den Berg, M. W. E.; Driess, M. *Angew. Chem., Int. Ed.* **2005,** *44,* 7892–7896. doi:10.1002/anie.200501212
48. Berardi, S.; La Ganga, G.; Natali, M.; Bazzan, I.; Puntoriero, F.; Sartorel, A.; Scandola, F.; Campagna, S.; Bonchio, M. *J. Am. Chem. Soc.* **2012,** *134,* 11104–11107. doi:10.1021/ja303951z
49. Evangelisti, F.; Güttinger, R.; Moré, R.; Luber, S.; Patzke, G. R. *J. Am. Chem. Soc.* **2013,** *135,* 18734–18737. doi:10.1021/ja4098302
50. Yin, Q.; Tan, J. M.; Besson, C.; Geletii, Y. V.; Musaev, D. G.; Kuznetsov, A. E.; Luo, Z.; Hardcastle, K. I.; Hill, C. L. *Science* **2010,** *328,* 342–345. doi:10.1126/science.1185372
51. Wasylenko, D. J.; Ganesamoorthy, C.; Borau-Garcia, J.; Berlinguette, C. P. *Chem. Commun.* **2011,** *47,* 4249–4251. doi:10.1039/c0cc05522k
52. Dogutan, D. K.; McGuire, R., Jr.; Nocera, D. G. *J. Am. Chem. Soc.* **2011,** *133,* 9178–9180. doi:10.1021/ja202138m
53. Das, B. K.; Chakrabarty, R. *J. Chem. Sci.* **2011,** *123,* 163–173. doi:10.1007/s12039-011-0111-6
54. Chakrabarty, R.; Bora, S. J.; Das, B. K. *Inorg. Chem.* **2007,** *46,* 9450–9462. doi:10.1021/ic7011759
55. Chakrabarty, R.; Sarmah, P.; Saha, B.; Chakravorty, S.; Das, B. K. *Inorg. Chem.* **2009,** *48,* 6371–6379. doi:10.1021/ic802115n

56. Wang, X.; Maeda, K.; Thomas, A.; Takanabe, K.; Xin, G.; Carlsson, J. M.; Domen, K.; Antonietti, M. *Nat. Mater.* **2009,** *8,* 76–80. doi:10.1038/nmat2317
57. Wang, X.; Chen, X.; Thomas, A.; Fu, X.; Antonietti, M. *Adv. Mater.* **2009,** *21,* 1609–1612. doi:10.1002/adma.200802627
58. Lin, Z.; Wang, X. *Angew. Chem., Int. Ed.* **2013,** *52,* 1735–1738. doi:10.1002/anie.201209017
59. Zhang, J.; Zhang, M.; Sun, R.-Q.; Wang, X. *Angew. Chem., Int. Ed.* **2012,** *51,* 10145–10149. doi:10.1002/anie.201205333
60. Cui, Y.; Ding, Z.; Fu, X.; Wang, X. *Angew. Chem., Int. Ed.* **2012,** *51,* 11814–11818. doi:10.1002/anie.201206534
61. Lin, J.; Ding, Z.; Hou, Y.; Wang, X. *Sci. Rep.* **2013,** *3,* No. 1056. doi:10.1038/srep01056
62. Wang, S.; Yao, W.; Lin, J.; Ding, Z.; Wang, X. *Angew. Chem., Int. Ed.* **2014,** *53,* 1034–1038. doi:10.1002/anie.201309426
63. Wang, S.; Ding, Z.; Wang, X. *Chem. Commun.* **2015,** *51,* 1517–1519. doi:10.1039/C4CC07225A
64. Kuriki, R.; Matsunaga, H.; Nakashima, T.; Wada, K.; Yamakata, A.; Ishitani, O.; Maeda, K. *J. Am. Chem. Soc.* **2016,** *138,* 5159–5170. doi:10.1021/jacs.6b01997
65. Kuriki, R.; Yamamoto, M.; Higuchi, K.; Yamamoto, Y.; Akatsuka, M.; Lu, D.; Yagi, S.; Yoshida, T.; Ishitani, O.; Maeda, K. *Angew. Chem., Int. Ed.* **2017,** *56,* 4867–4871. doi:10.1002/anie.201701627
66. Kuriki, R.; Sekizawa, K.; Ishitani, O.; Maeda, K. *Angew. Chem., Int. Ed.* **2015,** *54,* 2406–2409. doi:10.1002/anie.201411170
67. Wang, S.; Hou, Y.; Wang, X. *ACS Appl. Mater. Interfaces* **2015,** *7,* 4327–4335. doi:10.1021/am508766s
68. Zhang, M.; Wang, X. *Energy Environ. Sci.* **2014,** *7,* 1902–1906. doi:10.1039/c3ee44189j
69. Zhang, G.; Zang, S.; Lin, L.; Lan, Z.-A.; Li, G.; Wang, X. *ACS Appl. Mater. Interfaces* **2016,** *8,* 2287–2296. doi:10.1021/acsami.5b11167
70. Lin, J.; Pan, Z.; Wang, X. *ACS Sustainable Chem. Eng.* **2014,** *2,* 353–358. doi:10.1021/sc4004295

License and Terms

BEILSTEIN JOURNAL OF ORGANIC CHEMISTRY

Microfluidic light-driven synthesis of tetracyclic molecular architectures

Javier Mateos, Nicholas Meneghini, Marcella Bonchio, Nadia Marino, Tommaso Carofiglio, Xavier Companyó* and Luca Dell'Amico*

Letter

Open Access

Address:
Dipartimento di Scienze Chimiche and ITM-CNR UoS of Padova, Università di Padova, Via Marzolo 1, 35131 Padova, Italy

Email:
Xavier Companyó* - xavier.companyo@unipd.it; Luca Dell'Amico* - luca.dellamico@unipd.it

* Corresponding author

Keywords:
[4 + 2] photoenol; cycloaddition; flow chemistry; microfluidic photoreactor; photoredox catalysis; synthetic photochemistry

Beilstein J. Org. Chem. **2018,** *14,* 2418–2424.
doi:10.3762/bjoc.14.219

Received: 26 June 2018
Accepted: 31 August 2018
Published: 17 September 2018

This article is part of the thematic issue "Photoredox catalysis for novel organic reactions".

Guest Editor: P. H. Seeberger

Abstract

Herein we report an effective synthetic method for the direct assembly of highly functionalized tetracyclic pharmacophoric cores. Coumarins and chromones undergo diastereoselective [4 + 2] cycloaddition reactions with light-generated photoenol intermediates. The reactions occur by aid of a microfluidic photoreactor (MFP) in high yield (up to >98%) and virtually complete diastereocontrol (>20:1 dr). The method is easily scaled-up to a parallel setup, furnishing 948 mg of product over a 14 h reaction time. Finally, a series of manipulations of the tetracyclic scaffold obtained gave access to valuable precursors of biologically active molecules.

Introduction

In recent years synthetic photochemistry has become highly sophisticated [1]. The opportunity of using renewable energy sources to transform and functionalize organic molecules is receiving considerable interest from the scientific community [2]. Thus, innovative light-driven metal-free synthetic methods have been successfully developed [3]. More recently, the microfluidic photoreactor (MFP) technology has revealed to be a key technology applicable for diverse photochemical processes [4]. Microfluidic photoreactions allow an increased light penetration and surface-to-volume ratio together with a more uniform and effective irradiation of the reaction system [5], thus resulting in highly improved synthetic performances compared to the classical batch conditions. Recently, light-driven reactions of 2-methylbenzophenone (2-MBP) were reported to proceed smoothly under a MFP setup, furnishing highly diversified molecular scaffolds with enhanced yields and selectivities [6]. The chemistry is based on the ability of 2-MBP derivatives **A** of generating, upon light-irradiation, the highly reactive photoenol intermediate **A'** [7] and trapping of the latter by a competent electron-deficient reaction partner (Figure 1). The synthetic approach is not only restricted to electron-poor dienophiles such as maleimides **B** (see Figure 1a), but has also been imple-

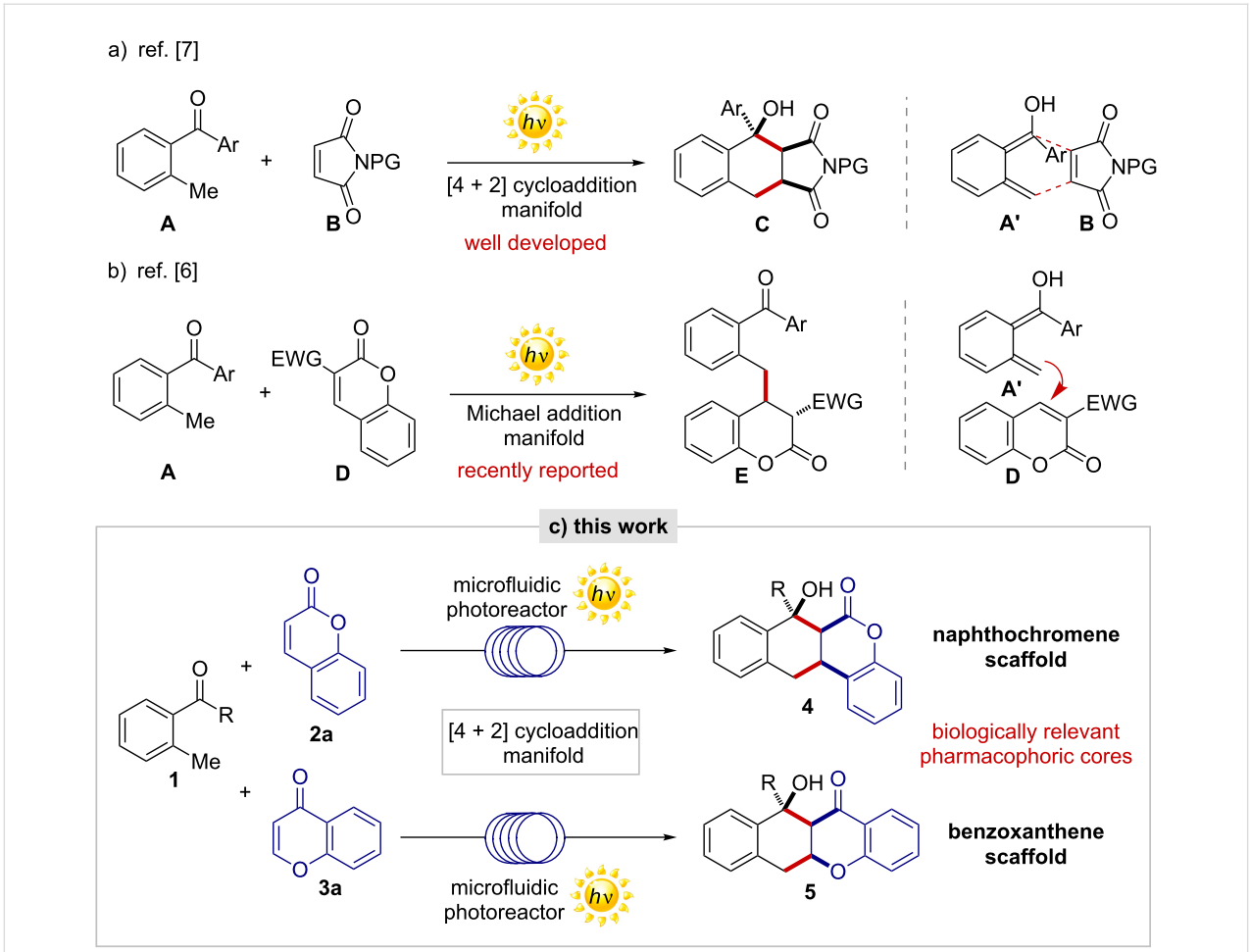

Figure 1: a) Light-driven reaction between 2-MBP **A** and maleimide **B** for the synthesis of **C** through a [4 + 2] cycloaddition manifold. b) Light-driven reaction between 2-MBP **A** and 3-substituted coumarin **D** for the synthesis of **E** through a Michael addition manifold. c) Light-driven reaction between 2-MBPs **1** and coumarin (**2a**) or chromone (**3a**) for the synthesis of privileged tetracyclic scaffolds **4** or **5**.

mented different reaction partners, allowing the light-promoted construction of biologically active natural products [8]. With this aim, electron-deficient chromophores, such as 3-coumarin-carboxylates **D**, have been used as competent reaction partners of 2-MBPs **A**, furnishing 3-benzylated chromanones **E** through a Michael addition pathway (see Figure 1b) [6].

Prompted by the interest of developing novel light-driven microfluidic methods for the construction of biologically relevant molecular scaffolds, we investigated the reaction between MBP **1** and 3-unsubstituted coumarin (**2a**) and chromone (**3a**, Figure 1c). It was anticipated that the successful development of these photoreactions would generate valuable privileged scaffolds, namely, naphthochromenones **4** and benzoxanthenes **5**, through a diastereoselective light-driven [4 + 2] cycloaddition reaction. Interestingly, the tetracyclic scaffolds **4** and **5** are embodied in different biologically active molecules, with diverse pharmacological activities [9]. To the best of our knowledge, diastereoselective methods for the direct construction of naphthochromenone **4** are still missing. On the other hand, the reported construction of the benzoxanthene scaffold **5** relies on the use of harsh reaction conditions (e.g., 250 °C), leading to a mixture of regio- and diastereoisomers in moderate yields [10]. Hence, the development of an efficient synthetic method to access these privileged motifs still represents an open task in synthetic chemistry.

The method presented herein is suited for a broad range of coumarins **2** and chromones **3**, used as precursors for the direct generation of the tetracyclic scaffold **4** and **5**, with high synthetic performances (up to >98% yield) and complete diastereocontrol (>20:1). Additionally, manipulations of the naphthochromenone scaffold **4** give access to highly diversified molecular architectures, which are valuable intermediates in the synthesis of different biologically active molecules [11]. Noteworthy, the photoreactions presented herein do not proceed

under conventional batch conditions, thus highlighting the importance of the MFP method enabling novel light-driven synthetic transformations.

Results and Discussion

The reaction between 2-methylbenzophenone (**1a**) and coumarin (**2a**) was initially screened in a MFP of 1000 µL volume, using 1.5 equiv of **1a** and a residence time of 26.6 min (Table 1 and Table S3 in the Supporting Information File 1). Under these reaction conditions, product **4a** formed in 57% yield as a single detectable diastereoisomer with a production of 0.077 mmol·h^{-1} (entry 1 in Table 1). For comparison, in entry 2 of Table 1 are reported the reaction conditions previously described for the synthesis of **4a** [6]. Interestingly, a higher MFP volume resulted in a higher productivity: 0.077 mmol·h^{-1} vs 0.063 mmol·h^{-1} (entry 1 vs entry 2, Table 1). Reversing the reagents ratio, i.e., using a slight excess of coumarin (**2a**), turned out to be highly beneficial, giving the cyclized product **4a** in 77% yield (Table 1, entry 3). Notably, the optimal reaction conditions for the light-driven [4 + 2] cycloaddition were achieved within a 1000 µL MFP with a residence time set at 35 min forming product **4a** in quantitative yield, complete diastereocontrol and a productivity of 0.104 mmol·h^{-1} (Table 1, entry 4). On the contrary, when the same reaction was performed under batch conditions, the expected [4 + 2] cycloaddition product **4a** was only formed in trace amounts along with extensive product decomposition (Table 1, entry 5). The enhanced reactivity under the MFP compared to the batch setup (Table 1, entry 4 vs entry 5) is attributed to the more efficient illumination and the shorter irradiation time within the MFP [6], thus successfully preventing the light-promoted product decomposition [12]. In fact, the irradiation for 8 h of an authentic sample of **4a** resulted in the formation of a series of undefined decomposition products. Control experiments showed that in the absence of light irradiation, the cyclization product was not detected (Table 1, entry 6), confirming the photochemical nature of the present reaction.

With the optimal reaction conditions in hand we next explored the generality and limitations of the photochemical transformation (Figure 2). First, different substitutions on the 2-MBP scaffold were evaluated. Electron-donating substituents on both aromatic rings gave excellent results, furnishing the corresponding naphthochromenones **4b** and **4c** as single detectable diastereoisomers (>20:1 dr), with yields spanning from 53% to 83% and short residence times (35 min). On the contrary, electron-withdrawing substituents resulted in inferior synthetic performances. Compounds **4d** and **4e** were isolated in 44% and 40%, respectively within 60 min. The optimized reaction conditions were also amenable to diverse coumarin scaffolds. Six and 7-substituted coumarins furnished the corresponding cyclic products **4f–h** in moderate to excellent yields (41 to >98%) in a pure diastereoisomeric form. As a limitation of the present microfluidic photochemical method, thioxocoumarin **2e** showed poor reac-

Table 1: Light-driven reaction between 2-methylbenzophenone (**1a**) and coumarin (**2a**); selected optimization results.

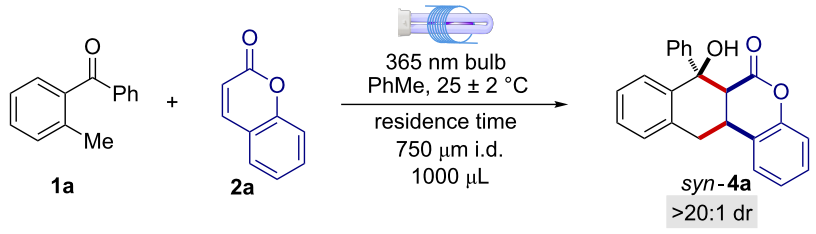

entry[a]	residence time (min)	reactor volume (µL)	reagent ratio (**1a**:**2a**)	yield	production (mmol·h^{-1})
1	26.6	1000	1.5:1	57	0.077
2[b]	26.6	400	1.5:1	70[c]	0.063
3	26.6	1000	1:3	77	0.104
4	35	1000	1:5	>98%[c]	0.104
5[d,e]	480	1000	1:5	–	–
6[f]	35	1000	1:5	–	–

[a]Unless otherwise noted, reaction conditions were as follows: a degassed solution of **1a** and **2a** in toluene (0.06 M) was irradiated for the indicated time at 25 ± 2 °C (see Supporting Information File 1 for details). All yields refer to NMR yields using trimethoxybenzene as the internal standard. The dr was inferred by ^{1}H NMR analysis on the crude reaction mixture and in all the cases resulted >20:1. [b]Reaction conditions as described in [6]. [c]Isolated yield. [d]Reaction performed in batch. [e]Extensive decomposition of both starting reagents **1a** and **2a** was observed by ^{1}H NMR analysis of the crude reaction mixture. [f]Reaction performed under MFP setup in the absence of light. i.d. = internal diameter.

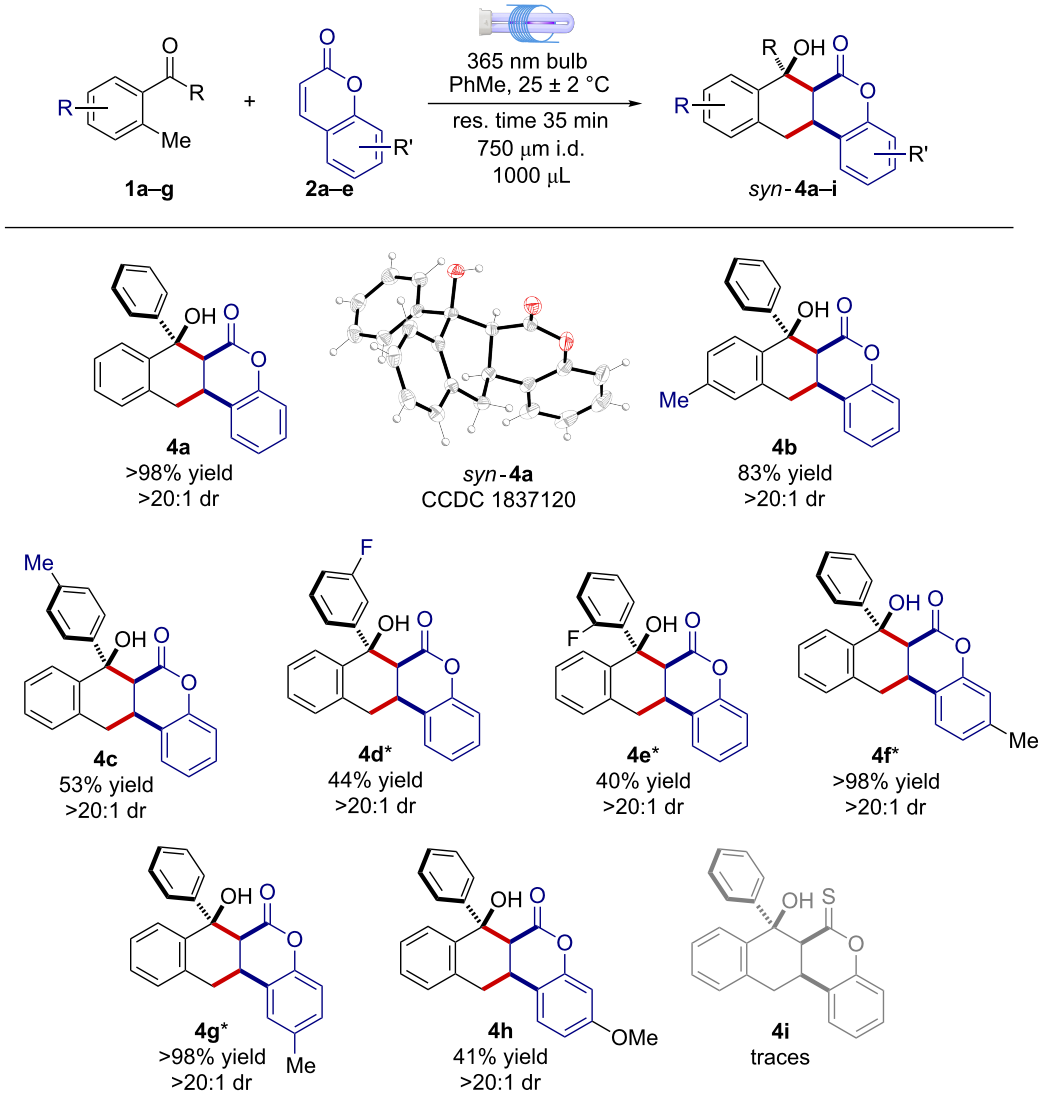

Figure 2: Generality and limits of the light-driven [4 + 2] cyclization reaction between 2-MBP **1a–g** and coumarins **2a–c** under MFP setup. *Residence time was 60 min.

tivity under the titled reaction conditions, producing only traces of the expected sulfur-containing adduct **4i**. As a matter of fact, compound **2e** showed a high tendency to undergo a light-promoted [2 + 2] dimerization reaction, thus preventing the envisaged [4 + 2] cycloaddition pathway [13].

Next, the chromone scaffold **3a**, which is a precursor of diverse classes of biologically active molecules [14], was evaluated under the developed MFP setup. Notably, the [4 + 2] cycloaddition product **5a** formed in 72% yield and >20:1 dr, without the need of further condition adjustments. The relative *syn* configuration within **5a** was inferred by 2D-NOESY experiments and confirmed by X-ray analysis of a suitable single crystal (Figure 3). Noteworthy, different 2-MBPs bearing electron-donating or electron-withdrawing groups underwent the light-driven [4 + 2] cycloaddition, affording the corresponding tetracyclic products **5b–f** with high dr and in good yields spanning from 41% to 72% (Figure 3).

In order to demonstrate the easy scalability of the present method (Scheme 1) two MFPs were used in a parallel setup producing 948 mg of **4a** after 14 h with an overall productivity rate of 0.196 mmol·h^{-1} [15]. Subsequently, a series of manipulations were conducted on product **4a**. Its treatment with a solution of sodium hydroxide in water promoted a quantitative lactone-opening/decarboxylation cascade sequence, yielding 2,4-dihydronaphthalene **6a** in quantitative yield without the need of chromatographic purification. Interestingly, scaffold **6a**

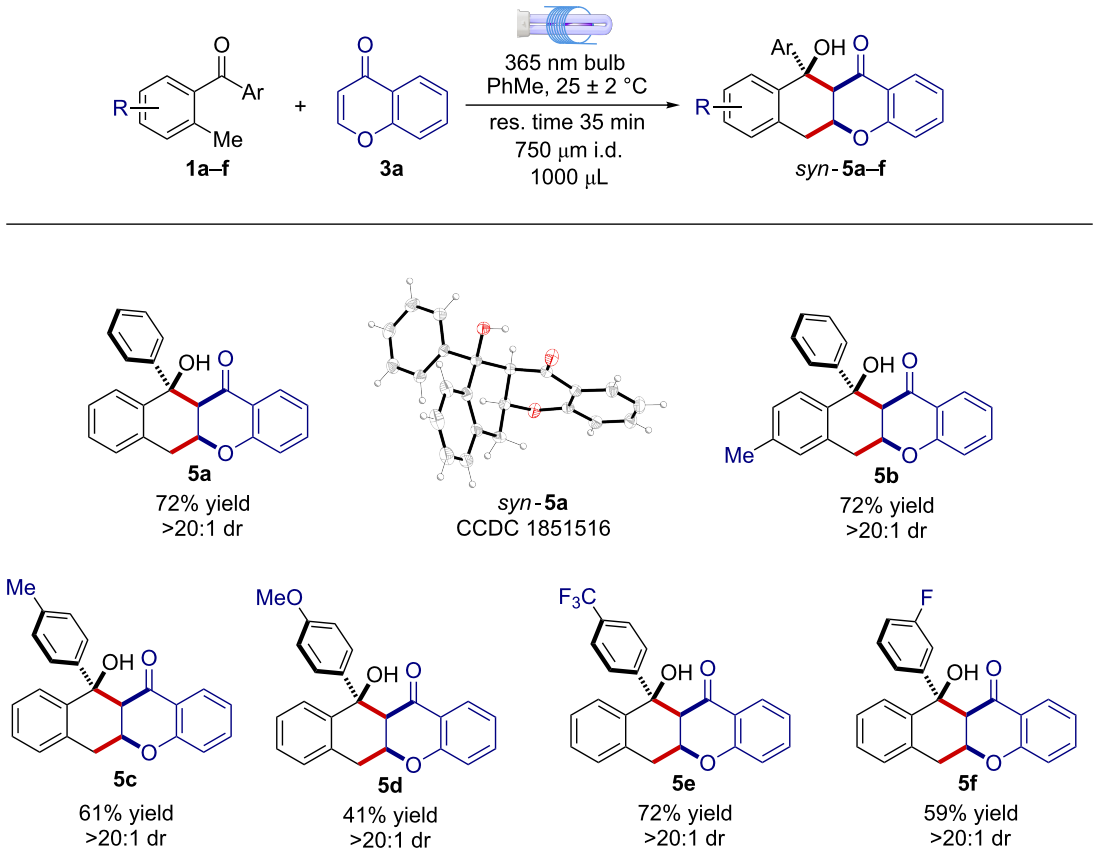

Figure 3: Generality and limits of the light-driven [4 + 2] cyclization reaction between 2-MBP **1a–f** and chromone (**3a**) under MFP setup.

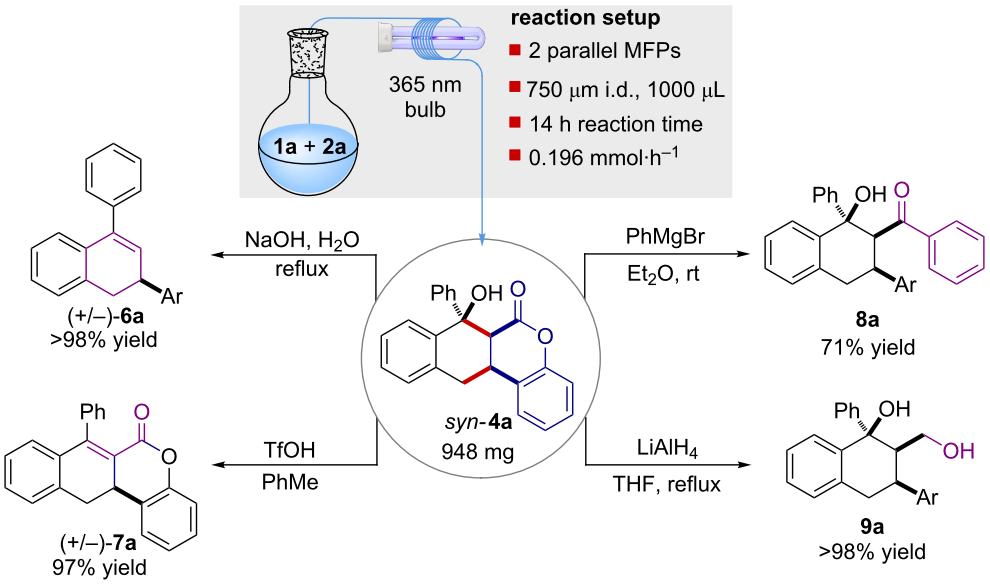

Scheme 1: MFP parallel setup for higher scale production of **4a** (top) and different molecular scaffolds **6a–9a** accessible after simple manipulation (Ar = *o*-OH-C_6H_4).

is a valuable intermediate for the synthesis of biologically active natural compounds [16] and industrially relevant drugs [17] reminiscent of the bioactive tetralinolic pharmacophore core [18].

Acidic treatment of **4a** generated, after a simple extraction, the corresponding α,β-unsaturated compound **7a** in 97% yield. A further manipulation involved the treatment of **4a** with PhMgBr, converting the lactone moiety into the corresponding aromatic ketone. Product **8a** formed in 71% yield without diastereoisomeric loss. Finally, $LiAlH_4$ reduction of **4a** furnished the bicyclic 1,3-diol **9a** in quantitative yield, again without the need of chromatographic purification. Noteworthy, compounds **6a**–**9a** embody different functionalities suitable for additional synthetic transformations.

Conclusion

In conclusion we have developed an effective light-driven microfluidic method for the synthesis of valuable tetracyclic molecular architectures using commercially available precursors and a common 365 nm bulb. The reaction does not proceed under conventional batch conditions, highlighting the essential role of the developed MFP. A wide series of naphthochromenones and benzoxanthenes were synthesized in high yields and excellent diastereoselectivity. Finally, the large-scale production and subsequent manipulations of product **4a** demonstrated the high synthetic potential of the present MFP method, which is well-suited for the construction of diverse biologically active molecules.

Supporting Information

Supporting Information File 1

Experimental procedures, characterization data for products **4a**–**h**, **5a**–**f** and **6a**–**9a**, NMR spectra, and CIF files for CCDC 1837120 and CCDC 1851516.
[https://www.beilstein-journals.org/bjoc/content/supplementary/1860-5397-14-219-S1.pdf]

Acknowledgements

L.D. thanks the CariParo Foundation for the AMYCORES starting grant 2015. X.C. thanks the University of Padova for the GREEN C-C STARS starting grant 2017. Andrea Rossa and Stefano Mercanzin are gratefully acknowledged for technical assistance.

ORCID® iDs

Javier Mateos - https://orcid.org/0000-0002-2358-9183
Nicholas Meneghini - https://orcid.org/0000-0003-1199-5624
Marcella Bonchio - https://orcid.org/0000-0002-7445-0296
Nadia Marino - https://orcid.org/0000-0002-7038-9715
Tommaso Carofiglio - https://orcid.org/0000-0002-4648-1458
Xavier Companyó - https://orcid.org/0000-0001-8969-7315
Luca Dell'Amico - https://orcid.org/0000-0003-0423-9628

References

1. Ravelli, D.; Protti, S.; Fagnoni, M. *Chem. Rev.* **2016,** *116,* 9850–9913. doi:10.1021/acs.chemrev.5b00662
See for a review.
2. Shaw, M. H.; Twilton, J.; MacMillan, D. W. C. *J. Org. Chem.* **2016,** *81,* 6898–6926. doi:10.1021/acs.joc.6b01449
3. Zou, Y.-Q.; Hörmann, F. M.; Bach, T. *Chem. Soc. Rev.* **2018,** *47,* 278–290. doi:10.1039/C7CS00509A
4. Cambié, D.; Bottecchia, C.; Straathof, N. J. W.; Hessel, V.; Noël, T. *Chem. Rev.* **2016,** *116,* 10276–10341. doi:10.1021/acs.chemrev.5b00707
5. Su, Y.; Straathof, N. J. W.; Hessel, V.; Noël, T. *Chem. – Eur. J.* **2014,** *20,* 10562–10589. doi:10.1002/chem.201400283
6. Mateos, J.; Cherubini-Celli, A.; Carofiglio, T.; Bonchio, M.; Marino, N.; Companyó, X.; Dell'Amico, L. *Chem. Commun.* **2018,** *54,* 6820–6823. doi:10.1039/C8CC01373J
7. Sammes, P. G. *Tetrahedron* **1976,** *32,* 405–422. doi:10.1016/0040-4020(76)80055-5
8. Nicolaou, K. C.; Gray, D.; Tae, J. *Angew. Chem., Int. Ed.* **2001,** *40,* 3675–3678. doi:10.1002/1521-3773(20011001)40:19<3675::AID-ANIE3675>3.0.CO;2-G
9. Wright, P. M.; Seiple, I. B.; Myers, A. G. *Angew. Chem., Int. Ed.* **2014,** *53,* 8840–8869. doi:10.1002/anie.201310843
10. Sandulache, A.; Silva, A. M. S.; Cavaleiro, J. A. S. *Tetrahedron* **2002,** *58,* 105–114. doi:10.1016/S0040-4020(01)01131-0
11. Allred, T. K.; Manoni, F.; Harran, P. G. *Chem. Rev.* **2017,** *117,* 11994–12051. doi:10.1021/acs.chemrev.7b00126
12. The batch reaction was performed using the same light source employed for the MFP setup and stopped at different reaction times. When the batch reaction was stopped at short reaction time (e.g., 2 h) the product **4a** was only detected in low amount (<10%) along with recovery of the unreacted starting material **1a** and **2a**. At longer reaction time (e.g., 8 h) decomposition products were detected by ^{1}H NMR analysis of the crude reaction mixture. See Supporting Information File 1 for details.
13. ^{1}H NMR analysis of the crude reaction mixture collected after 30 min residence time under the MFP setup, showed a large amount of the [2 + 2] dimerization side product of **2e** (57% conversion with respect to **2e**). Other coumarins **2a**–**c** showed inferior conversion to the corresponding dimerization side product (10–20%).
14. Bauvois, B.; Puiffe, M.-L.; Bongui, J.-B.; Paillat, S.; Monneret, C.; Dauzonne, D. *J. Med. Chem.* **2003,** *46,* 3900–3910. doi:10.1021/jm021109f
15. Su, Y.; Kuijpers, K.; Hessel, V.; Noël, T. *React. Chem. Eng.* **2016,** *1,* 73–81. doi:10.1039/C5RE00021A
16. Lantaño, B.; Aguirre, J. M.; Drago, E. V.; de la Faba, D. J.; Pomilio, N.; Mufato, J. D. *Magn. Reson. Chem.* **2017,** *55,* 619–633. doi:10.1002/mrc.4564
17. Sook, O.; Jang, B. S. *Arch. Pharmacal Res.* **1995,** *18,* 277–281.
18. Hanaya, K.; Onodera, S.; Ikegami, Y.; Kudo, H.; Shimaya, K. *J. Chem. Soc., Perkin Trans. 2* **1981,** 944–947. doi:10.1039/p29810000944

BEILSTEIN JOURNAL OF ORGANIC CHEMISTRY

Synthesis of aryl sulfides via radical–radical cross coupling of electron-rich arenes using visible light photoredox catalysis

Amrita Das, Mitasree Maity, Simon Malcherek, Burkhard König* and Julia Rehbein*

Full Research Paper

Open Access

Address:
Department of Chemistry and Pharmacy, Institute of Organic Chemistry, University of Regensburg, Universitätsstraße 31, 93053 Regensburg, Germany

Email:
Burkhard König* - Burkhard.Koenig@chemie.uni-regensburg.de;
Julia Rehbein* - Julia.Rehbein@chemie.uni-regensburg.de

* Corresponding author

Keywords:
arenes; oxidation; photocatalysis; thiolation; visible light

Beilstein J. Org. Chem. **2018,** *14,* 2520–2528.
doi:10.3762/bjoc.14.228

Received: 02 July 2018
Accepted: 18 September 2018
Published: 27 September 2018

This article is part of the thematic issue "Photoredox catalysis for novel organic reactions".

Guest Editor: P. H. Seeberger

Abstract

Electron-rich arenes react with aryl and alkyl disulfides in the presence of catalytic amounts of $[Ir(dF(CF_3)ppy)_2(dtbpy)]PF_6$ and $(NH_4)_2S_2O_8$ under blue light irradiation to yield arylthiols. The reaction proceeds at room temperature and avoids the use of prefunctionalized arenes. Experimental evidence suggests a radical–radical cross coupling mechanism.

Introduction

The generation of carbon–sulfur bonds is an important task in organic synthesis, because of their abundance in target structures, such as natural products and drugs [1-3]. They are found in organic semiconductors, antidepressant or antileukotriene agents (Figure 1). Three of the five most selling drugs in 2015 were organosulfur compounds. The majority of methods for C–S bond synthesis use transition metal-catalyzed cross coupling of thiols and their derivatives with organohalides [4-6], arylboronic acids [7], aryl triflates [8], and diazonium salts [9]. Typical metals used are palladium [10-13], copper [14-21], nickel [22-24], iron [25-29], cobalt [30-32], and rhodium [33,34]. Aryl sulfides are also synthesized by cross coupling of thiols and aryl Grignard/arylzinc reagents [35,36]. However, most of these methods require harsh reaction conditions, external additives and high temperatures. The reactions need prefunctionalized arenes, while a direct C–S sulfenylation by C–H functionalization would be more desirable and cost effective. So far, only a few reports on direct C–H functionalization using transition metals or metal free [37-39] conditions and different sources of sulfur, for example arylsulfonyl chlorides, sodium arylsulfinates, sulfinic acids and arylsulfonyl hydrazides have been reported (Scheme 1). However, the protocols require prefunctionalized sulfenylating reagents. Recently Lei and co-workers reported a DDQ-mediated selective radical–radical cross coupling between electron-rich arenes and thiols [40]. Miyake et al. reported the visible light-promoted cross-cou-

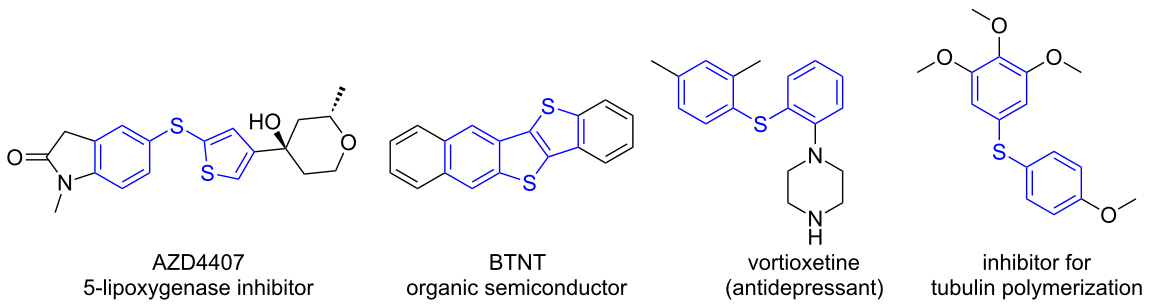

Figure 1: Selected examples of sulfenylated heterocycles used in pharmaceuticals and material chemistry.

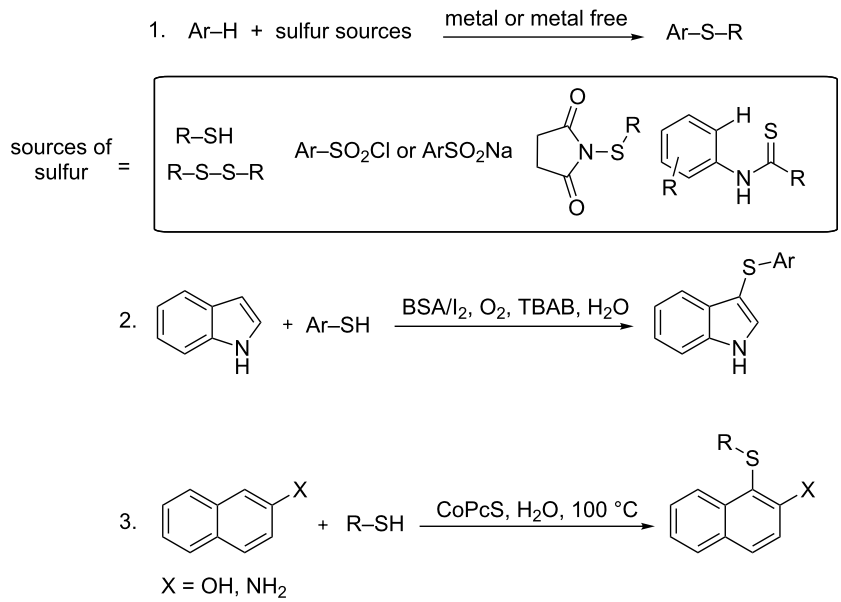

Scheme 1: Synthetic routes to organosulfur compounds.

pling reaction between aryl halides and arylthiols via an intermolecular charge transfer using Cs_2CO_3 as base [41]. Two recent reports showed the synthesis of C-3 sulfenylated indoles and 3-sulfenylimidazopyridine via C–H functionalization using Rose Bengal as photocatalyst [42,43]. In general, the arylation reactions use the reductive cycle of the photocatalyst and for this, electron poor arenes are required. In this article, we report the development of a mild and efficient oxidative photocatalytic method of thiolation of electron-rich di- and trimethoxybenzene arenes with aryl disulfides and $(NH_4)_2S_2O_8$ as terminal oxidant (Scheme 2).

Results and Discussion

1,2,4-Trimethoxybenzene and diphenyl disulfide were employed as the model substrates to test our proposal and to optimize the reaction conditions. Our developed photocatalytic method allows the activation of electron-rich alkoxyarenes for the direct C–H sulfenylation reaction using visible light and $[Ir(dF(CF_3)ppy)_2(dtbpy)]PF_6$ as the photocatalyst. The reaction was carried out under nitrogen under visible-light irradiation at 455 nm. The oxidation potential of this test arene is 1.02 V vs SCE, which allows oxidation by $[Ir(dF(CF_3)ppy)_2(dtbpy)]PF_6$ having an estimated excited state oxidation potential of 1.21 V vs SCE. Other photocatalysts like $Ru(bpy)_3Cl_2$, $Ru(bpz)_3PF_6$, DDQ, acridinium dyes, Eosin Y, Eosin Y disodium salt and 4-CzIPN were evaluated, but under our reaction conditions either low substrate conversion or the degradation of the photocatalyst was observed (see Supporting Information File 1, Table S1). The organic dye 9-mesityl-10-phenylacridinium tetrafluoroborate completely decomposed in the presence of excess disulfide within 30 minutes of irradiation. $[Ir(dF(CF_3)ppy)_2(dtbpy)]PF_6$ was found to be the best photocatalyst and in this case, CH_3CN was the best solvent compared to DMF, DMSO and DCE. When thiophenol was used as the

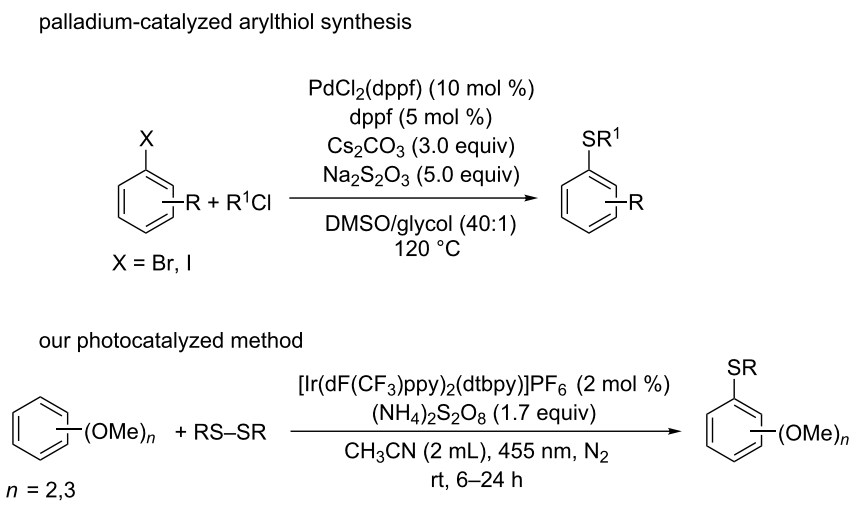

Scheme 2: Aryl sulfide synthesis.

sulfur source, diphenyl disulfide was obtained as a major side product, which in turn hindered the arylation process and resulted in several other oxidized products of thiophenol. So, the readily available diphenyl disulfide was added as the thiolating agent. Addition of excess disulfide (e.g., 5 equivalents) resulted in the formation of thiophenol as a major side product along with other oxidized sulfur species. The amount of disulfide was varied from 0.5 equivalents to five equivalents; 1.7 equivalents of disulfide gave the best result. The photocatalytic reaction was very slow when air was used as an oxidant, also it led to various oxidation products of the sulfur and the degradation of the photocatalyst was observed upon irradiation. Therefore, $(NH_4)_2S_2O_8$ was used as terminal oxidant. The addition of *tert*-butyl hydroperoxide (TBHP) as an oxidant led to degradation of the reaction mixture, also when nitrobenzene ($PhNO_2$) was used as oxidant, trace amounts of product were observed along with the formation of aniline, likely arising from the regeneration of the catalyst. Control experiments confirmed that light and photocatalyst were essential for the arylation reaction (see Supporting Information File 1, Table S2). With these conditions in hand, electron rich di- and trimethoxyarenes were reacted. The reactions were complete within 6 to 24 hours and the products were obtained in moderate yields. The best yield of 85% was observed when the electron-rich bis(4-methoxyphenyl) disulfide was employed as the thiolating agent (**3h**). With symmetrical arenes, diarylation was observed. The initially formed mono-arylated product is more reactive than the starting material and reacts to the diarylthiol product. When 1-phenyl-1*H*-pyrrole-2,5-dione was employed as the arene, the sulfenylation occurred exclusively at the double bond instead at the arene to give the product **3k** in 58% yield and a trace amount of diarylation product of the aromatic ring. When the more difficult to oxidize 2-methoxynaphthalene was used as substrate, the product **3l** was obtained in only 30% yield indicating the limit of the scope of the method. The substrate scope is shown in Scheme 3. The structures of compounds **3a**, **3d**, **3e** and **3i** in the solid state were determined by X-ray structure analysis (Figure 2).

We performed various control experiments to support the proposed reaction mechanism, which is shown in Scheme 4. Two equivalents of 2,2,6,6-tetramethylpiperidyl-1-oxyl (TEMPO), a radical scavenger were added to 1,2,4-trimethoxybenzene (Scheme 4a), in the presence of $[Ir(dF(CF_3)ppy)_2(dtbpy)]PF_6$, ammonium thiosulfate and 455 nm LED irradiation. The reaction mixture was analyzed by mass spectrometry, which showed the molecular ion indicating the formation of the proposed TEMPO adduct with the arene radical intermediate. Also, when diphenyl disulfide was irradiated with TEMPO in the presence and absence of the photocatalyst, (Scheme 4b and Scheme 4c) the adduct 2,2,6,6-tetramethyl-1-((phenylthio)oxy)piperidine was obtained in both cases. See Supporting Information File 1 for the HRMS analysis of the TEMPO adduct. These radical trapping experiments show that initially a radical cation of the arene is formed by the excited photocatalyst, which then is trapped by the radical scavenger TEMPO. S–S bond cleavage has been reported for alkyl and aryl disulfides in an oxidative [44-46] and triplet sensitized mechanism [47]. It is also well known in literature that aromatic disulfides are cleaved homolytically under UV irradiation yielding the corresponding radicals [48]. A recent study from Nicewicz showed that an aryl disulfide could be cleaved by irradiation with visible light [49].

Some spectroscopic investigations (Figure 3) gave valuable information about the mechanism of the photoredox catalytic cycle. The luminescence intensity of $[Ir(dF(CF_3)ppy)_2(dtbpy)]$-

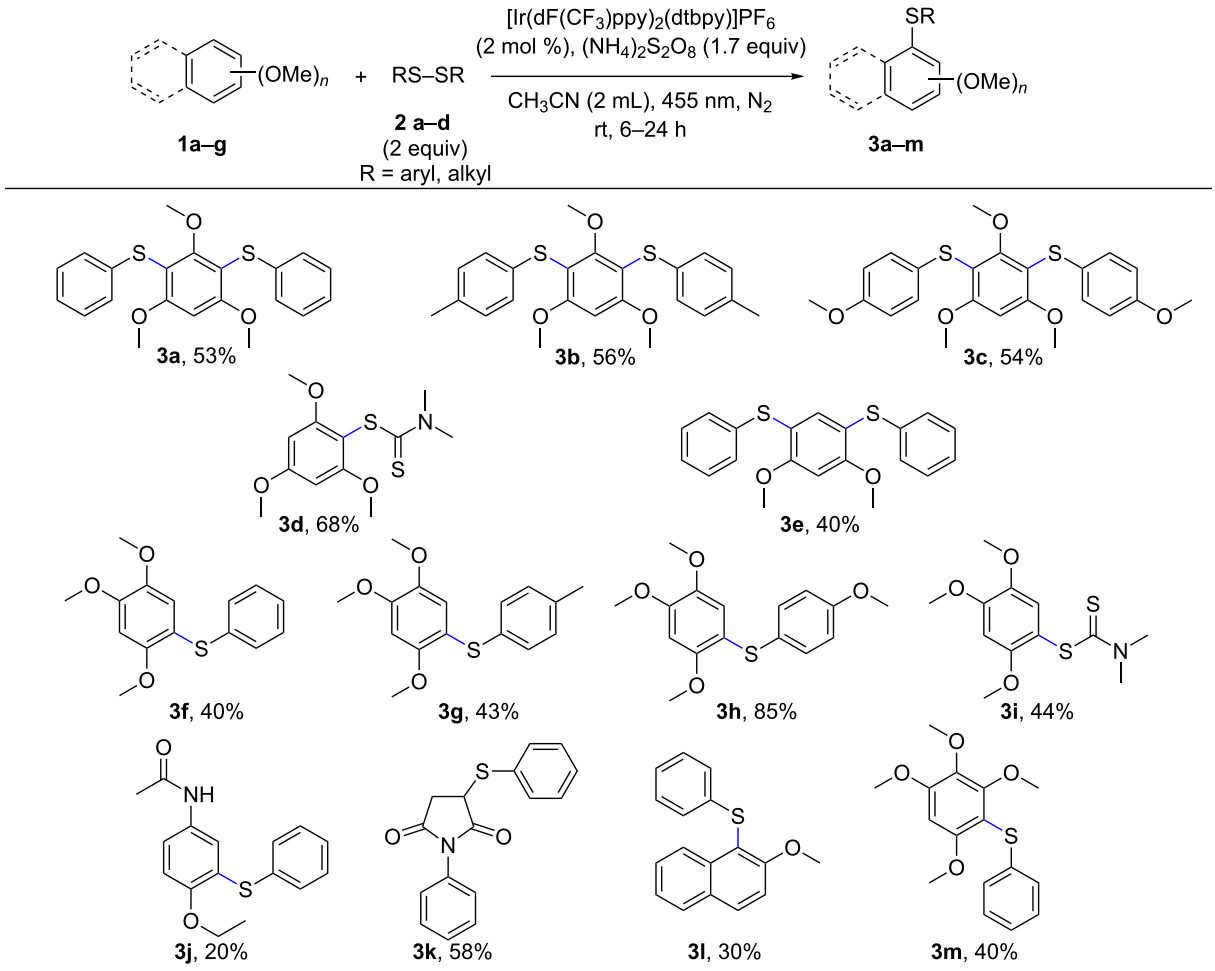

Scheme 3: Substrate scope for arylthiol syntheses. The reaction was performed with **1a–g** (0.1 mmol) and **2a–d** (2 equiv), $(NH_4)_2S_2O_8$ (1.7 equiv) and $[Ir(dF(CF_3)ppy)_2(dtbpy)]PF_6$ (2 mol %) in 2 mL CH_3CN. For reaction times see Supporting Information File 1.

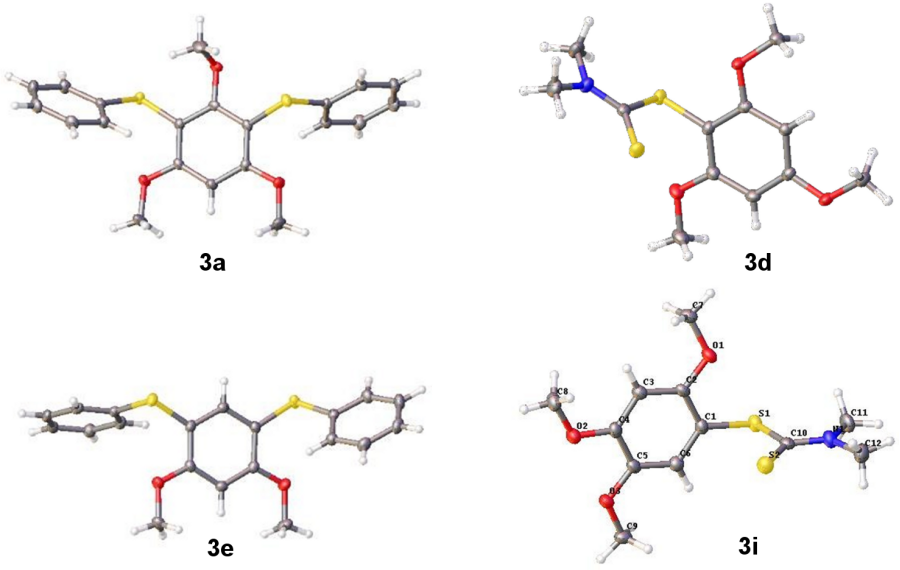

Figure 2: Crystal structures of compounds **3a**, **3d**, **3e** and **3i**.

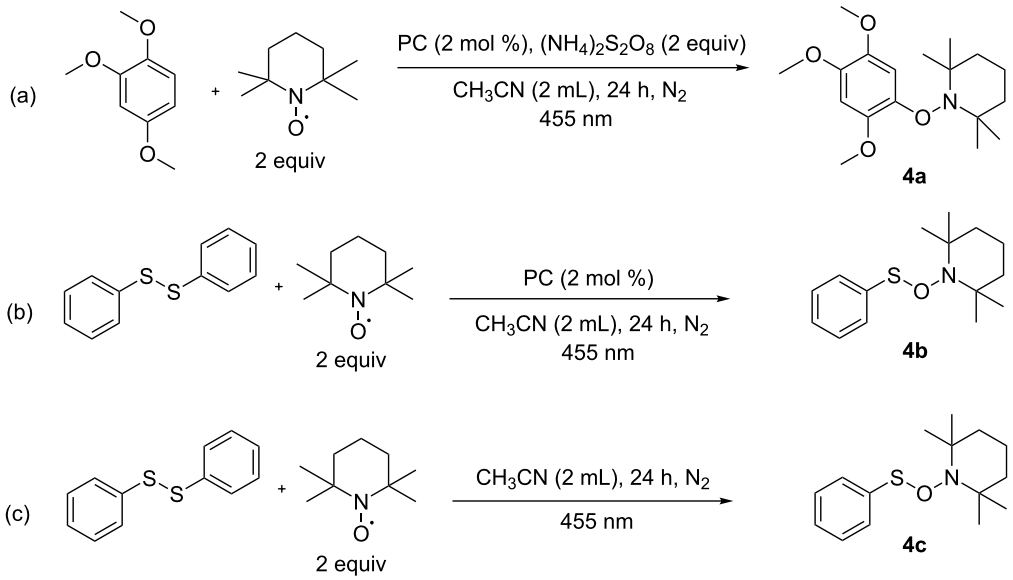

Scheme 4: Radical trapping experiments.

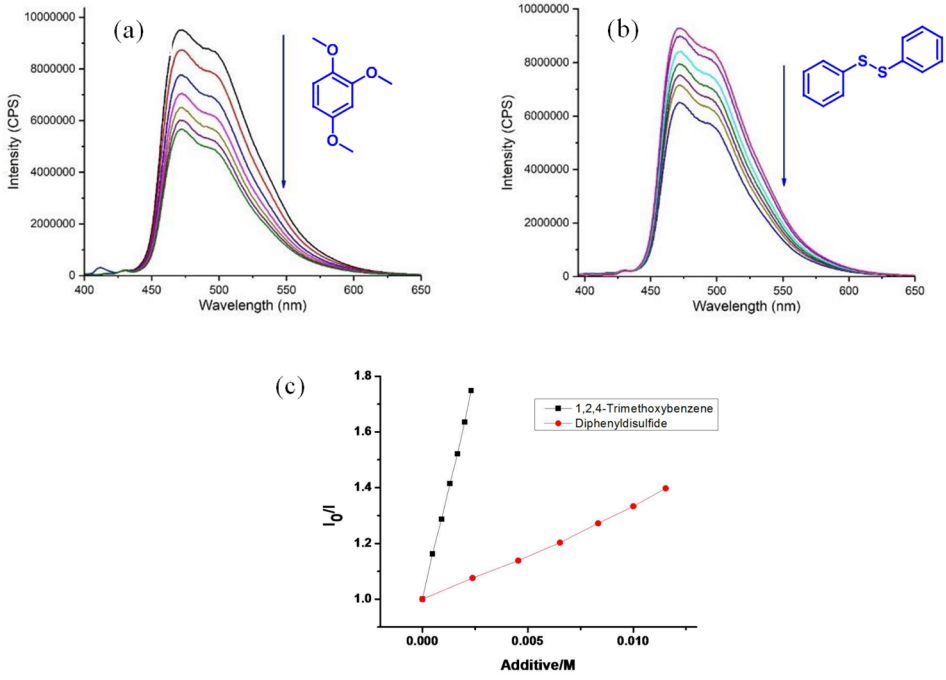

Figure 3: (a) Changes in the fluorescence spectra (in this case intensity, λ_{Ex} = 455 nm) of $[Ir(dF(CF_3)ppy)_2(dtbpy)]PF_6$ upon the addition of 1,2,4-trimethoxybenzene in CH_3CN. (b) Changes in the fluorescence spectra upon the addition of diphenyl disulfide in CH_3CN. (c) Stern–Volmer quenching plot of iridium catalyst in the presence of 1,2,4-trimethoxybenzene and diphenyl disulfide. K_q (arene) = 318 ± 2.6 M^{-1} L and K_q (disulfide) = 36 ± 0.7 M^{-1} L.

PF_6 was quenched upon successive addition of 1,2,4-trimethoxybenzene (oxidation potential 1.02 V vs SCE, Figure 3a). The values are similar to the estimated excited state oxidation potential of $[Ir(dF(CF_3)ppy)_2(dtbpy)]PF_6$ (+1.21 V vs SCE in acetonitrile). On the other hand, the luminescence was quenched negligible on addition of diphenyl disulfide

(Figure 3b). Stern–Volmer quenching studies showed that the arene is quenched at a much higher rate than the disulfide (Figure 3c). This indicates that the oxidation of the arene is the key step in the C–H sulfenylation reaction. Anisole does not quench the luminescence of $[Ir(dF(CF_3)ppy)_2(dtbpy)]PF_6$ and also did not give a sulfenylated product under our photocatalytic conditions. This is rationalized by the oxidation potential of anisole of 1.76 V vs SCE, which is higher than the estimated excited state oxidation potential of the photocatalyst.

To elucidate, if the 1,3,5-TMB radical cation (1,3,5-TMB$^{\bullet+}$) is formed indeed during the quenching process of the catalyst by 1,3,5-TMB (Scheme 5) ns-time-resolved transient absorption spectroscopy was used [50]. To allow for a decomposition of the multicomponent spectra we conducted laser flash photolysis (LFP) experiments on the single components (**I** = [Ir], **II** = 1,3,5-TMB, **III** = $(PhS)_2$ in ACN, fpt-degassed) and the 2- and 3-component mixtures (**A** = [Ir]/[TMB] = 1:1500; **B** = [Ir]/[TMB]/[$(PhS)_2$] = 1:1500:25 in ACN, fpt-degassed) [51]. Analyzing the single component solutions by LFP experiments with different time-resolutions and time-scales (400 ps/div, 10 ns/div, 10µs/div; t_{max} = 3.5 µs to 10 µs) provided information on photophysics and photochemistry of the single reactants. Figure 4 shows the strong luminescence of the catalyst (red line) that overlaps with the transient absorption of the postulated 1,3,5-TMB$^{\bullet+}$ in the 2-component mixture **A** [52]. The half-life time $\tau_{1/2}$ of the catalyst's emission was determined to be 1.5 µs (mono-exponential fit at 520 nm) and corresponds well with published data on related compounds [53-55]. The 1,3,5-TMB on its own did not show any transients initiated by the 355 nm pulse. $(PhS)_2$ produced under 355 nm irradiation, a broad transient absorption from 300 nm to 390 nm that did not decline over the measurement time (up to 10 µs, see Supporting Information File 1). In the UV–vis spectra recorded after the LFP experiment a significant change in absorption in the 300–370 nm region was observed, indicating that probably a fragmentation of the disulfide bond took place due to the laser irradiation. Since this effect occurred also under reduced laser power (70% of the original 58 mJ/pulse) we restricted the current analysis to the two-component solution (**A**). Since 1,3,5-TMB did not show any transient formation in solution **II**, the deconvolution of the spectra of **A** were achieved with the help of spectra derived of **I**. Taking the difference spectra on different time intervals revealed a transient absorption spectrum that corresponds to literature data of 1,3,5-TMB$^{\bullet+}$ (Figure 4). 1,3,5-TMB$^{\bullet+}$ emerges within the first 20 ns and has a life-time of around 4 µs. The presence of TMB led to a slower decay kinetics at wavelength where both fluorescence of that catalyst and the transient 1,3,5-TMB$^{\bullet+}$ occur, for instance at 447 nm $k_{decay,\mathbf{I}}/k_{decay,\mathbf{A}}$ = 1.4.

Based on the above experimental results, spectroscopic investigations and literature reports, we propose a photocatalytic mechanism (Scheme 5). Upon photoexcitation, $[Ir(dF(CF_3)ppy)_2(dtbpy)]PF_6$ accepts an electron from the arene and converts it into the corresponding radical cation **1**. Ammonium persulfate present in the reaction mixture could oxidize the reduced photocatalyst and complete the catalytic cycle forming the sulfate dianion **5** and sulfate radical anion **6**. The phenyl sulfide radical **2** formed upon homolytic cleavage of diphenyl disulfide adds to the radical cation of the arene to form the unstable cationic intermediate **3**. Aromatization by deprotonation leads to the desired product **7**.

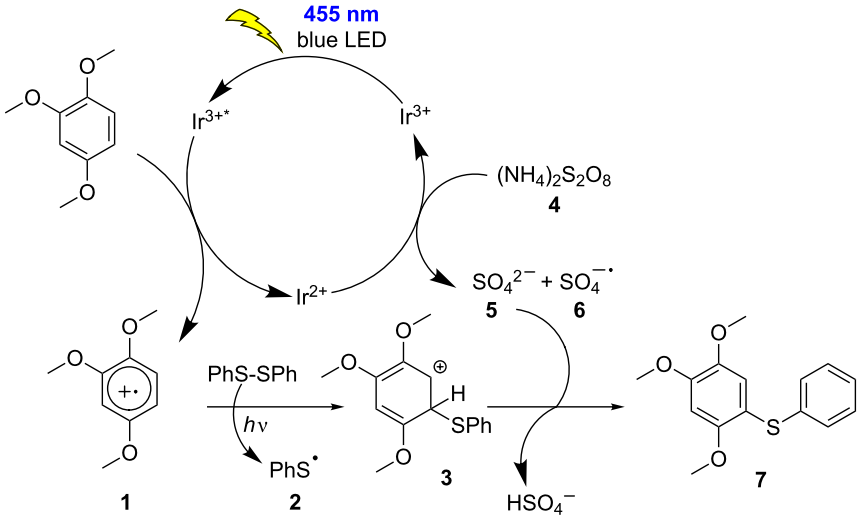

Scheme 5: Proposed mechanism for visible light mediated direct C–H sulfenylation.

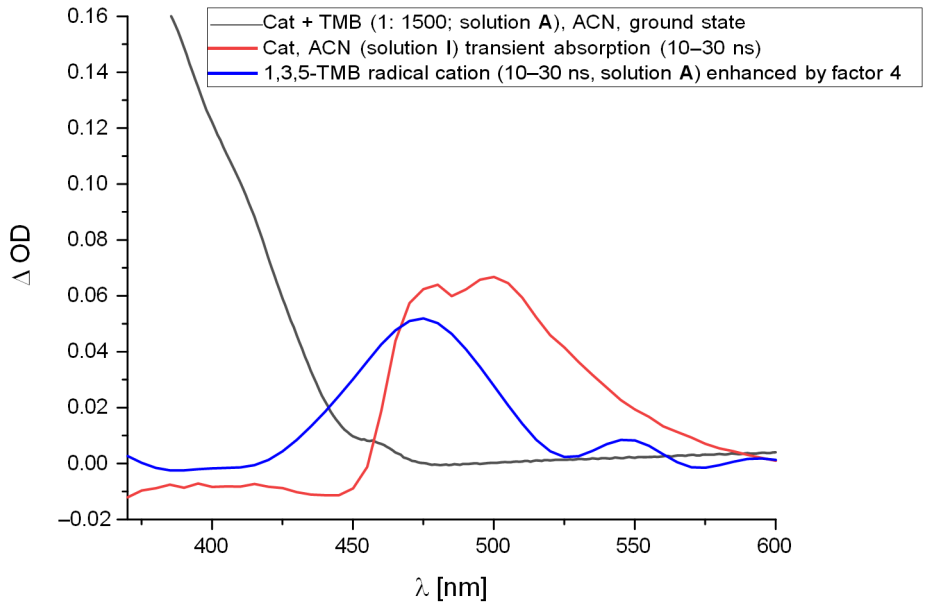

Figure 4: Black line: UV–vis spectrum of the degassed [Ir] + 1,3,5-TMB mixture (solution **A**) in ACN. Blue and red lines: Absorption spectra averaged over 10–30 ns after 355 nm laser-pulse with red being derived from the [Ir] solution **I** and representing the emission spectrum of the catalyst. Whereas, the blue line was obtained from the difference spectrum [Ir] and [Ir] + TMB and represents the transient absorption spectrum of 1,3,5-TMB$^{\bullet+}$ with λ_{max} of 473 nm (solution **A**).

Conclusion

In conclusion, we have developed a photocatalytic method for the synthesis of aryl sulfides via a radical–radical cation cross coupling of electron rich arenes with aryl and alkyl disulfides. The reaction proceeds at room temperature and avoids the use of prefunctionalized arenes.

Supporting Information

Supporting Information File 1

Experimental details, LFP data and NMR spectra of all compounds.
[https://www.beilstein-journals.org/bjoc/content/supplementary/1860-5397-14-228-S1.pdf]

Supporting Information File 2

X-ray crystallographic data for **3a** (CCDC 1847083), **3d** (CCDC 1847084), **3e** (CCDC 1847085 and **3i** (CCDC 1847086). These data can be obtained free of charge from The Cambridge Crystallographic Data Centre.
[https://www.beilstein-journals.org/bjoc/content/supplementary/1860-5397-14-228-S2.zip]

Acknowledgements

A.D., M.M, J.R. and S.M. thank the Deutsche Forschungsgemeinschaft (GRK 1626 and Emmy-Noether grant, 251211948) for financial support. We thank Dr. Rudolf Vasold and Mrs. R. Hoheisel for GC–MS and electrochemical measurements.

ORCID® iDs

Amrita Das - https://orcid.org/0000-0001-8737-8177
Burkhard König - https://orcid.org/0000-0002-6131-4850
Julia Rehbein - https://orcid.org/0000-0001-9241-0637

References

1. Dunbar, K. L.; Scharf, D. H.; Litomska, A.; Hertweck, C. *Chem. Rev.* **2017,** *117,* 5521–5577. doi:10.1021/acs.chemrev.6b00697
2. Vazquez-Prieto, M. A.; Miatello, R. M. *Mol. Aspects Med.* **2010,** *31,* 540–545. doi:10.1016/j.mam.2010.09.009
3. Feng, M.; Tang, B.; Liang, S. H.; Jiang, X. *Curr. Top. Med. Chem.* **2016,** *16,* 1200–1216. doi:10.2174/1568026615666150915111741
4. Kondo, T.; Mitsudo, T.-a. *Chem. Rev.* **2000,** *100,* 3205–3220. doi:10.1021/cr9902749
5. Eichman, C. C.; Stambuli, J. P. *Molecules* **2011,** *16,* 590–608. doi:10.3390/molecules16010590
6. Wong, Y.-C.; Jayanth, T. T.; Cheng, C.-H. *Org. Lett.* **2006,** *8,* 5613–5616. doi:10.1021/ol062344l
7. Singh, R.; Allam, B. K.; Singh, N.; Kumari, K.; Singh, S. K.; Singh, K. N. *Adv. Synth. Catal.* **2015,** *357,* 1181–1186. doi:10.1002/adsc.201400983
8. Pandya, V. G.; Mhaske, S. B. *Org. Lett.* **2014,** *16,* 3836–3839. doi:10.1021/ol5018646
9. Li, Y.; Xie, W.; Jiang, X. *Chem. – Eur. J.* **2015,** *21,* 16059–16065. doi:10.1002/chem.201502951

10. Li, G. Y. *Angew. Chem., Int. Ed.* **2001,** *40,* 1513–1516. doi:10.1002/1521-3773(20010417)40:8<1513::AID-ANIE1513>3.0.CO;2-C
11. Fernández-Rodríguez, M. A.; Hartwig, J. F. *Chem. – Eur. J.* **2010,** *16,* 2355–2359. doi:10.1002/chem.200902313
12. Teverovskiy, G.; Surry, D. S.; Buchwald, S. L. *Angew. Chem., Int. Ed.* **2011,** *50,* 7312–7314. doi:10.1002/anie.201102543
13. Li, J.; Li, C.; Yang, S.; An, Y.; Wu, W.; Jiang, H. *J. Org. Chem.* **2016,** *81,* 7771–7783. doi:10.1021/acs.joc.6b01428
14. Gan, J.; Ma, D. *Org. Lett.* **2009,** *11,* 2788–2790. doi:10.1021/ol900943b
15. Saha, A.; Saha, D.; Ranu, B. C. *Org. Biomol. Chem.* **2009,** *7,* 1652–1657. doi:10.1039/b819137a
16. Ma, D.; Xie, S.; Xue, P.; Zhang, X.; Dong, J.; Jiang, Y. *Angew. Chem., Int. Ed.* **2009,** *48,* 4222–4225. doi:10.1002/anie.200900486
17. Ma, D.; Geng, Q.; Zhang, H.; Jiang, Y. *Angew. Chem., Int. Ed.* **2010,** *49,* 1291–1294. doi:10.1002/anie.200905646
18. Chen, C.-K.; Chen, Y.-W.; Lin, C.-H.; Lin, H.-P.; Lee, C.-F. *Chem. Commun.* **2010,** *46,* 282–284. doi:10.1039/B918117B
19. Ma, D.; Lu, X.; Shi, L.; Zhang, H.; Jiang, Y.; Liu, X. *Angew. Chem., Int. Ed.* **2011,** *50,* 1118–1121. doi:10.1002/anie.201005787
20. Deng, H.; Li, Z.; Ke, F.; Zhou, X. *Chem. – Eur. J.* **2012,** *18,* 4840–4843. doi:10.1002/chem.201103525
21. Uyeda, C.; Tan, Y.; Fu, G. C.; Peters, J. C. *J. Am. Chem. Soc.* **2013,** *135,* 9548–9552. doi:10.1021/ja404050f
22. Zhang, Y.; Ngeow, K. C.; Ying, J. Y. *Org. Lett.* **2007,** *9,* 3495–3498. doi:10.1021/ol071248x
23. Jammi, S.; Barua, P.; Rout, L.; Saha, P.; Punniyamurthy, T. *Tetrahedron Lett.* **2008,** *49,* 1484–1487. doi:10.1016/j.tetlet.2007.12.118
24. Zhang, C. P.; Vicic, D. A. *J. Am. Chem. Soc.* **2012,** *134,* 183–185. doi:10.1021/ja210364r
25. Correa, A.; Mancheño, O. G.; Bolm, C. *Chem. Soc. Rev.* **2008,** *37,* 1108–1117. doi:10.1039/b801794h
26. Correa, A.; Carril, M.; Bolm, C. *Angew. Chem., Int. Ed.* **2008,** *47,* 2880–2883. doi:10.1002/anie.200705668
27. Wu, W.-Y.; Wang, J.-C.; Tsai, F.-Y. *Green Chem.* **2009,** *11,* 326–329. doi:10.1039/b820790a
28. Wu, J.-R.; Lin, C.-H.; Lee, C.-F. *Chem. Commun.* **2009,** 4450–4452. doi:10.1039/B907362K
29. Lin, Y.-Y.; Wang, Y.-J.; Lin, C.-H.; Cheng, J.-H.; Lee, C.-F. *J. Org. Chem.* **2012,** *77,* 6100–6106. doi:10.1021/jo3008397
30. Wong, Y.-C.; Jayanth, T. T.; Cheng, C.-H. *Org. Lett.* **2006,** *8,* 5613–5616. doi:10.1021/ol062344l
31. Lan, M.-T.; Wu, W.-Y.; Huang, S.-H.; Luo, K.-L.; Tsai, F.-Y. *RSC Adv.* **2011,** *1,* 1751–1755. doi:10.1039/c1ra00406a
32. Huang, X.; Chen, Y.; Zhen, S.; Song, L.; Gao, M.; Zhang, P.; Li, H.; Yuan, B.; Yang, G. *J. Org. Chem.* **2018,** *83,* 7331–7340. doi:10.1021/acs.joc.7b02718
33. Ajiki, K.; Hirano, M.; Tanaka, K. *Org. Lett.* **2005,** *7,* 4193–4195. doi:10.1021/ol051588n
34. Arisawa, M.; Suzuki, T.; Ishikawa, T.; Yamaguchi, M. *J. Am. Chem. Soc.* **2008,** *130,* 12214–12215. doi:10.1021/ja8049996
35. Cheng, J.-H.; Ramesh, C.; Kao, H.-L.; Wang, Y.-J.; Chan, C.-C.; Lee, C.-F. *J. Org. Chem.* **2012,** *77,* 10369–10374. doi:10.1021/jo302088t
36. Yonova, I. M.; Osborne, C. A.; Morrissette, N. S.; Jarvo, E. R. *J. Org. Chem.* **2014,** *79,* 1947–1953. doi:10.1021/jo402586v
37. Shen, C.; Zhang, P.; Sun, Q.; Bai, S.; Hor, T. S. A.; Liu, X. *Chem. Soc. Rev.* **2015,** *44,* 291–314. doi:10.1039/C4CS00239C
38. Parumala, S. K. R.; Peddinti, R. K. *Green Chem.* **2015,** *17,* 4068–4072. doi:10.1039/C5GC00403A
39. Zhao, W.; Xie, P.; Bian, Z.; Zhou, A.; Ge, H.; Niu, B.; Ding, Y. *RSC Adv.* **2015,** *5,* 59861–59864. doi:10.1039/C5RA10763F
40. Huang, Z.; Zhang, D.; Qi, X.; Yan, Z.; Wang, M.; Yan, H.; Lei, A. *Org. Lett.* **2016,** *18,* 2351–2354. doi:10.1021/acs.orglett.6b00764
41. Liu, B.; Lim, C.-H.; Miyake, G. M. *J. Am. Chem. Soc.* **2017,** *139,* 13616–13619. doi:10.1021/jacs.7b07390
42. Guo, W.; Tan, W.; Zhao, M.; Tao, K.; Zheng, L.-Y.; Wu, Y.; Chen, D.; Fan, X.-L. *RSC Adv.* **2017,** *7,* 37739–37742. doi:10.1039/C7RA08086G
43. Rahaman, R.; Das, S.; Barman, P. *Green Chem.* **2018,** *20,* 141–147. doi:10.1039/C7GC02906C
44. Giordan, J.; Bock, H. *Chem. Ber.* **1982,** *115,* 2548–2559. doi:10.1002/cber.19821150718
45. Töteberg-Kaulen, S.; Steckhan, E. *Tetrahedron* **1988,** *44,* 4389–4397. doi:10.1016/S0040-4020(01)86141-X
46. Lakkaraju, P. S.; Zhou, D.; Roth, H. D. *J. Chem. Soc., Perkin Trans. 2* **1998,** *2,* 1119–1122. doi:10.1039/a800341f
47. Wallace, W. L.; Van Duyne, R. P.; Lewis, F. D. *J. Am. Chem. Soc.* **1976,** *98,* 5319–5326. doi:10.1021/ja00433a044
48. Dénès, F.; Pichowicz, M.; Povie, G.; Renaud, P. *Chem. Rev.* **2014,** *114,* 2587–2693. doi:10.1021/cr400441m
49. Romero, N. A.; Nicewicz, D. A. *J. Am. Chem. Soc.* **2014,** *136,* 17024–17035. doi:10.1021/ja506228u
50. For details on spectrometer set-up, see Supporting Information File 1.
51. To achieve a maximum of 1,3,5-TMB to 1,3,5-TMB$^{\bullet+}$ conversion and render the bimolecular kinetics to pseudo-first order we used a 1500-fold excess of 1,3,5-TMB.
52. Dogadkin, D. N.; Dolotova, E. V.; Soboleva, I. V.; Kuzmin, M. G.; Plyusnin, V. F.; Pozdnyakov, I. P.; Grivin, V. P.; Vauthey, E.; Brodard, P.; Nicolet, O. *High Energy Chem.* **2004,** *38,* 392–400. doi:10.1023/B:HIEC.0000048237.12132.26
53. Lu, Y.; Wang, J.; McGoldrick, N.; Cui, X.; Zhao, J.; Caverly, C.; Twamley, B.; Ó Máille, G. M.; Irwin, B.; Conway-Kenny, R.; Draper, S. M. *Angew. Chem., Int. Ed.* **2016,** *55,* 14688–14692. doi:10.1002/anie.201608442
54. Flamigni, L.; Ventura, B.; Barigelletti, F.; Baranoff, E.; Collin, J.-P.; Sauvage, J.-P. *Eur. J. Inorg. Chem.* **2005,** 1312–1318. doi:10.1002/ejic.200400801
55. Hofbeck, T.; Yersin, H. *Inorg. Chem.* **2010,** *49,* 9290–9299. doi:10.1021/ic100872w

BEILSTEIN JOURNAL OF ORGANIC CHEMISTRY

Oxidative and reductive cyclization in stiff dithienylethenes

Michael Kleinwächter, Ellen Teichmann, Lutz Grubert, Martin Herder and Stefan Hecht*

Full Research Paper

Open Access

Address:
Department of Chemistry & IRIS Adlershof, Humboldt-Universität zu Berlin, Brook-Taylor-Straße 2, 12489 Berlin, Germany

Email:
Stefan Hecht* - sh@chemie.hu-berlin.de

* Corresponding author

Keywords:
diarylethenes; electrochromism; molecular switches; (spectro)electrochemistry

Beilstein J. Org. Chem. **2018,** *14,* 2812–2821.
doi:10.3762/bjoc.14.259

Received: 26 July 2018
Accepted: 30 October 2018
Published: 09 November 2018

This article is part of the thematic issue "Photoredox catalysis for novel organic reactions".

Guest Editor: P. H. Seeberger

Abstract

The electrochemical behavior of stiff dithienylethenes, undergoing double bond isomerization in addition to ring-closure, has been investigated. Electrochromism was observed in almost all cases, with the major pathway being the oxidatively induced cyclization of the open isomers. The influence of the ring size (to lock the reactive antiparallel conformation) as well as substituents (to modulate the redox potential) on the electrocyclization was examined. In the series of derivatives with 6-membered rings, both the *E*- and the *Z*-isomer convert to the closed isomer, whereas for the 7-membered rings no cyclization from the *E*-isomer was observed. For both stiff and normal dithienylethenes bearing benzonitrile substituents an additional and rare reductive electrocyclization was observed. The mechanism underlying both observed electrocyclization pathways has been elucidated.

Introduction

Diarylethenes (DAEs) are a rich family of organic photoswitches formally derived from stilbene [1,2]. Upon irradiation they are able to undergo reversible photoisomerization based on 6π-electrocyclization and -cycloreversion, respectively, between two thermally stable states, which make them interesting components for optical memories [3,4]. In addition to photochemistry, the isomerization of DAEs can also be triggered by electrochemical means, therefore providing a stimulus orthogonal to light [5].

Electrochemically induced isomerization of DAEs is almost exclusively based on oxidation. Either cyclization [5-13] or cycloreversion [14-21] can be observed, while correlation of both reaction modes to the molecular structure is still under discussion [22-26]. There are only few reports about reductive isomerization, each involving the ionic methylpyridinium group as a substituent on the photochromic unit [27-29]. However, by a combination of suitable substituents, a bidirectional system able to operate in both switching directions either electrochemically or photochemically has been reported [28].

We have recently developed a new subclass of DAEs without the geometric constraint of the central endocyclic olefin bridge yet with two rings each involving one of the bridge's carbon atoms to lock the photoreactive antiparallel conformation and thus provide stiff dithienylethenes (sDTEs), in analogy to stiff

stilbenes [30-32]. Due to enabled isomerization of the central exocyclic double bond, sDTEs form a three-state system undergoing interconversion between ring-open *E*- and *Z*-isomers and a ring-closed *C*-isomer (Scheme 1).

Here we describe the oxidatively and reductively induced isomerization behavior of sDTEs as investigated by cyclovoltammetry (CV) and spectro-electrochemistry (SEC) [33]. Our present study is aiming to: 1) elucidate the influence of possible double bond isomerization on the electrochromism of sDTEs; 2) explore the structural effect of varying ring size as well as electronic modification; and 3) contribute to the mechanistic understanding of electrochromism in DAEs in general.

First, we discuss the simple methyl-substituted sDTE derivative **sDTE$_{66}$-Me**, consisting of two 6-membered rings, and subsequently relate to other members of this new family of compounds, possessing either different ring sizes or aromatic substituents with different electronic properties (Scheme 2). Interestingly, we found that oxidative cyclization can occur from both double bond isomers. In addition, a reductive cyclization was discovered in bis(benzonitrile)-substituted DTEs and also in a DTE with an extended π-system.

Results and Discussion

Cyclization by anodic oxidation

In initial experiments, the electrochemical behavior of the methyl-substituted derivative bearing six-membered rings (**sDTE$_{66}$-Me**) was investigated. For both configurational isomers, i.e., ***E*-** and ***Z*-sDTE$_{66}$-Me**, an irreversible oxidation wave corresponding to the transfer of two electrons was observed in the cyclic voltammograms (Figure 1a), with the *Z*-isomer (blue dashed line) being slightly easier to oxidize than

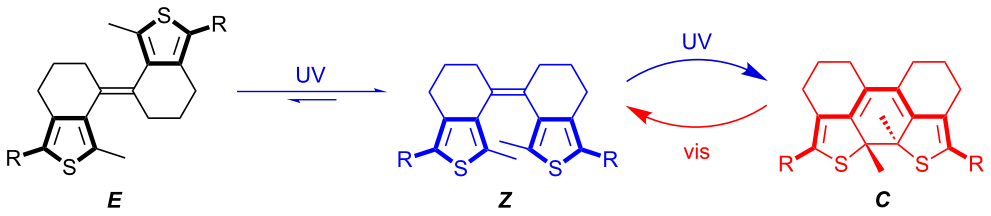

Scheme 1: Combining double bond isomerization (***E*/*Z***) and cyclization/cycloreversion (***Z*/*C***) in three-state switching sDTEs. Photochemically, both ring-open isomers are converted to the closed isomer ***C*** in high yield when irradiated with near UV light. Upon irradiation with visible light the *C*-isomer undergoes quantitative cycloreversion exclusively to the *Z*-isomer [33].

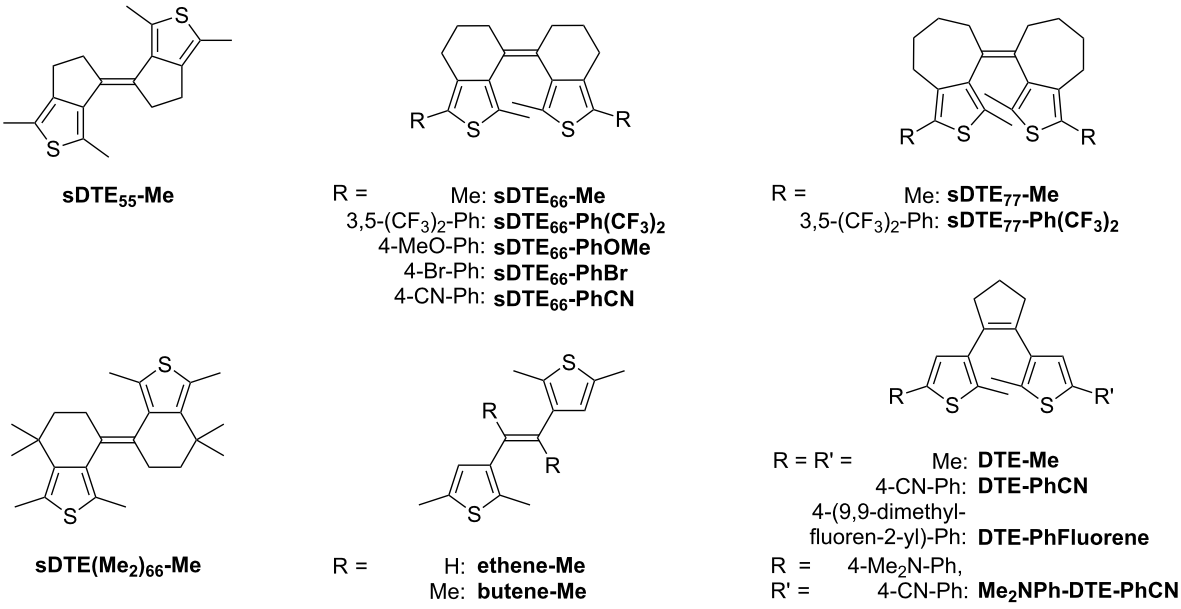

Scheme 2: Overview of all sDTE and reference DTE compounds investigated in this study. The compound names indicate the molecular frame (e.g., sDTE$_{66}$) and the substituents attached to the 5-position of the thiophenes (e.g., -PhOMe). For all compounds, the major isomer obtained in the synthesis [33] is shown.

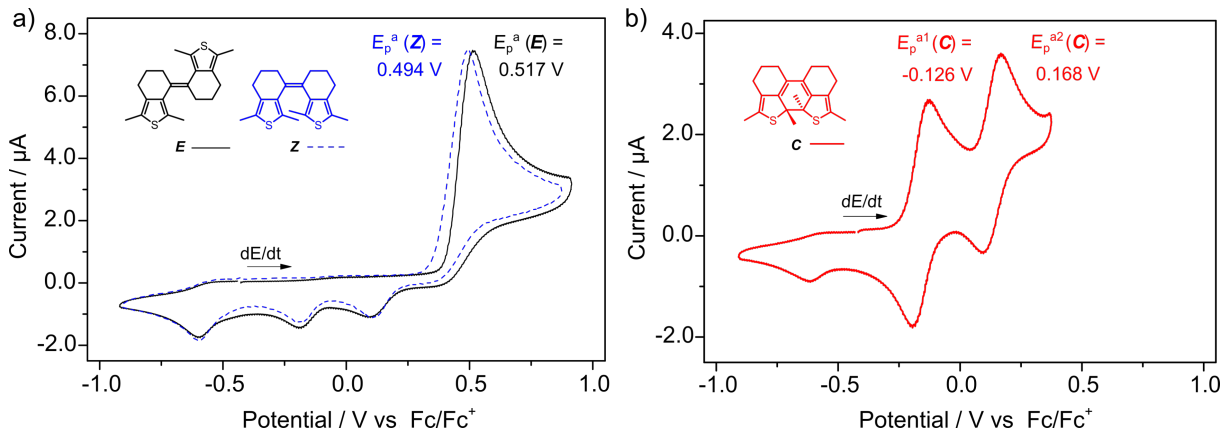

Figure 1: Cyclic voltammograms of **sDTE$_{66}$-Me**. a) Both *E*- (black line) and *Z*-isomer (blue dashed line) display one irreversible oxidation wave, which is assigned to the formation of the closed isomer. b) The closed isomer (red line), generated in situ from ***Z*-sDTE$_{66}$-Me** upon irradiation with 313 nm light prior to the CV measurement, displays two distinct oxidation waves. The first one is reversible whereas the second is quasi-reversible. Experiments were carried out in MeCN with 0.1 M Bu_4NPF_6, $c = 1 \cdot 10^{-3}$ M, $dE/dt = 1$ V s^{-1}.

***E*-sDTE$_{66}$-Me** (black line). In contrast to both open isomers, two separate one-electron oxidation waves were observed for the closed isomer ***C*-sDTE$_{66}$-Me** (Figure 1b), generated either in the irreversible oxidation process or photochemically. Both of these oxidation events occur at significantly lower potentials compared to the open isomers, reflecting the increased energy of the HOMO due to the extended π-system generated upon ring-closure.

Irreversible oxidation of the open isomer of DAEs has already been observed and was ascribed to cyclization [6-13]. Indeed, the two separate one-electron reduction waves arising during the back-sweep after oxidation of the *E*- and *Z*-isomer match exactly those of the independently photochemically prepared closed isomer (Figure 1b). Furthermore, in a second consecutive redox cycle (Figure S11, Supporting Information File 1) also two oxidation waves for ***C*-sDTE$_{66}$-Me** are observed. Interestingly, oxidatively induced cyclization seems to occur similarly from both *Z*- and *E*-configured open isomers, i.e., regardless of the double bond geometry. Since ring-closure requires the two reactive α-thienyl carbon atoms to approach each other, presumably an additional electrochemically induced $E \rightarrow Z$ isomerization occurs prior to cyclization. Indeed, there are scattered reports about configurational isomerism in stilbene radical cations [34,35] and simple dithienylethenes [36-38]. As such, we postulate an equilibrium between both *E*- and *Z*-radical cations with the latter rapidly reacting to the closed isomer.

To gain a deeper mechanistic understanding of the oxidative cyclization, the evolution of the UV–vis absorption spectra during a CV cycle was recorded in a SEC cell. It was found that both ***E*-** and ***Z*-sDTE$_{66}$-Me** convert from their colorless initial charge-neutral state into the same oxidized species which displays characteristic absorption bands centered at 493 nm and 621 nm (Figure 2a and b; for an overlay of spectra see Figure S29, Supporting Information File 1).

To identify the nature of this product, SEC was performed on the photochemically generated closed isomer (Figure 2c,d). Herein, the reversible first oxidation step yields the radical cation $\boldsymbol{C}^{+\bullet}$ (Figure 2c, light blue), identified by its characteristic red-shifted absorption at 731 nm and 912 nm due to an unpaired electron. The radical cation $\boldsymbol{C}^{+\bullet}$ is stable even at the slow scan rates of SEC and builds up continuously as evidenced by clean isosbestic points. In a subsequent, second oxidation step, the radical cation $\boldsymbol{C}^{+\bullet}$ is converted to the dication $\boldsymbol{C}^{2+}$ (Figure 2d, green), as indicated by the hypsochromic shift due to the absence of an open-shell system. The formed dication exhibits characteristic absorption bands centered at 493 nm and 621 nm, identical to the species formed upon oxidation of the open isomers.

Notably, while the first oxidation step of the closed isomer ($\boldsymbol{C} \rightarrow \boldsymbol{C}^{+\bullet}$) is fully reversible, the second oxidation ($\boldsymbol{C}^{+\bullet} \rightarrow \boldsymbol{C}^{2+}$) is only quasi-reversible. Formation of an unknown follow-up product (**FP**) occurs at the low scan rates of the SEC experiment, indicated by the appearance of a reduction wave at a significantly lower potential ($E_p^c = -0.530$ V) during the return scan (Figure 2d). At the same time the reduction waves corresponding to the closed isomer, as observed in the CV experiment with high scan rates (Figure 1), disappear. Furthermore, the UV–vis spectrum recorded in the SEC after reduction is an overlay of that of the closed isomer and the new species **FP**

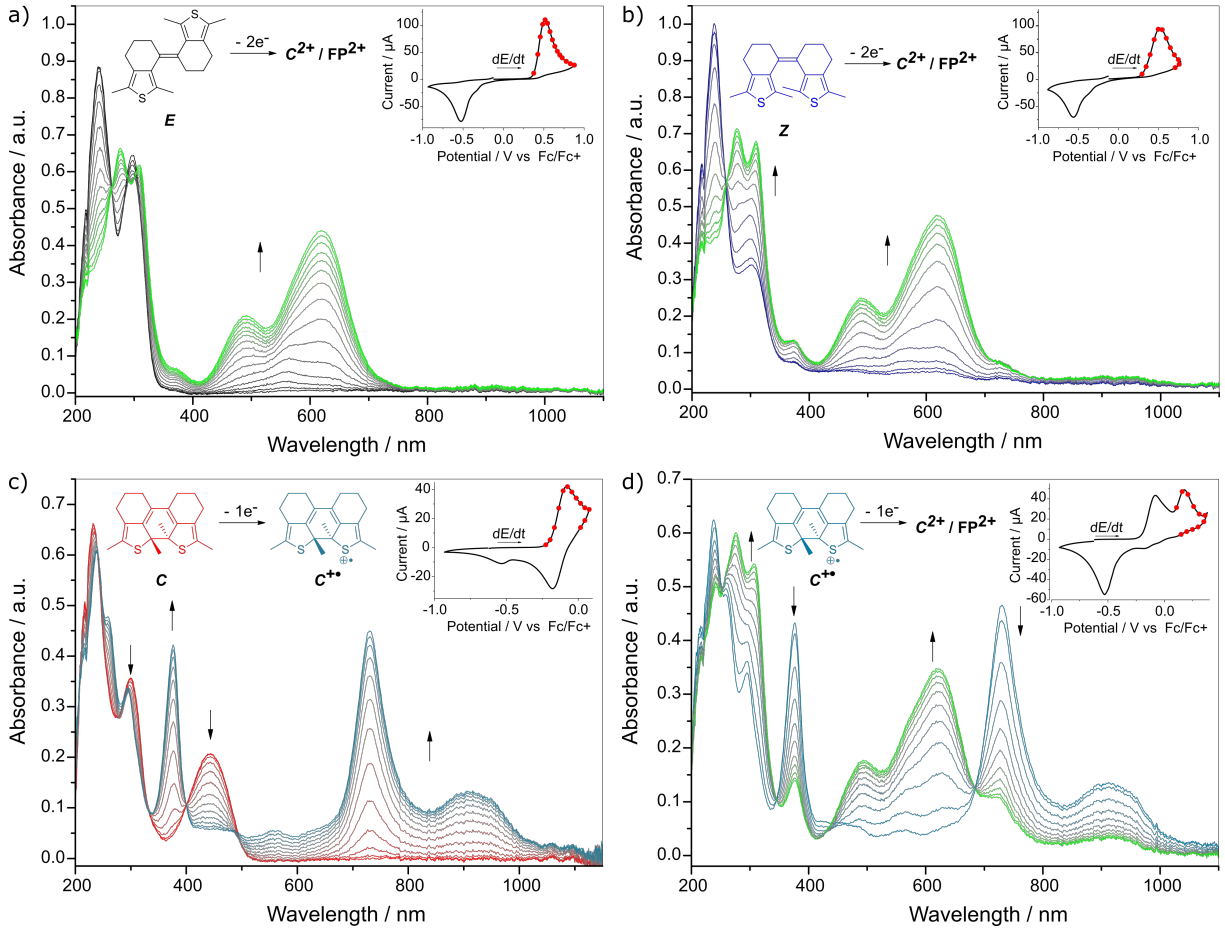

Figure 2: Spectroelectrochemistry of **sDTE$_{66}$-Me**. Absorption changes during CV, insets showing the corresponding cyclovoltammograms with red dots marking when UV–vis–NIR spectra were measured. A stable intermediate is formed upon oxidation of: a) ***E*-sDTE$_{66}$-Me** and b) ***Z*-sDTE$_{66}$-Me**. c) Oxidation of photogenerated ***C*-sDTE$_{66}$-Me** to the stable radical cation $C^{+\bullet}$. d) Further oxidation of $C^{+\bullet}$ to the dication FP^{2+}, measured in a separate experiment. At the low sweep rates of SEC an irreversible reduction wave at E_p^c = −0.530 V occurs in a), b), and d). Experiments were carried out in MeCN with 0.1 M Bu_4NPF_6, c = 5·10^{-4} M, dE/dt = 10 mV s^{-1}.

possessing an absorbance maximum at 358 nm (Figure S29, Supporting Information File 1). This kind of irreversible process from an oxidized closed isomer has already been observed for DAEs [7], but its nature has not been further discussed except that it is different from the typical photochemical byproduct of DAEs [39,40].

Although the exact identity of **FP**/FP^{2+} remains elusive, several characteristics can be summarized: 1) FP^{2+} is formed from both the open and the closed isomers upon oxidation (Figure S41 and Figure S42, Supporting Information File 1) and its reduction wave is shifted to lower potentials compared to C^{2+} for all observed cases by up to >600 mV (see Table S1, Supporting Information File 1). 2) The amount of FP^{2+} formed depends on both the electronic structure of the photoswitch and the scan rate. While at slow scan rates (10 mV s^{-1}) the conversion is quantitative for **sDTE$_{66}$-Me**, it can still be observed at the fast scan rates (1 V s^{-1}). Notably, for phenyl-substituted sDTEs the extent of FP^{2+}-formation is lower, and for the donor-substituted ***C*-sDTE$_{66}$-PhOMe** the initial absorption spectrum after a complete redox cycle is fully recovered, even at low scan rates (for a comparison of full redox cycles of ***C*-sDTE$_{66}$-Me** and ***C*-sDTE$_{66}$-PhOMe** see Figure S30, Supporting Information File 1). This observation confirms the enhanced stabilization of the C^{2+} cation by electron-donating groups [8]. 3) Upon reduction of FP^{2+}, both **FP** as well as ***C*** are formed. UPLC analysis of a preparative scale oxidation and subsequent reduction of ***Z*-sDTE$_{66}$-Me** as well as ***C*-sDTE$_{66}$-Me** (Figure S41 and Figure S42, Supporting Information File 1) showed mainly the closed isomer after the reduction step. However, in these experiments an insoluble off-red film deposited on the platinum electrode that resisted further analysis (for a photograph, see Figure

S41d, Supporting Information File 1). 4) The absorption spectrum of **FP** is red-shifted compared to the two open isomers yet blue-shifted compared to the closed isomer (Figure S29b, Supporting Information File 1). 5) Upon reduction, a species analogous to **FP** was not observed (vide infra and Figure S43, Supporting Information File 1).

Considering all these findings, a mechanism for the oxidative cyclization of **sDTE$_{66}$-Me** (Scheme 3) can be derived: Starting from either open isomer fast isomerization to the same dication C^{2+} takes place upon oxidation. Both, the isomerization of the double bond of the *E*-isomer as well as the cyclization reaction are instantaneous on the timescale of the experiment. The closed dication C^{2+} can be reduced stepwise to its neutral form. In addition, when C^{2+} is not stabilized by donor substituents it undergoes a subsequent reaction to the structurally yet unidentified follow-up product FP^{2+}, which upon reduction, at least partially, transforms into the charge-neutral closed isomer ***C***. Note that during oxidative cyclization the characteristic absorption of the cation radical $C^{+\bullet}$ at 731 nm is not observed (Figure 2a and b), suggesting a concerted two-electron oxidation of the open isomers and thermal cyclization in the dicationic state (vide infra).

Influence of ring size and substitution

To correlate structural parameters with the observed electrochemical behavior, sDTEs with other ring sizes (**sDTE$_{55}$-Me** and **sDTE$_{77}$-R**) and derivatives bearing peripheral phenyl substituents with different electronic properties (-OMe, -Br, -CN, $(-CF_3)_2$) as well as various reference compounds were examined. The oxidation potentials for the investigated compounds (see Scheme 2) are summarized in Figure 3 and Table S1 (Supporting Information File 1).

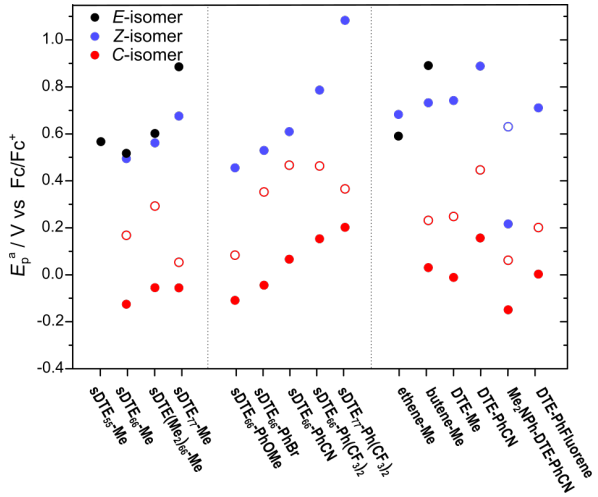

Figure 3: Anodic peak potentials (E_p^a) of sDTEs and reference compounds in MeCN. Solid circles refer to the first oxidation potential, hollow circles to the second oxidation potential (if available). For detailed data, see Table S1, for all respective cyclovoltammograms, see Figure S10 to Figure S27 in Supporting Information File 1.

For most ring-open compounds investigated, the *E*-isomer displayed a higher or at least equal oxidation potential when compared to the *Z*-isomer. This difference for both open isomers is rather surprising in view of their very similar absorption maxima in first approximation reflecting the HOMO–LUMO gap. The sole exception to this trend is the only derivative with an H-substituted double bond **ethene-Me**, which exhibit the expected behavior of a less facile oxidation of the *Z*-isomer due to its somewhat twisted π-system leading to less pronounced π-conjugation and lowering the HOMO level. Even

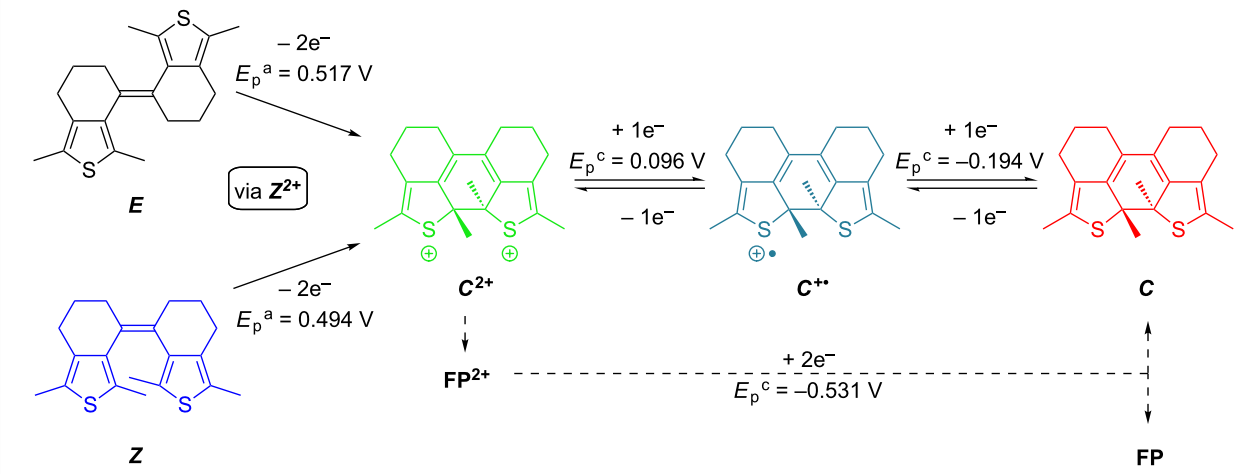

Scheme 3: Proposed mechanism for the oxidative cyclization of **sDTE$_{66}$-Me**. Upon two-fold oxidation, both open isomers cyclize to the dication C^{2+}. This dication can reversibly be reduced to the closed isomer ***C*** in two consecutive steps. Upon low sweep rates, an unidentified follow-up product **FP** forms that at least partially can be reduced to ***C***.

more surprising is the comparison of methyl-substituted derivatives of different ring sizes. Instead of the expected ease of oxidation with an increasing number of carbons due to their donating inductive (+I) effect, the exact opposite trend was observed with **sDTE$_{77}$-Me** being most difficult to oxidize. In the group of sDTE$_{66}$-R derivatives, however, the influence of the substituent is in accordance with its electron-donating or electron-withdrawing ability.

The closed isomers are, in general, much easier to oxidize as the open isomers, even in cases such as **sDTE$_{77}$-Me**, in line with the largely reduced HOMO–LUMO gap of the colored closed isomers implying an energetically higher and thus more accessible HOMO level. The first and second oxidation potential are shifted depending on the electron-donating or electron-withdrawing character of the attached substituents, similarly to what is known for normal DAEs [40,41]. The differences between the first and second oxidation wave seem to depend on the nature of the substituents with donors reducing the gap, presumably by more efficient stabilization of the dication, and on conformational rigidity dictating the extent of π-conjugation between both hemispheres.

Similar to the model compound **sDTE$_{66}$-Me**, all available sDTE$_{66}$ derivatives as well as both *Z*-configured sDTE$_{77}$ derivatives undergo electrocyclization upon oxidation. This also holds true for all cyclopentene-bridged DTE derivatives. However, in **butene-Me** the formation of **FP^{2+}** is the predominant reaction pathway even at high scan rates, while for ***E*-sDTE$_{55}$-Me** as well as both isomers of **ethene-Me** no characteristic cathodic waves of the closed isomers were observed. For ***E*-sDTE$_{77}$-Me** neither oxidative cyclization nor formation of **FP^{2+}** was found despite its irreversible oxidation wave.

Cyclization by cathodic reduction

Except for rare examples of methylpyridinium substituted DTEs [27,28] and dithiazolylethenes [29], ring closure under reductive conditions has not been reported for DAEs. For most structures the reduction potential of the open isomer is too negative to be reached within the redox window determined by the electrolyte. Thus, a strongly electron-deficient substituent such as pyridinium is necessary to shift the reduction potential to accessible values. However, not every electron-withdrawing group appears to be suited to induce cathodic cyclization [40,42].

In the case of the electron-deficient benzonitrile derivative **sDTE$_{66}$-PhCN** the reduction potential could be reached and for the *Z*-isomer an irreversible two-electron reduction wave at $E_p^c = -2.526$ V was detected (Figure 4). Upon re-oxidation, a new peak matching that of the photochemically generated closed isomer, determined in a separate experiment, was observed. Likewise, in a second cycle (Figure S24, Supporting Information File 1), the reduction wave of the closed isomer at $E_p^c = -1.920$ V appeared, clearly indicating reductive cyclization. The reductive formation of ***C*-sDTE$_{66}$-PhCN** was unequivocally proven by a preparative electrolysis of ***Z*-sDTE$_{66}$-PhCN** and subsequent product analysis, showing a closed to *Z*-isomer ratio of 69:31 (Figure S43, Supporting Information File 1). Interestingly and in strong contrast to the *Z*-isomer, for the *E*-isomer a reversible reduction wave was observed and no cyclization product was formed (Figure 4a). Note that, however, both open isomers undergo oxidative cyclization (Figure S19b and Figure S20b, Supporting Information File 1).

To investigate the generality of reductive cyclization mediated by cyano groups, we subjected the cyclopentene-bridged DTE with benzonitrile substituents (**DTE-PhCN**) to these conditions.

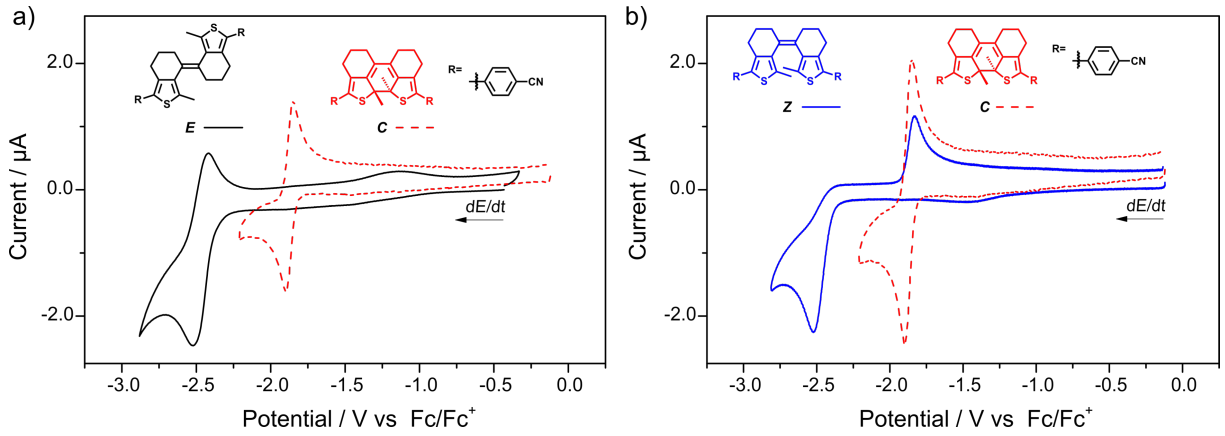

Figure 4: Cyclic voltammograms of **sDTE$_{66}$-PhCN**. The reduction of a) ***E*-sDTE$_{66}$-PhCN** (black line) is reversible, whereas the reduction of b) ***Z*-sDTE$_{66}$-PhCN** (blue line) yields the closed isomer, indicated by the characteristic oxidation wave of ***C*-sDTE$_{66}$-PhCN** (red dashed line), generated photochemically. Experiments in a) DMF with 0.1 M Bu_4NPF_6, $c = 5{\cdot}10^{-4}$ M, $dE/dt = 1$ V s^{-1} and b) MeCN with 0.1 M Bu_4NPF_6, $c = 5{\cdot}10^{-4}$ M, $dE/dt = 1$ V s^{-1}.

The electrochemistry of this compound [8] and its hexafluorocyclopentene derivative [43] have already been investigated, but its behavior under reductive conditions has not been discussed. Indeed, an irreversible reduction wave at $E_p^c = -2.436$ V was found, giving rise to an oxidation wave corresponding to the closed isomer (Figure S23, Supporting Information File 1). Once formed, the closed isomers of both nitrile-substituted compounds, i.e., **sDTE$_{66}$-PhCN** and **DTE-PhCN**, can be reversibly reduced and oxidized (Figure S20 and Figure S23, Supporting Information File 1). The two-electron reduction of the closed isomer was found to occur in a stepwise manner as indicated by SEC of ***C*-DTE-PhCN** clearly showing an intermediate radical anionic species ***C*$^{-\bullet}$** (Figure S40, Supporting Information File 1).

Moreover, the phenomenon of reductive cyclization appears not to be restricted to DTEs with strongly electron-withdrawing groups. We found that the electronic effects of an extended π-system lead to similar results. As such, the bis(4-(9,9-dimethyl-9*H*-fluoren-2-yl)phenyl)-substituted **DTE-PhFluorene** undergoes reductive as well as oxidative cyclization (Figure 5), a phenomenon that we have recently also observed for reductively and oxidatively induced azobenzene *Z*→*E* isomerization [44,45].

Mechanism of the electrochemical isomerization

In the literature, either mono- [7,18,22,23,46] or bis-oxidized [9-11] open DAEs have been reported and discussed [8,47] as the key intermediate undergoing thermal cyclization or cycloreversion, typically in the context of so-called "ECE" and "EEC" mechanisms, respectively [48]. To contribute to this discussion, nonsymmetrical DAEs bearing two electronically distinct aryl moieties (CF_3- and Me-thiazole) [5] or thiophenes possessing donor and acceptor substituents (-Ph/-PhOMe, -Ph(CF_3)$_2$/-PhNMe$_2$, and -Ph(CF_3)$_2$/-PhOMe) have been investigated [8,40]. However, sufficient separation of the oxidation waves in order to assure a fully stepwise oxidation process is difficult to achieve and could only be realized in the case of modified thiazoles [5] or using the strongly donating -PhNMe$_2$ substituent [40]. In these compounds, the first oxidation wave is fully reversible and anodic cyclization occurs only after the second step, forming the open dication (EEC mechanism).

By combining strongly electron-donating and electron-withdrawing substituents within one molecule (**Me$_2$NPh-DTE-PhCN**), we could access an open isomer showing two separated one-electron waves upon both oxidation and reduction (Figure 6). As in the examples above, the first oxidation wave of ***O*-Me$_2$NPh-DTE-PhCN** is fully reversible and anodic cyclization occurs only from the open dication (Figure 6b). In addition, also the first reduction wave is fully reversible (Figure 6a). However, because the second reduction potential was not accessible, no cyclization was observed. It is noteworthy that the reduction of ***O*-Me$_2$NPh-DTE-PhCN** and ***O*-DTE-PhCN** occur at very similar potentials (−2.457 V and −2.436 V, respectively), thus indicating that both hemispheres in open DTEs are only very weakly conjugated.

From the fact that the radical anion does not undergo cyclization we conclude that a concerted EEC mechanism is valid for both oxidative and reductive cyclization in our compounds (Scheme 4). There is, however, a marked difference between the oxidative and reductive pathway: In the dicationic state a

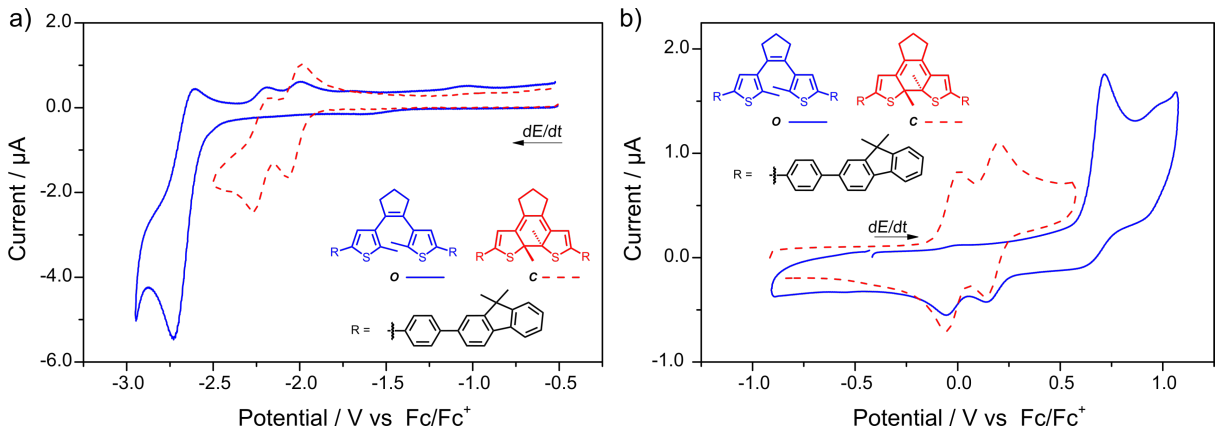

Figure 5: Cyclic voltammogram of **DTE-PhFluorene**. The ring-closed isomer (red dashed line) is formed both under a) reductive and b) oxidative conditions from ***O*-DTE-PhFluorene** (blue line), as shown by the emerging characteristic oxidation and reduction waves, respectively. Experiments in a) DMF with 0.1 M Bu_4NPF_6, $c = 1{\cdot}10^{-3}$ M, $dE/dt = 1$ V s^{-1} and b) DCM with 0.2 M Bu_4NPF_6 $c = 7{\cdot}10^{-4}$ M, $dE/dt = 100$ mV s^{-1}. For two consecutive oxidation and reduction cycles, see Figure S25 in Supporting Information File 1.

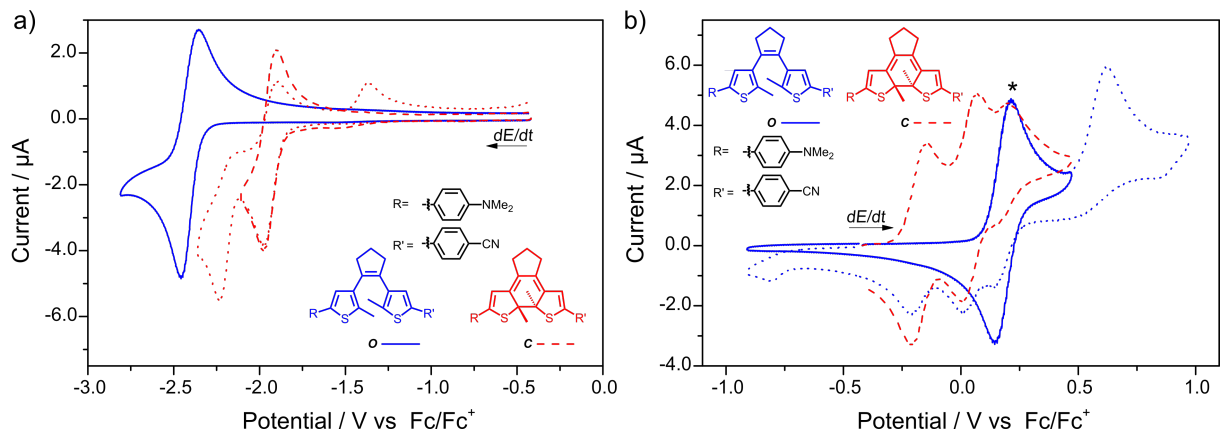

Figure 6: Cyclic voltammograms of **Me_2NPh-DTE-PhCN** displaying separated one-electron anodic and cathodic waves. a) Reversible first one-electron reduction (blue line) of ***O*-Me_2NPh-DTE-PhCN**. The second reduction potential cannot be accessed. First (red dashed line) and second one-electron reduction (red dotted line) of ***C*-Me_2NPh-DTE-PhCN** are shown for comparison. b) Oxidative cyclization of ***O*-Me_2NPh-DTE-PhCN** occurs only at the second oxidation/reduction step (blue dotted line), whereas the first step (blue line) is reversible. The oxidation waves of the closed isomer (red dashed line) are shown for comparison. The asterisk marks the oxidation wave of residual open isomer after irradiation. Experiments in MeCN with 0.1 M Bu_4NPF_6, $c = 1 \cdot 10^{-3}$ M, $dE/dt = 1$ V s^{-1}.

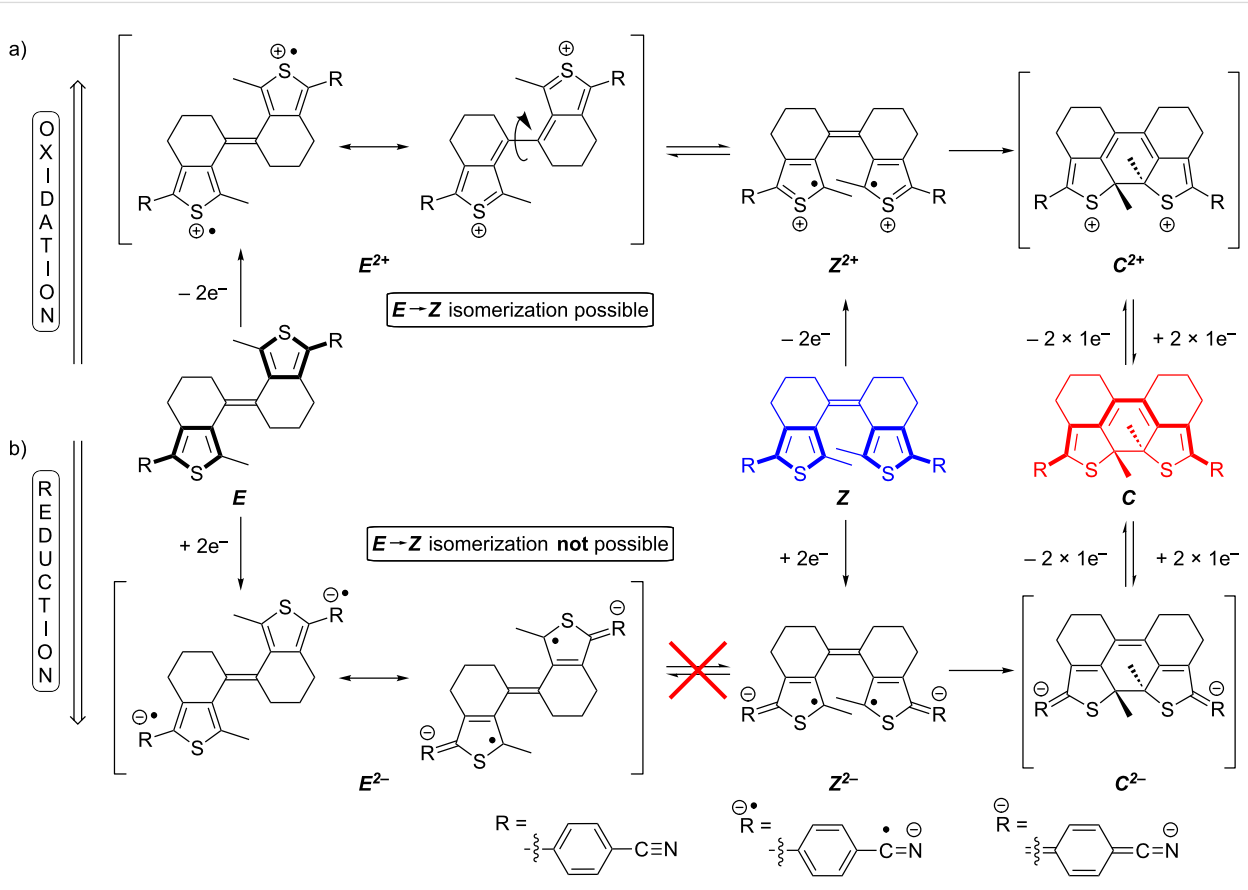

Scheme 4: Proposed mechanism to explain the observed selectivity of anodic and cathodic cyclization in $sDTE_{66}$ derivatives: a) Upon two-fold oxidation, an equilibration between the two dications of the *E*- and *Z*-isomers is possible due to rotation about the formed central single bond. Once formed, Z^{2+} is trapped as C^{2+}. b) In contrast, bond rotation is not possible for the dianion E^{2-} and as a consequence, reductive cyclization is only possible from Z^{2-}.

resonance structure exists in which the central double bond is resolved and thus bond rotation is allowed. This is reflected by the fact that both the *E*- and the *Z*-isomers of sDTEs are able to undergo oxidative cyclization. In contrast, in the dianionic state formal cross-conjugation between the thiophene moieties and the central double bond persists and no rotation takes place. Thus, only the dianion of the *Z*-isomer undergoes cyclization while the reduction of the *E*-isomer is reversible. This behavior differs strongly from that of stilbene, in which reduction occurs at the double bond and causes an equilibration of the double bond isomers in favor of the *E*-stilbene [49].

Conclusion

We have investigated the electrochemical behavior of sDTEs, a new family of photoswitches possessing three switching states (*E*/*Z*/*C*). The oxidation potentials of a series of compounds with either 5-, 6-, or 7-membered rings attached to the central exocyclic double bond as well as the electronic influence of substituents were compared. We found that in particular the derivatives with 6-membered rings undergo efficient cyclization upon two-electron oxidation. Notably, both *E*- and *Z*-isomers undergo 6π-electrocyclization because rotation about the central bond is possible in the dication. Furthermore, we discovered three examples undergoing cyclization upon two-electron reduction that so far has only rarely been observed. Remarkably, only the *Z*-isomer ring-closes under reductive conditions, whereas the *E*-isomer is reduced reversibly. In addition, the investigation of a nonsymmetrically substituted DTE showed that a two-fold change of the oxidation state is necessary to achieve cyclization, via both the oxidative and reductive pathway.

Experimental

A detailed description of the experimental conditions and applied analytical methods, including synthesis, photochemistry, and electrochemistry, can be found in Supporting Information File 1.

Supporting Information

Supporting Information File 1

Experimental part.
[https://www.beilstein-journals.org/bjoc/content/supplementary/1860-5397-14-259-S1.pdf]

Acknowledgements

Generous support by the European Research Council (ERC via ERC-2012-STG_308117 “Light4Function”) and the German Research Foundation (DFG via SFB 658 and via the Cluster of Excellence “Unifying Concepts in Catalysis”, EXC 314-2) is gratefully acknowledged.

ORCID® iDs

Ellen Teichmann - https://orcid.org/0000-0002-4301-1530
Stefan Hecht - https://orcid.org/0000-0002-6124-0222

References

1. Irie, M.; Mohri, M. *J. Org. Chem.* **1988,** *53,* 803–808. doi:10.1021/jo00239a022
2. Nakamura, S.; Irie, M. *J. Org. Chem.* **1988,** *53,* 6136–6138. doi:10.1021/jo00261a035
3. Irie, M. *Chem. Rev.* **2000,** *100,* 1685–1716. doi:10.1021/cr980069d
4. Irie, M.; Fukaminato, T.; Matsuda, K.; Kobatake, S. *Chem. Rev.* **2014,** *114,* 12174–12277. doi:10.1021/cr500249p
5. Herder, M.; Utecht, M.; Manicke, N.; Grubert, L.; Pätzel, M.; Saalfrank, P.; Hecht, S. *Chem. Sci.* **2013,** *4,* 1028–1040. doi:10.1039/C2SC21681G
6. Peters, A.; Branda, N. R. *Chem. Commun.* **2003,** 954–955. doi:10.1039/B211378C
7. Browne, W. R.; de Jong, J. J. D.; Kudernac, T.; Walko, M.; Lucas, L. N.; Uchida, K.; van Esch, J. H.; Feringa, B. L. *Chem. – Eur. J.* **2005,** *11,* 6414–6429. doi:10.1002/chem.200500162
8. Browne, W. R.; de Jong, J. J. D.; Kudernac, T.; Walko, M.; Lucas, L. N.; Uchida, K.; van Esch, J. H.; Feringa, B. L. *Chem. – Eur. J.* **2005,** *11,* 6430–6441. doi:10.1002/chem.200500163
9. Liu, Y.; Lagrost, C.; Costuas, K.; Tchouar, N.; Le Bozec, H.; Rigaut, S. *Chem. Commun.* **2008,** 6117–6119. doi:10.1039/b815899a
10. He, B.; Wenger, O. S. *J. Am. Chem. Soc.* **2011,** *133,* 17027–17036. doi:10.1021/ja207025x
11. Staykov, A.; Areephong, J.; Browne, W. R.; Feringa, B. L.; Yoshizawa, K. *ACS Nano* **2011,** *5,* 1165–1178. doi:10.1021/nn102806z
12. Harvey, E. C.; Areephong, J.; Cafolla, A. A.; Long, C.; Browne, W. R.; Feringa, B. L.; Pryce, M. T. *Organometallics* **2014,** *33,* 3309–3319. doi:10.1021/om4005719
13. Meng, F.; Hervault, Y.-M.; Shao, Q.; Hu, B.; Norel, L.; Rigaut, S.; Chen, X. *Nat. Commun.* **2014,** *5,* No. 3023. doi:10.1038/ncomms4023
14. Koshido, T.; Kawai, T.; Yoshino, K. *J. Phys. Chem.* **1995,** *99,* 6110–6114. doi:10.1021/j100016a055
15. Peters, A.; Branda, N. R. *J. Am. Chem. Soc.* **2003,** *125,* 3404–3405. doi:10.1021/ja028764x
16. Zhou, X.-H.; Zhang, F.-S.; Yuan, P.; Sun, F.; Pu, S.-Z.; Zhao, F.-Q.; Tung, C.-H. *Chem. Lett.* **2004,** *33,* 1006–1007. doi:10.1246/cl.2004.1006
17. Nakashima, T.; Kajiki, Y.; Fukumoto, S.; Taguchi, M.; Nagao, S.; Hirota, S.; Kawai, T. *J. Am. Chem. Soc.* **2012,** *134,* 19877–19883. doi:10.1021/ja309275q
18. Lee, S.; You, Y.; Ohkubo, K.; Fukuzumi, S.; Nam, W. *Org. Lett.* **2012,** *14,* 2238–2241. doi:10.1021/ol300604n
19. Massaad, J.; Micheau, J.-C.; Coudret, C.; Serpentini, C. L.; Guirado, G. *Chem. – Eur. J.* **2013,** *19,* 12435–12445. doi:10.1002/chem.201301566
20. Lee, S.; You, Y.; Ohkubo, K.; Fukuzumi, S.; Nam, W. *Chem. Sci.* **2014,** *5,* 1463–1474. doi:10.1039/c3sc52900b
21. Calupitan, J. P.; Nakashima, T.; Hashimoto, Y.; Kawai, T. *Chem. – Eur. J.* **2016,** *22,* 10002–10008. doi:10.1002/chem.201600708
22. Moriyama, Y.; Matsuda, K.; Tanifuji, N.; Irie, S.; Irie, M. *Org. Lett.* **2005,** *7,* 3315–3318. doi:10.1021/ol051149o
23. Guirado, G.; Coudret, C.; Hliwa, M.; Launay, J.-P. *J. Phys. Chem. B* **2005,** *109,* 17445–17459. doi:10.1021/jp052459r
24. Coudret, C.; Guirado, G.; Hortholary, C.; Launay, J.-P.; Battaglini, N.; Klein, H.; Dumas, P. *Mol. Cryst. Liq. Cryst.* **2005,** *431,* 501–508. doi:10.1080/15421400590947225

25. Yuan, N.; Zhang, Z.; Wang, X.; Wang, X. *Chem. Commun.* **2015,** *51,* 16714–16717. doi:10.1039/C5CC06755C
26. Zhang, Z.-X.; Wang, P.-X.; Bai, F.-Q.; Kong, C.-P.; Zhang, H.-X. *Phys. Chem. Chem. Phys.* **2017,** *19,* 9281–9291. doi:10.1039/C7CP00262A
27. Gorodetsky, B.; Samachetty, H. D.; Donkers, R. L.; Workentin, M. S.; Branda, N. R. *Angew. Chem.* **2004,** *116,* 2872–2875. doi:10.1002/ange.200353029
28. Gorodetsky, B.; Branda, N. R. *Adv. Funct. Mater.* **2007,** *17,* 786–796. doi:10.1002/adfm.200600902
29. Léaustic, A.; Anxolabéhère-Mallart, E.; Maurel, F.; Midelton, S.; Guillot, R.; Métivier, R.; Nakatani, K.; Yu, P. *Chem. – Eur. J.* **2011,** *17,* 2246–2255. doi:10.1002/chem.201002451
30. Ogawa, K.; Suzuki, H.; Futakami, M. *J. Chem. Soc., Perkin Trans. 2* **1988,** 39–43. doi:10.1039/P29880000039
31. Oelgemöller, M.; Brem, B.; Frank, R.; Schneider, S.; Lenoir, D.; Hertkorn, N.; Origane, Y.; Lemmen, P.; Lex, J.; Inoue, Y. *J. Chem. Soc., Perkin Trans. 2* **2002,** 1760–1771. doi:10.1039/B203167A
32. Oelgemöller, M.; Frank, R.; Lemmen, P.; Lenoir, D.; Lex, J.; Inoue, Y. *Tetrahedron* **2012,** *68,* 4048–4056. doi:10.1016/j.tet.2012.03.038
33. Kleinwächter, M.; Teichmann, E.; Schwarz, J.; Hecht, S. *manuscript in preparation.*
34. Lewis, F. D.; Petisce, J. R.; Oxman, J. D.; Nepras, M. J. *J. Am. Chem. Soc.* **1985,** *107,* 203–207. doi:10.1021/ja00287a037
35. Majima, T.; Tojo, S.; Ishida, A.; Takamuku, S. *J. Org. Chem.* **1996,** *61,* 7793–7800. doi:10.1021/jo960598m
36. Bragadin, M.; Cescon, P.; Berlin, A.; Sannicolò, F. *Makromol. Chem.* **1987,** *188,* 1425–1430. doi:10.1002/macp.1987.021880618
37. Onoda, M.; Iwasa, T.; Kawai, T.; Yoshino, K. *J. Phys. Soc. Jpn.* **1991,** *60,* 3768–3776. doi:10.1143/JPSJ.60.3768
38. Benincori, T.; Brenna, E.; Sannicolò, F.; Trimarco, L.; Schiavon, G.; Zecchin, S.; Zotti, G. *Macromol. Chem. Phys.* **1996,** *197,* 517–528. doi:10.1002/macp.1996.021970208
39. Irie, M.; Lifka, T.; Uchida, K.; Kobatake, S.; Shindo, Y. *Chem. Commun.* **1999,** 747–750. doi:10.1039/a809410a
40. Herder, M.; Schmidt, B. M.; Grubert, L.; Pätzel, M.; Schwarz, J.; Hecht, S. *J. Am. Chem. Soc.* **2015,** *137,* 2738–2747. doi:10.1021/ja513027s
41. Herder, M.; Eisenreich, F.; Bonasera, A.; Grafl, A.; Grubert, L.; Pätzel, M.; Schwarz, J.; Hecht, S. *Chem. – Eur. J.* **2017,** *23,* 3743–3754. doi:10.1002/chem.201605511
42. Berberich, M.; Würthner, F. *Asian J. Org. Chem.* **2013,** *2,* 250–256. doi:10.1002/ajoc.201200179
43. Liu, G.; Pu, S. Z.; Zheng, C. H.; Le, Z. G.; Luo, M. B. *Phys. Scr.* **2007,** *T129,* 278. doi:10.1088/0031-8949/2007/T129/062
44. Goulet-Hanssens, A.; Utecht, M.; Mutruc, D.; Titov, E.; Schwarz, J.; Grubert, L.; Bléger, D.; Saalfrank, P.; Hecht, S. *J. Am. Chem. Soc.* **2017,** *139,* 335–341. doi:10.1021/jacs.6b10822
45. Goulet-Hanssens, A.; Rietze, C.; Titov, E.; Abdullahu, L.; Grubert, L.; Saalfrank, P.; Hecht, S. *Chem* **2018,** *4,* 1740–1755. doi:10.1016/j.chempr.2018.06.002
46. Matsuda, K.; Yokojima, S.; Moriyama, Y.; Nakamura, S.; Irie, M. *Chem. Lett.* **2006,** *35,* 900–901. doi:10.1246/cl.2006.900
47. Logtenberg, H.; Browne, W. R. *Org. Biomol. Chem.* **2013,** *11,* 233–243. doi:10.1039/C2OB26723C
48. Testa, A. C.; Reinmuth, W. H. *Anal. Chem.* **1961,** *33,* 1320–1324. doi:10.1021/ac60178a010
49. Abdul-Rahim, O.; Simonov, A. N.; Boas, J. F.; Rüther, T.; Collins, D. J.; Perlmutter, P.; Bond, A. M. *J. Phys. Chem. B* **2014,** *118,* 3183–3191. doi:10.1021/jp500786j

License and Terms

BEILSTEIN JOURNAL OF ORGANIC CHEMISTRY

Organometallic vs organic photoredox catalysts for photocuring reactions in the visible region

Aude-Héloise Bonardi[1,2], Frédéric Dumur*[3], Guillaume Noirbent[3], Jacques Lalevée*[1,2] and Didier Gigmes[3]

Review

Open Access

Address:
[1]Université de Haute-Alsace, CNRS, IS2M UMR 7361, F-68100 Mulhouse, France, [2]Université de Strasbourg, France and [3]Aix Marseille Univ, CNRS, ICR UMR 7273, F-13397 Marseille, France

Email:
Frédéric Dumur* - frederic.dumur@univ-amu.fr; Jacques Lalevée* - jacques.lalevee@uha.fr

* Corresponding author

Keywords:
photoinitiator; photopolymerization; photoredox catalysis; photoredox catalyst

Beilstein J. Org. Chem. **2018,** *14,* 3025–3046.
doi:10.3762/bjoc.14.282

Received: 30 August 2018
Accepted: 23 November 2018
Published: 12 December 2018

This article is part of the thematic issue "Photoredox catalysis for novel organic reactions".

Guest Editor: P. H. Seeberger

Abstract

Recent progresses achieved in terms of synthetic procedures allow now the access to polymers of well-defined composition, molecular weight and architecture. Thanks to these recent progresses in polymer engineering, the scope of applications of polymers is far wider than that of any other class of material, ranging from adhesives, coatings, packaging materials, inks, paints, optics, 3D printing, microelectronics or textiles. From a synthetic viewpoint, photoredox catalysis, originally developed for organic chemistry, has recently been applied to the polymer synthesis, constituting a major breakthrough in polymer chemistry. Thanks to the development of photoredox catalysts of polymerization, a drastic reduction of the amount of photoinitiators could be achieved, addressing the toxicity and the extractability issues; high performance initiating abilities are still obtained due to the catalytic approach which regenerates the catalyst. As it is a fast-growing field, this review will be mainly focused on an overview of the recent advances concerning the development of organic and organometallic photoredox catalysts for the photoreticulation of multifunctional monomers for a rapid and efficient access to 3D polymer networks.

Introduction

Photopolymerization reactions are now widely used both in industry and in academic laboratories. These processes usually lead to the transformation of a liquid resin in a 3D solid polymer upon light exposure. These photochemical processes offer potential advantages compared to thermal polymerization. First, it is a greener technology, i.e., the system does not need to be heated and no (or low content of) volatile organic compounds are released. Secondly, mild conditions can be employed. It is now possible to perform photopolymerizations upon soft irradiation conditions with, for example, household light bulbs, LED light, low intensity lasers and even sunlight [1-4]. The first reason is the low cost and infiniteness character

of light (more particularly when using visible light). The "on-off" aspect of a lamp offers good possibilities of external regulator of the reaction. Another advantage is the spatial control, i.e., the reaction only occurs in the light-irradiated areas. For all these advantages, photopolymerization reactions are already encountered for applications in a lot of sectors such as coatings, adhesives, paints, inks, composites, 3D-printing, dentistry, data storage ... [5-7].

Review

1 Photopolymerization processes and uses of photocatalysts (PCs)

Traditionally, polymer manufacturing is made through thermal curing. However, this route has many limitations: these processes are usually slow, expensive by requiring high temperature and high energy and release solvent (VOC). As an alternative of thermal polymerizations, polymerization upon light irradiation offers a good alternative. In both cases, polymerization occurs by the action of an initiating system in a monomer blend. In the case of photopolymerization, a photoinitiating system (PIs) is required to convert light in initiating species. Many factors affect the photopolymerization kinetics. However, the PIs is the most important key factor and that's why enhancing its properties have drawn many interest in the past few decades. The development of photoredox catalysts is one of the major advances.

1.1 Photoinitiating system (PIs)

Photoinitiated polymerization processes are polymerizations initiated by light irradiation. For that, a photoinitiator (PI) or a photoinitiating system (PIs) is mixed with the monomer or a monomer blend. The PI is a component which absorbs light and initiates polymerization alone whereas a photoinitiating system comprises different compounds [8-10]. Under irradiation, PI or PIs generate active species: free radicals and/or ions and/or acid. When the active species are produced, a wide range of monomers can be polymerized via a free radical or a cationic mechanism (anionic mechanisms are still rare) [8]. A PI can also be used in combination with a photosensitizer (PS) to extend the spectral sensitivity to longer wavelengths. The development of new photoinitiating systems has been the subject of many researches in the last decades [11,12].

For a PIs to be efficient, it requires several properties:

i) Excellent light absorption (meaning high molar extinction coefficients) in the region of the emission spectrum of the irradiation source.

ii) Appropriated excited state energy and redox potentials to interact with additives [13].

Parallel to this, the environmental issues impose the use of new polymerization methods that are safer for the manipulator, contribute to lower the amount of released volatile organic compounds and can reduce the energy consumption used to produce the polymers. At present, most of the photoinitiating systems in use in the industry required high light intensity, the emission of these lamps being mainly centered in the UV range. To create safer photoinitiating systems, photoinitiators exhibiting a strong absorption in the near UV or visible range with high molar extinction coefficients are actively researched. As far as the extractability of the photoinitiators and the side-products that can be formed during the polymerization process is concerned, a good strategy is to reduce the amount of photoinitiator. Thus, inspired by catalytic cycles used in organic chemistry, the development of photoredox catalysis for photopolymerization reactions has been proposed. It has emerged as a significant innovation in the field of photoinitiated polymerization. Photoredox catalysis is a new strategy to generate radicals and/or cations upon soft irradiation [14].

1.2 Development of photoredox catalysts

In the field of photoinitiated polymerization, a photoredox catalyst is a photoinitiating system capable of regeneration during the polymerization reaction [14]. This regeneration is based on an oxidoreduction reaction between the light absorbing compound and suitable additives under light to induce a catalytical cycle.

As light is an inexhaustible and renewable energy, photochemistry has dealt a great interest into organic chemistry and green chemistry since the early 20th century [15]. By absorbing light, the compound reaches an electronically excited state which significantly changes the distribution of electrons in the molecule. Thus, chemical properties such as reactivity, oxidation potential or reduction potential change drastically. With appropriate donors or acceptors, electron charge transfer is possible via this excited state and redox reactions are possible. This process is called photoinduced electron transfer (PET).

In this context, photoredox catalysis was developed. Light is used to excite the photoredox catalyst which allows electron transfer processes with additives. Both oxidation and reduction reactions can be possible. Indeed, when the photoredox catalyst is excited, one electron moves from the HOMO (abbreviation for highest occupied molecular orbital) to the LUMO (abbreviation for lowest unoccupied molecular orbital). Thus, there is a lack of one electron in the HOMO and an electron available in the LUMO. That's why the excited photoredox catalyst is at the same time a stronger oxidant and a stronger reductant than its ground state. Therefore, the PC can react more easily with an oxidant or a reductant (see in Figure 1) [16]. By addition of

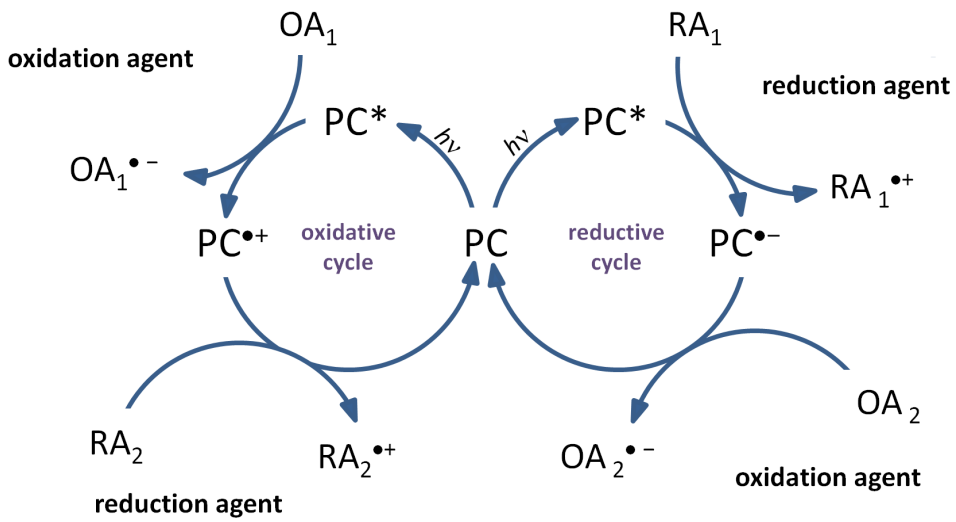

Figure 1: Typical oxidative and reductive cycle for a photoredox catalyst (PC).

another reduction or oxidation agent, the catalytic cycle can be created as illustrated in Figure 1 to regenerate the PC.

As illustrated, for an oxidative cycle, the excited photocatalyst (PC*) reacts first with an electron acceptor (also named oxidation agent, OA_1 in Figure 1) which leads to $PC^{\bullet+}$ and $OA_1^{\bullet-}$. Then, PC can be regenerated with an electron donor (also named reduction agent, RA_2 in Figure 1) by a redox reaction. In a reductive cycle, the PC* reacts first with a reduction agent (in Figure 1, RA_1) which leads to $PC^{\bullet-}$ and $RA_1^{\bullet+}$. Then, PC can be regenerated with an oxidation agent (OA_2). Radicals and cations are generated in these cycles [16]. As we can observe, this process offers the possibility to regenerate the catalyst. Consequently, the amount of PC used for the photochemical transformation is added only in catalytic amount and recovered after the reaction. That's why the definition of photocatalyst is fulfilled.

For a compound to be efficient as photoredox catalyst in the visible range, several parameters have to be fulfilled: [17]

i) The molecule should strongly absorb in the near UV or visible range with high molar extinction coefficients.

ii) The redox potentials of the excited state of photoredox catalysts must be in appropriateness to those of the additives to be incorporated into oxidative or reductive cycles (see Figure 1).

iii) The oxidation or the reduction of the photoredox catalyst should be reversible in order to be regenerated (to avoid any side reaction from $PC^{\bullet+}$ or $PC^{\bullet-}$).

iv) The excited state lifetimes of photoredox catalyst should be long enough to exhibit a high quenching efficiency with the additives, i.e., to have enough time to react with the additives.

This is frequently referred as the Golden Rules of photoredox catalysis.

Photoredox catalysis has been largely developed in organic chemistry in the last decades and already found wide applications such as in water splitting, solar energy storage, proton-coupled electron transfer or photovoltaic for example [18].

1.3 Electronic transitions involved into photoredox processes

For selected photoredox catalysts, light irradiation has enough energy for the excitation of the PC from the ground state S0 to an excited stated (S1). This is usually a transition between the HOMO and the LUMO. Both can be different type of molecular orbital (MO) regarding the compound chosen and the different transitions will be presented.

1.3.1 n–π* transition: The n–π* transition (depicted in Figure 2) is a transition where the HOMO is a non-bonding orbital (n) and π* an anti-bonding orbital. Both orbitals have different symmetries and this transition is observed for molecules with a heteroatom such as nitrogen, oxygen or sulfur which are carrying free electron pair. Most compounds concerned by this transition usually absorbs around 300 and 380 nm and rarely up to the visible range [19].

1.3.2 π–π* transition: π referred to a bonding orbital. The π and π* molecular orbitals have generally the same symmetry which allow the π–π* transition (depicted in Figure 2).

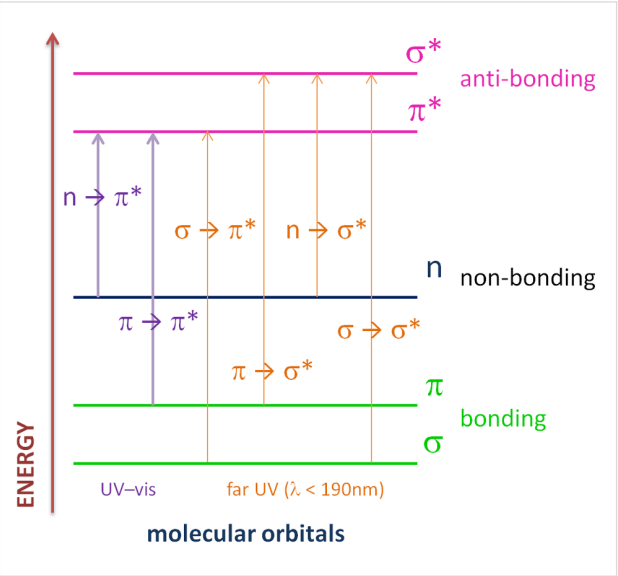

Figure 2: Transitions involved in absorbing species containing π, σ and n electrons.

This transition is generally observed for molecules with extended π-conjugated systems. As π and π* are more distant from each other than n and π* orbitals, the absorption is generally observed in higher wavelength than for n–π* transition. Moreover, the longer the π-system, the higher are the wavelengths needed to excite the molecule.

1.3.3 Charge transfer transition (CT): A charge transfer transition is mostly observed from interaction between the LUMO on an electron accepting group and the HOMO on an electron-donating group. This can be an intermolecular or intramolecular process. For an intramolecular process, this type of transition mostly concerned polarized molecules with both groups on its structure. Intermolecular charge transfer transition is observed for example with charge transfer complex formed by interaction an acceptor and a donor. The interaction between the two compounds induced a complex with a smaller energy gap between HOMO and LUMO than the energy gap between the HOMO of the acceptor and the LUMO of the donor when the two compounds are separated. This transition is generally observed with high intensity on the UV–visible spectra [20].

1.3.4 Ligand to metal charge transfer (LMCT): The LMCT transition is observed for organometallic compounds for example with organic molecules as ligands. This ligand possesses σ, σ*, π, π* and n molecular orbitals [21]. When orbitals of this ligand are fully occupied, a charge transfer is possible from it to the empty or partially filled metal d-orbitals as illustrated in Figure 3. Absorption band observable are very intense.

1.3.5 Metal to ligand charge transfer (MLCT): The MLCT transition is a second type of charge transfer observed with metal complexes. More particularly, it is observed for complexes whose ligands have relatively high-energy lone pairs or in case of metal with low-lying empty orbitals. For coordination compounds with π-acceptor ligand, MLCT transition are common and can be generate through light excitation. This absorption results from the movement of an electron from the metal orbitals to the ligand π* orbitals [22]. This process is illustrated in the case of a d^5 high spin octahedral complex in Figure 4. As for LMCT, MLCT give intense band in UV spectrum.

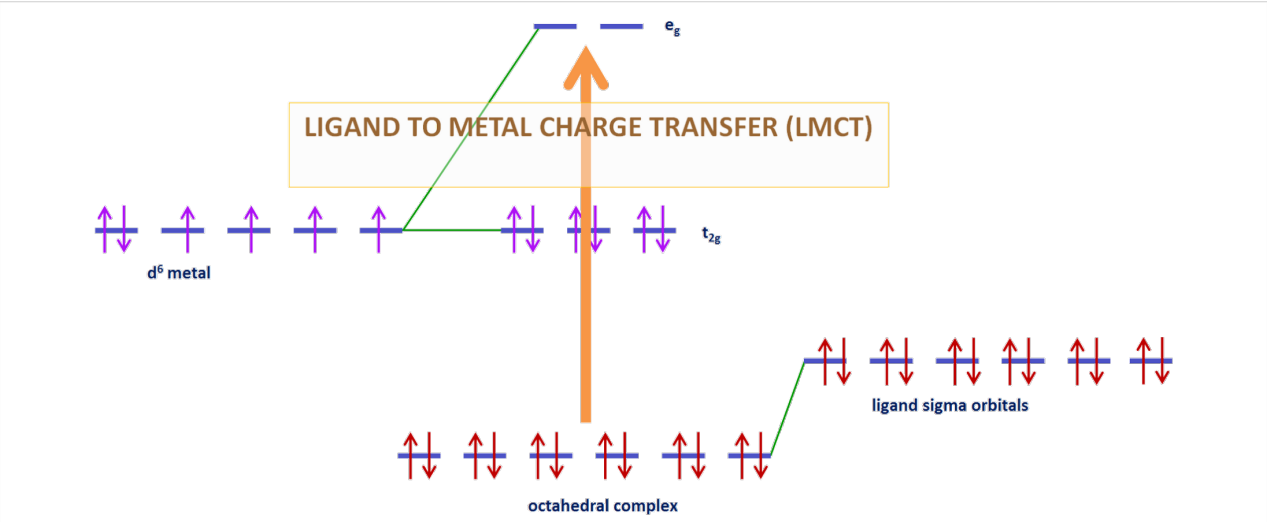

Figure 3: Ligand to metal charge transfer (illustrated here for a d^6 metal complex).

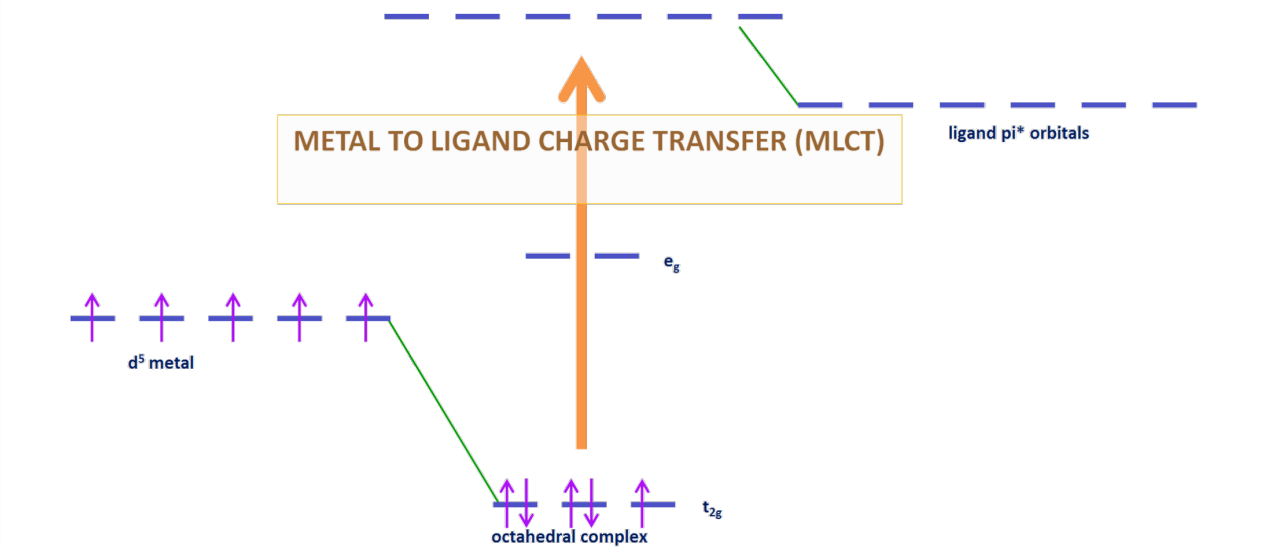

Figure 4: Metal to ligand charge transfer (illustrated here for a d^5 metal complex).

1.4 Mechanisms in polymerization reactions

Free radical polymerization or/and cationic polymerization can be initiated by photoredox catalysis. Respectively, radicals or/and cations must be produced to initiate the polymerization. By formation of radicals, the polymerization of C=C functions such as (meth)acrylates or styrene can be initiated. With cations or acids as initiating species, epoxy monomers can be polymerized. Both types of polymerization are widely used both in academic and industrial fields. About 45% of the manufactured plastic material and 40% of synthetic rubber are produced by free radical polymerization worldwide [23].

In both cases, the photoredox catalyst, used as PS, absorbs the light and goes to its excited state. Then, there are two possibilities: the photoredox catalyst can react through an oxidative or a reductive cycle as presented in Figure 1. Herein, we will present four additives that can be used in combination with a photoredox catalyst to initiated photopolymerization (Scheme 1).

As reduction agent, silanes such as tris(trimethylsilyl)silane (abbreviated $(TMS)_3SiH$), amines such as ethyl 4-(dimethylamino)benzoate (abbreviated EDB) or carbazole derivatives such as 9-vinylcarbazole (NVK) are presented. As oxidizing agent, it is possible to use a iodonium salt such as diphenyliodonium (Ph_2I^+).

With these additives, three systems involving catalytic cycles for photopolymerization are presented: [14,23,24]

- PC/Ph_2I^+/$(TMS)_3SiH$
- PC/Ph_2I^+/NVK
- PC/Ph_2I^+/EDB

With these three systems, both free radical and cationic polymerizations are possible. The chemical mechanisms for these different systems are depicted in Figure 5.

With appropriated photoredox catalysts, formations of interpenetrated polymer networks (IPN) are also mentioned. For the three systems proposed above, formation of aryl radicals is observed. These radicals are able to initiate the free radical polymerization of (meth)acrylates [1]. In the photocatalytic cycle (Figure 5C), $EDB_{(-H)}^{\bullet}$ radicals are also produced and able to

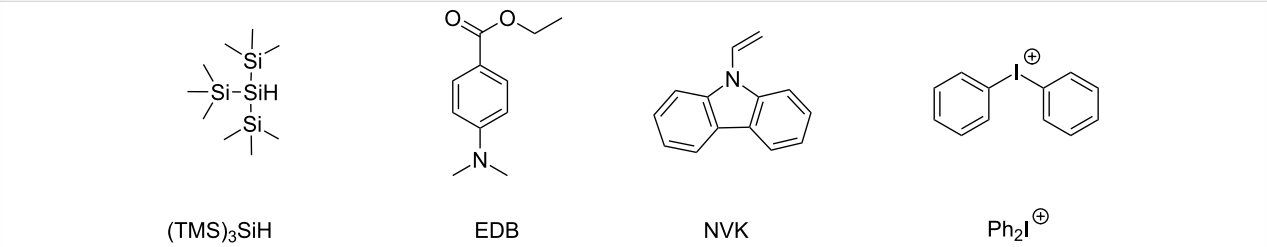

Scheme 1: Structures of additives involved in the photoredox catalytic cycles.

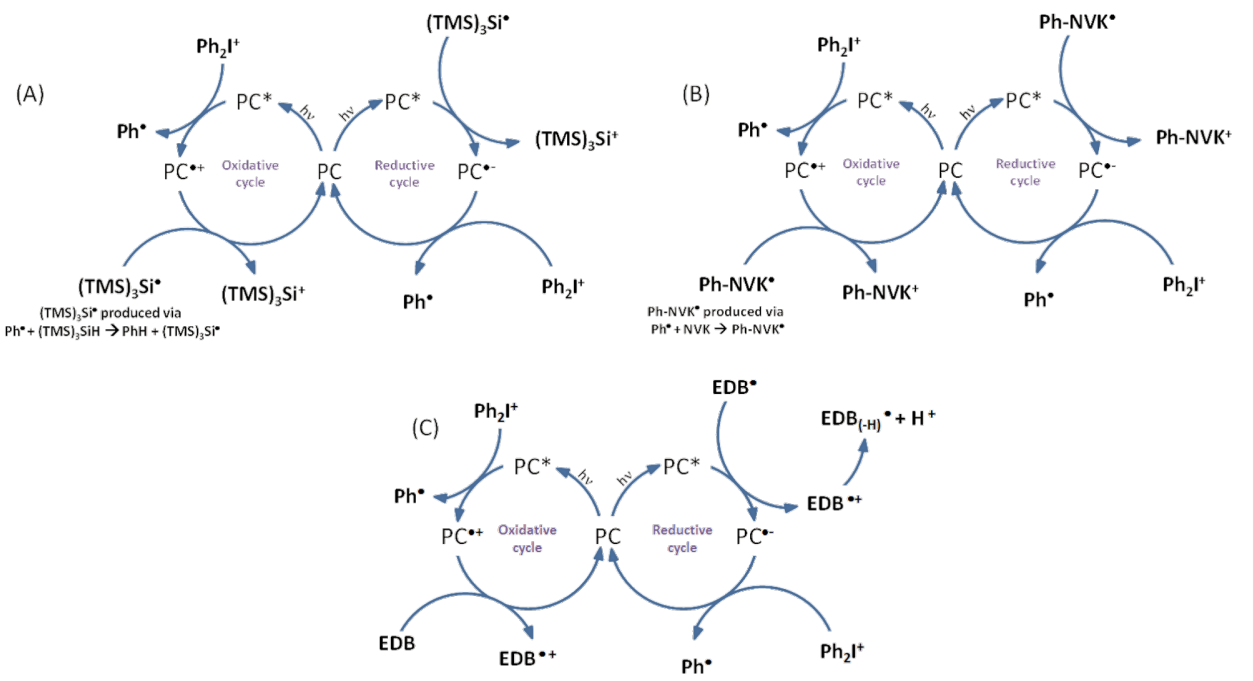

Figure 5: Catalytic cycles involved with iodonium salt and (A) $(TMS)_3SiH$, (B) NVK and (C) EDB.

initiate the free radical polymerization. Concerning the cationic polymerization, initiating cations are also produced in the three systems proposed, e.g., in the catalytic cycle (Figure 5A). Thanks to the low ionization potential of the silyl radicals $(TMS)_3Si^•$, the generation of silylium cations is possible. These cations have been described in the literature for initiation of ring-opening polymerization processes [25]. Cations Ph-NVK$^+$ produced in catalytic cycle (Figure 5B) have also been well noted in the literature as highly reactive structures [26,27]. Amines, such as EDB presented in photoredox catalytic cycle (Figure 5C), are also well mentioned as efficient co-initiators for free-radical-promoted cationic polymerizations [1,28,29].

In Part 2, a photoredox catalyst useable in such a photocatalytic system will be presented. To be involved properly into the photocatalytical cycle, photoredox catalysts must be chosen with suitable redox potential to perform an oxidation or a reduction with other additives presented above. Thus, redox potentials of additives are resumed in Table 1.

Indeed, additives and photoredox catalysts are involved into redox mechanisms. From a single or triplet state of the photoredox catalyst, an electron is transferred. According to Rehm–Weller, an electron can be transferred from the electron donor to the electron acceptor in the excited state if the free

Table 1: Redox properties of additives [1,30,31].

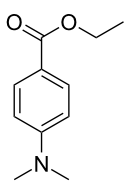

EDB

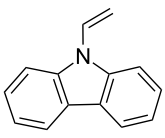

NVK

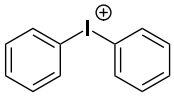

$Ph_2I^⊕$

additives	reaction	redox potential associated	references
Ph_2I^+	reduction	−0.2 V	1
NVK	oxidation	1.17 V	30
EDB	oxidation	1.1 V	31

energy change ΔG_{et} is negative. ΔG_{et} can be calculated from the equation:

$$\Delta G_{et} = E_{ox} - E_{red} - E^* + C \quad (1)$$

where E_{ox} is the oxidation potential of the electron donor, E_{red} the reduction potential of the electron acceptor, E^* the excited state energy level and C the coulombic term for the initially formed ion pair (if there are ions in solution). For polar solvent, C is neglected.

$(TMS)_3SiH$ is not presented in Table 1 because the driving force of its reactivity is more its bond dissociation energy (BDE) than its redox potential. Indeed, this compound obeys to a pure hydrogen transfer mechanism. This corresponds to a hydrogen transfer from $(TMS)_3SiH$ to the triplet excited state of the PC. Thus, to react, the PC must have a lifetime of its triplet excited state that is long enough. The bond dissociation energy of the Si–H of $(TMS)_3SiH$ has been calculated: 79.8 kcal/mol (methods of calculation optimized at the B3LYP/6-31G* level as referred in [32]). Polymerization performances of photoredox catalysts given in example in the present review will be presented in Part 3.

2 The different classes of photoredox catalysts (PCs)

The main characteristics of the different classes of photoredox catalysts will be given below. If historically, photoredox catalysts were based on metals, but recent developments have promoted the emergence of metal-free catalysts that could in the future discard those based on metals, notably due to cost and environmental issues. Both categories of photoredox catalysts (PCs) will be described in this part and a series of structures is given in Scheme 2.

2.1 Metal-based photoredox catalysts

The first photoredox catalysts to emerge were the metal-based complexes. Indeed, metal complexes, also named coordination compounds, have been recognized in the photochemistry field since the second half of the last century [33-35]. However, these compounds are still the subject of extensive researches [36]. Coordination compounds have interesting properties for photochemical reactions. First, by absorption of visible light, transitions described in part 1.3 can be observed. Thus, the complex goes from its ground state to one electronically excited state which produced reactive species. Most of the transitions observed for this complex are LMCT and MLCT (respectively,

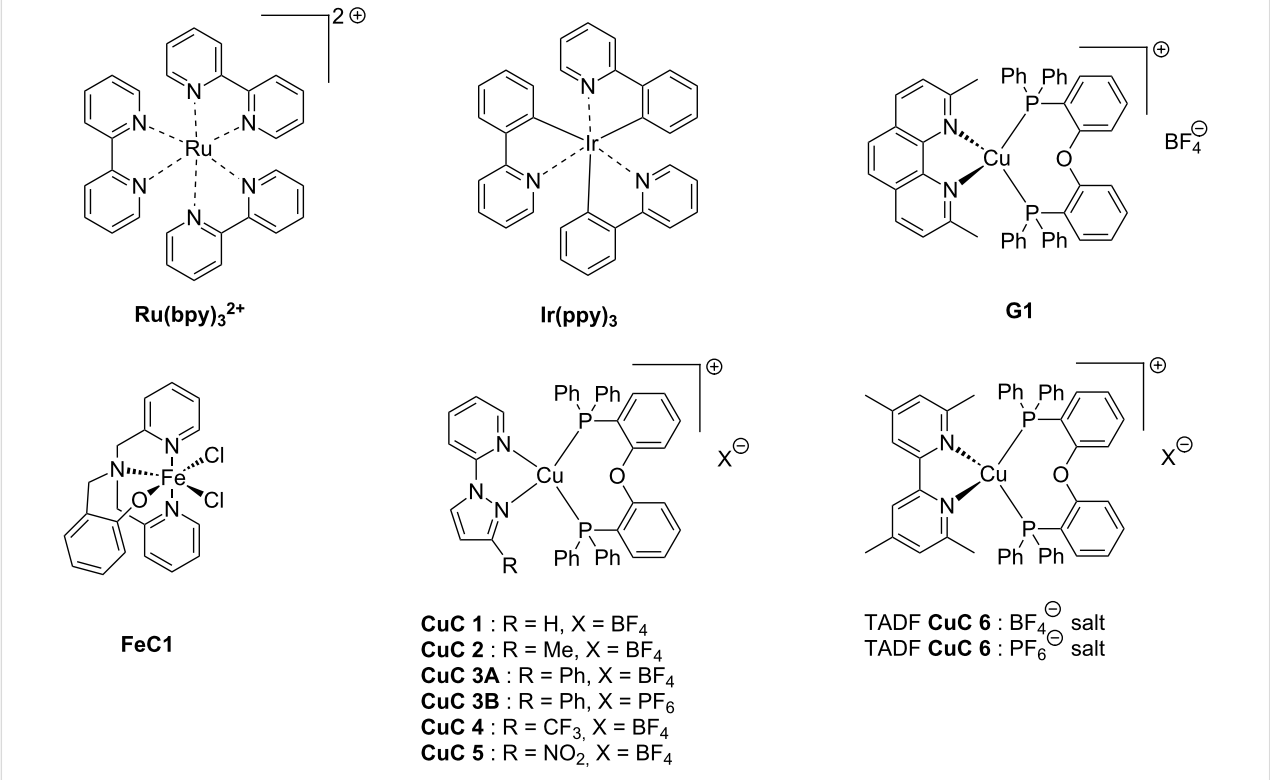

Scheme 2: Structures of photoredox metal-based catalysts.

described in 1.3.4 and 1.3.5). After electron transfer, the metal complex is promoted to an oxidation or reduction state. With well adapted redox potentials and relatively long-lived excited states, these metal-based complexes can be used into photoredox catalysis with suitable oxidation or reductive agents [37-39].

2.1.1 The first generation of metal-based PCs: ruthenium and iridium complexes: The first generation of coordination compounds used for the photoredox catalysis comprises ruthenium and iridium complexes. These two types of metal-based complexes have been substantially developed in the last 40 years for different photochemical applications [40-42] and found wide applications in solar cells [43] or OLEDs (organic light-emitting devices) fabrication [44] and more recently in free radical polymerization [45]. Both complex families can react through oxidative or reductive pathways (Figure 1) depending on the other chemical compounds mixed with them (see below in Part 3 for the polymerization initiated by photoredox catalysis). The light absorption properties of these complexes can be tuned by modification of the structure and more specially by choosing the appropriate ligands. Photochemical reactions can occur upon different light expositions with wavelengths ranging from UV to red light. Low light intensity can be used too, such as the one delivered by household LED bulbs [14]. **$Ru(bpy)_3^{2+}$** is probably the most studied Ru-based photoredox catalyst (abbreviation for ruthenium tris(2,2'-bipyridyl) dichloride; depicted in Scheme 2). The photochemical properties of this complex, commercially available, are gathered in Table 2.

By irradiation of the ruthenium complex, there is a formation of a triplet excited state through metal to ligand charge transfer (Scheme 3, reaction 1). As described in Table 2, the irradiation must be around 450 nm. Thus, as the triplet excited state is long enough and thanks to the values of oxidation potentials, a single electron transfer (SET) to the iodonium salt occurred (Scheme 3, reaction 2) [46]. The formation of phenyl radicals is observed. Another product of reaction 2 is $Ru(bpy)_3^{3+}$. This species is able to react with $(TMS)_3Si^{\bullet}$ to regenerate

Table 2: Characteristics of **$Ru(bpy)_3^{2+}$** [45-48].

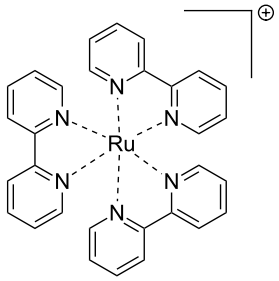

$Ru(bpy)_3^{2+}$

		references
appearance	red solid	
transitions observed	MLCT transition (strong absorption around 450 nm) d–d transition (weak absorption around 350 nm) ligand centered π–π* transition (285 nm)	[45]
nature of the excited state	triplet	[46]
excited state lifetime	1100 ns	[47]
oxidation potentials reduction potentials	$E_{1/2}^{ox}$ = +1.29 V; $E_{1/2}^{+II/I}$ = +0.77 V $E_{1/2}^{III/+II}$ = −0.81 V; $E_{1/2}^{red}$ = −1.33 V	[48]

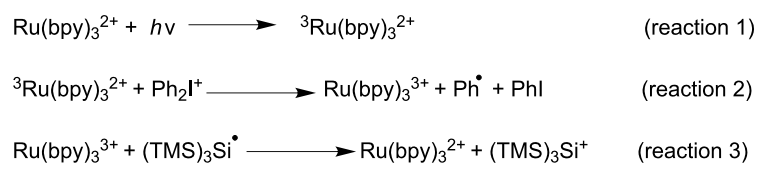

Scheme 3: Photocatalytical cycle for the Ru complex.

$Ru(bpy)_3^{2+}$ (reaction 3). Thus, the photocatalytical cycle is observed.

To conclude, oxidative and reductive photoredox cycles can be observed with $Ru(bpy)_3$. Other ruthenium complexes which can be used into photocatalytical cycles have been described in the literature and more particularly with other type of ligands. Modification of the ligands has an influence on the redox potentials and the lifetime of the excited states [40]. The more the ligand has an electron-donating behavior, the easier is the oxidation of the metal center. For example, adding methyl substituents to the bipyridine ligands of the **$Ru(bpy)_3^{2+}$** complex, the reduction potential shifts from −1.33 V to −1.45 V [49].

Redox potentials of the complex can also be tuned by changing the metal. For example, smaller Stokes shifts are observed using iridium rather than ruthenium metal. That's why Ir-based complexes have also been widely described in the literature as metal-based photoredox catalysts [19]. As an example, **$Ir(ppy)_3$** (abbreviation for tris(2-phenylpyridine)iridium) has been chosen and is depicted in Scheme 2. This metal complex is also commercially available. **$Ir(ppy)_3$** exhibits a MLCT transition in the near UV–visible range. The photochemical properties of this complex are gathered in Table 3.

Interestingly, it is also possible to tune both the light absorption and redox properties through well selected ligands [52]. This Ir-based complex reacts in the photoredox catalytical cycle with iodonium salt and $(TMS)_3SiH$ as the Ru-based complex in reactions 1, 2 and 3. Moreover, Iridium complexes can be interesting for applications in ring-opening photopolymerization initiation as shown in [53] (see Part 3). For this purpose, the Ir complex was more interesting than the Ru one because of the longer excited state lifetime, lower oxidation potential leading to higher interaction rate constants with additives used for ring-opening photopolymerization (e.g., iodonium salt). Thus, promising photoinitiating systems using Ir complexes have been proposed for polymerization under household fluorescence bulbs and even under sun radiation (useful for development of green technologies) [54]. Despite the really interesting properties of Ru and Ir complexes, they have also strong drawbacks limiting their applications to photosensitive systems. First of all, this first generation of complexes is very expensive and can be pretty hard to synthesize. Moreover, the complexes can be toxic [55]. Therefore, it was essential to develop new photoredox catalysts based on low-cost metals such as copper complexes or iron complexes which will be described in detail in the paragraph below.

2.1.2 The second generation of metal-based PCs: copper and iron complexes: Due to their earth-abundant property, iron and copper have received increasing attention and development of Fe and Cu complexes as highly efficient photoredox catalysis has been the subject of many studies [55-58]. These complexes have been identified as really efficient for developing low-cost electroluminescent devices or light-mediated reaction such as polymerization upon near UV or visible light applications (see Part 3).

Table 3: Characteristics of **$Ir(ppy)_3$** [40,50,51]:

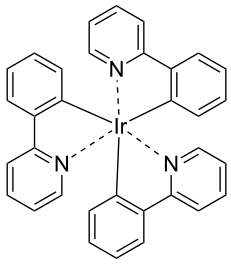

$Ir(ppy)_3$

		references
appearance	yellow to orange solid	
transitions observed	MLCT transition (strong absorption around 375 nm) d–d transition (weak absorption around 278 nm) ligand centered π–π* transition (230 nm)	[40]
nature of the excited state	triplet	[50]
excited state lifetime	1900 ns	[50]
oxidation potentials reduction potentials	$E_{1/2}^{ox}$ = +0.78 V; $E_{1/2}^{+II/I}$ = +0.31 V $E_{1/2}^{III/+II}$ = −1.73 V; $E_{1/2}^{red}$ = −2.20 V	[51]

The development of efficient photoluminescent copper complexes is possible by choosing appropriate ligands. The fine tunings of both redox potentials and visible light absorption properties are also possible [59]. Copper complexes can show really interesting properties for photoredox catalyst applications. Some of them exhibit high emission quantum yields, long excited-state lifetimes and high oxidation potentials adequate for photoredox catalysis [59-62].

One example of highly efficient copper complex developed for photoredox applications is [Cu(neo)(DPEphos)]BF_4 also named **G1** (depicted in Scheme 2). The synthesis of this complex is detailed in references [63] and [64]. The photochemical properties of **G1** are gathered in Table 4.

The multidentate ligands confer to the complex MLCT possibilities like the Ru complexes or Ir complexes described above. This transition is observed after a strong absorption of the complex centered at 380 nm (Table 4). Thus, it can react through a redox cycle with similar reaction than the Ru-based complexes under irradiation by different visible light such as a halogen lamp, laser diodes (405 and 457 nm) or LEDs (405 and 455 nm) [63].

Iron oxide photoredox catalysts have been also developed but not for polymer applications [65]. Iron oxide can offer the same advantages than TiO_2 but with a lower gap between its HOMO and its LUMO which enable visible light excitation and thus, wide applications in heterogeneous photocatalysis for example. Therefore, a large series of iron complexes were also reported as photoredox catalysts. The photosensitivity of this class of transition metal has been recognized since the middle of the last century. Intense absorption bands of these complexes are located in the ultraviolet range and are related to a charge-transfer transition [33]. An example of an iron complex photoredox catalyst **FeC1** is given in Scheme 2 and the associated photochemical properties gathered in Table 5. A synthesis of this complex is detailed in reference [66].

This iron complex with tetradentate monophenolate ligands has raised interest for catalytic reduction of hydrogen gas [64]. Such an iron polypyridyl complex has also really good photoredox catalyst properties to initiate a polymerization upon sunlight exposure in a three-component system [68]. Functionalization of the ligand can change the photochemical properties of the complex as described in [68], i.e., nitro-functionalization and sulfino-functionalization decreased the photocatalytic activity of the complex. Moreover, this functionalization affects the oxidative quenching rate and the stability of the complex. Thus, as for other complexes described above, the choice of the ligand is essential for good properties.

2.1.3 The latest generation of metal-based catalysts: Emergence of the TADF complexes: Metal complexes are still at the origin of numerous researches as photoredox catalysts, these researches being notably motivated by their remarkable long-lived excited state lifetimes that make these structures highly reactive structures. Since 2012 and thanks to the pioneering works of Adachi et al. in this field [69-71], a new class of metal-based complexes has been developed for photoredox application: TADF (abbreviation for Thermally Activated Delayed Fluorescence) complexes.

Table 4: Characteristics of **G1** [63-65].

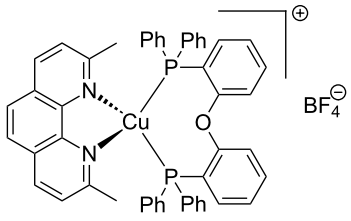

G1

		references
appearance	yellow solid	
transition observed	MLCT transition (strong absorption at 380 nm) more intense intraligand transitions appear at shorter wavelength	[63]
nature of the excited state	triplet	[63]
excited state lifetime	3000 ns	[64]
oxidation potential	$E_{1/2}^{ox}$ = +1.35 V	[65]

Table 5: Characteristics of **FeC1** from [66-68].

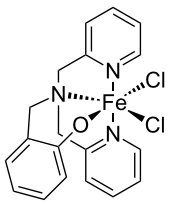

FeC1

		references
appearance	solid	
transitions observed	MLCT transition : pπ → dσ* transition centered at 360 nm pπ → dπ* transition centered at 590 nm	[66]
nature of the excited state	triplet	[66]
lifetime of the excited state	>1 ns	[67]
reduction potential	$E_{1/2}^{red}$ = −1.57 V	[68]

These compounds have singular excited states: their HOMO and their LUMO have been designed to avoid the overlap of the frontier molecular orbitals [32,69]. The energy between the singlet excited state and the triplet excited state becomes inferior to 0.1 eV, an energy easily overcome by thermal activation. Thus, the excited states can be thermally upconverted to the singlet state by reverse intersystem crossing (RISC), giving rise to a luminescence process arising from the singlet state (fluorescence). The concept of delayed fluorescence is based on the unusual and transient localization of the electrons on the triplet state, which upconvert to the singlet state thermally (i.e., at room temperature) and can promote a radiative decay from the singlet excited state. This property gives to TADF complex lifetime of their excited state comparable to the lifetime of the excited state of phosphorescent molecules, e.g., in the microsecond time scale [69].

Due to these really interesting properties, metal-based and metal-free TADF fluorescent materials have been extensively studied over the past few years, improving the photophysics of this new class of materials by molecular design [72-74]. This year, the first use of TADF complexes as photoredox catalysts in polymerization was reported [75]. **CuC 4** whose properties are presented in Table 6 is one of them. The synthesis of this complex has been reported in ref [58]. Other TADF copper complexes which can be used in photoredox cycles are described in this reference.

By their broad absorptions extending from 350 to 450 nm, theses complexes are excellent candidates for photoinitiation in the visible range. Moreover, the reactivity of the chromophores can be tuned by the counter anion, PF_6^- being less nucleophilic than BF_4^-. In this context, both the polymerization rate and the final conversion were both improved by reducing the nucleophilicity of the anion in cationic polymerization. The photochemical properties of TADF **CuC 4** are summarized in Table 6.

From Table 6, it is observable that the properties of **CuC 4** are compatible with its use in a photoredox cycle with similar reactions than Ru-based complexes. Indeed, MLCT is also observed in the near-UV range to reach a triplet excited state with a long lifetime and oxidation potential is compatible with additives involved into a photocatalytical cycle.

2.2 The organophotoredox catalysts

For some specific applications, it can be essential to develop metal-free systems because of potential toxicity, storage stability or bioaccumulation of metal for example. Organic photoredox catalysis has been largely studied in the past few years and is the topic of many reviews [17,40,45,49,52]. Thanks to the ability of some chromophores to transfer electrons when irradiated, they can participate in catalytic processes. These later catalytic processes can be widely applied to organic synthesis or photopolymerization [17]. More than just a “metal-free” alternative, some chromophores allow access to unique chemistries such as photocatalysis at different wavelength or photoconductivity for example [76]. Moreover, they can be characterized by lower costs. For examples, methylene blue or eosin-Y are examples of widespread photoredox catalytic dyes [18].

Table 6: Characteristics of TADF **CuC 4** from [58].

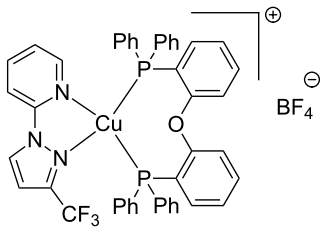

CuC 4

appearance	solid
transition observed	MLCT transition (strong absorption at 355 nm)
nature of the excited state	triplet
lifetime of the excited state	2500 ns
oxidation potential	$E_{1/2}^{ox}$ = +1.42 V

There is a wide range of organophotoredox catalysts. Here, only two examples of photoredox catalysts will be detailed: the carbazole derivatives and the TADF compounds presented as the last generation of organophotoredox catalysts. These examples are depicted in Scheme 4.

2.2.1 Carbazole derivatives: Carbazole derivatives are a good example of organophotoredox catalysts. A carbazole is an aromatic tricyclic organic compound with two six-membered benzene rings fused on either side of a five-membered nitrogen-containing ring. They exhibit unusual optical and electronic properties such as photoconductivity and photorefractivity [77]. More particularly, they are interesting for their high triplet energies, their ability to be quenched by either an electron donor or acceptor, and their reversible oxidation processes [78,79]. To finish, these compounds absorb in the near UV or visible range and related extinction coefficients are found relatively high. Thus, carbazole and its derivatives are good candidates for photoredox catalytic applications.

As an illustration, **C2** (abbreviation for 3-nitro-9-octyl-9*H*-carbazole) has been chosen and is depicted in Scheme 4. This photoredox catalyst can be synthetized as presented in [81]; its photochemical properties are given in Table 7.

We observe from Table 7 that by irradiation in the near-UV range, the excited state of **C2** is reached. This phenomenon can be observed upon exposure to different light irradiation such as light emitting diodes (LEDs) from 405 to 477 nm or a household device for example [80]. The triplet excited state is obtained. From the triplet state of carbazole, similar reactions with ruthenium triplet state (reactions 1, 2, and 3 in Section 2.1.1) can be observed. Moreover, as both oxidation and reduction potential are compatible with additives presented in Scheme 1, both oxidative photocatalytical cycle and reductive photocatalytical cycle are observed with this type of compounds [80]. This is possible only with an appropriate lifetime of the excited state which is remarkably high as we can see in Table 7.

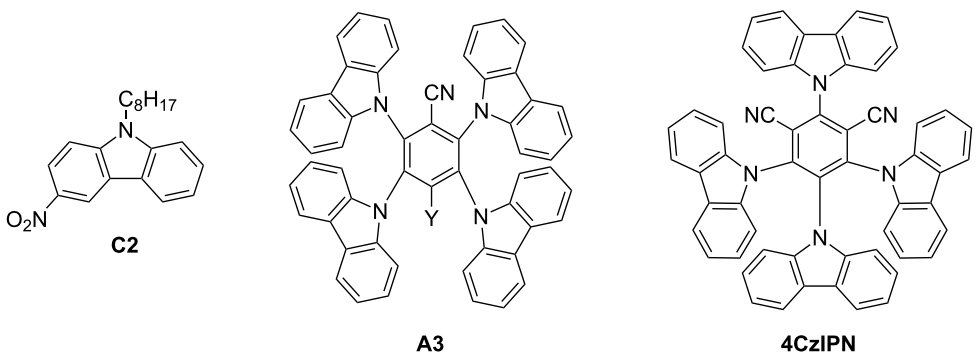

C2 **A3** **4CzIPN**

Scheme 4: Structures of photoredox organocatalysts.

Table 7: Characteristics of **C2** from [80].

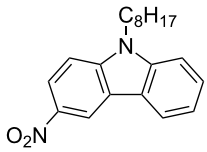

C2

appearance	powder
transition observed	π → π* transition centered at 374 nm
nature of the excited state	triplet
lifetime of the excited state	10 µs under nitrogen and 330 ns under air
oxidation potential	$E_{1/2}^{ox}$ = +1.5 V
reduction potential	$E_{1/2}^{red}$ = −1.38 V

2.2.2 Emergence of the TADF carbazole derivatives: TADF compounds as good candidates for photoredox catalysis have already been presented in Section 2.1.3. It is also possible to find in the literature metal-free TADF compounds with successful application in the photoredox catalysis field [81]. With adequate substituents on the carbazole structures described above, this thermally activated delayed fluorescence property has been observed combined with photoredox catalytical behaviour from UV to 450 nm light.

A3 (abbreviation for 2,3,5,6-tetrakis(*N*-carbazolyl)benzonitrile) is one of those compounds (Scheme 4). A synthetic pathway of **A3** has been detailed in reference [81]. Its absorption extends from UV until 450 nm and can thus be activated at 405 nm with a blue light. Eventually, the peripheral carbazoles can be substituted with halogens. This increases the rate of RISC, and red-shifts the absorption spectrum [81]. For example, with a bromo atom on the peripheral carbazole of **A3**, the absorption at 470 nm is around 800 $M^{-1}{\cdot}cm^{-1}$ where for **A3** almost no absorption is observed. Main characteristics of **A3** have been resumed in Table 8.

The **A3** component can be used both as electron donor and electron acceptor. Indeed, the free energy change (calculated with the Rehm–Weller equation and the redox potential in Table 8) for the electron-transfer reaction is possible both with electron acceptor such as iodonium salt and electron donor such as EDB [76]. In a three-component system **A3**/Iod/EDB (where Iod

Table 8: Characteristics of **A3** [81].

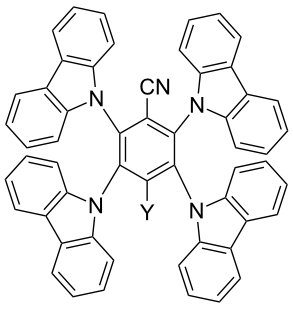

A3

appearance	powder
transition observed	π → π* transition at 333 nm
nature of the excited state	both singlet and triplet
lifetime of the singlet excited state	7.24 µs under nitrogen and 350 ns under air for both states (TADF properties)
oxidation potential	$E_{1/2}^{ox}$ = +1.61 V
reduction potential	$E_{1/2}^{red}$ = −1.63 V

stands for bis(4-*tert*-butylphenyl)iodonium hexafluorophosphate), both oxidative and reductive cycle can be observed and the two routes are even in competition and occur simultaneously. This is reinforced by remarkably long lifetime excited state (Table 8).

In organic chemistry, TADF molecules can also be used as organocatalysts for classical organic reactions that are traditionally carried out in the presence of transition metal complexes. In this field, **4CzIPN** (Scheme 4) that was reported in the first work of Adachi et al. as a green emitter for OLEDs [69,83,84] was revisited numerous times in organocatalysis. In 2017, it was notably used for the chemoselective and regioselective hydroformylation of aromatic olefins [84]. Interestingly, if transition metals can initiate an ionic hydroformylation reaction of aryl olefins, a free radical pathway could be promoted by use of diethoxyacetic acid and **4CzIPN**, inducing the in situ generation of an equivalent of a formyl radical.

Parallel to this, **4CzIPN** was also used as an organoredox catalyst for the alkylation of heteroarenes [85], the oxidation of silicates [86], the alkylation of imines [87], the α-arylation/heteroarylation of 2-trifluoroboratochromanones [88]. In these different situations, comparisons with reference transition metal catalysts classically used as initiators were established and **4CzIPN** could provide performances comparable to that obtained with metal complexes. As specificity, **4CzIPN** is characterized by a broad absorption extending from 250 nm to ≈500 nm. Its different photophysical characteristics are detailed in Table 9.

In order to be concise, only three kinds of organophotocatalysts have been described in the present review. However, over the years, a large number of different organophotocalysts has been described in the literature. Notably, pyrene [89], truxene [90-92], polyaromatic hydrocarbons [93], heteropolyacenes [90,91], carbazoles [80,81,94], triazines [95], pentacenes [96], diketopyrrolopyrroles [24] and perylene [97,98] derivatives have been investigated as organocatalysts as exemplified in Scheme 5.

3 Comparison of the efficiency of these photoredox catalysts in polymerization reactions

Polymerization reactions whose initiation is induced by photoredox catalysts has been detailed in part 1.4. Representative monomer conversions with different photoredox catalysts and upon different irradiation light for free radical polymerization and for cationic polymerization are, respectively, gathered in Table 10 and Table 11.

Additives used for both free radical polymerization and cationic polymerization are discussed in Section 1 and depicted in Scheme 1. Photocatalysts mentioned in Table 10 and Table 11 are the ones described in Section 2 and depicted in Scheme 2 and Scheme 4. To finish, monomers used as example for photopolymerization performance are shown in Scheme 6.

Two types of monomers are presented in Scheme 6. EPOX is a diepoxide which can be polymerized by cationic polymerization. Photopolymerization of the EPOX monomer can be

Table 9: Characteristics of **4CzIPN** [69,82,83].

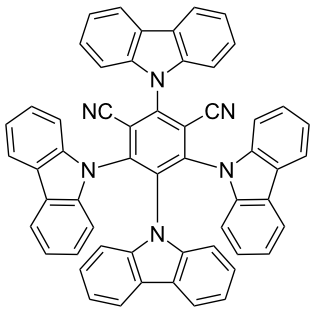

4CzIPN

		references
appearance	powder	
transition observed	π → π* transition around 290 nm	[69]
excited state	singlet and triplet	[82]
lifetime of the excited state	5.1 μs under nitrogen and 91 ns under air for both states (TADF)	[83]
oxidation potential	$E_{1/2}^{ox}$ = +1.35 V	[83]

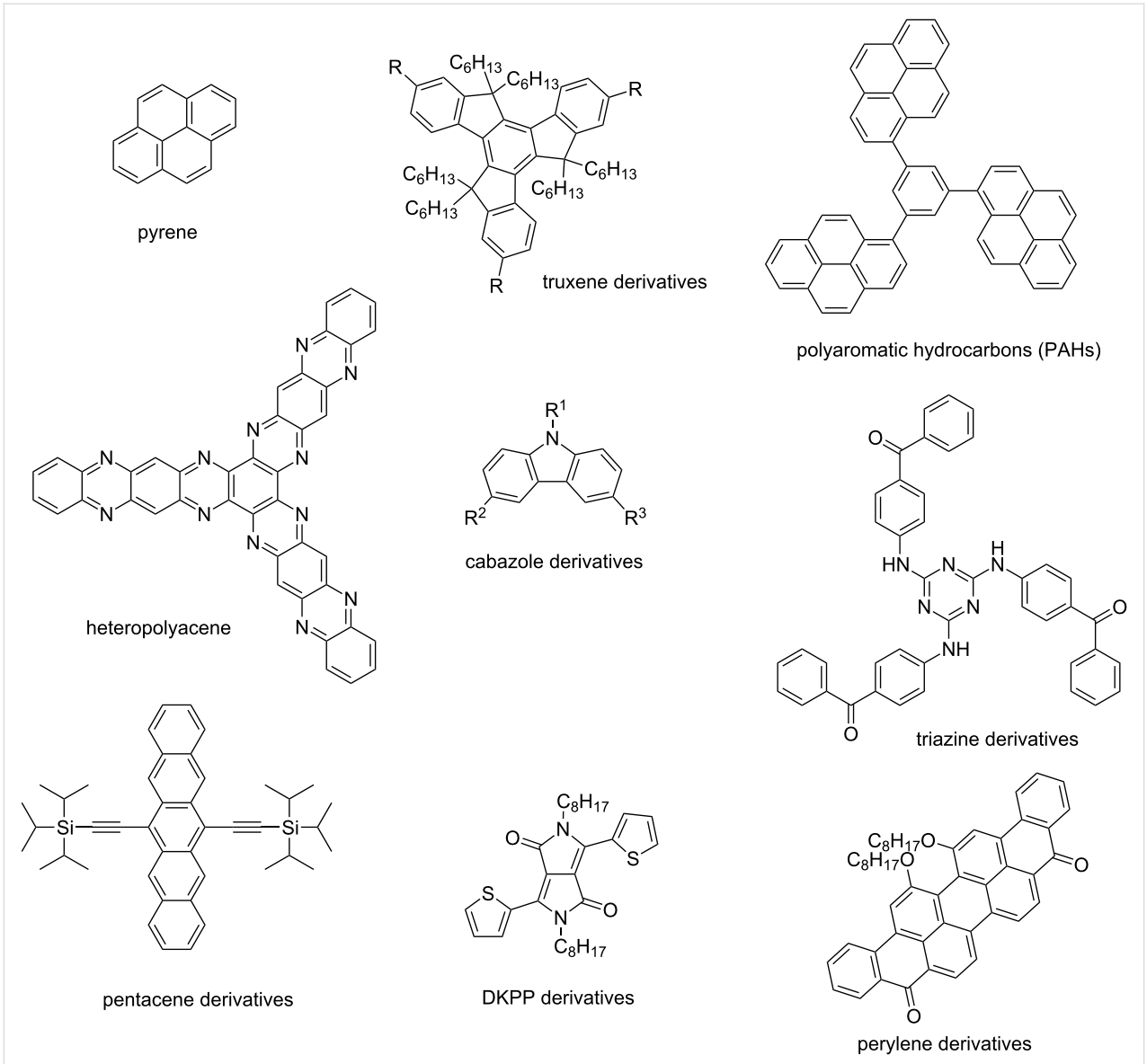

Scheme 5: Diversity of the chemical structures of photoredox organocatalysts.

followed by real-time Fourier transformation infrared spectroscopy, following the epoxy function. Other monomers presented in Scheme 6 are acrylates and methacrylates and can be polymerized by free radical polymerization. Photopolymerization of these compounds can also be characterized by FTIR measurement, following the C=C double bound conversion. The photopolymerization performance of the free radical polymerization using photoredox catalysis is presented in Table 10 and for cationic polymerization in Table 11.

As observed in Table 10, all photocatalysts presented before lead to a free radical polymerization. The first interesting property of a photopolymerization using a photoredox catalyst is the percentage of photoredox catalyst used. Actually, we observed that all polymerizations are performed using less than 0.5 wt % of photoredox catalyst. In most cases, the photoredox catalyst is the most expensive compound of the formulation and using a catalytic system instead of "traditional" PIs, can drastically reduce the final price of the system. Secondly, we noticed that there is no notably difference between the reactivities using a metal-based and a metal-free photoredox catalyst. The choice of the photocatalyst has to be done regarding the application. We observe that different types of light sources are used depending on the system.

For metal-based photocatalysts, the TADF derivative presented gives a remarkably high rate of final conversion for TMPTA.

Table 10: Free radical polymerization performances with metal-based and metal-free photocatalysts [46,53,58,63,80,81,99].

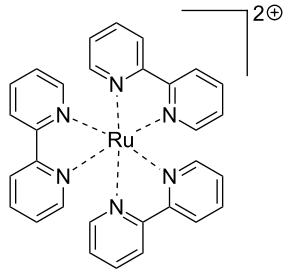

$Ru(bpy)_3^{2+}$

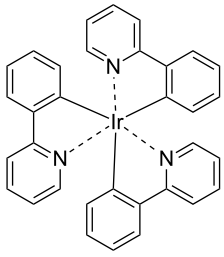

$Ir(ppy)_3$

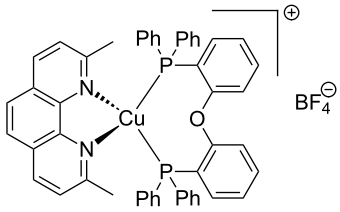

G1

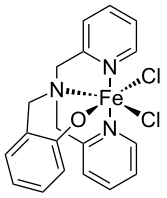

FeC1

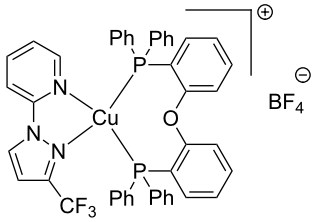

CuC 4

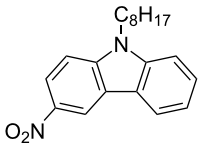

C2

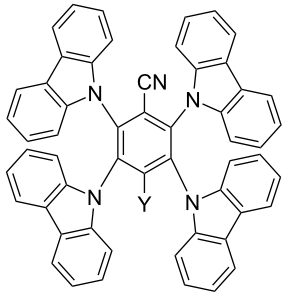

A3

photocatalyst	class of PC	monomer	irradiation	additives	conversion	references
$Ru(bpy)_3^{2+}$ (0.2 wt %)	ruthenium complex	TMPTA	xenon lamp (λ > 390 nm)	Ph_2I^+ (2 wt %) $(TMS)_3SiH$ (3 wt %)	23% laminated 20 μm 200 s of irradiation	[46]
$Ir(ppy)_3$ (0.2 wt %)	irridium complex	TMPTA	xenon lamp (λ > 390 nm)	Ph_2I^+ (2 wt %) $(TMS)_3SiH$ (3 wt %)	40% laminated 25 μm 200 s of irradiation	[53]
G1 (0.1 wt %)	copper complex	TMPTA	LED@455 nm (80 mW/cm²)	Ph_2I^+ (2 wt %) NVK (3 wt %)	56% laminated 20 μm 400 s of irradiation	[63]
FeC1 (0.2 wt %)	iron complex	TMPTA	LED@405 nm (110 mW/cm²)	Ph_2I^+ (2 wt %) NVK (3 wt %)	31% laminated 20 μm 400 s of irradiation	[99]
CuC 4 (0.5 wt %)	copper complex (TADF)	BisGMA/ TEGDMA	LED@405 nm (110 mW/cm²)	Ph_2I^+ (1 wt %) EDB (1 wt %)	80% under air 1.4 mm 800 s of irradiation	[58]
C2 (0.5 wt %)	organic	TMPTA	LED@405 nm (110 W/cm²)	Ph_2I^+ (1 wt %) EDB (1.5 wt %)	57% laminated 25 μm 800 s of irradiation	[80]
		BisGMA/ TEGDMA	LED@477 nm (110 W/cm²)		44% laminated 25 μm 800 s of irradiation	[80]
A3 (0.5 wt %)	organic	TMPTA	LED@405 nm (110 W/cm²)	Ph_2I^+ (1 wt %) EDB (1 wt %)	62% laminated 25 μm 800 s of irradiation	[81]

Table 11: Cationic photopolymerization performance with metal-based and metal-free photoredox catalysts [46,53,58,63,80,81,99,100].

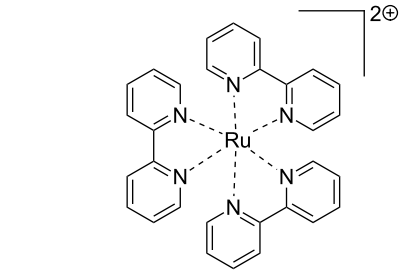

$Ru(bpy)_3^{2+}$

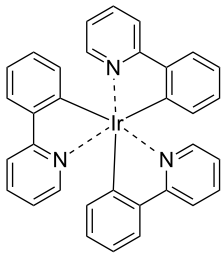

$Ir(ppy)_3$

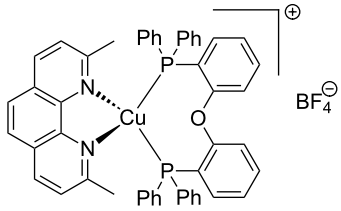

G1

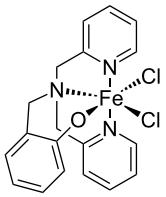

FeC1

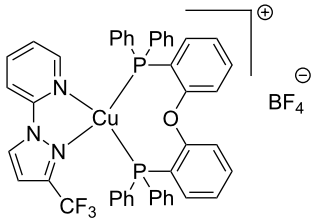

CuC 4

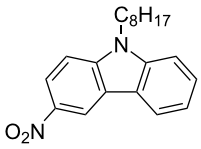

C2

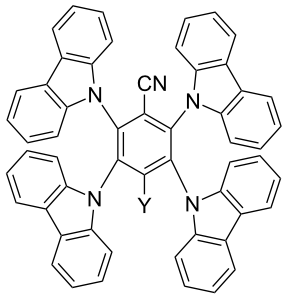

A3

photocatalyst	class of PC	monomer	irradiation	additives	conversion	references
$Ru(bpy)_3^{2+}$ (2 wt %)	ruthenium complex	EPOX	laser diode @457 nm (100 mW/cm^2)	Ph_2I^+ (2 wt %) $(TMS)_3SiH$ (3 wt %)	60% laminated 20 µm 200 s of irradiation	[46]
$Ir(ppy)_3$ (0.2 wt %)	irridium complex	EPOX	blue LED bulb (15 mW/cm²)	Ph_2I^+ (2 wt %) $(TMS)_3SiH$ (3 wt %)	63% laminated 25 µm 180 s of irradiation	[53]
G1 (0.1 wt %)	copper complex	EPOX	LED@455 nm (80 mW/cm^2)	Ph_2I^+ (2 wt %) NVK (3 wt %)	58% under air 20 µm 800 s of irradiation	[63]
FeC1 (0.2 wt %)	iron complex	EPOX	LED@405 nm (110 mW/cm^2)	Ph_2I^+ (2 wt %) NVK (3 wt %)	25% under air 20 µm 800 s of irradiation	[99]
CuC 4 (0.5 wt %)	copper complex (TADF)	EPOX	LED@405 nm (110 mW/cm^2)	Ph_2I^+ (1 wt %) CARET[a] (1 wt %)	63% under air 1.4 mm 800 s of irradiation	[58]
C2 (0.5 wt %)	organic	EPOX	LED@405 nm (110 mW/cm^2)	Ph_2I^+ (1 wt %) EDB (1 wt %)	50% 1.4mm under air 800 s of irradiation	[80]
A3 (0.5 wt %)	organic	EPOX	LED@405 nm (110 mW/cm^2)	Ph_2I^+ (1 wt %) EDB (1 wt %)	54% 25 µm under air 800 s of irradiation	[81]

[a]See Scheme 7 below.

Moreover, the photopolymerization is done under air whereas other photopolymerizations are conducted in a laminated environment. This polymerization is really challenging due to the oxygen inhibition which prove the great efficiency of the system. The organobased photoredox catalyst **A3** gives also a really interesting final conversion.

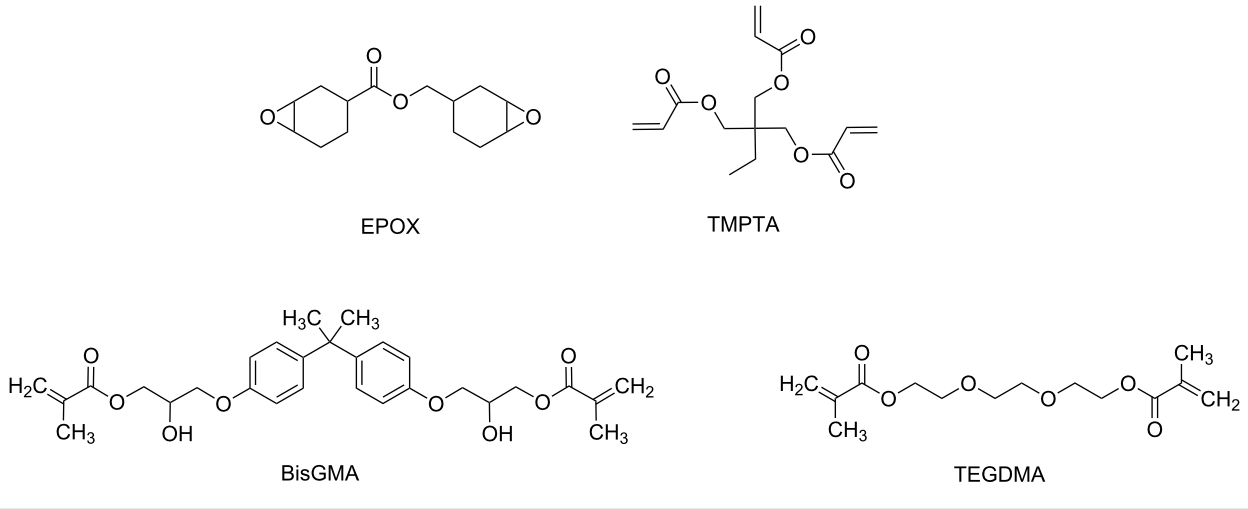

Scheme 6: Structures of benchmarked monomers.

The **CuC 4** photoredox catalyst has been described in the literature using the CARET additive for photopolymerization of EPOX. CARET is depicted in Scheme 7.

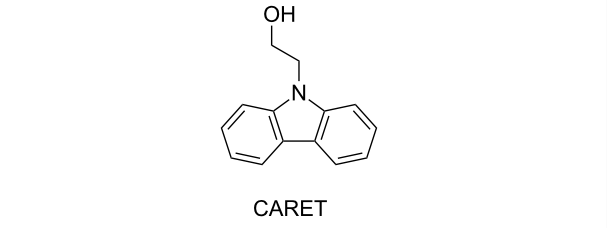

Scheme 7: Structure of the CARET additive.

This compound has exactly the same mechanism of reaction than EDB. There is first a hydrogen abstraction on the compound followed by a reaction with the iodonium salt into the photoredox catalytic cycle as described in Part 1.4, Figure 5.

Regarding the photopolymerization performances reported in Table 11, similar remarks can be made. Photopolymerization of cationic monomer is possible using only a catalytic content of PC and both metal-based and metal-free PC gives polymerization under the conditions tested. The choice of the photoredox catalyst has also to be done regarding the application: final toxicity, choice of the device to perform the polymerization (light irradiation, under air or not…), price of the formulation, etc.

For both free radical and cationic polymerizations, only a very small part of the wide diversity of possible photoredox catalyst has been presented here. Moreover, wavelength of irradiation is here restricted from 300 to 500 nm. In the recent literature, free radical polymerization using a photoredox catalyst has for example been presented using NIR light with both metal-based and metal-free photoredox catalyst [101].

4 Photoredox catalysts in controlled radical polymerization

Photoredox catalysis can also be used in a controlled free radical polymerization. The controlled radical polymerization is a powerful tool for the synthesis of polymers with precise average molar masses, diverse compositions and well-defined architectures [102]. The controlled radical polymerization has raised lots of interest and allows high chain end fidelity and ability to reinitiate the polymer chain.

The use of light to mediate radical photopolymerization can influence two different processes: intramolecular photochemical processes and/or photoredox processes. In this review, we will focus only on photoredox processes. In a photoredox-controlled radical polymerization, a photoredox catalyst is used. By irradiation, it undergoes a single electron transfer with an appropriate initiator. Thus, radicals are produced to initiate the polymerization. The polymerization can be controlled through oxidative or reductive pathways.

An example is provided where the controlled photopolymerizations are based on an oxidative quenching mechanism. This means that the photoredox catalyst is irradiated to go to its excited state and then oxidized by the initiator or the dormant species (R-Mn-Br) [102]. To regenerate the PC, a single electron transfer reaction must be involved as shown in Scheme 8.

Through these single electron transfer processes, photo-ATRP has been successfully achieved (ATRP stands for atom transfer radical polymerization) [104,105]. It is defined by IUPAC by

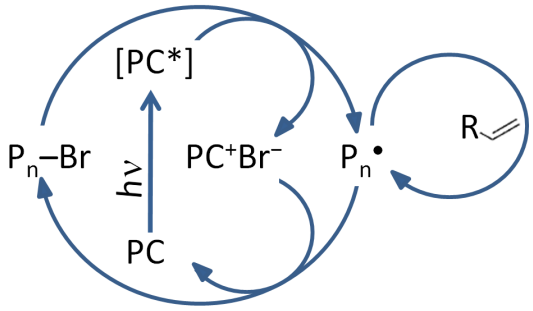

Scheme 8: Photoredox catalysis mechanism of a visible light-mediated living radical polymerization. (Abbreviation: PC for photoredox catalyst, [PC]* the photoredox catalyst at its excited state, P_n the polymeric chain), extracted from [103].

"Controlled reversible-deactivation radical polymerization in which the deactivation of the radicals involves reversible atom transfer or reversible group transfer catalyzed usually, though not exclusively, by transition metal complexes" [106]. In this mechanism, the catalyst is the most important component: it determines the equilibrium constant between the active and dormant species which is directly linked to the distribution of chain lengths [107].

As photoredox catalysts for ATRP applications, copper(II)-complexes have been widely used. For example, bis(1,10-phenanthroline)copper(I) (abbreviated $Cu(phen)_2^{2+}$) is reported in ref [37] as an efficient photoredox catalyst for ATRP upon a simple household blue LED. Ir-based photoredox catalyst are also efficient in this mechanism such as tris(2-phenylpyridinato)iridium(III) reported in ref [37] for photocontrolled radical polymerization of methacrylates. The use of a Fe complex or dye (for metal-free PC) is also possible to performed ATRP as described in reference [107].

A ROMP mechanism is also possible thanks to the photoredox catalyst. ROMP stands for ring-opening metathesis polymerization. This polymerization is based on cyclic olefins whose ring strain is released during polymerization. This reaction needs a catalyst to occur [108]. Metal-free photoredox catalysts for ROMP were proposed in [109]. For example, pyrylium and acridinium salts can be used as good candidates for photooxidation of vinyl ether initiators. A Ru-based ROMP precatalyst: $[Ru(IMesH_2)(CF_3CO_2)(t\text{-}BuCN)_4)]^+ CF_3CO_2^-$ which is a thermally stable photoredox catalyst has been also proposed in [110]. To finish, the RAFT polymerization can be also extended in a photocontrolled polymerization accessible via a photoredox catalyst. RAFT is the abbreviation of reversible addition-fragmentation chain transfer. A RAFT agent is necessary to perform the polymerization [111]. However, ruthenium or iridium PCs have been used in RAFT polymerizations through a photoredox catalytic cycle to suppress oxygen inhibition [112]. Organic photoredox catalysts can also be used to perform a RAFT polymerization, i.e., in [113] trithiocarbonates were proposed as intrinsic photoredox catalysts and RAFT agents.

Conclusion

In the present paper, some examples of metal and metal-free photoredox catalysts are provided for photoreticulation processes of multifunctional radical (acrylate, methacrylate…) or cationic (epoxide) monomers. Undoubtedly, the advantage of the photoredox catalysis approach is the high efficiency of the system to initiate the polymerization upon mild light irradiation conditions (as the catalyst is regenerated) and the low content required. All these works on PC pave the way for highly reactive photosensitive systems that can be used for high tech applications: functional coatings, smart materials, new 3D printing resins, preparation of composites. Other development of PC can be expected in near future.

ORCID® iDs

Aude-Héloise Bonardi - https://orcid.org/0000-0001-5433-5883
Frédéric Dumur - https://orcid.org/0000-0003-4872-094X
Guillaume Noirbent - https://orcid.org/0000-0002-3547-0278

References

1. Fouassier, J. P.; Lalevée, J. *Photoinitiators for Polymer Synthesis;* Wiley-VCH Verlag GmbH: Weinheim, Germany, 2012. doi:10.1002/9783527648245
2. Schnabel, W. *Polymers and Light: Fundamentals and Technical Applications;* Wiley-VCH Verlag GmbH & Co. KGaA, 2007.
3. Fouassier, J. P.; Rabek, J. F., Eds. *Radiation Curing in Polymer Science and Technology—Volume II;* Springer Netherlands: Dordrecht, Netherlands, 1993. doi:10.1007/978-94-011-1876-7
4. Lalevée, J.; Fouassier, J.-P., Eds. *Dyes and Chromophores in Polymer Science;* John Wiley & Sons, Inc.: Hoboken, NJ, U.S.A., 2015. doi:10.1002/9781119006671
5. Glöckner, P. *Radiation Curing: Coatings and Printing Inks;* Technical Basics, Applications and Trouble Shooting: 2008.
6. Moszner, N.; Salz, U. *Macromol. Mater. Eng.* **2007,** *292,* 245–271. doi:10.1002/mame.200600414
7. Ibrahim, A.; Stefano, L. D.; Tarzi, O.; Tar, H.; Ley, C.; Allonas, X. *Photochem. Photobiol.* **2013,** *89,* 1283–1290. doi:10.1111/php.12132
8. Fouassier, J. P.; Allonas, X.; Burget, D. *Prog. Org. Coat.* **2003,** *47,* 16–36. doi:10.1016/s0300-9440(03)00011-0
9. Dietlin, C.; Schweizer, S.; Xiao, P.; Zhang, J.; Morlet-Savary, F.; Graff, B.; Fouassier, J.-P.; Lalevée, J. *Polym. Chem.* **2015,** *6,* 3895–3912. doi:10.1039/c5py00258c
10. Lalevée, J.; Blanchard, N.; Tehfe, M.-A.; Peter, M.; Morlet-Savary, F.; Gigmes, D.; Fouassier, J. P. *Polym. Chem.* **2011,** *2,* 1986–1991. doi:10.1039/c1py00140j
11. Lalevée, J.; Fouassier, J.-P., Eds. *Photopolymerisation Initiating Systems;* Polymer Chemistry Series; Royal Society of Chemistry: Cambridge, United Kingdom, 2018. doi:10.1039/9781788013307
12. A. Al Mousawi, Université de Haute-Alsace, 2018.

13. Lalevée, J.; Peter, M.; Dumur, F.; Gigmes, D.; Blanchard, N.; Tehfe, M.-A.; Morlet-Savary, F.; Fouassier, J. P. *Chem. – Eur. J.* **2011,** *17,* 15027–15031. doi:10.1002/chem.201101445
14. Lalevée, J.; Tehfe, M.-A.; Dumur, F.; Gigmes, D.; Blanchard, N.; Morlet-Savary, F.; Fouassier, J. P. *ACS Macro Lett.* **2012,** *1,* 286–290. doi:10.1021/mz2001753
15. Crivello, J. V.; Lam, J. H. W. *Macromolecules* **1977,** *10,* 1307–1315. doi:10.1021/ma60060a028
16. Lalevée, J.; Tehfe, M.-A.; Morlet-Savary, F.; Graff, B.; Dumur, F.; Gigmes, D.; Blanchard, N.; Fouassier, J.-P. *Chimia* **2012,** *66,* 439–441. doi:10.2533/chimia.2012.439
17. Romero, N. A.; Nicewicz, D. A. *Chem. Rev.* **2016,** *116,* 10075–10166. doi:10.1021/acs.chemrev.6b00057
18. Nicewicz, D. A.; Nguyen, T. M. *ACS Catal.* **2014,** *4,* 355–360. doi:10.1021/cs400956a
19. Crivello, J. V.; Lam, J. H. W. *J. Polym. Sci., Polym. Chem. Ed.* **1978,** *16,* 2441–2451. doi:10.1002/pol.1978.170161004
20. Garra, P.; Graff, B.; Morlet-Savary, F.; Dietlin, C.; Becht, J.-M.; Fouassier, J.-P.; Lalevée, J. *Macromolecules* **2018,** *51,* 57–70. doi:10.1021/acs.macromol.7b02185
21. Stöver, H. D. H.; Li, K. In *Polymeric Materials Encyclopedia;* Salamone, J. C., Ed.; CRC Press: New York, 1996.
22. Atkins, P.; Overton, T. *Shriver and Atkins' Inorganic Chemistry;* OUP Oxford, 2010.
23. Braun, D. *Int. J. Polym. Sci.* **2009,** No. 893234. doi:10.1155/2009/893234
24. Bouzrati-Zerelli, M.; Zivic, N.; Dumur, F.; Gigmes, D.; Graff, B.; Fouassier, J. P.; Lalevée, J. *Polym. Chem.* **2017,** *8,* 2028–2040. doi:10.1039/c7py00202e
25. Kim, D.; Scranton, A. B.; Stansbury, J. W. *J. Polym. Sci., Part A: Polym. Chem.* **2009,** *47,* 1429–1439. doi:10.1002/pola.23252
26. Neckers, D. C.; Valdes-Aguilera, O. M. Photochemistry of the Xanthene Dyes, Chapter 4. *Advances in Photochemistry;* John Wiley & Sons, Inc.: Hoboken, NJ, U.S.A., 2007; pp 315–394. doi:10.1002/9780470133491.ch4
27. Lalevée, J.; Tehfe, M.-A.; Zein-Fakih, A.; Ball, B.; Telitel, S.; Morlet-Savary, F.; Graff, B.; Fouassier, J. P. *ACS Macro Lett.* **2012,** *1,* 802–806. doi:10.1021/mz3002325
28. Hua, Y.; Crivello, J. V. *Macromolecules* **2001,** *34,* 2488–2494. doi:10.1021/ma0018502
29. Ledwith, A. *Polymer* **1978,** *19,* 1217–1219. doi:10.1016/0032-3861(78)90073-3
30. Fouassier, J. P.; Burr, D.; Crivello, J. V. *J. Photochem. Photobiol., A* **1989,** *49,* 317–324. doi:10.1016/1010-6030(89)87130-8
31. Geißler, U.; Hallensleben, M. L.; Toppare, L. *Synth. Met.* **1993,** *55,* 1483–1488. doi:10.1016/0379-6779(93)90272-x
32. El-Roz, M.; Lalevée, J.; Allonas, X.; Fouassier, J. P. *Macromolecules* **2009,** *42,* 8725–8732. doi:10.1021/ma9017313
33. Adamson, A. W.; Waltz, W. L.; Zinato, E.; Watts, D. W.; Fleischauer, P. D.; Lindholm, R. D. *Chem. Rev.* **1968,** *68,* 541–585. doi:10.1021/cr60255a002
34. Lehn, J.-M. In *Perspectives in coordination chemistry;* Williams, A. F.; Floriani, C.; Merbach, A. E., Eds.; 1992; p 447.
35. Balzani, V.; Credi, A.; Venturi, M. *Coord. Chem. Rev.* **1998,** *171,* 3–16. doi:10.1016/s0010-8545(98)90005-4
36. *Photochemistry and Photophysics of Coordination Compounds II;* Springer-Verlag: Berlin Heidelberg, 2007; Vol. 281.
37. Fors, B. P.; Hawker, C. J. *Angew. Chem., Int. Ed.* **2012,** *51,* 8850–8853. doi:10.1002/anie.201203639
38. Balzani, V.; Bolletta, F.; Gandolfi, M. T.; Maestri, M. Bimolecular electron transfer reactions of the excited states of transition metal complexes. *Organic Chemistry and Theory;* Topics in Current Chemistry; Springer-Verlag: Berlin, Germany; pp 1–64. doi:10.1007/bfb0048835
39. Ohtsuki, A.; Goto, A.; Kaji, H. *Macromolecules* **2013,** *46,* 96–102. doi:10.1021/ma302244j
40. Prier, C. K.; Rankic, D. A.; MacMillan, D. W. C. *Chem. Rev.* **2013,** *113,* 5322–5363. doi:10.1021/cr300503r
41. Singh, A.; Kubik, J. J.; Weaver, J. D. *Chem. Sci.* **2015,** *6,* 7206–7212. doi:10.1039/c5sc03013g
42. Campagna, S.; Puntoriero, F.; Nastasi, F.; Bergamini, G.; Balzani, V. Photochemistry and Photophysics of Coordination Compounds: Ruthenium. *Photochemistry and Photophysics of Coordination Compounds I;* Topics in Current Chemistry; Springer Berlin: Berlin, Germany, 2007; pp 117–214. doi:10.1007/128_2007_133
43. Adeloye, A.; Ajibade, P. *Molecules* **2014,** *19,* 12421–12460. doi:10.3390/molecules190812421
44. Okada, S.; Okinaka, K.; Iwawaki, H.; Furugori, M.; Hashimoto, M.; Mukaide, T.; Kamatani, J.; Igawa, S.; Tsuboyama, A.; Takiguchi, T.; Ueno, K. *Dalton Trans.* **2005,** 1583–1590. doi:10.1039/b417058j
45. Nicewicz, D. A.; MacMillan, D. W. C. *Science* **2008,** *322,* 77–80. doi:10.1126/science.1161976
46. Kalyanasundaram, K. *Coord. Chem. Rev.* **1982,** *46,* 159–244. doi:10.1016/0010-8545(82)85003-0
47. Juris, A.; Balzani, V.; Barigelletti, F.; Campagna, S.; Belser, P.; von Zelewsky, A. *Coord. Chem. Rev.* **1988,** *84,* 85–277. doi:10.1016/0010-8545(88)80032-8
48. Juris, A.; Balzani, V.; Belser, P.; von Zelewsky, A. *Helv. Chim. Acta* **1981,** *64,* 2175–2182. doi:10.1002/hlca.19810640723
49. Tucker, J. W.; Stephenson, C. R. J. *J. Org. Chem.* **2012,** *77,* 1617–1622. doi:10.1021/jo202538x
50. Farney, E. P.; Yoon, T. P. *Angew. Chem., Int. Ed.* **2014,** *53,* 793–797. doi:10.1002/anie.201308820
51. Singh, A.; Teegardin, K.; Kelly, M.; Prasad, K. S.; Krishnan, S.; Weaver, J. D. *J. Organomet. Chem.* **2015,** *776,* 51–59. doi:10.1016/j.jorganchem.2014.10.037
52. Teegardin, K.; Day, J. I.; Chan, J.; Weaver, J. *Org. Process Res. Dev.* **2016,** *20,* 1156–1163. doi:10.1021/acs.oprd.6b00101
53. Lalevée, J.; Blanchard, N.; Tehfe, M.-A.; Peter, M.; Morlet-Savary, F.; Fouassier, J. P. *Macromol. Rapid Commun.* **2011,** *32,* 917–920. doi:10.1002/marc.201100098
54. Lalevée, J.; Blanchard, N.; Tehfe, M.-A.; Morlet-Savary, F.; Fouassier, J. P. *Macromolecules* **2010,** *43,* 10191–10195. doi:10.1021/ma1023318
55. Mokbel, H.; Anderson, D.; Plenderleith, R.; Dietlin, C.; Morlet-Savary, F.; Dumur, F.; Gigmes, D.; Fouassier, J.-P.; Lalevée, J. *Polym. Chem.* **2017,** *8,* 5580–5592. doi:10.1039/c7py01016h
56. Garra, P.; Carré, M.; Dumur, F.; Morlet-Savary, F.; Dietlin, C.; Gigmes, D.; Fouassier, J.-P.; Lalevée, J. *Macromolecules* **2018,** *51,* 679–688. doi:10.1021/acs.macromol.7b02491
57. Dumur, F. *Org. Electron.* **2015,** *21,* 27–39. doi:10.1016/j.orgel.2015.02.026
58. Al Mousawi, A.; Kermagoret, A.; Versace, D.-L.; Toufaily, J.; Hamieh, T.; Graff, B.; Dumur, F.; Gigmes, D.; Fouassier, J. P.; Lalevée, J. *Polym. Chem.* **2017,** *8,* 568–580. doi:10.1039/c6py01958g
59. McMillin, D. R.; McNett, K. M. *Chem. Rev.* **1998,** *98,* 1201–1220. doi:10.1021/cr9601167

60. Harkins, S. B.; Peters, J. C. *J. Am. Chem. Soc.* **2005,** *127,* 2030–2031. doi:10.1021/ja043092r
61. Dumur, F.; Gigmes, D.; Fouassier, J.-P.; Lalevée, J. *Acc. Chem. Res.* **2016,** *49,* 1980–1989. doi:10.1021/acs.accounts.6b00227
62. Cuttell, D. G.; Kuang, S.-M.; Fanwick, P. E.; McMillin, D. R.; Walton, R. A. *J. Am. Chem. Soc.* **2002,** *124,* 6–7. doi:10.1021/ja012247h
63. Xiao, P.; Dumur, F.; Zhang, J.; Fouassier, J. P.; Gigmes, D.; Lalevée, J. *Macromolecules* **2014,** *47,* 3837–3844. doi:10.1021/ma5006793
64. Lalevée, J.; Xiao, P.; Gigmes, D.; Dumur, F. Light induced free radical and/or cationic photopolymerization method. Eur. Pat. EP3114148A1, 2015.
65. Laurier, K. G. M.; Vermoortele, F.; Ameloot, R.; De Vos, D. E.; Hofkens, J.; Roeffaers, M. B. J. *J. Am. Chem. Soc.* **2013,** *135,* 14488–14491. doi:10.1021/ja405086e
66. Cavell, A. C.; Hartley, C. L.; Liu, D.; Tribble, C. S.; McNamara, W. R. *Inorg. Chem.* **2015,** *54,* 3325–3330. doi:10.1021/ic5030394
67. Creutz, C.; Chou, M.; Netzel, T. L.; Okumura, M.; Sutin, N. *J. Am. Chem. Soc.* **1980,** *102,* 1309–1319. doi:10.1021/ja00524a014
68. Hartley, C. L.; DiRisio, R. J.; Screen, M. E.; Mayer, K. J.; McNamara, W. R. *Inorg. Chem.* **2016,** *55,* 8865–8870. doi:10.1021/acs.inorgchem.6b01413
69. Uoyama, H.; Goushi, K.; Shizu, K.; Nomura, H.; Adachi, C. *Nature* **2012,** *492,* 234–238. doi:10.1038/nature11687
70. Mamada, M.; Inada, K.; Komino, T.; Potscavage, W. J., Jr.; Nakanotani, H.; Adachi, C. *ACS Cent. Sci.* **2017,** *3,* 769–777. doi:10.1021/acscentsci.7b00183
71. Adachi, C. *Jpn. J. Appl. Phys.* **2014,** *53,* 060101. doi:10.7567/jjap.53.060101
72. Im, Y.; Kim, M.; Cho, Y. J.; Seo, J.-A.; Yook, K. S.; Lee, J. Y. *Chem. Mater.* **2017,** *29,* 1946–1963. doi:10.1021/acs.chemmater.6b05324
73. Dias, F. B.; Penfold, T. J.; Monkman, A. P. *Methods Appl. Fluoresc.* **2017,** *5,* 012001. doi:10.1088/2050-6120/aa537e
74. Zhang, W.; Jin, J.; Huang, Z.; Zhuang, S.; Wang, L. *Sci. Rep.* **2016,** *6,* 30178. doi:10.1038/srep30178
75. Bouzrati-Zerelli, M.; Guillaume, N.; Goubard, F.; Bui, T.-T.; Villotte, S.; Dietlin, C.; Morlet-Savary, F.; Gigmes, D.; Fouassier, J. P.; Dumur, F.; Lalevée, J. *New J. Chem.* **2018,** *42,* 8261–8270. doi:10.1039/c7nj04394e
76. Luo, J.; Zhang, J. *ACS Catal.* **2016,** *6,* 873–877. doi:10.1021/acscatal.5b02204
77. Zhang, Y.; Wada, T.; Sasabe, H. *J. Mater. Chem.* **1998,** *8,* 809–828. doi:10.1039/a705129h
78. Valeur, B.; Berberan-Santos, M. N. *Molecular Fluorescence: Principles and Applications;* John Wiley & Sons, 2012. doi:10.1002/9783527650002
79. Ambrose, J. F.; Nelson, R. F. *J. Electrochem. Soc.* **1968,** *115,* 1159–1164. doi:10.1149/1.2410929
80. Al Mousawi, A.; Dumur, F.; Garra, P.; Toufaily, J.; Hamieh, T.; Graff, B.; Gigmes, D.; Fouassier, J. P.; Lalevée, J. *Macromolecules* **2017,** *50,* 2747–2758. doi:10.1021/acs.macromol.7b00210
81. Al Mousawi, A.; Lara, D. M.; Noirbent, G.; Dumur, F.; Toufaily, J.; Hamieh, T.; Bui, T.-T.; Goubard, F.; Graff, B.; Gigmes, D.; Fouassier, J. P.; Lalevée, J. *Macromolecules* **2017,** *50,* 4913–4926. doi:10.1021/acs.macromol.7b01114
82. Im, Y.; Lee, J. Y. *J. Inf. Disp.* **2017,** *18,* 101–117. doi:10.1080/15980316.2017.1333046
83. Hosokai, T.; Matsuzaki, H.; Nakanotani, H.; Tokumaru, K.; Tsutsui, T.; Furube, A.; Nasu, K.; Nomura, H.; Yahiro, M.; Adachi, C. *Sci. Adv.* **2017,** *3,* e1603282. doi:10.1126/sciadv.1603282
84. Huang, H.; Yu, C.; Zhang, Y.; Zhang, Y.; Mariano, P. S.; Wang, W. *J. Am. Chem. Soc.* **2017,** *139,* 9799–9802. doi:10.1021/jacs.7b05082
85. Matsui, J. K.; Primer, D. N.; Molander, G. A. *Chem. Sci.* **2017,** *8,* 3512–3522. doi:10.1039/c7sc00283a
86. Lévêque, C.; Chenneberg, L.; Corcé, V.; Ollivier, C.; Fensterbank, L. *Chem. Commun.* **2016,** *52,* 9877–9880. doi:10.1039/c6cc04636c
87. Patel, N. R.; Kelly, C. B.; Siegenfeld, A. P.; Molander, G. A. *ACS Catal.* **2017,** *7,* 1766–1770. doi:10.1021/acscatal.6b03665
88. Matsui, J. K.; Molander, G. A. *Org. Lett.* **2017,** *19,* 436–439. doi:10.1021/acs.orglett.6b03448
89. Telitel, S.; Dumur, F.; Faury, T.; Graff, B.; Tehfe, M.-A.; Gigmes, D.; Fouassier, J.-P.; Lalevée, J. *Beilstein J. Org. Chem.* **2013,** *9,* 877–890. doi:10.3762/bjoc.9.101
90. Tehfe, M.-A.; Lalevée, J.; Telitel, S.; Contal, E.; Dumur, F.; Gigmes, D.; Bertin, D.; Nechab, M.; Graff, B.; Morlet-Savary, F.; Fouassier, J.-P. *Macromolecules* **2012,** *45,* 4454–4460. doi:10.1021/ma300760c
91. Tehfe, M.-A.; Dumur, F.; Contal, E.; Graff, B.; Gigmes, D.; Fouassier, J.-P.; Lalevée, J. *Macromol. Chem. Phys.* **2013,** *214,* 2189–2201.
92. Lalevée, J.; Tehfe, M.-A.; Dumur, F.; Gigmes, D.; Graff, B.; Morlet-Savary, F.; Fouassier, J.-P. *Macromol. Rapid Commun.* **2013,** *34,* 239–245. doi:10.1002/marc.201200578
93. Tehfe, M.-A.; Lalevée, J.; Morlet-Savary, F.; Graff, B.; Blanchard, N.; Fouassier, J.-P. *Macromolecules* **2012,** *45,* 1746–1752. doi:10.1021/ma300050n
94. Pan, X.; Fang, C.; Fantin, M.; Malhotra, N.; So, W. Y.; Peteanu, L. A.; Isse, A. A.; Gennaro, A.; Liu, P.; Matyjaszewski, K. *J. Am. Chem. Soc.* **2016,** *138,* 2411–2425. doi:10.1021/jacs.5b13455
95. Tehfe, M.-A.; Dumur, F.; Graff, B.; Morlet-Savary, F.; Fouassier, J.-P.; Gigmes, D.; Lalevée, J. *Macromolecules* **2012,** *45,* 8639–8647. doi:10.1021/ma301931p
96. Tehfe, M.-A.; Lalevée, J.; Morlet-Savary, F.; Graff, B.; Blanchard, N.; Fouassier, J.-P. *ACS Macro Lett.* **2012,** *1,* 198–203. doi:10.1021/mz200140y
97. Xiao, P.; Dumur, F.; Frigoli, M.; Graff, B.; Morlet-Savary, F.; Wantz, G.; Bock, H.; Fouassier, J. P.; Gigmes, D.; Lalevée, J. *Eur. Polym. J.* **2014,** *53,* 215–222. doi:10.1016/j.eurpolymj.2014.01.024
98. Tehfe, M.-A.; Lalevée, J.; Morlet-Savary, F.; Graff, B.; Fouassier, J.-P. *Macromolecules* **2011,** *44,* 8374–8379. doi:10.1021/ma2017265
99. Xiao, P.; Zhang, J.; Campolo, D.; Dumur, F.; Gigmes, D.; Fouassier, J. P.; Lalevée, J. *J. Polym. Sci., Part A: Polym. Chem.* **2015,** *53,* 2673–2684. doi:10.1002/pola.27762
100. Zhang, J.; Campolo, D.; Dumur, F.; Xiao, P.; Fouassier, J. P.; Gigmes, D.; Lalevée, J. *J. Polym. Sci., Part A: Polym. Chem.* **2015,** *53,* 42–49. doi:10.1002/pola.27435
101. Bonardi, A. H.; Dumur, F.; Grant, T. M.; Noirbent, G.; Gigmes, D.; Lessard, B. H.; Fouassier, J.-P.; Lalevée, J. *Macromolecules* **2018,** *51,* 1314–1324. doi:10.1021/acs.macromol.8b00051
102. Chen, M.; Zhong, M.; Johnson, J. A. *Chem. Rev.* **2016,** *116,* 10167–10211. doi:10.1021/acs.chemrev.5b00671
103. Leibfarth, F. A.; Mattson, K. M.; Fors, B. P.; Collins, H. A.; Hawker, C. J. *Angew. Chem., Int. Ed.* **2013,** *52,* 199–210. doi:10.1002/anie.201206476
104. Wang, J.-S.; Matyjaszewski, K. *J. Am. Chem. Soc.* **1995,** *117,* 5614–5615. doi:10.1021/ja00125a035

105. Matyjaszewski, K.; Xia, J. *Chem. Rev.* **2001,** *101,* 2921–2990. doi:10.1021/cr940534g
106. Jenkins, A. D.; Jones, R. G.; Moad, G. *Pure Appl. Chem.* **2009,** *82,* 483–491. doi:10.1351/pac-rep-08-04-03
107. Treat, N. J.; Sprafke, H.; Kramer, J. W.; Clark, P. G.; Barton, B. E.; Read de Alaniz, J.; Fors, B. P.; Hawker, C. J. *J. Am. Chem. Soc.* **2014,** *136,* 16096–16101. doi:10.1021/ja510389m
108. Frech, C. M.; Blacque, O.; Berke, H. *Pure Appl. Chem.* **2006,** *78,* 1877–1887. doi:10.1351/pac200678101877
109. Ogawa, K. A.; Goetz, A. E.; Boydston, A. J. *J. Am. Chem. Soc.* **2015,** *137,* 1400–1403. doi:10.1021/ja512073m
110. Wang, D.; Wurst, K.; Knolle, W.; Decker, U.; Prager, L.; Naumov, S.; Buchmeiser, M. R. *Angew. Chem., Int. Ed.* **2008,** *47,* 3267–3270. doi:10.1002/anie.200705220
111. Yeole, N. *Synlett* **2010,** 1572–1573. doi:10.1055/s-0029-1219938
112. Xu, J.; Jung, K.; Atme, A.; Shanmugam, S.; Boyer, C. *J. Am. Chem. Soc.* **2014,** *136,* 5508–5519. doi:10.1021/ja501745g
113. Fu, Q.; Xie, K.; McKenzie, T. G.; Qiao, G. G. *Polym. Chem.* **2017,** *8,* 1519–1526. doi:10.1039/c6py01994c

License and Terms

BEILSTEIN JOURNAL OF ORGANIC CHEMISTRY

N-Arylphenothiazines as strong donors for photoredox catalysis – pushing the frontiers of nucleophilic addition of alcohols to alkenes

Fabienne Speck, David Rombach and Hans-Achim Wagenknecht*

Full Research Paper

Open Access

Address:
Institute of Organic Chemistry, Karlsruhe Institute of Technology (KIT), Fritz-Haber-Weg 6, 76131 Karlsruhe, Germany

Email:
Hans-Achim Wagenknecht* - Wagenknecht@kit.edu

* Corresponding author

Keywords:
addition; phenothiazine; photochemistry; photoredox catalysis; redox potential

Beilstein J. Org. Chem. **2019,** *15,* 52–59.
doi:10.3762/bjoc.15.5

Received: 13 July 2018
Accepted: 12 December 2018
Published: 04 January 2019

This article is part of the thematic issue "Photoredox catalysis for novel organic reactions".

Guest Editor: P. H. Seeberger

Abstract

A new range of *N*-phenylphenothiazine derivatives was synthesized as potential photoredox catalysts to broaden the substrate scope for the nucleophilic addition of methanol to styrenes through photoredox catalysis. These *N*-phenylphenothiazines differ by their electron-donating and electron-withdrawing substituents at the phenyl group, covering both, σ and π-type groups, in order to modulate their absorbance and electrochemical characteristics. Among the synthesized compounds, alkylaminylated *N*-phenylphenothiazines were identified to be highly suitable for photoredox catalysis. The dialkylamino substituents of these *N*-phenylphenothiazines shift the estimated excited state reduction potential up to −3.0 V (vs SCE). These highly reducing properties allow the addition of methanol to α-methylstyrene as less-activated substrate for this type of reaction. Without the help of an additive, the reaction conditions were optimized to achieve a quantitative yield for the Markovnivkov-type addition product after 20 h of irradiation.

Introduction

Visible-light photoredox catalysis has become a precious tool in modern synthetic organic chemistry and experiences a continuously growing interest in industrial applications. The access to electronically excited states of organic molecules allows unlocking new and sometimes complementary chemical reactivities that cannot be tackled by using thermally driven chemical reactions [1]. This complementarity allows for the development of so far unknown transformations [2]. The photochemical reactivity can be tuned by the absorption and excited state characteristics of the photocatalyst. In this context, organic dyes represent a perfectly suited class of photocatalysts as they can easily be modified by the introduction of functional groups that allow

fine-tuning the optoelectronic properties of the molecules. Photochemical methods have allowed to overcome some of the current limitations in thermally driven chemistry and to substitute conventional energy demanding chemistry by highly sustainable photochemical methods [3-12].

Phenothiazines have become a precious class of organic molecules, not only due to their widespread use in medicinal chemistry [13] but also because of their fascinating electronic properties. Recently their use in photoredox catalysis allowed for the development of some novel transformations, namely dehalogenation [14] as well as the first pentafluorosulfanylation method starting from sulfur hexafluoride [2]. We are convinced that the value of phenothiazine derivatives in photoredox catalysis is still underestimated. While these compounds found widespread use in ATRA (atom transfer radical addition) polymerization [15,16] the interest of using this class of catalysts only gained limited interest during the last years. The advantage of using *N*-phenylphenothiazine catalysts in photoredox chemistry is attributed to their beneficial redox properties. Moreover, a modification of the core is rather simple and allows fast access to a wide variety of catalysts. Recently it was shown that the radical cation of the photoredox catalyst can play a key role in photoinduced oxidation chemistry [16]. This is rather unusual due to the usually short lifetime of radical cations in solution attributed to their low-lying excited states. Normally, this is the reason why photochemical processes can hardly compete with photophysical decay processes. However, a pre-coordination of the substrate may facilitate electron transfer under non-diffusional controlled conditions. Very recently, the fast (picosecond) excited state dynamics of the radical cation of *N*-phenylphenothiazine was investigated by Wasielewski et al. This radical cation had a high reduction potential of about +2.1 V (vs SCE) [17] allowing the reduction of poorly oxidizing agents. The combination of both properties in one system is a remarkable feature for chemical redox dynamics between −2.1 V up to +2.1 V. One of the key problems in photochemistry, which was recently addressed by the development of the consecutive photoelectron transfer process (conPET) [5], is the need to push the frontiers by accessing high reduction potentials. While the classical photoredox concept is based on the photophysical properties of the excited photoredox catalyst, the idea of the conPET concept mimics nature's light collection system and consecutively collects the energy of two photons stored in the excited state of the initially pre-promoted photoredox catalyst's radical ion. This was one of the features to use *N*-phenylphenothiazine for the photoactivation of SF_6 for the pentafluorosulfanylation of styrenes [2]. This two photon concept can further be extended to the photoredox catalytically generation of hydrated electrons as very powerful reductants (E = −2.8 V (vs NHE)) for organic reactions [18].

During the last years, we investigated the photoredox chemistry of new classes of catalysts like perylene bisimides, for their suitability in these types of processes [19] and evaluated the addition of methanol to alkenes as a simple model system. Due to the insufficient reduction potential of the photoredox catalyst, the Markovnikov addition of alcohols through oxidative quenching is yet limited to highly activated, aromatic alkenes. To the best of our knowledge no methods are known today that allow the addition of alcohols to α-methyl-substituted styrenes through photoredox catalysis. The currently available methods are based on a two-step procedure involving an iodoalkoxylation with NIS followed by the reduction of the formed alkyl iodide generating the product in moderate yields [20], or through the direct addition of MeOH catalyzed by either acidic conditions or heated ion exchange resin [21,22]. These methods are therefore not suitable for the alkoxylation of acid or base-labile substrates. To overcome the current limitations of reduction potentials of single electron transfer processes in photoredox catalysis we present herein a range of new *N*-phenylphenothiazine derivatives **1**–**11** as photoredox catalysts. Three of them were identified to be highly suitable for the addition of methanol to alkenes affording the corresponding Markovnikov products.

Results and Discussion

Activated aromatic olefins, such as 1,1-diphenylethylene (**12**), have reduction potentials $E_{red}(S/S^{-\bullet})$ in the range of −2.2 to −2.3 V [23,24], α- and β-methylstyrene (**13a** and **13b**) have an $E_{red}(S/S^{-\bullet})$ of −2.5 to −2.7 V [25], and styrene (**14**) an $E_{red}(S/S^{-\bullet})$ of −2.6 V (Figure 1) [25,26]. For non-aromatic, alkylated olefins, like 1-methylcyclohex-1-ene (**15**), the reduction potentials are estimated to values of $E_{red}(S/S^{-\bullet})$ = −3.0 V [25]. In our initial photoredox catalyst screening [26], we identified 1-(*N*,*N*-dimethylamino)pyrene (**16**) having an excited-state reduction potential $E^*_{ox}(P^{+\bullet}/P^*)$ of −2.4 V (determined by cyclic voltammetry and E_{00}). Thus, we are able to photoreduce 1,1-diphenylethylene (**12**), but not yet α-methylstyrene (**13**), and clearly not non-aromatic (alkylated) olefins, such as methylated cyclohexene **15**, as basic structures. The absorption of *N*-phenylphenothiazine (**1**) disappears at around 390 nm. This feature requires the excitation of the molecule using UV light sources and contradicts the use of visible light irradiation due to vanishing extinction coefficients at the edge to the visible region. To reach for high excited state reduction potentials and excite at rather long irradiation wavelengths an energetically high lying electronic groundstate potential has to be connected with a small S_0–S_1 gap for the development of strongly reducing photoredox catalysts. Thus, we first focused our strategy in catalyst development on the synthesis of some highly electron-rich phenothiazines **2**–**5** as well as some electron-deficient phenothiazines **6**–**9** to analyze the influences of

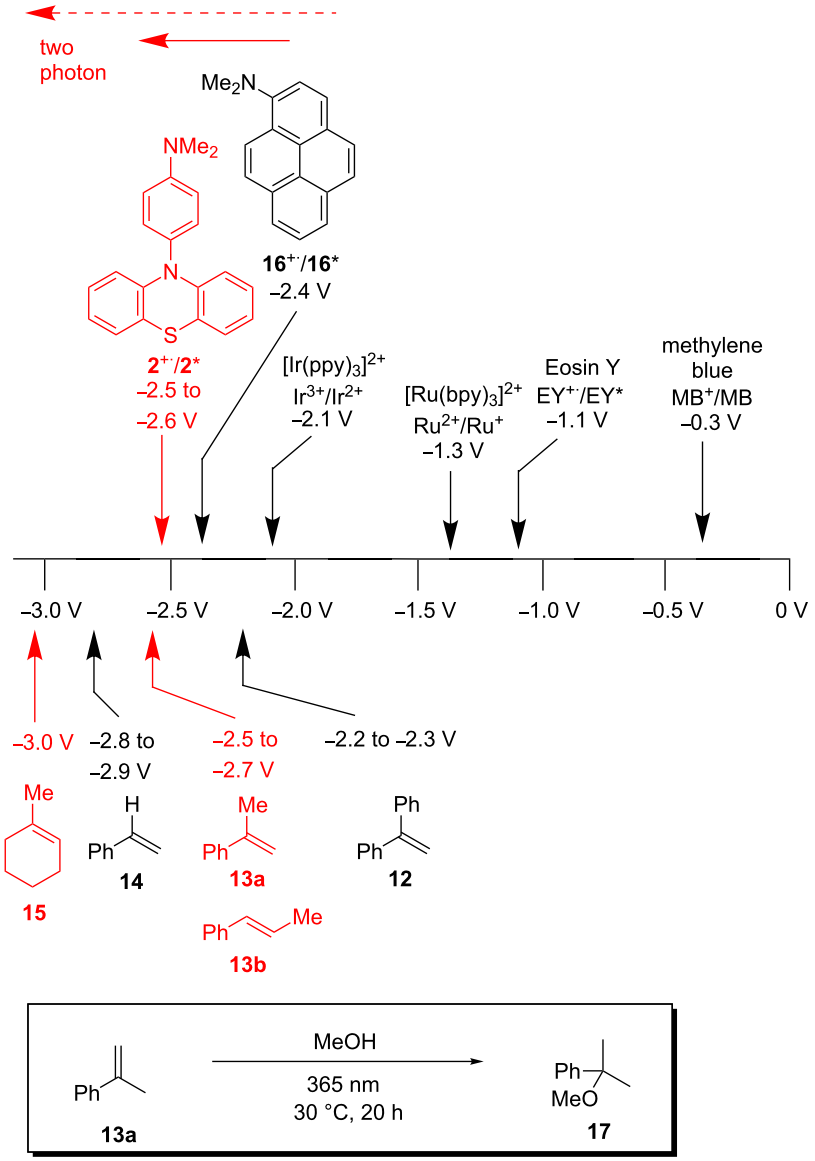

Figure 1: Reduction potentials (vs SCE) of common photoredox catalysts, pyrene **16** and phenothiazine **2**, in comparison to addressable substrate scope **12**–**15**. Bottom: photoredox catalytic addition of MeOH to α-methylstyrene (**13a**).

modifications of the core and the aryl moiety (Figure 2). The observed trends allowed us to come up with a set of strongly reducing photoredox catalysts that operate under UV-A conditions close to the visible range. In order to extend the scope of available reduction potentials we expected that the *N*-phenylphenothiazine core having installed additional electron-donating groups, like NR_2 in **2**, reaches very low reduction potentials in the range of $E(P^{+\cdot}/P^*) = -2.5$ to -3.0 V which is in the range of solid sodium [27], that would be able to attack low-substituted styrenes like **13a** and **13b**.

Firstly, the absorbance characteristics of the derivatives **1**–**9** were analyzed and compared (Figure 3). The parent compound *N*-phenylphenothiazine (**1**) shows an absorption maximum at 320 nm. Substitution of the arene moiety results in a shift of the absorption maxima due to a change in the HOMO–LUMO gaps. It turned out that the introduction of the π-donating dimethylamino substituent in **2** induces a hypsochromic shift of the absorption maximum by 7 nm to 313 nm, while the mesityl group present in **5** as a σ-donor causes a bathochromic shift of about 8 nm. The detailed structure of the alkyl group attached to the amino part in the phenothiazines **2**, **10** and **11** showed no significant change in the absorption maximum of the S_1 transition (**10** in comparison to **2**), but replacement of the methyl groups by branched isobutyl groups in **11** resulted in a hypsochromic shift of the bathochromic features of absorption.

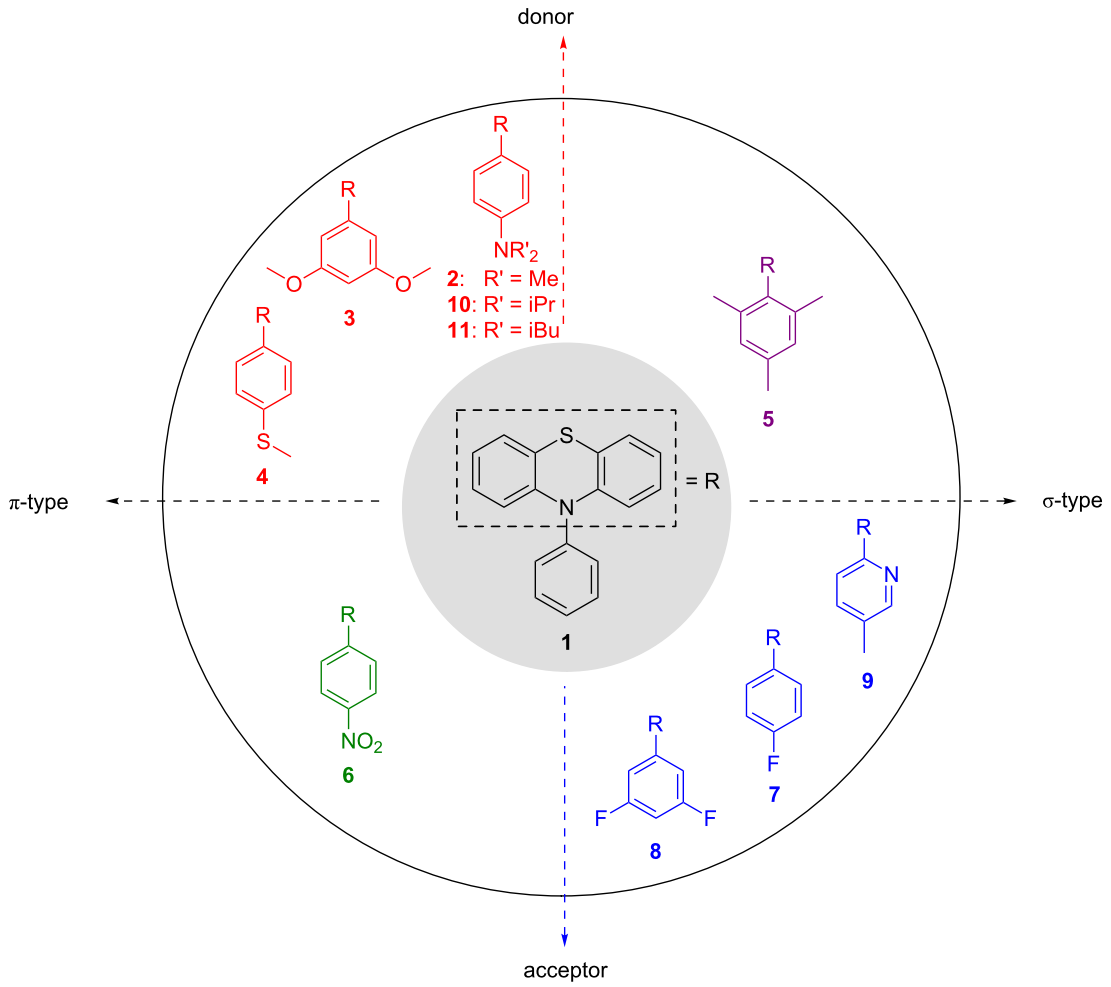

Figure 2: Acceptor or donor-modified phenothiazines **1**–**11** as potential photoredox catalysts.

The nitro compound **6** turned out to show a distinct long wavelength absorption that is apart from the region of absorption of all other catalysts by a shift of about 40 nm which is probably due to a charge transfer state. Interestingly, the spectrum of the methylpyridine derivative **9** showed a rather short absorption maximum at 302 nm.

All *N*-phenylphenothiazines **1**–**11** were additionally characterized by cyclic voltammetry (Figure 3 and Table 1) [28]. We found the first oxidation half wave of the unsubstituted *N*-phenylphenothiazine (**1**) as a fully reversible process as it was described in literature recently [18]. The second oxidation process of **1** is almost reversible but induces to some extent an irreversible oxidation process that shows up as further reduction half wave in the cyclic voltammogram. This is true for almost all synthesized derivatives **3**–**9**. The radical dication is known to undergo disproportionation reactions [27], which potentially explain the results. Only the amino derivatives **2**, **10** and **11** managed to undergo a second completely reversible oxidation process. To exclude interference with water and oxygen the measurements were carried under strict exclusion of any contaminants. The first oxidation of the lead structure **1** was found to occur at $E(\mathbf{1}^{+\bullet}/\mathbf{1})$ = 0.75 V (vs SCE). The substitution of the arene moiety by one (see **7**) or two fluorine substituents (see **8**) only leads to a shift in the reduction potential of about 0.06 V. This trend was expected due to the lower electron density of these two *N*-phenylphenothiazines at the arene moiety. However, the effect by the pure σ-acceptor fluorine is not very pronounced. In the case of the 4-NO_2 substituted derivative **6** the pronounced influence of the π-acceptor shifts the reduction potential to a value of up to $E(\mathbf{6}^{+\bullet}/\mathbf{6})$ = 0.89 V (vs SCE). Substitution of the *N*-aryl moiety by electron-donating substituents shifts the potentials correspondingly towards lower reduction potentials, as expected. By introducing the thioether substituent (see **4**) to the arene the potential drops to about $E(\mathbf{4}^{+\bullet}/\mathbf{4})$ = 0.71 V (vs SCE). If the steric bulk is enhanced by a

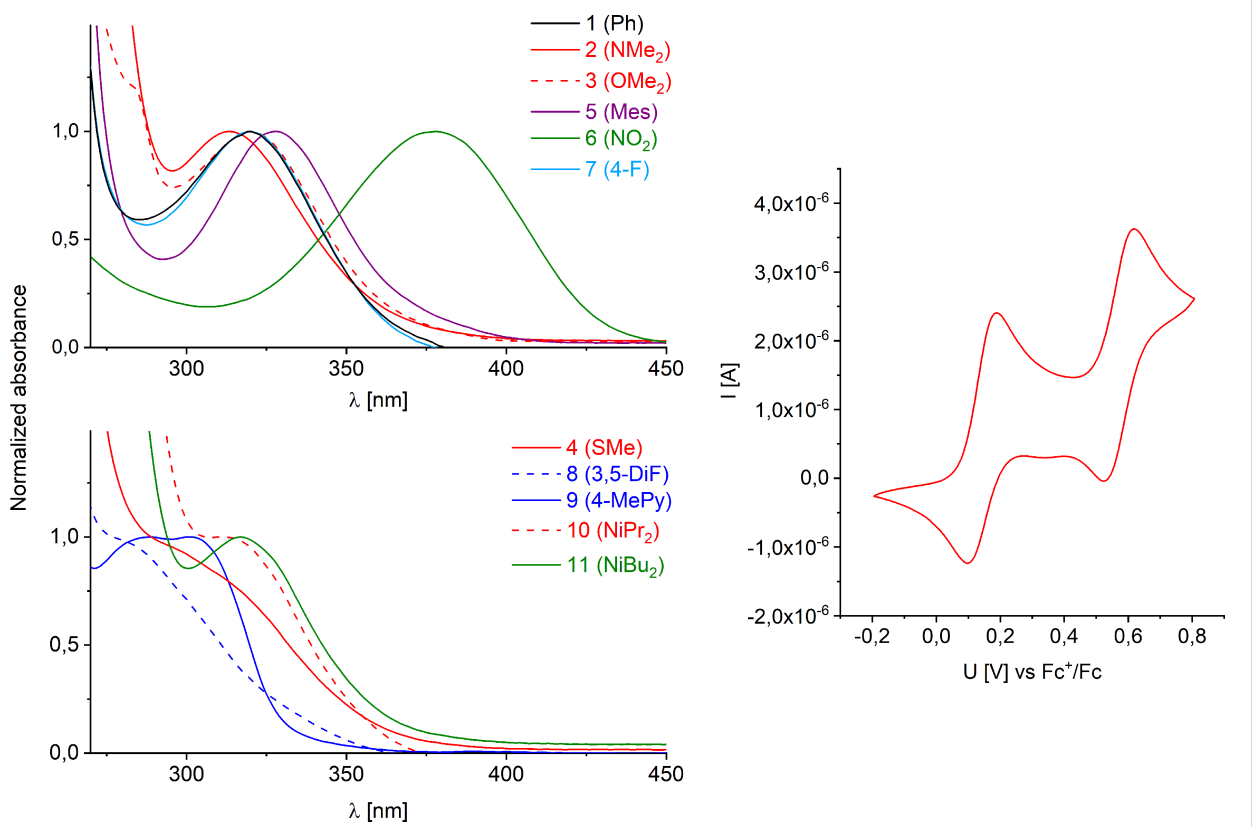

Figure 3: Normalized UV–vis absorption spectra above 290 nm of *N*-phenylphenothiazines **1**–**11** (left) and representative cyclic voltammogram of **2** (right).

Table 1: Reduction potentials $E_{red}(\mathbf{X}^{+\cdot}/\mathbf{X})$ of *N*-phenylphenothiazines **1**–**11** (determined by cyclic voltammetry using ferrocene as standard).

compound	$E_1(\mathbf{X}^{+\cdot}/\mathbf{X})$[a]	$E_2(\mathbf{X}^{+\cdot}/\mathbf{X})$	$E_1(\mathbf{X}^{+\cdot}/\mathbf{X}^*)$	E_{00}[b]
1	0.75 V	1.50 V[c]	−2.5 V	3.2 eV
2	0.57 V	1.00 V	−2.5 V	3.1 eV
3	0.73 V	1.49 V	−2.5 V	3.2 eV
4	0.71 V	–	−3.0 V	3.7 eV[d]
5	0.67 V	1.59 V	−2.5 V	3.1 eV
6	0.89 V	1.55 V	−2.1 V	3.0 eV
7	0.75 V	1.50 V[c]	−2.5 V	3.3 eV
8	0.77 V	1.05 V[c]	−2.6 V	3.4 eV
9	0.80 V	–	−2.6 V	3.4 eV
10	0.53 V	0.98 V	−2.9 V	3.4 eV
11	0.49 V	0.96 V	−2.9 V	3.4 eV

[a]Converted from the ferrocene scale to the scale vs SCE: +0.38 V [30]. [b]E_{00} was estimated by using the method of determination of the intersection of the normalized absorption and fluorescence. [c]Irreversible. [d]Fluorescence in the UV-A range, see Figure S27 (Supporting Information File 1).

mesityl substituent (see **5**) the reduction potential interestingly is higher than in the parent compound **1** although there are electron-donating alkyl groups present in the molecular structure. This can be explained by a twist of the arene moieties due to steric bulk causing an interruption of the delocalization. The electron transfer is found to occur at $E(\mathbf{5}^{+\cdot}/\mathbf{5})$ = 0.67 V (vs SCE). However, the introduction of the π-donating dimethylamino substituent dramatically shifts the reduction potential to up to $E(\mathbf{2}^{+\cdot}/\mathbf{2})$ = 0.57 V (vs SCE). We hypothesized that the introduction of even more donating substituents could reduce the reduction potential further. Therefore, we synthesized the modified alkylated compounds **10** and **11**, respectively. Indeed, both compounds showed a lower potential with **11** having an $E_{red}(\mathbf{11}^{+\cdot}/\mathbf{11})$ = 0.49 V (vs SCE). This made us curious about the excited state potential of the catalysts. Using the Rehm–Weller equation (without considering the solvent term) [29] we estimated the excited state potential of these catalysts to be as low as $E_{red}(\mathbf{X}^{+\cdot}/\mathbf{X}^*) \approx -2.9$ to −3.0 V (vs SCE).

The proposed photoredox catalytic mechanism (Figure 4) for the nucleophilic addition of methanol to olefins starts with photoinduced electron transfer from the *N*-phenylphenothiazine (**1**) as photocatalyst to **13a** as substrate. The resulting substrate radical anion $\mathbf{13a}^{-\cdot}$ is instantaneously protonated to radical $\mathbf{13a}^{\cdot}$ and back-electron transfer to the intermediate phenothiazine radical cation $\mathbf{1}^{+\cdot}$ yields the substrate cation $\mathbf{13a}^{+}$. The latter is

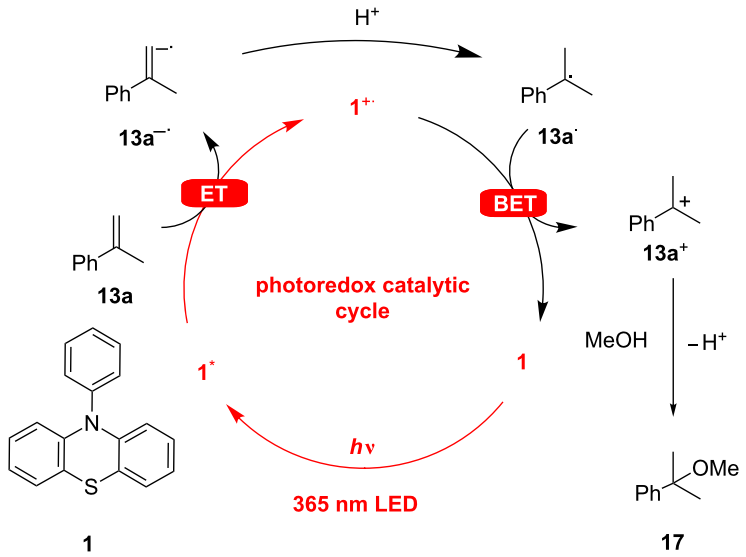

Figure 4: Proposed mechanism for the photoredox-catalyzed addition of methanol to α-methylstyrene (**13a**). (ET = electron transfer, BET = back-electron transfer).

attacked by methanol as nucleophile and finally deprotonation gives rise to the product **17** (see Figure 4). The principal problem of this type of photoredox catalytic cycle is that the back-electron transfer cannot compete with the initial electron transfer because both components, $\mathbf{1}^{+\cdot}$ and $\mathbf{13}^{-\cdot}$, are formed only in stationary low concentrations. In the past, we used electron mediators as additives (triethylamine) [19,26] or peptides with substrate-binding sites [31,32] to overcome this problem. For the current work, we propose a radical ion pair in a solvent cage that undergoes an extremely fast proton transfer followed by the intracage back-electron transfer, since triethylamine is no longer needed (vide infra).

The evaluation of both the optical and electrochemical properties of the prepared phenothiazine derivatives **1**–**11** leads to the conclusion that only the dialkylamino derivatives **2**, **10** and **11** come up with an estimated excited state reduction potential capable of reducing α-methylstyrene (**13a**). The optoelectronic properties and the excited state reduction potential of $E_{red}(\mathbf{2}^{+\cdot}/\mathbf{2}^{*}) = -2.5$ V of dimethylamino compound **2** that is close to the reduction potential of the substrate **13a** encouraged us to approach the so far not yet observed addition of methanol to this less activated substrate promoted by catalyst **2**. After optimizing our catalytic system with catalyst **2**, we could also confirm the expected reactivity of the branched dialkylamino-substituted derivatives **10** and **11** (entry 12 and 13, Table 2).

The initial conditions included irradiation of substrate **13a** in the presence of the catalyst (5 mol %) in methanol and triethyl-

Table 2: Screening of reaction conditions for the methanol addition to α-methylstyrene (**13a**).[a]

entry	**13a** [mM]	catalyst	mol %	additive	solvent	yield
1	84.6	**2**	5	NEt_3[b]	MeOH	31%
4	84.6	**2**	5	–	MeOH	84%
5	42.3	**2**	10	–	MeOH	quant.
6	42,3	**2**	10	–	MeOH	–[c]
7	42.3	**2**	10	–	MeOH	–[d]
8	42.3	–	–	NEt_3	MeOH	–[d]
9	42.3	**2**	10	–	MeOD	78%[e]
11	170	**2**	10	–	MeOD	quant.[e]
12	170	**10**	10	–	MeOH	quant.[e]
13	170	**11**	10	–	MeOH	quant.[e]

[a]Conditions: 30 °C, 65 h, 365 nm LEDs. [b]10 equiv. [c]No light. [d]No catalyst. [e]20 h.

amine (10% (v/v)) as the additive according to our previously reported photoredox catalysis with pyrene **16** [18]. Under these conditions the product **17** was formed in a yield of 31%. It turned out that omitting the additive as electron shuttle enhanced the catalytic efficiency and the yield increased up to 84%. Obviously, this is a major difference between the photoredox catalysis with pyrene **16**, where triethylamine was absolutely crucial to obtaining good product yields, and *N*-phenylphenothiazine **1**. Having this electron shuttle (ca. 1 M) in the reaction mixture efficiently leads to silent or non-silent quenching of the reactive species due to the following modes of quenching. While the back-electron transfer under generation of the triethylamine radical cation unproductively consumes electrons while oxidizing triethylamine, the hydrogen abstraction pathway generates the reduced phenylethane, which is observed in small concentrations in the reaction mixture. The analysis of the reaction mixture still showed some unreacted starting material. Assuming the first electron transfer as the rate-determining step the substrate concentration was reduced to 42 mM and the catalyst concentration was increased to 10 mol %. This change in the reaction conditions led to a quantitative product formation after 65 h. Finally, the rather long reaction times were addressed by speeding up the reaction simply by raising the concentration of all components to 170 mM. This reduced the reaction time to 20 h irradiation producing the product **17** in quantitative yield. However, a further increase of substrate concentration slowed down the reaction again by speeding up silent electron transfer processes.

Conclusion

One of the major current challenges in photoredox catalysis is the design of chromophores suitable for the most reductive chemical reactions, like for instance reductions by alkaline metals, affording reaction conditions that are easier to handle. While solid sodium comes up with a reduction potential of −3.0 V (vs SCE) the present novel *N*-phenylphenothiazine-based photoredox catalysts reach impressive excited state reduction potentials with up to −3.0 V (vs SCE) in case of catalyst **10**. We applied the strongly reducing *N*-phenylphenothiazines **2**, **10** and **11** for the photoredox catalytic reduction of α-methylstyrene (**13a**) as a less activated styrene that could not be addressed before. After optimization, the photoredox catalytic addition of methanol proceeded in quantitative yield within 20 h without any further additive, like triethylamine as electron shuttle. We could speed up the reaction by using increased concentrations of the substrate and the catalyst affording the product in quantitative yield after 20 h reaction time. We believe that photoredox catalysis with synthetically easily accessible *N*-phenylphenothiazines will lead to the development of new photoredox catalytic approaches based on their strongly reducing excited states.

Supporting Information

Supporting Information File 1

Copies of ^{1}H and ^{13}C NMR spectra, mass spectra, absorption and emission spectra and cyclic voltammetry data of **1**–**11** and **17**.
[https://www.beilstein-journals.org/bjoc/content/supplementary/1860-5397-15-5-S1.pdf]

Acknowledgements

Financial support by the Deutsche Forschungsgemeinschaft (Wa 1386/16-2) and KIT is gratefully acknowledged. DR thanks the GRK 1626 “Chemical photocatalysis” (funded by the Deutsche Forschungsgemeinschaft) for participation in their qualification program and the Landesgraduiertenförderung Baden Württemberg for financial support.

ORCID® iDs

Fabienne Speck - https://orcid.org/0000-0003-2183-375X
David Rombach - https://orcid.org/0000-0002-6673-9567
Hans-Achim Wagenknecht - https://orcid.org/0000-0003-4849-2887

References

1. Papadakis, R.; Ottosson, H. *Chem. Soc. Rev.* **2015,** *44,* 6472–6493. doi:10.1039/c5cs00057b
2. Rombach, D.; Wagenknecht, H.-A. *ChemCatChem* **2018,** *10,* 2955–2961. doi:10.1002/cctc.201800501
3. Nguyen, T. M.; Manohar, N.; Nicewicz, D. A. *Angew. Chem., Int. Ed.* **2014,** *53,* 6198–6201. doi:10.1002/anie.201402443
4. Shaw, M. H.; Twilton, J.; MacMillan, D. W. C. *J. Org. Chem.* **2016,** *81,* 6898–6926. doi:10.1021/acs.joc.6b01449
5. Ghosh, I.; Ghosh, T.; Bardagi, J. I.; König, B. *Science* **2014,** *346,* 725–728. doi:10.1126/science.1258232
6. Reckenthäler, M.; Griesbeck, A. G. *Adv. Synth. Catal.* **2013,** *355,* 2727–2744. doi:10.1002/adsc.201300751
7. Rueping, M.; Nikolaienko, P.; Lebedev, Y.; Adams, A. *Green Chem.* **2017,** *19,* 2571–2575. doi:10.1039/c7gc00877e
8. McTeague, T. A.; Jamison, T. F. *Angew. Chem., Int. Ed.* **2016,** *55,* 15072–15075. doi:10.1002/anie.201608792
9. Lang, S. B.; Wiles, R. J.; Kelly, C. B.; Molander, G. A. *Angew. Chem., Int. Ed.* **2017,** *56,* 15073–15077. doi:10.1002/anie.201709487
10. Lévesque, F.; Seeberger, P. H. *Angew. Chem., Int. Ed.* **2012,** *51,* 1706–1709. doi:10.1002/anie.201107446
11. Amador, A. G.; Yoon, T. P. *Angew. Chem., Int. Ed.* **2016,** *55,* 2304–2306. doi:10.1002/anie.201511443
12. Douglas, J. J.; Albright, H.; Sevrin, M. J.; Cole, K. P.; Stephenson, C. R. J. *Angew. Chem., Int. Ed.* **2015,** *54,* 14898–14902. doi:10.1002/anie.201507369
13. Ohlow, M. J.; Moosmann, B. *Drug Discovery Today* **2011,** *16,* 119–131. doi:10.1016/j.drudis.2011.01.001
14. Discekici, E. H.; Treat, N. J.; Poelma, S. O.; Mattson, K. M.; Hudson, Z. M.; Luo, Y.; Hawker, C. J.; Read de Alaniz, J. *Chem. Commun.* **2015,** *51,* 11705–11708. doi:10.1039/c5cc04677g

15. Dadashi-Silab, S.; Pan, X.; Matyjaszewski, K. *Chem. – Eur. J.* **2017,** *23,* 5972–5977. doi:10.1002/chem.201605574
16. Pan, X.; Fang, C.; Fantin, M.; Malhotra, N.; So, W. Y.; Peteanu, L. A.; Isse, A. A.; Gennaro, A.; Liu, P.; Matyjaszewski, K. *J. Am. Chem. Soc.* **2016,** *138,* 2411–2425. doi:10.1021/jacs.5b13455
17. Christensen, J. A.; Phelan, B. T.; Chaudhuri, S.; Acharya, A.; Batista, V. S.; Wasielewski, M. R. *J. Am. Chem. Soc.* **2018,** *140,* 5290–5299. doi:10.1021/jacs.8b01778
18. Kerzig, C.; Goez, M. *Chem. Sci.* **2016,** *7,* 3862–3868. doi:10.1039/c5sc04800a
19. Weiser, M.; Hermann, S.; Penner, A.; Wagenknecht, H.-A. *Beilstein J. Org. Chem.* **2015,** *11,* 568–575. doi:10.3762/bjoc.11.62
20. Murphy, J. A.; Khan, T. A.; Zhou, S.-z.; Thomson, D. W.; Mahesh, M. *Angew. Chem., Int. Ed.* **2005,** *44,* 1356–1360. doi:10.1002/anie.200462038
21. Ziegler, K.; Dislich, H. *Chem. Ber.* **1957,** *90,* 1107–1115. doi:10.1002/cber.19570900634
22. Ouardad, S.; Wirotius, A.-L.; Kostjuk, S.; Ganachaud, F.; Peruch, F. *RSC Adv.* **2015,** *5,* 59218–59225. doi:10.1039/c5ra08557h
23. Ruoff, R. S.; Kadish, K. M.; Boulas, P.; Chen, E. C. M. *J. Phys. Chem.* **1995,** *99,* 8843–8850. doi:10.1021/j100021a060
24. Senboku, H.; Komatsu, H.; Fujimura, Y.; Tokuda, M. *Synlett* **2001,** 418–420. doi:10.1055/s-2001-11417
25. Mattay, J. *Tetrahedron* **1985,** *41,* 2405–2417. doi:10.1016/s0040-4020(01)96636-0
26. Penner, A.; Bätzner, E.; Wagenknecht, H.-A. *Synlett* **2012,** *23,* 2803–2807. doi:10.1055/s-0032-1317532
27. Ong, S. P.; Chevrier, V. L.; Hautier, G.; Jain, A.; Moore, C.; Kim, S.; Ma, X.; Ceder, G. *Energy Environ. Sci.* **2011,** *4,* 3680. doi:10.1039/c1ee01782a
28. Yasukouchi, K.; Taniguchi, I.; Yamaguchi, H.; Ayukawa, J.; Ohtsuka, K.; Tsuruta, Y. *J. Org. Chem.* **1981,** *46,* 1679–1683. doi:10.1021/jo00321a031
29. Rehm, D.; Weller, A. *Ber. Bunsen-Ges.* **1969,** *73,* 834–839.
30. Pavlishchuk, V. V.; Addison, A. W. *Inorg. Chim. Acta* **2000,** *298,* 97–102. doi:10.1016/s0020-1693(99)00407-7
31. Hermann, S.; Wagenknecht, H.-A. *J. Pept. Sci.* **2017,** *23,* 563–566. doi:10.1002/psc.2966
32. Hermann, S.; Sack, D.; Wagenknecht, H.-A. *Eur. J. Org. Chem.* **2018,** 2204–2207. doi:10.1002/ejoc.201800319

License and Terms